

Investigating the mechanisms and outcomes of Sprouty-2 S-acylation

A thesis presented by

Carolina Locatelli

In fulfilment of the requirement for the degree of

Doctor of Philosophy

2021

University of Strathclyde

Strathclyde Institute of Pharmacy and Biomedical Sciences

Declaration of Authenticity and Author's Rights

This thesis is the result of the author's original research. It has been composed by the author and has not been previously submitted for examination which has led to the award of a degree.

The copyright of this thesis belongs to the author under the terms of the United Kingdom Copyright Acts as qualified by University of Strathclyde Regulation 3.50. Due acknowledgement must always be made of the use of any material contained in, or derived from, this thesis.

Signed:

A handwritten signature in cursive script that reads "Cardina Foster".

Date: 01/03/21

Acknowledgements

First and foremost, my biggest thank you goes to my supervisor Prof. Luke H. Chamberlain. His constant support, guidance and patience made this journey so enjoyable. Truly, I could have not wished for a better mentor. Thank you so much for this opportunity Luke, it will be difficult to find another work environment as welcoming and friendly!

I would also like to thank all the lab members I had the pleasure to work with during my PhD. Dr. Christine Salaun, thank you with all my heart for your great help and patience, best bench mate ever. I will miss our chats and breaks! Dr. Kimon Lemonidis, thanks for replying to my monthly emails and for your valuable feedbacks. Dr. Filip Zmuda, Dr. Jennifer Greaves and Dr. Marianna Kouskou, it was a pleasure meeting you!

Thanks to my PhD colleagues, for the pre-Covid19 nights out and the endless streams of beers, and to all the SIPBS staff that made me feel so welcomed and never an outsider. I will miss you all!

While I was in Glasgow, I was lucky enough to meet many awesome friends. Alex, always so full of energy, thanks for explaining the chemistry behind things. Mirna, soon-to-be Dr., it was a pleasure to share this “PhD life” with you. To you and Kristijan, two great friends, a million thanks for all the laughs and beautiful moments we shared! Laurie, what to say, I am so grateful our paths crossed. Thank you for our endless chats and all the time spent together. Let us not forget about our plans. I will miss you!

To my beautiful Italian friends, for always being on the other end of the phone. Raffa, la mia BFF (meglio nota come patatona) dopo tutti questi anni sei ancora e sempre qui con me, vicinissima al mio cuore, ti voglio un bene immenso! Giorgia, la mia valvola di sfogo, grazie per ascoltare le mie lunghissime lamentele e capire i miei dubbi come fossero i tuoi, mi mancano le nostre avventure! Mau, se non ci fossi bisognerebbe inventarti, grazie per esserci sempre e comunque, ti voglio bene amico

mio! Jessi, grazie per la tua sincerità e la gioia che mi trasmetti ogni volta che ci ritroviamo, sei sempre un punto di riferimento importantissimo! Mavi, alle nostre convinzioni e conversazioni in anglo-italo-ispano, grazie per credere in me e per avermi supportato lungo questo percorso, siamo ancora troppo lontane amica mia!

To Ginés, from the bottom of my heart thank you for your love, tenderness and endless patience. I hope to do an equally good job now that you have undertaken a PhD. I am always on your side!

A mio fratello, mia mamma e mio papà, tutto questo non sarebbe stato possibile senza il vostro supporto e immenso amore, vi amo infinitamente!

Publications

Locatelli, C., Lemonidis, K., Salaun, C., Tomkinson, N.C.O., Chamberlain, L.H., 2020. Identification of key features required for efficient S-acylation and plasma membrane targeting of Sprouty-2. *J. Cell Sci.* jcs.249664. <https://doi.org/10.1242/jcs.249664>

Salaun, C., Locatelli, C., Zmuda, F., Cabrera González, J., Chamberlain, L.H., 2020. Accessory proteins of the zDHHC family of S-acylation enzymes. *J. Cell Sci.* <https://doi.org/10.1242/jcs.251819>

Poster communications

Locatelli, C., Lemonidis, K., Salaun, C., and Chamberlain, L.H. (2019) Protein interactions mediated by the Ankyrin-Repeat Domain of the S-acyltransferase zDHHC17. Unpublished poster presentation at FASEB conference: “The protein lipidation conference: enzymology, signalling, and therapeutics” 7-12th July, Olean, NY, USA. Appendix I.

Locatelli, C., Lemonidis, K., and Chamberlain, L.H. (2018) zDHHC17 protein-protein interactions mediated by the Ankyrin-Repeat Domain. Unpublished poster presentation at Biochemical Society conference: “Acylation of intracellular and secreted proteins: mechanisms and functional outcomes” 10-12th September, Brighton, UK. Appendix II.

Table of Contents

Declaration of Authenticity and Author's Rights	I
Acknowledgements	II
Publications	IV
Poster communications	V
List of Figures	XII
List of Tables	XVI
List of Abbreviations	XVII
Abstract	XXIV
Chapter 1 Introduction	1
1.1 S-acylation is a type of protein lipidation.....	1
1.2 Regulatory effects of S-acylation.....	2
1.2.1 S-Acylation of soluble proteins	3
(i) Isoprenylated and S-acylated substrates.....	4
(ii) N-myristoylated and S-acylated substrates	6
(iii) Exclusively S-acylated substrates.....	12
1.2.2 S-acylation of transmembrane (TM) proteins	16
1.2.3 S-acylation and protein stability	20
1.2.4 S-acylation and anterograde transport	22
1.3 Deacylation mediated by protein thioesterases	24
1.4 S-acylation mediated by the zDHHC family of enzymes	28
1.4.1 Subcellular and tissue-distribution of zDHHC enzymes.....	35
1.5 Regulation of zDHHC enzymes	37
1.6 Substrate specificity of zDHHC enzymes	41

1.6.1 The ankyrin-repeat (ANK) domain of zDHHC17 and zDHHC13 mediates substrate recognition and binding.....	42
1.6.2 Identification of a zDHHC-ANK-binding motif (zDABM)	43
1.6.3 Critical residues for zDHHC17 ANK domain - substrate interaction.....	44
1.7 zDHHC17 S-acyltransferase: (patho)physiology	47
1.7.1 zDHHC17 and Huntington disease	48
1.7.2 zDHHC17 and diabetes mellitus	50
1.7.3 zDHHC17 and other diseases	52
1.8 The Sprouty (SPRY) family of proteins.....	52
1.8.1 General domain structure of SPRY proteins	53
1.8.2 Subcellular localisation of SPRY proteins.....	56
1.8.3 Regulation of RTK signalling by SPRY proteins	59
(i) FGF signalling	62
(ii) EGF signalling	67
(iii) VEGF signalling	70
1.8.4 Regulation of SPRY proteins by post-translational modifications (PTMs). 72	
1.9 SPRY proteins and development	74
1.10 SPRY2 and tumorigenesis	76
1.10.1 SPRY2 and prostate cancer (PC)	77
1.10.2 SPRY2 and glioblastoma multiforme (GBM).....	80
1.11 Aims of the thesis	82
Chapter 2 Materials and Methods	84
2.1 Cellular Biology	84
2.1.1 Mammalian Cell Culture	84
2.1.2 Plasmids	85

2.1.3 DNA Transfection	88
2.1.4 Cycloheximide experiments.....	89
2.2 Molecular Biology	89
2.2.1 Site-Directed Mutagenesis.....	89
2.2.2 Agarose Gel electrophoresis.....	94
2.2.3 Purification of the PCR products.....	95
2.2.3.1 DNA extraction from agarose gel.....	95
2.2.3.2 DpnI treatment	95
2.2.4 Gateway Cloning System	96
2.2.5 Production of competent TOP10 E. Coli cells	96
2.2.6 Bacterial transformation and culture for plasmid DNA amplification	97
2.2.7 Plasmid DNA purification.....	98
2.2.7.1 Miniprep plasmid purification	98
2.2.7.2 Restriction Enzyme digestion.....	98
2.2.7.3 Sequencing.....	99
2.2.7.4 Midiprep plasmid purification	99
2.2.8 Protein Expression and Purification.....	99
2.2.9 Pull-down assay using His ₆ -tagged protein immobilised on Ni ²⁺ -NTA	101
2.3 Protein Biochemistry	103
2.3.1 Click Chemistry.....	103
2.3.2 Co-Immunoprecipitation assay.....	103
2.3.3 Click Chemistry coupled with immunoprecipitation	105
2.3.4 Subcellular fractionation by ultracentrifugation	106
2.3.6 Sodium Dodecyl Sulphate-Polyacrylamide Gel Electrophoresis (SDS-PAGE)	106

2.3.7 Immunoblotting	108
2.3.8 Total Protein Stain	108
2.3.9 Antibodies	109
2.3.10 Peptide Array and Far Western blotting.....	110
2.4 Confocal microscopy	111
2.5 Bioinformatics tools.....	111
2.6 Data quantification and statistical analysis	112
Chapter 3 Identification of key features required for efficient S-acylation and plasma membrane targeting of SPRY2 protein	115
3.1 Introduction.....	115
3.2 Results	117
3.2.1 SPRY2 is S-acylated by zDHHC17 promoting protein stability.....	117
3.2.2 The increase in SPRY2 levels following S-acylation is independent of the highly conserved Tyr-55 (Y55)	121
3.2.3 Region 260-290, within the CRD of SPRY2, is important for zDHHC17- mediated stability	123
3.2.4 SPRY2 is differentially S-acylated by zDHHC17, zDHHC7, and zDHHC3 enzymes	125
3.2.5 S-acylation of SPRY2 by zDHHC17 requires cysteines 265 and 268	127
3.2.6 Cys-265 and Cys-268 are located in a hydrophobic patch within an α - helical region of the CRD of the protein	134
3.2.7 Specific regions in the CRD are required for efficient S-acylation of SPRY2	137
3.2.8 Identification of the key residues within the sequence 'SAQNVIDYGT---- VKGL' important for SPRY2 S-acylation by zDHHC17	143

3.2.9 Combined substitutions of Asn-211 (N211), Asp-214 (D214) and Lys-223 (K223) block S-acylation of SPRY2 by both zDHHC17 and zDHHC7	151
3.2.10 The NDK mutant undergoes more rapid degradation than wild-type SPRY2	155
3.2.11 S-acylation-deficient mutants are membrane-associated and display a distinct migration pattern on SDS-PAGE	157
3.2.12 Disruption of S-acylation leads to mis-localisation of SPRY2 and loss of plasma membrane association	158
3.3 Discussion	161
Chapter 4 Characterisation of SPRY2 interactions with the ankyrin-repeat domain of zDHHC17	170
4.1 Introduction.....	170
4.2 Results	172
4.2.1 Alanine substitution of Trp-130 (W130A) within the ANK domain of zDHHC17 severely impairs the binding of SPRY2 and several other proteins that contain zDABM sequences	172
4.2.2 N100A and W130A substitutions have no effect on S-acylation of SPRY2 by zDHHC17	174
4.2.3 Mutation of the zDABM sequence(s) in SPRY2 has no effect on S-acylation mediated by zDHHC17	176
4.2.4 Disruption of the zDABM sequence in SPRY2 diminishes but does not abolish interaction with ANK17 in pull-down assays	178
4.2.5 Mutation of Pro-154 in SPRY2 leads to reduced but not abolished interaction with full-length zDHHC17.....	180
4.2.6 Truncation analysis suggests that the SPRY domain is sufficient for S-acylation of SPRY2 by zDHHC17	182

4.2.7 The ANK domain is required for zDHHC17-mediated S-acylation of SPRY2	186
4.2.8 Peptide array experiments suggest the presence of a second binding site upstream of the zDABM of SPRY2	188
4.2.9 In PC12 cells, SPRY2 P154A and SPRY2 155-315 are efficiently S-acylated by endogenous enzymes and targeted to the plasma membrane similar to wild-type SPRY2	191
4.3 Discussion	194
Chapter 5 Homo- and hetero- multimerisation of zDHHC17, the enzyme that modifies SPRY2	202
5.1 Introduction	202
5.2 Results	204
5.2.1 The ANK domain of zDHHC17 interacts with zDHHC17 and zDHHC13 ...	204
5.2.2 zDHHC17 interaction with the ANK domain reflects ANK-ANK interaction	206
5.2.3 Self-association of the ANK domain of zDHHC17 requires the substrate binding pocket (Asn-100 and Trp-130)	208
5.2.4 Co-immunoprecipitation experiments suggest a second mode of zDHHC17 self-association	210
5.3 Discussion	212
Chapter 6 Final Discussion	218
Chapter 7 Bibliography	226
Appendix I	272
Appendix II	273

List of Figures

Chapter 1

Figure 1.1 Two-step mechanism of action by zDHHC enzymes.....	31
Figure 1.2 Structure of a zDHHC enzyme.....	33
Figure 1.3 S-acylation of zDHHC enzymes.....	34
Figure 1.4 Interaction between ANK17 and SNAP25b ₁₁₁₋₁₂₀ peptide	46
Figure 1.5 Structure of <i>D. melanogaster</i> and human SPRY proteins.....	55
Figure 1.6 Schematic representation of human SPRY2 protein.....	56
Figure 1.7 Schematic representation of hSPRY2 interactors.....	61
Figure 1.8 Modulation of FGF signalling by SPRY proteins	66
Figure 1.9 Modulation of EGF signalling by SPRY proteins	69
Figure 1.10 Modulation of VEGF signalling by SPRY proteins.....	71

Chapter 3

Figure 3.1 S-acylation of SPRY2 by zDHHC17 enhances protein levels	119
Figure 3.2 Loss of the slower migrating band of SPRY2 after replacement of either Ser-111 or Ser-120 with alanine residues	120
Figure 3.3 S-acylation-dependent increase in SPRY2 levels is independent of phosphorylation at the highly conserved Tyr-55.....	122
Figure 3.4 SPRY2 region 260-290 is important for the zDHHC17-mediated increase in SPRY2 levels.....	124
Figure 3.5 SPRY2 is S-acylated by zDHHC17, zDHHC7 and zDHHC3 enzymes	126
Figure 3.6 Efficient S-acylation by zDHHC17 requires Cys-265 and Cys-268 within the CRD of SPRY2.....	129
Figure 3.7 Analysis of the effects of cysteine substitutions on the level of SPRY2 .	131
Figure 3.8 S-acylation of SPRY2 mutants with substitutions of Cys-265 and Cys-268	133
Figure 3.9 Cys-265 and Cys-268 are predicted to lie within an α -helical region	134

Figure 3.10 Wheel projection of region 249-286 of SPRY2 using NetWheel software	135
Figure 3.11 Analysis of the hydrophobicity of the cysteine-rich domain (CRD) of SPRY2	136
Figure 3.12 SPRY2 S-acylation by zDHHC17 requires the presence of specific regions within the CRD	138
Figure 3.13 Residues within the SPRY2 region 208-225 are important for S-acylation by zDHHC17.....	140
Figure 3.14 Residues within the SPRY2 region 208-225 are important for S-acylation by zDHHC7.....	142
Figure 3.15 Analysis of SPRY2 mutants S208A, Q210A, N211A, and V212A S-acylation by zDHHC17.....	146
Figure 3.16 Analysis of SPRY2 mutants I213A, D214A, Y215A, G216A, and T217A S-acylation by zDHHC17	148
Figure 3.17 Analysis of SPRY2 mutants V222A, K223A, G224A, and L225A S-acylation by zDHHC17.....	150
Figure 3.18 Asp-214 (D214) and Lys-223 (K223) are highly conserved across species	151
Figure 3.19 Asp-214 and Lys-223 are positioned on opposite sides of the same α -helix	152
Figure 3.20 Combined alanine substitution of Asn-211, Asp-214, and Lys-223 in the CRD leads to a loss of SPRY2 S-acylation by both zDHHC17 and zDHHC7.....	154
Figure 3.21 Cycloheximide-block experiments reveal a shorter half-life for the S-acylation-deficient NDK mutant.....	156
Figure 3.22 Membrane localisation and electrophoretic properties of S-acylation-deficient mutants of SPRY2.....	158
Figure 3.23 Analysis of localisation of SPRY2 WT and SPRY2 S-acylation defective mutants NDK, and C265/268A	160

Chapter 4

Figure 4.1 Effect of the W130A substitution of the ANK domain on substrate binding by zDHHC17	173
Figure 4.2 S-acylation of SPRY2 by zDHHC17 does not require Trp-130 or Asn-100	175
Figure 4.3 S-acylation of SPRY2 by zDHHC17 does not require zDABM sequences	177
Figure 4.4 Mutation of Pro-154 within the zDABM of SPRY2 reduces but does not abolish binding to ANK17	179
Figure 4.5 Mutation of Pro-154 in SPRY2 diminishes but does not abolish interaction with full-length zDHHC17	181
Figure 4.6 Residues 155-315 of SPRY2, encompassing the SPRY domain, are sufficient for S-acylation by zDHHC17	183
Figure 4.7 SPRY2 S-acylation by zDHHC17 does not require its C-terminal domain	185
Figure 4.8 Deletion of ANK17 or the C-terminal tail of zDHHC17 prevents SPRY2 S-acylation	187
Figure 4.9 A potential second ANK17 binding domain is present at position 106-120 of human SPRY2	190
Figure 4.10 SPRY2 P154A and 155-315 mutants are endogenously S-acylated in PC12 cells.....	192
Figure 4.11 Intracellular localisation of SPRY2 P154 and 155-315 mutants in PC12 cells	193

Chapter 5

Figure 5.1 zDHHC17 and zDHHC13 bind to the ANK domain of zDHHC17	205
Figure 5.2 ANK17 displays a loss of interaction with a zDHHC17 mutant lacking the ANK domain	207
Figure 5.3 The N100/W130 binding pocket in the ANK domain is important for zDHHC17 homo-dimerisation	209
Figure 5.4 zDHHC17 self-association in cells does not require ANK domain dimerisation	211

Chapter 6

Figure 6.1 Main findings of this study and key outstanding questions 219

List of Tables

Chapter 1

Table 1.1 Fatty acyl chain length preference in the zDHHC enzyme family	35
Table 1.2 Intracellular distribution of zDHHC S-acyltransferases	36
Table 1.3 Expression of SPRY2 in various human cancer types	77

Chapter 2

Table 2.1 Sequences of oligonucleotide primers used to generate zDHHC17 and SPRY2 mutants by site-direct mutagenesis PCR	94
--	----

List of Abbreviations

17-ODA: 17-octadecynoic acid

2-BP: 2-bromopalmitate (zDHHC enzymes/S-acylation inhibitor)

ABHD17A-C: α/β hydrolase domain containing protein 17 members A-C

Acyl-RAC: Acyl Resin-Assisted Capture

AMPA: α -amino-3-hydroxy-5-methyl-4-isoxazole propionate receptor

ANK/ANK17: ankyrin repeat domain/zDHHC17 ankyrin repeat domain

APT1/2 or LYPLA1/2: acyl protein thioesterase 1/2 lysophospholipase 1/2

ATR/TEM8: anthrax toxin receptor/tumour-endothelial marker-8

BDNF: brain-derived neurotrophic factor

BHK: baby hamster kidney

BPH: benign prostatic hyperplasia

BRET: bioluminescence resonance energy transfer

CASP6: caspase-6

c-Cbl: Casitas B-lineage lymphoma

CCR5: C-C chemokine receptor type 5

CGN: *cis*-Golgi network

CGN: cerebellar granule neurons

CHO: Chinese hamster ovary

CIN85: Cbl-interacting protein of 85 kDa

CK1: casein kinase 1

ClipR-59/CLIP3: CAP-Gly domain-containing linker protein 3

CMG2: capillary morphogenesis protein 2

CRD: cysteine-rich domain

CSP α : cysteine-string protein α ; also known as DnaJ homolog subfamily C member 5 (DNAJC5)

DHHC: Aspartate-Histidine-Histidine-Cysteine (Asp-His-His-Cys)

DRMs: detergent-resistant membranes

DYRK1A: dual specificity tyrosine phosphorylation regulated kinase 1A

EGF(R): epidermal growth factor (receptor)

EGFRvIII: EGFR variant III

ER: endoplasmic reticulum

ERAD: endoplasmic reticulum-associated degradation

Erf2/Erf4: Effector of Ras function

ERK: extracellular signal-regulated kinase

Erp57/PDIA3: protein disulphide-isomerase A3

FGF(R): fibroblast growth factor (receptor)

FRAP: fluorescence recovery after photobleaching

FRET: Forster resonance energy transfer

FRS2: FGF-receptor substrate-2

FTase: farnesyltransferase

GAD65: glutamate decarboxylase 65 kDa isoform

GAP43: growth associated protein 43

GBM: glioblastoma multiforme

GCP16/Golga7: Golgi complex protein of 16 kDa

GDNF(R): glial cell-derived neurotrophic factor (receptor)

GGTase: geranylgeranyltransferase

GluR and GluNR: glutamate receptor subunits of AMPA and NMDA receptors, respectively

Glut4: glucose transporter 4

GPCR: G-protein-coupled receptors

GPMV: giant plasma membrane vesicles

Grb2: growth factor receptor bound protein-2

GSK3 β : glycogen synthase kinase 3 beta

GTP/GDP: guanosine-triphosphate/guanosine-diphosphate

GTPase: GTP hydrolase enzyme

H-bonds: hydrogen-bonds

HD: Huntington disease

HEK293/HEK293T: human embryonic kidney cells

HER2: human epidermal growth factor receptor 2

HGF-c-Met: hepatocyte growth factor - c-Mesenchymal-epithelial transition

HIP14/HIP14L: Huntingtin Interacting Protein 14/Huntingtin Interacting Protein 14-like

HTT: Huntingtin protein

HUVEC: human umbilical vein endothelial cells

IFITM1/3: interferon-induced transmembrane protein 1/3

IL-1 β : interleukin 1 beta

IL6: interleukin 6

INF- γ : interferon-gamma

JNK: c-Jun N terminus kinase

LFQ-MS: Label-Free Quantification-mass spectrometry

LRP6: low-density lipoprotein receptor-related protein 6

MAM: mitochondria-associated membrane

MAPK: mitogen-activated protein kinase

MC1R: melanocortin 1 receptor

MEK1/2 or MAPKK: mitogen-activated protein kinase kinase

MIAPaCa-2: human pancreatic tumour cells

MLE15: mouse lung epithelial cells

Mnk1/2: mitogen-activated protein kinase-interacting kinase 1/2

mSH: metabolic serine hydrolases

MVB: multivesicular body

NCX1: sodium-calcium (Na^+ - Ca^{2+}) exchanger 1

NF1: neurofibromin 1

NGF: neuronal growth factor

NMDAR: N-methyl-D-aspartate receptor

NMT: N-myristoyltransferase

NRVM: neonatal rat ventricular myocytes

NSF: N-ethylmaleimide sensitive factor

PaCCT: Palmitoyltransferase Conserved C-terminus

PAT: protein acyltransferase

PC: prostate cancer

PC12: pheochromocytoma (rat adrenal gland)

PDGF(R): platelet-derived growth factor (receptor)

PI3K-AKT: phosphoinositide-3-kinase-AKT/PKB (protein kinase B)

PIN: prostatic intraepithelial neoplasia

PIP: phosphatidylinositol

PIP₂: phosphatidylinositol (4,5)-bisphosphate

PIP₃: phosphatidylinositol (3,4,5)-trisphosphate

PLC γ : phospholipase C gamma

PM: plasma membrane

PP2A: protein phosphatase 2A

PPT1: palmitoyl protein thioesterase 1

PSD-95: post-synaptic density protein 95 (also known as disc large homolog 4)

PTEN: phosphatase and tensin homolog

Rab: members of the Ras superfamily of small GTPases

RE: recycling endosomes

RER: rough ER

ROS: reactive oxygen species

RTK: Receptor Tyrosine Kinase

SERCA2b: sarcoendoplasmic reticulum Ca²⁺ transport ATPase 2b

SFK: Src-family of non-receptor tyrosine kinases

Shp2 phosphatase: SH2 domain-containing protein tyrosine phosphatase-2

shRNA: short/small hairpin RNA

Siah2: seven-in-absentia homolog-2

SIM: super-resolution microscopy

siRNA: small interference RNA

SNAP: soluble NSF attachment protein

SNAP25/23: synaptosomal-associated protein of 25/23 kDa

SNARE: soluble NSF-attachment protein (SNAP) receptor

SOS: son of sevenless

SPRY: sprouty protein(s)

SPRY1-4: Sprouty 1-4

SRM: serine-rich motif

SUS: split ubiquitin system

SYT I: synaptotagmin I

$t_{1/2}$: half-life (i.e. the time required for a quantity to reduce to half of its initial value)

Tesk1: testicular protein kinase 1

Tgl1: t-SNARE affecting a late Golgi compartment protein 1 (*S. Cerevisiae*)

TGN: *trans*-Golgi network

TKB: tyrosine kinase-binding

TM(D): transmembrane (domain)

TNF(R): tumour necrosis factor (receptor)

TfR: transferrin receptor

Tsg101: tumour-susceptibility gene 101

vdW: van der Waals

VEGF(R): vascular-growth factor (receptor)

VSV-G: vesicular stomatitis virus G protein

Wnt: wingless-related integration site

Yck: type I casein kinases

zDABM: zDHHC-ANK domain binding motif

zDHHC: zinc finger DHHC enzymes

Abstract

S-acylation is a reversible post-translational modification (PTM) that regulates proteins in several ways, including by modulating trafficking, stability and protein interactions. This PTM is mediated by twenty-three zinc finger DHHC (zDHHC) enzymes that display distinct activity and substrate selectivity profiles. Sprouty (SPRY) proteins are regulators of Receptor Tyrosine Kinase (RTK) signalling and play a major role in maintaining cellular homeostasis. Indeed, their deregulation is linked to tumorigenesis, developmental defects and neurological diseases. The defining feature of SPRY proteins is a large cysteine-rich domain (CRD), which is modified by S-acylation. In this thesis, cell-based and cell-free assays, extensive mutagenesis analysis and confocal imaging techniques were employed to examine the mechanisms and outcomes of SPRY2 S-acylation. The results presented show that SPRY2 is differentially modified by zDHHC enzymes: zDHHC17 displayed apparent selectivity for Cys-265/268, whereas zDHHC7 and zDHHC3 mediated more expansive S-acylation of the CRD. S-acylation mediated by both zDHHC17 and zDHHC7 required the presence of a novel NDK (Asn-Asp-Lys) motif in the CRD. Regardless of the modifying enzyme, S-acylation correlated with increased levels of SPRY2 protein, which is linked to an increase in SPRY2 stability. Furthermore, confocal microscopy revealed that S-acylation is also required for efficient plasma membrane targeting. The interaction between SPRY2 and zDHHC17 was further explored and although SPRY2 interacted with the ankyrin repeat (ANK) domain of zDHHC17 through a canonical mechanism, this mode of binding was dispensable for S-acylation. Binding assays suggested the presence of an additional lower affinity interaction site, which might involve amino acid regions 155-290 and/or 106-120 of SPRY2. Finally, evidence is presented that zDHHC17 forms dimers or higher-order oligomers, which involve ANK-ANK interactions. It is speculated that the formation of these zDHHC17 oligomers might be relevant to the function of the enzyme. Overall, this thesis highlights that S-acylation regulates multiple aspects of SPRY2, including protein stability and plasma membrane targeting. As expression levels and localisation are

two fundamental properties of a protein and because alterations in these properties can cause disease, we propose that targeting SPRY2 S-acylation might represent a novel therapeutic strategy in cancer and other diseases.

Chapter 1 Introduction

1.1 S-acylation is a type of protein lipidation

A large number of eukaryotic proteins are modified with a variety of lipid and lipid-like groups in a process known as lipidation. Lipidation plays an important role in regulating protein function, localisation, stability, and hydrophobicity (Chamberlain and Shipston, 2015; Nadolski and Linder, 2007). The attachment of lipid groups takes place either during protein translation (i.e. co-translational modifications) or after protein synthesis (i.e. post-translational modifications). Additionally, lipidation can take place in the cytoplasm, at the membrane-cytosol interface or in the lumen of the secretory pathway (Nadolski and Linder, 2007).

The three major lipidation types found on intracellular proteins to-date are isoprenylation, N-myristoylation and S-acylation (Chamberlain and Shipston, 2015; Nadolski and Linder, 2007). Isoprenylation involves the addition of farnesyl (C15:0) and geranylgeranyl chains (C20:0) to cysteine residues in a post-translational fashion. N-myristoylation on the other hand is the attachment of a myristic acid group (C14:0) onto an N-terminal glycine, and is almost exclusively a co-translational process (Nadolski and Linder, 2007). Both isoprenylation and N-myristoylation are irreversible modifications catalysed by soluble enzymes which recognise well-defined consensus motifs. During isoprenylation, CAAX box and non-CAAX box sequences (where X indicates any amino acid and A denotes an aliphatic/hydrophobic residue) are recognised and modified by either farnesyltransferases (FTase) or geranylgeranyltransferases (GGTase) based on the identity of the amino acid X. In N-myristoylation, a glycine residue in the consensus sequence MGXXS/T (M, methionine; G, glycine; S/T, serine/threonine) is modified by N-myristoyltransferase (NMT) enzymes following removal of the initiating methionine by methionine aminopeptidase (Chamberlain and Shipston, 2015).

S-acylation, the focus of this thesis, is the post-translational attachment of long-chain fatty acyl groups onto free cysteine residues *via* covalent thioester bonds. In contrast

to the aforementioned lipidation events, S-acylation is a reversible modification mediated by protein acyltransferase (PAT) enzymes and reversed by acyl protein thioesterases (APTs). There is no strict consensus motif for S-acylation and the only requirement for this modification has been suggested to be the presence of accessible cysteine residues in substrate proteins positioned at the cytosol-membrane interface (Chamberlain and Shipston, 2015; Rana et al., 2018b). Since palmitic acid (C16:0) is the most commonly incorporated fatty acid, S-acylation is also referred to as “palmitoylation” (Chamberlain and Shipston, 2015). However, substrate proteins can be modified with acyl chains of different length and saturation (Greaves et al., 2017) with addition of myristate (C14:0), stearate (C18:0), oleate (C18:1), linoleate (C18:2), and arachidonate (C20:4) all been reported (Hallak et al., 1994; Muszbek et al., 1999; Veit et al., 1996a). Based on this, the term S-acylation will be preferentially used within this thesis.

1.2 Regulatory effects of S-acylation

The identification of S-acylation as a protein modification dates back to 1979 when the Sindbis viral glycoproteins E1 and E2 were first reported to be covalently modified by fatty acids (Schmidt et al., 1979). To date, an estimated 12,688 substrates from 68 organisms have been identified either through targeted studies or through wider proteome studies (Blanc et al., 2015; Collins et al., 2017; Kang et al., 2008; Roth et al., 2006; W. Yang et al., 2010). Of these, more than 4,500 have been identified in human and mouse, 240 in the yeast *Schizosaccharomyces pombe*, and 59 in *Saccharomyces cerevisiae*. More than 400 substrates have been reported in parasites such as *Toxoplasma gondii* and *Plasmodium falciparum*, the causative agents of toxoplasmosis and malaria in humans, respectively (Blanc et al., 2019, 2015). It is important to note, however, that the large majority of proteins identified through proteome level studies have not yet been validated as *bona fide* S-acylated proteins. The addition of fatty acyl chains during S-acylation increases the local hydrophobicity of modified substrates, which can have several consequences. One of the main

regulatory effects of S-acylation is to regulate the intracellular trafficking of proteins, including retention to, or release from, the Golgi apparatus, and protein cycling through vesicles (Greaves et al., 2009b; Greaves and Chamberlain, 2007; Linder and Deschenes, 2007). Indeed, recent findings revealed a key role for S-acylation in controlling anterograde protein transport throughout the Golgi system (Ernst et al., 2019, 2018). S-acylation can also mediate membrane association of soluble proteins or soluble loops of transmembrane proteins, and targeting of substrates to specific membrane sub- and micro-domains (Fukata et al., 2016; Greaves et al., 2009b; Levental et al., 2010; Salaun et al., 2010). Furthermore, S-acylation can protect against ubiquitination, and prevents the degradation of a number of proteins (Linder and Deschenes, 2007). These regulatory effects impact the function of many physiological systems in the body and are particularly relevant within the brain where S-acylation regulates synaptic function and plasticity and neuronal development (El-Husseini and Brecht, 2002; Fukata and Fukata, 2010).

The plethora of intracellular proteins undergoing S-acylation can be broadly classified into either soluble or transmembrane proteins (Chamberlain and Shipston, 2015; Linder and Deschenes, 2007), and this classification is used in the following discussion.

1.2.1 S-acylation of soluble proteins

Soluble S-acylated proteins can be further classified as (i) dually isoprenylated and S-acylated (e.g. H- and N-Ras), (ii) dually N-myristoylated and S-acylated (e.g. Src-family kinases, G α subunits), and (iii) exclusively S-acylated proteins (e.g. G α subunits, SNAP25/23, CSP α , PSD95) (Chamberlain and Shipston, 2015; Smotrýs and Linder, 2004).

The examples discussed below represent a selection of soluble proteins for which the main outcomes of S-acylation have been extensively studied.

(i) Isoprenylated and S-acylated substrates

H- and N-Ras proteins

Perhaps the best-characterised example of how S-acylation affects intracellular trafficking and localisation is represented by H- and N-Ras, which are monomeric G proteins (Chamberlain et al., 2013; Linder and Deschenes, 2007). Synthesised as soluble proteins, Ras GTPases are primarily active at the plasma membrane where they function as molecular switches (based on GTP or GDP binding) and play a key role in the transduction of pathways involved in cell growth, differentiation, and survival. H- and N-Ras undergo dual lipidation and are modified by both isoprenyl and S-acyl groups (Shahinian and Silviu, 1995). While the first lipidation event (i.e. isoprenylation) confers weak and transient membrane affinity, the second modification (i.e. S-acylation) provides a more stable association to membranes in a process also known as “kinetic trapping” (Shahinian and Silviu, 1995).

Shortly after synthesis, cytosolic H- and N-Ras are farnesylated on their CAAX box by FTase, and this is followed by proteolysis of the -AAX residues, and carboxymethylation of the farnesylated cysteine (Cys-186) (Casey et al., 1989; Gutierrez et al., 1989; Zhao et al., 2002). The farnesylated Ras proteins freely and rapidly exchange between the cytosol and the endoplasmic reticulum (ER) and Golgi membranes (Choy et al., 1999; Goodwin et al., 2005). Their subsequent trafficking from these compartments (i.e. ER and Golgi membranes) to the plasma membrane is vesicle-mediated and depends upon membrane trapping of the proteins by S-acylation (Goodwin et al., 2005). While H-Ras can be modified on either one or both of two cysteine residues, Cys-181 and Cys-184, N-Ras is exclusively S-acylated on Cys-184 (Hancock et al., 1989).

H- and N-Ras constitutively cycle between the plasma membrane and the Golgi apparatus with a quick turnover, which is suggested to be mediated by an S-acylation cycle that involves Ras S-acylation at the Golgi and deacylation at the plasma membrane (Rocks et al., 2005). Early pulse-chase studies, using radiolabelling with ³[H] palmitic acid, estimated a palmitate turnover for N-Ras of about 20 min and for

H-Ras of about 90 min (Magee et al., 1987). More recently, using photoactivatable Ras proteins, Rocks and colleagues showed that such turnover may be much quicker. In fact, plasma membrane-to-Golgi trafficking of H- and N-Ras was found to occur within 10.8 ± 1.1 and 1.8 ± 0.2 min, respectively. Using synthetic Ras constructs with a non-cleavable thioester bond, it was further demonstrated that S-acylation turnover is key for this retrograde transport of Ras proteins. Thus, a model was proposed in which S-acylation at the Golgi drives vesicle transport of H- and N-Ras to the plasma membrane, whereas subsequent deacylation redistributes farnesylated Ras to intracellular membranes, *via* non-vesicular exchange (Goodwin et al., 2005), including the ER and Golgi membranes where the cycle can start again (Rocks et al., 2005).

Interestingly, the degree of S-acylation, and presumably the rate of deacylation, dictate differences in the spatial distribution of the two Ras isoforms. The dually S-acylated H-Ras is predominantly localised at the plasma membrane, whereas singly S-acylated N-Ras displays a predominant Golgi distribution (Apolloni et al., 2000). Furthermore, cysteine substitutions of H-Ras revealed that the two S-acylated cysteines may not be functionally equivalent. S-acylation at Cys-181 (H-Ras C184S mutant) mediated efficient trafficking to the plasma membrane, whereas S-acylation at Cys-184 (H-Ras C181S mutant) retained H-Ras within the Golgi apparatus (Rocks et al., 2005; Roy et al., 2005). Using a combination of confocal live-cell imaging and electron microscopy, the differential S-acylation state between H- and N-Ras was reported to be also important for the spatial organisation within the Golgi apparatus with H-Ras (i.e. dually S-acylated) evenly distributing throughout the Golgi membranes and N-Ras (i.e. singly S-acylated) partitioning toward the *cis*-Golgi (Lynch et al., 2015). Overall, these observed localisation differences between H- and N-Ras and between different cysteine mutants of H-Ras most likely reflect how rapidly (or not) the proteins convert between S-acylated and non-acylated states. Thus, the presence of two S-acylated cysteines in H-Ras may increase the lag period between S-acylation and complete deacylation and therefore promote enhanced plasma membrane localisation, whereas the more rapid deacylation of N-Ras facilitates

retrograde movement to the Golgi, leading to a more pronounced localisation at this compartment.

Similarly to H- and N-Ras, K-Ras undergoes post-translational modifications including farnesylation, proteolysis of the CAAX box, and carboxymethylation of Cys-186 (Apolloni et al., 2000). However, in contrast to H- and N-Ras, K-Ras is not modified by S-acylation and is instead directed to the plasma membrane, bypassing the Golgi, by a polybasic region (multiple Lys residues) located at its C-terminal domain (Apolloni et al., 2000; Choy et al., 1999).

The effects of S-acylation on Ras proteins extend beyond Golgi-to-plasma membrane trafficking and this modification has also been suggested to affect the micro-localisation of Ras proteins at the plasma membrane. Although H-, N- and K-Ras all localise in defined microdomains at the plasma membrane, these are largely non-overlapping, and the S-acylated isoforms preferentially localise in cholesterol-rich microdomains. H-Ras exists in a dynamic equilibrium between lipid rafts and non-cholesterol-dependent microdomains, whereas K-Ras is totally excluded from lipid rafts (Janosi et al., 2012; Plowman et al., 2005; Prior et al., 2003).

(ii) N-myristoylated and S-acylated substrates

Src-family kinases

Another example of how S-acylation mediates trafficking and membrane localisation of peripheral proteins is provided by the Src-family of non-receptor tyrosine kinases (SFKs) (Chamberlain and Shipston, 2015). Coupling surface receptors with downstream intracellular effectors, SFKs play a critical role in several pathways controlling cell proliferation, differentiation, migration and survival. SFK proteins include Src, Lyn, Yes, Fyn, Lck, Blk, Hck, Fgr and Yrk kinases. While Src, Yes, Fyn and Yrk are ubiquitously expressed, Lyn, Lck, Blk, Hck, Fgr are mainly found in hematopoietic cells (Parsons and Parsons, 2004). All SFKs are co-translationally N-myristoylated and post-translationally S-acylated, except for Src and Blk which are exclusively N-myristoylated (Deschenes, Rj. 2013, Aicart-Ramos et al., 2011; Resh,

1999). N-myristoylation of SFKs occurs at Gly-2, in the general motif Met-Gly-Cys, within the conserved N-terminal Src homology 4 (SH4) domain (Resh, 1999; Shenoy-Scaria et al., 1994). S-acylation occurs on cysteines at different positions, immediately downstream of the myristoylated Gly-2. For instance, Lyn, Yes, Hck and Fgr are S-acylated on Cys-3, whereas Fyn and Lck are dually S-acylated on Cys-3 and Cys-6, and Cys-3 and Cys-5, respectively (Alland et al., 1994; Koegl et al., 1994; Shenoy-Scaria et al., 1994; Yurchak and Sefton, 1995). No data is currently available for the S-acylation status of Yrk.

In a series of comprehensive studies, the Yamaguchi group highlighted how subcellular localisation and trafficking of SFKs is driven by their S-acylation status. In fractionation experiments in both HeLa and HEK293 cells, endogenous Src (non S-acylated) and Lyn (S-acylated) were found predominantly at the plasma membrane and the Golgi apparatus, respectively, suggesting S-acylation may impart specific subcellular localisations (Kasahara et al., 2007). In follow-up studies, combining fluorescence recovery after photobleaching (FRAP) and site-directed mutagenesis in COS-1 cells, the intracellular trafficking of Src, Lyn, Yes, and Fyn was further characterised. Src protein (non S-acylated) was shown to localise at the plasma membrane and focal adhesions where it underwent rapid exchange with endosomes/lysosomes (Kasahara et al., 2007). On the hand, the singly S-acylated Lyn and Yes (Cys-3) accumulated at the Golgi apparatus shortly after synthesis and at the plasma membrane at later phases of expression. Furthermore, Lyn and Yes co-localised with caveolin (a vesicular/perinuclear protein) and GalT (a *trans*-Golgi protein) suggesting that they route to the plasma membrane *via* the secretory pathway (Kasahara et al., 2007; Sato et al., 2009). In contrast, Fyn, which is doubly S-acylated (on Cys-3 and Cys-6), associated with the plasma membrane within 5 min of its synthesis (Van 't Hof and Resh, 1997) without any evident Golgi accumulation (Sato et al., 2009). Similar results were observed in transfected HeLa cells in which Lyn, Yes and Fyn expression could be synchronised by doxycycline (Dox) (Sato et al., 2009). Interestingly, blocking Lyn S-acylation by mutating Cys-3 (Lys C3S mutants) resulted in the protein displaying Src-like trafficking and recruitment at focal

adhesions, suggesting that S-acylation excludes SFKs from these cytoskeletal structures (Kasahara et al., 2007). Furthermore, a singly S-acylated Fyn (Fyn C6S) accumulated at Golgi regions before trafficking to the plasma membrane, similarly to the singly S-acylated Lyn and Yes proteins. Notably, Fyn-Lyn and Fyn-Yes chimera constructs, containing two S-acylation sites, mainly localised at the plasma membrane bypassing the Golgi system, resembling wild-type Fyn (Sato et al., 2009).

Based on these observations, it was proposed that SFKs translocate to the plasma membrane using at least three different “routes”, depending on the degree of S-acylation (Sato et al., 2009): (i) N-myristoylated and non S-acylated SFKs (e.g. Src) rapidly exchange between late endosomes or lysosomes and the plasma membrane *via* the cytosol (Kasahara et al., 2007), (ii) N-myristoylated and singly S-acylated SFKs (e.g. Lyn and Yes) reach the plasma membrane through the secretory pathway and, (iii) N-myristoylated and dually S-acylated SFKs (e.g. Fyn) are directed to the plasma membrane directly after synthesis and bypass the Golgi system (Sato et al., 2009; Van 't Hof and Resh, 1997).

Early studies in HeLa and COS cells showed that inhibition of Lck S-acylation (Lck Ser-3/Ser-5 double mutant) disrupted both its plasma membrane localisation and activity (Yurchak and Sefton, 1995). Like Fyn, Lck is dually S-acylated, thus it would be expected to be targeted to the plasma membrane independently of the secretory pathway. However, pulse-chase experiments in SupT1 human T cells suggested that newly synthesised Lck is transported to the plasma membrane *via* a slow exocytic pathway (30 to 40 min), involving CD4 receptor-binding in the *trans*-Golgi network (TGN). The authors further suggested that the faster rate of trafficking reported for Fyn by Van 't Hof and Resh (1997) might be due to the presence of positively-charged amino acids that are absent in Lck (Bijlmakers and Marsh, 1999). In a more recent study, S-acylation was shown to be important for plasma membrane targeting of Lck in HeLa cells, but not in Jurkat T cells, suggesting that different localisation mechanisms might exist in T cells (Akimzhanov et al., 2015). Employing biorthogonal labelling with the palmitic acid analogue 17-ODYA (17-octadecynoic acid), Akimzhanov et al. (2015) also showed that Lck was characterised by a rapid and highly

dynamic S-acylation turnover (labelling visible within 1 min), whereas the closely-related Fyn displayed much slower S-acylation kinetics (labelling visible after 1 h). Thus, despite strong similarities, Lck and Fyn display differential S-acylation with different outcomes.

Hck is the only SFK for which two isoforms have been reported, p61^{Hck} and p59^{Hck}. Both isoforms are N-myristoylated on Gly-2, but only p59^{Hck} undergoes S-acylation, at Cys-3 (Carreno et al., 2000). The non-S-acylated p61^{Hck} was shown to associate with both the Golgi apparatus and lysosomes, whereas the S-acylated p59^{Hck} was found at both the Golgi system and the plasma membrane. However, when S-acylation of p59^{Hck} was blocked by cysteine-to-serine substitution (p59^{Hck} C3S mutant), the protein was excluded from the plasma membrane and co-localised with the lysosomal marker Ig95, similarly to p61^{Hck}. Therefore, the S-acylation state of Hck determines whether the protein will be recruited at the plasma membrane or at the lysosomal compartments (Carreno et al., 2000).

Finally, S-acylation with heterologous unsaturated or polyunsaturated fatty acids was shown to reduce Fyn affinity for lipid-rafts, revealing a link between S-acylation and distribution of SFKs to specialised plasma membrane sub-domains (Liang et al., 2001; Sezgin et al., 2017).

α subunits of heterotrimeric G proteins (Gα)

S-acylation also regulates the intracellular trafficking and plasma membrane targeting of the α subunits of heterotrimeric G proteins (El-Husseini and Brecht, 2002). Working downstream of G-protein-coupled-receptors (GPCRs), heterotrimeric G proteins are composed of three subunits: α, β and γ, and couple a large array of extracellular stimuli with downstream intracellular effectors, including ion channels and enzymes. The β and γ subunits are irreversibly associated into Gβγ heterodimers, whereas the α subunit dynamically associates and dissociates to and from the Gβγ pairs while switching between an inactive (GDP-bound) and active (GTP-bound) status, respectively (Alberts et al., 2015).

There are four sub-families of $G\alpha$ proteins: $G\alpha_s$ (stimulatory - includes $G\alpha_s$ and $G\alpha_{olf}$), $G\alpha_i$ (inhibitory - includes $G\alpha_{i1-3}$, $G\alpha_{o1-2}$, $G\alpha_{t1-3}$ and $G\alpha_z$), $G\alpha_q$ (includes $G\alpha_q$, $G\alpha_{11}$, $G\alpha_{14}$ and $G\alpha_{16}$) and $G\alpha_{12/13}$ (includes $G\alpha_{12}$ and $G\alpha_{13}$) (Milligan and Kostenis, 2006; Strathmann and Simon, 1991). Similar to SFKs, $G\alpha_i$ (e.g. $G\alpha_{i1-3}$, $G\alpha_{o1}$ and $G\alpha_z$) are N-myristoylated (on Gly-2) and S-acylated (on Cys-3) within the general motif Met-Gly-Cys (Linder et al., 1993; Mumby et al., 1994). In contrast, $G\alpha_s$, $G\alpha_q$ (e.g. $G\alpha_q$, $G\alpha_{14}$, $G\alpha_{16}$) and $G\alpha_{12/13}$ are exclusively S-acylated at one or more cysteine residues within the first 20 N-terminal amino acids. Finally, $G\alpha_{t1-3}$ are only N-myristoylated (Jennings and Linder, 2010; Wedegaertner, 2012).

α , β and γ subunits are all synthesised on soluble ribosomes. After synthesis, the α subunits undergo S-acylation and associate with the $\beta\gamma$ heterodimers (pre-assembled and isoprenylated), most likely at the ER or Golgi apparatus before trafficking to the plasma membrane (Marrari et al., 2007). Interestingly, S-acylation of α has also been suggested to favour binding to $\beta\gamma$ which, in turn, may protect S-acyl moieties from hydrolysis. It was proposed that S-acylation enhanced the association of $G\alpha_s$ to $G\beta\gamma$ either by (i) enhancing the avidity for membranes containing the pre-formed $\beta\gamma$ heterodimers or by (ii) inducing conformational changes in $G\alpha_s$ itself, increasing the binding affinity for $G\beta\gamma$ (Iiri et al., 1996). Tsutsumi and colleagues demonstrated that knockdown of specific S-acyltransferases reduced the S-acylation levels of $G\alpha_q$ and $G\alpha_{11}$ and also redistributed them from the plasma membrane to the cytoplasm, suggesting that S-acylation is a prerequisite for plasma membrane association of α subunits. In the same study, S-acylation was further shown to be needed for the continuous shuttling of $G\alpha_q/G\alpha_{11}$ between the plasma membrane and the Golgi system (Tsutsumi et al., 2009). The exact route used by heterotrimeric G proteins to traffic to the plasma membrane is still an open question with reports showing that this may occur *via* both Golgi-independent and -dependent pathways (Jennings and Linder, 2010; Marrari et al., 2007; Wedegaertner, 2012).

In an independent study, three-dimensional modelling and electrostatic surface mapping predictions were used to analyse the N-terminal regions of $G\alpha$ proteins. While α subunits with a single S-acylated cysteine (and no N-myristoylation site) were

found to contain polybasic motifs in this region, such sequences were shown to be much smaller in the dually-lipidated, or N-myristoylated G α proteins. In the α subunits with only a single S-acylation site, these positive patches may confer first weak and transient membrane binding to ensure efficient S-acylation and plasma membrane localisation. In crystal structures, these positive sequences orientated opposite to the surface that binds the $\beta\gamma$ pairs, potentially allowing the α subunits to interact at the same time with negatively charged elements of the plasma membrane and the $\beta\gamma$ subunits (Kosloff et al., 2002).

Once at the plasma membrane, inactive G α subunits are both GDP-bound and $\beta\gamma$ -associated. Upon GPCR-stimulation, G α subunits release the bound GDP to bind GTP molecules. GTP-binding causes conformational changes which allow the α subunits to dissociate from the $\beta\gamma$ pairs and move off the plasma membrane to the cytoplasm/intracellular compartments through a not yet completely understood mechanism (Marrari et al., 2007; Wedegaertner, 2012). Whether this redistribution occurs *via* simple diffusion or *via* vesicle-mediated pathways, deacylation has been shown to play a key role for some α subunits. In S49 *cyc*⁻ and COS cells, it was shown that isoproterenol treatments (an agonist of the β -adrenergic receptors) activated and relocated G α_s subunits to the cytosol while accelerating the turnover of ³[H]palmitate (Mumby et al., 1994; Wedegaertner and Bourne, 1994). Once GTP molecules have been hydrolysed to GDP, these α subunits must undergo new S-acylation cycles and move back to the plasma membrane.

More recently, using fluorescence recovery after photobleaching (FRAP) and fluorescence resonance energy transfer (FRET), inactive heterotrimeric G proteins were found to rapidly shuttle ($t_{1/2} < 1$ min) between the plasma membrane and intracellular membranes (e.g. Golgi apparatus) in the absence of extracellular stimuli. Interestingly, this basal shuttling was inhibited by treating cells with 2-bromopalmitate (2-BP), a general inhibitor of protein S-acylation (Chisari et al., 2007). Thus, it was suggested that constitutive S-acylation (at the Golgi complex) and deacylation (at the plasma membrane) of G α proteins might play a crucial role in

maintaining their basal shuttling, similar to what previously described for H- and N-Ras (Rocks et al., 2005; Saini et al., 2009; Tsutsumi et al., 2009).

(iii) Exclusively S-acylated substrates

SNARE proteins: SNAP23 and SNAP25

The importance of S-acylation in mediating membrane association of soluble proteins is also exemplified by the two t-SNARE proteins SNAP25 and SNAP23 (Chamberlain and Shipston, 2015). At the plasma membrane of cells, SNARE proteins mediate fusion of membranes during exocytotic events, thus playing a key role in secretory pathways (Jahn and Scheller, 2006). SNAP25 is mainly involved in the exocytosis of neurotransmitters into the synaptic cleft and regulated exocytosis pathways in endocrine and neuroendocrine cells (Kádková et al., 2019), whereas SNAP23 is more ubiquitously expressed and regulates exocytosis also in other cell types (Jahn and Scheller, 2006).

Both SNAP25 and SNAP23 are highly abundant proteins, characterised by a conserved cysteine-rich domain (CRD) which is extensively S-acylated shortly after synthesis, most likely at the Golgi apparatus (Greaves et al., 2010, 2009a; Jahn and Scheller, 2006). Similar to some G α subunits, these SNARE proteins are exclusively S-acylated and their initial (transient/weak) membrane binding prior to S-acylation has been proposed to rely on the hydrophobicity of the CRD and other surrounding residues (Greaves et al., 2009a; Greaves and Chamberlain, 2011a, 2006). While SNAP25 contains four cysteine residues at positions 85, 88, 90 and 92, SNAP23 has five cysteines at positions 79, 80, 83, 85 and 87 (Greaves et al., 2010; Lane and Liu, 1997; Vogel and Roche, 1999).

S-acylation of the CRD of SNAP25 and SNAP23 has been established by several *in vitro* studies as the pre-requisite for plasma membrane attachment (Gonzalo et al., 1999; Gonzalo and Linder, 1998; Salaün et al., 2004; Vogel and Roche, 1999). In SNAP25, the minimal S-acylation region, encompassing amino acids 85-120, was shown to be sufficient for targeting the protein to the plasma membrane (Gonzalo et al., 1999). In

line with this, deletion of the SNAP25 CRD, or mutation of the four cysteine residues (4CL mutant), led to cytosolic accumulation of the protein (Greaves et al., 2009a; Hess et al., 1992; Veit et al., 1996b). Interestingly, when the cysteine residues were individually mutated membrane binding was affected to different degrees: simultaneous mutation of Cys-85 and Cys-88 reduced membrane interaction more than that of Cys-92 and/or Cys-90 (Greaves et al., 2009a; Lane and Liu, 1997). Furthermore, while a fully S-acylated SNAP25 preferentially associated with the plasma membrane, mutation of one cysteine (either SNAP25 C88L or C90L) enhanced the association with recycling endosomes (REs) and *trans*-Golgi network (TGN) (Greaves and Chamberlain, 2011a). Based on this, it was proposed that the degree of S-acylation controls SNAP25 localisation at the plasma membrane, REs and TGN, allowing the same pool of protein to constantly recycle between these compartments (Aikawa et al., 2006; Chamberlain et al., 2013; Greaves and Chamberlain, 2011a). While this mechanism would facilitate the described function of SNAP25 at both the plasma membrane and endosomal system (Aikawa et al., 2006), it implies that SNAP25 undergoes dynamic S-acylation. However, over the years, inconsistent results have been obtained on the degree to which SNAP25 S-acylation turns over. In early studies on PC12 cells, SNAP25 was found to undergo rapid and dynamic S-acylation with a ³[H]palmitate turnover of ~ 3 h and a protein half-life of 8 h (Lane and Liu, 1997). In contrast, other studies reported stable attachment of S-acyl chains in unstimulated PC12 cells (Heindel et al., 2003) as well as cortical neurons (Kang et al., 2004). However, in cortical neurons, S-acylation was shown to be modulated by changes in synaptic activity, such as long-term inhibition (Kang et al., 2004). In another study, in which PC12 cells were incubated with the inhibitor of protein synthesis cycloheximide to remove [³H] palmitate labelling of newly-synthesised SNAP25, the protein was still radiolabelled consistent with the mature form of the protein undergoing dynamic S-acylation (Greaves and Chamberlain, 2011a).

S-acylation has been also shown to modulate the affinity of SNAP25 and SNAP23 for membrane lipid rafts with important cellular consequences (Salaün et al., 2005a, 2005b). While in PC12 cells only 20% of endogenous SNAP25 (four S-acylation sites)

was found to associate with detergent-resistant “raft” domains, greater than 60% of SNAP23 (five S-acylation sites) was detected in these fractions (Salaün et al., 2005a). Intriguingly, mutation of the extra cysteine in the CRD of SNAP23 to a phenylalanine (as present in SNAP25) reduced SNAP23 affinity for insoluble rafts to a level similar to that seen with SNAP25. Conversely, introduction of an extra cysteine in the CRD of SNAP25 (F84C; comparable to SNAP23), enhanced its affinity for lipid rafts to the same level seen for SNAP23 (Salaün et al., 2005a). Importantly, the strength of association to these detergent-insoluble raft domains negatively correlated with the ability of these SNARE proteins to sustain exocytosis. Thus, by affecting the raft distribution of SNAP25/23 at the plasma membrane, S-acylation may directly modulate exocytosis (Salaün et al., 2005b).

Cysteine-string-protein α (CSP α)

Similar to SNARE proteins, cysteine-string-protein α (CSP α /DNAJC5) plays a key role in regulated exocytosis and is characterised by a large S-acylated CRD (also known as the cysteine-string domain) containing 14 cysteine residues (Gundersen et al., 1994). In immunoblotting assays, the extensive S-acylation of CSP α correlated with a protein band shift of ~ 8 kDa which was lost when samples were treated with hydroxylamine (HA), a compound that cleaves the thioester bonds (Gundersen et al., 1994). Interestingly, the 14 cysteines within the string domain are not all equally important for S-acylation of the protein: those at positions 1-7 (numbered from the N-terminal end of the CRD) are essential for S-acylation of the entire CRD whilst substitution of cysteines 8-14 does not prevent S-acylation of cysteines 1-7. Furthermore, removal of cysteines 1-7 also blocks membrane association and intracellular sorting of CSP α (Diez-Ardanuy et al., 2017; Greaves and Chamberlain, 2006). Based on this, it was proposed that cysteines 1-7 (and their hydrophobic character) may be important for initial membrane interaction of CSP α prior to S-acylation. In support of this idea, substitution of these cysteines with serine residues had a more pronounced effect than alanine substitutions on membrane association and S-acylation of CSP α (Greaves and Chamberlain, 2006). The intrinsic membrane affinity of these cysteines was suggested to mediate CSP α “sampling” of intracellular membranes, preceding S-

acylation (at the Golgi apparatus) and subsequent targeting to the plasma membrane and secretory organelles (Greaves et al., 2008).

Post-synaptic density protein 95 (PSD95)

In neurons, local and dynamic S-acylation allows the post-synaptic density protein 95 (PSD95) to constantly shuttle between the cytoplasm and the post-synaptic membranes where it plays a key role in synapse function and development. Like some G α subunits and SNARE proteins, PSD95 is an exclusively S-acylated protein (El-Husseini and Brecht, 2002; Fukata and Fukata, 2010). Newly synthesised PSD95 molecules are initially S-acylated at the Golgi apparatus on two N-terminal cysteine residues (Cys-3 and Cys-5) which are essential for post-synaptic targeting as their mutation (PSD95 C3S, C5S and C3/5S) results in PSD95 being redistributed to the cytosol with no specific enrichment at post-synaptic dendrites (Craven et al., 1999; Noritake et al., 2009; Topinka and Brecht, 1998). PSD95 S-acylation was also shown to require a short NH₂-terminal sequence (MDCLCIVTTKKYR), composed of five consecutive hydrophobic amino acids (i.e. underlined residues) and including the two S-acylated Cys-3 and Cys-5 (El-Husseini et al., 2000). Once S-acylated, PSD95 traffics to the post-synaptic membranes of excitatory neurons where it clusters into specific domains known as the post-synaptic densities (PSDs). Here, PSD95 undergoes rapid and dynamic S-acylation/deacylation cycles (Fukata et al., 2013). Pulse-chase studies conducted on hippocampal neurons using ¹²⁵I]palmitate, suggested that the half-life of PSD95 S-acylation is around 2 h. However, this turnover can be further modulated by glutamate receptor activity. Inhibition of glutamate receptors by kynurenic acid blocks ¹²⁵I]palmitate turnover, preventing PSD95 declustering (El-Husseini et al., 2002). Similarly, blockage of synaptic activity by tetrodotoxin (TTX) promotes PSD95 S-acylation and clustering at the post-synaptic membranes (Hayashi et al., 2009; Noritake et al., 2009). Conversely, glutamate treatments, as well as prolonged stimulation of synaptic activity (i.e. activation of glutamate receptors), were shown to reduce the ¹²⁵I]palmitate half-life on PSD95, thus promoting dissociation from the PSDs (El-Husseini et al., 2002). The importance of this dynamic association to and dissociation from the PSDs is further highlighted by the fact that PSD95 modulates

the membrane recruitment of other key neuronal proteins, such as the glutamate receptors AMPAR and NMDAR (further discussed below). Together with PSD95, these receptors regulate key functions in neurons such as synaptic transmission and long-term synaptic strength and plasticity (El-Husseini et al., 2002; Fukata and Fukata, 2010). Intriguingly, more recent data also suggest that while PSD95 S-acylation turnover is quite rapid during synaptic maturation, it slows down in more mature neurons (Yokoi et al., 2016).

1.2.2 S-acylation of transmembrane (TM) proteins

In contrast to soluble proteins where S-acylation is needed for stable membrane attachment, transmembrane (TM) proteins are defined by the presence of one or more domains intrinsically embedded within the phospholipid bilayer. In these substrates, S-acylation usually takes place on cysteine residues located at the cytosol-membrane interface or within the transmembrane domains (TMDs). Nonetheless, cytosolic domains can also be modified (Blaskovic et al., 2013). In these substrates, S-acylation often regulates trafficking and sorting by (i) affecting the three-dimensional arrangement of the transmembrane domains, (ii) promoting the lateral distribution of TM proteins and their association with specific membrane sub-domains, (iii) modulating protein-protein interactions and, (iv) interplaying with other post-translational modifications (Blaskovic et al., 2013; Greaves et al., 2009b; Greaves and Chamberlain, 2007). Interestingly, a recent study, in which native mass spectrometry was used to study S-acylation of membrane proteins, suggested that addition of S-acyl chains to cysteine residues occurs *via* a stochastic process. According to this model, any cysteine residue can be modified as long as it is accessible to the catalytic domain of S-acyltransferase enzymes (Rodenburg et al., 2017), however it is not clear how generally applicable this model is, as many transmembrane proteins have been shown to require specific PAT enzymes for their S-acylation (Chamberlain and Shipston, 2015; Gök et al., 2020; Zaballa and van der Goot, 2018). A few key examples of TM proteins undergoing S-acylation are further discussed below.

Lipoprotein receptor-related protein 6 (LRP6)

S-acylation plays a key role in regulating ER exit of lipoprotein receptor-related protein 6 (LRP6) (Abrami et al., 2008). LRP6 is a single-pass receptor involved in the transduction of Wnt signalling, a key pathway in both embryonic development and cancer pathways (Clevers, 2006). LRP6 is characterised by a single TMD slightly longer than most single-pass membrane proteins, containing 23 amino acids (Abrami et al., 2008). Stable S-acylation on Cys-1394 and/or Cys-1399 was shown to take place at the ER and was proposed to tilt the long transmembrane domain of LRP6, thus reducing hydrophobic mismatches and resultant aggregation (Joseph and Nagaraj, 1995), thereby promoting ER exit and plasma membrane targeting (Abrami et al., 2008). Interestingly, while S-acylation-deficient LRP6 was retained at the ER (by a mechanism involving monoubiquitination of Lys-1403), shortening the TMD by just 2 amino acids was found to rescue this phenotype and restore plasma membrane trafficking of cysteine mutants (Abrami et al., 2008).

Sodium-calcium (Na^+ - Ca^{2+}) exchanger 1 (NCX1)

The transmembrane sodium-calcium (Na^+ - Ca^{2+}) exchanger 1 (NCX1) is formed by 10 transmembrane domains and a large regulatory intracellular loop (f-loop) located between TMD5 and TMD6 and covering amino acids 219-761. The f-loop encompasses the exchange inhibitory peptide (XIP, residues 219–238), the two Ca^{2+} -binding domains (CBD1 and CBD2) (Gök and Fuller, 2020) and the S-acylation site, corresponding to Cys-739 (Reilly et al., 2015). On the plasma membrane of cells NCX1 can form functional dimers (Ren et al., 2008). In a recent study, S-acylation of NCX1 has been shown to modulate NCX1 structure, enhance the affinity for lipid raft domains and promote XIP-mediated inhibition (Gök et al., 2020). First, in neonatal rat ventricular myocytes (NRVMs) and HEK293 cells, FRET signal (measured between two NCX1 protomers) was increased following S-acylation and decreased when this was blocked by either mutating Cys-739 or treating cells with 2-BP, suggesting that S-acylation can trigger conformational changes on the cytoplasmic face of NCX1 (Gök et al., 2020). Second, in giant plasma membrane vesicles (GPMV), NCX1 C739A

exclusively localised in non-raft domains, whereas NCX1 wild-type associated with both raft- and non-raft domains, thus suggesting that S-acylation affects the ability of NCX1 to associate with lipid-ordered regions (Gök et al., 2020). Third, NCX1 C739A pulled down less XIP than wild-type NCX1, suggesting that S-acylation promotes XIP association, further mapped to occur at region 709-728 of NCX1 (also in the cytosolic f-loop). Therefore, it was proposed that following S-acylation of Cys-739, the inhibitory XIP module is recruited at region 709-728 of NCX1, where destabilisation of the nearby CBD2 (involved in NCX1 activation) promotes NCX1 inactivation (Gök et al., 2020). Importantly, NCX1 S-acylation status was found to modulate the intracellular content of Ca^{2+} with S-acylation decreasing and deacylation increasing Ca^{2+} fluxes (Gök et al., 2020).

AMPA and NMDA receptors

S-acylation also regulates post-synaptic trafficking and internalisation of the two glutamate receptors, AMPAR (α -amino-3-hydroxy-5-methyl-4-isoxazole propionate receptor) and NMDAR (N-methyl-D-aspartate receptor) (Fukata and Fukata, 2010). Both AMPAR and NMDAR are integral membrane proteins, and together with PSD95 are fundamental components of the post-synaptic neuronal membranes where they mediate synaptic transmission and plasticity (Fukata et al., 2016). Modulation of AMPAR affects synaptic strength, whereas modulation of NMDAR affects neuronal plasticity and development (Hayashi et al., 2009).

AMPARs are composed of four subunits, glutamate receptors 1 to 4 (GluR1-R4). Each GluR subunit has two S-acylated cysteines: one in the second TMD (GluR1 Cys-811; GluR2 Cys-836; GluR3 Cys-841; GluR4 Cys-817) and one within the C-terminal region, just after TMD4 (GluR1 Cys-585; GluR2 Cys-610; GluR3 Cys-615; GluR4 Cys-611). Interestingly, in both HEK293T cells and cortical neurons, S-acylation of TMD2 promoted retention of AMPARs at the Golgi, negatively affecting Golgi-to-plasma membrane trafficking. In contrast, the S-acylation status of the C-terminal region (i.e. TMD4) was found not to be important for receptor Golgi trafficking. However, once at the post-synaptic plasma membrane, deacylation of the C-terminal region

promoted the interaction of AMPAR with the cytoskeletal protein 4.1N which, in turn, enhanced the surface expression of AMPAR. Conversely, S-acylation at the C-terminus was shown to support GluR1/2 internalisation and endocytosis, most likely by disrupting the interactions with the cytoskeleton (Hayashi et al., 2005). As briefly mentioned before, AMPAR trafficking can also be modulated by PSD95. For example, decreased synaptic activity correlated with increased S-acylation of PSD95 as well as AMPAR clustering, whereas increased synaptic activity induced PSD95 deacylation and AMPAR internalisation (El-Husseini et al., 2002; Fukata and Fukata, 2010). Thus, the S-acylation status of both PSD95 and AMPAR contributes to the regulation of post-synaptic clustering of AMPAR (Blaskovic et al., 2013).

Similar to AMPAR, surface expression and internalisation of NMDAR is also regulated by dual S-acylation. The two subunits GluNR2A and GluNR2B of NMDAR undergo S-acylation at two distinct cysteine clusters: Cys cluster I and Cys cluster II, both located within the cytosolic C-terminal tail, downstream of the TMD4. At the plasma membrane, S-acylation of Cys cluster I, as well as phosphorylation of specific tyrosine residues (Fyn-mediated), was shown to ensure stable surface expression of NMDAR, whereas deacylation promoted receptor internalisation. S-acylation of Cys cluster II, on the other hand, retains NR2 subunits within the Golgi system, preventing trafficking to the post-synaptic membranes (Hayashi et al., 2009).

Calnexin

S-acylation also modulates the spatial organisation of the chaperone calnexin at two different ER sub-domains: (i) the perinuclear rough ER (RER) and (ii) the mitochondria-associated membrane (MAM). At steady state, the bulk of calnexin was shown to be modified at the ER on two juxtamembrane cysteines, Cys-502 and Cys-503, which have been reported to be stably S-acylated (Lakkaraju et al., 2012). At the RER, calnexin associates with the ribosome translocon complex, thus acting as a molecular chaperone and participating in the folding of newly synthesised glycoproteins. At the MAMs, S-acylated calnexin was found to interact with SERCA2b (sarcoendoplasmic reticulum Ca^{2+} transport ATPase 2b) and regulate mitochondrial

Ca²⁺ uptake from the ER. In contrast, non-acylated calnexin (the amount of which could be further increased under ER stress conditions) was shown to bind to ERp57 (protein disulphide-isomerase A3, PDIA3) to fulfil its ER quality control functions (Lynes et al., 2013). Combining mathematic modelling with experimental data, it was recently shown that calnexin undergoes S-acylation after around 8 h following its biosynthesis, first at position 502 and immediately after at position 503. At steady state, about 70% of the protein was predicted to be fully-modified, with S-acylation increasing the half-life of calnexin from 5 to 45 h. Also, S-acylation was negatively regulated by phosphorylation at specific serine residues, and a calnexin S3A mutant (in which Ser-554, Ser-564, and Ser-583 phosphorylation sites were simultaneously alanine-substituted) was characterised by both increased S-acylation and stability (Dallavilla et al., 2016).

1.2.3 S-acylation and protein stability

Another well-established function of S-acylation is that of increasing substrate stability. In some cases, this has been shown to occur through preventing ubiquitination and proteasomal and/or lysosomal degradation; a few key examples are further discussed below (Blaskovic et al., 2013; Chamberlain and Shipston, 2015; Linder and Deschenes, 2007).

Chemokine receptor CCR5

One of the first evidence that S-acylation can affect the stability of protein substrates, came from studies on the chemokine and HIV receptor CCR5 (C-C chemokine receptor type 5) (Blanpain et al., 2001). CCR5 is a GPCR and S-acylation is known to regulate many aspects of GPCRs, including trafficking, phosphorylation, receptor responsiveness and G protein coupling (Neve et al., 2003). In CCR5, S-acylation takes place at the boundary between the last TMD and the C-terminal cytosolic tail on three consecutive sites: Cys-321, Cys-323, and Cys-324 regulating intracellular trafficking, surface expression as well as receptor stability (Blanpain et al., 2001; Percherancier et al., 2001). In fact, when S-acylation was blocked by cysteine mutation, CCR5 half-

life was drastically reduced. However, the reduced half-life could be rescued by treating HeLa cells with bafilomycin A1, a mycotic compound that inhibits lysosomal proteases, suggesting that S-acylation prevents CCR5 destruction by the lysosomes (Percherancier et al., 2001).

Yeast SNARE protein Tlg1

In another key study by Valdez-Taubas and Pelham (2005), it was demonstrated that S-acylation of the yeast protein Tlg1 prevented its ubiquitination and degradation by the vacuole. Tlg1 is a single-pass SNARE protein, which is fundamental for membrane fusion events in the yeast *S. cerevisiae* (Linder and Deschenes, 2007). Tlg1 has two juxtamembrane cysteine residues (Cys-205 and/or Cys-206) modified by the S-acyltransferase Swf1 (Roth et al., 2006; Valdez-Taubas and Pelham, 2005). In *swf1Δ* cells (ablation of *SWF1* gene), Tlg1 half-life was reduced, ubiquitination increased, and the protein accumulated in multivesicular bodies (MVBs), which mediate vacuole-dependent degradation. Similar results were obtained when S-acylation was prevented by cysteine-mutation of the two C-terminal cysteine residues (Valdez-Taubas and Pelham, 2005). At the molecular level, S-acylation was proposed to induce conformational changes which mask specific acidic residues (i.e. Asp-203 and Asp-204) otherwise recognised by the ubiquitin-ligase Tul1 at the membrane interface (Valdez-Taubas and Pelham, 2005).

Anthrax toxin receptor (ATR/TEM8)

S-acylation also prevents ubiquitination and proteasomal degradation of the anthrax toxin receptor (ATR), also known as tumour-endothelial marker-8 (TEM8) (Abrami et al., 2006). The two isoforms of TEM8 undergo dynamic S-acylation on multiple cysteine residues: Cys-346, Cys-347, Cys-481, and Cys-521 in TEM8/1; Cys-346 and Cys-347 in TEM8/2. Mutation of one, two, three or all of these cysteines correlates with decreased TEM8 expression (Abrami et al., 2006). This is attributable to reduced protein half-life which could be rescued by treating cells with the proteasome inhibitor MG-132. Intriguingly, in transiently transfected CHO cells, S-acylated TEM8 mainly associated with detergent-soluble fractions (i.e. non-raft domains). In

contrast, S-acylation-deficient TEM8 (AAA TEM8/1) was constitutively associated with detergent-resistant membranes (DRMs, i.e. raft-like domains) and was also ubiquitinated (Abrami et al., 2006). In fact, it was proposed that when TEM8 associates with raft-like domains, it is recognised and modified by the E3 ubiquitin ligase c-Cbl which, in turn, results in TEM8 internalisation and subsequent degradation by the proteasome/lysosomes. Given that S-acylation negatively regulates the association with raft-domains, this results in physical segregation of TEM8 from c-Cbl ultimately preventing premature ubiquitination, internalisation and degradation (Abrami et al., 2006).

The interplay between S-acylation and ubiquitination has been reported in other proteins, including LRP6, the human capillary morphogenesis protein 2 (CMG2), which also functions as anthrax receptor; the interferon-induced transmembrane proteins 1 and 3 (IFITM1 and IFITM3) which block the entry of viruses, including influenza A, dengue and hepatitis C viruses into human cells; and sortilin which sorts proteins to the secretory or endocytic compartments (Chamberlain and Shipston, 2015; Zaballa and van der Goot, 2018).

1.2.4 S-acylation and anterograde transport

Recently, S-acylation was shown to operate as a sorting signal to control the anterograde transport of membrane proteins through the Golgi apparatus (Ernst et al., 2019, 2018). The Golgi system represents a major hub for modification and sorting of newly synthesised proteins and is often described as a series of flat compartments, called *cisternae*, which are held together by GRASP proteins. Each stack contains five-to-six *cisternae* and both a *cis*- and a *trans*-face which are also referred to as *cis*-Golgi network (CGN) and *trans*-Golgi network (TGN), respectively; the *cis*-side is closest to the ER and nucleus, hence proteins enter at the *cis*- and leave from the *trans*-face (Alberts et al., 2015).

In a pivotal study by Ernst et al. (2018), the exocytic pathway of S-acylated proteins was finely characterised by combining click-chemistry and pulse-chase experiments

with super-resolution microscopy (SIM). Following S-acylation at the *cis*-Golgi, proteins were shown to move forward towards the *trans*-Golgi where they could be observed after a 10-min chase. Within 20 min time, all cargo had left the Golgi and the proteins localised at the plasma membrane, or in other subcellular compartments. Employing two model cargo proteins, VSV-G and transferrin receptor (TfR), it was shown that S-acylation accelerated the rate of transport of proteins throughout the Golgi system. Experiments in HeLa cells, in which release from the ER of newly synthesised VSV-G and TfR was synchronised, suggest that both wild-type and S-acylation defective proteins enter the Golgi apparatus at the same time but do not traffic through it equally; S-acylation deficient proteins consistently reached the plasma membrane at later time points than their wild-type counterparts. Furthermore, following 2-BP treatment, plasma membrane delivery of wild-type VSV-G and/or TfR was perturbed, whereas that of S-acylation-defective proteins was not. When the intra-Golgi distribution of TfR was examined by 3D-SIM, S-acylated TfR was found to be preferentially accumulated in the highly curved (< 50 nm) rims of the Golgi, whereas the non-S-acylated variant was exclusively found at the flat regions of the *cis*-Golgi cisternae (Ernst et al., 2018). Based on these observations, it was proposed that in an attempt to lower their free-energy (and increase their stability), S-acylated membrane cargos promptly diffuse from the flat regions of the *cis*-Golgi to the highly curved cisternal rims from which budding of vesicles (involved in anterograde transport) takes place. Thus, S-acylation would function as a green-light for proteins that need to move forward (i.e. anterograde cargo) and as a red-light for those moving backwards (i.e. retrograde cargo) by simply excluding them and their receptors located at the cisternal rims (Ernst et al., 2019, 2018).

Although the described model relates to transmembrane cargos, S-acylation also accelerates the anterograde transport of both soluble and even non-S-acylated proteins. These, can in fact be “captured” when TM proteins diffuse from the flat *cis*-Golgi to the distal rims to be concentrated into the same budding vesicles. Importantly, most of the enzymes mediating S-acylation were observed at the *cis*-Golgi compartment and modulation of their expression was shown to affect the

anterograde routing of cargo proteins, highlighting how protein S-acyltransferase levels can further regulate the rate of intracellular trafficking (Ernst et al., 2019, 2018).

1.3 Deacylation mediated by protein thioesterases

One of the most prominent aspects of S-acylation is its reversible nature (Chamberlain and Shipston, 2015). The hydrolysis of fatty acyl chains from S-acylated substrates, a process also known as deacylation or depalmitoylation, is mediated by a series of enzymes belonging to the superfamily of metabolic serine hydrolases (mSH). Structurally, mSH enzymes are characterised by a central β -sheet surrounded by α -helices and a catalytic active site including a serine residue (Long and Cravatt, 2011). Also, most of the deacylases so far identified undergo dynamic S-acylation at their N-termini (Won et al., 2018; Zaballa and van der Goot, 2018).

The first deacylation enzyme to be identified was palmitoyl protein thioesterase 1 (PPT1) (Camp and Hofmann, 1993). Active against H-Ras *in vitro* (Camp and Hofmann, 1993), PPT1 was later found to co-sediment in epithelial-like Madin-Darby bovine kidney cells with lysosomes and late endosomes (Verkruyse and Hofmann, 1996) and to colocalise in fibroblast-like cells (i.e. COS-1) with the lysosomal enzyme β 3-hexosaminidase (Hellsten et al., 1996). A similar subcellular localisation was observed in baby hamster kidney (BHK) and Chinese hamster ovary (CHO) cells by others (Lehtovirta et al., 2001). Thus, PPT1 was proposed to contribute to the degradation of S-acylated proteins in lysosomes rather than their dynamic deacylation in the cytosol (Hellsten et al., 1996). However, in mouse brain and cultured primary neurons, PPT1 was primarily detected in the pre-synaptic compartment, specifically the synaptosomes and synaptic vesicles (Kim et al., 2008; Lehtovirta et al., 2001). Also, lack of PPT1 correlated with abnormal membrane association and sorting of synaptic vesicle proteins such as SNAP25, syntaxin I, VAMP2, GAD65 and SYT I, most of which are known to be S-acylated (Kim et al., 2008). Recently, the synaptic activity of PPT1 has been finely characterised by (Gorenberg et al., 2020). In this study,

proteome-wide screening was carried out employing Acyl Resin-Assisted Capture (Acyl-RAC) and Label-Free Quantification-mass spectrometry (LFQ-MS) to identify PPT1 substrates. Analysis of synaptosomes, purified from wild-type and PPT1-KO mice, revealed that S-acylation of several synaptic proteins was increased in PPT1 KO compared to WT synaptosomes or whole brain. Further validation of these putative substrates using *in vitro* deacylation assays and MS analysis, identified more than 100 *bona fide* substrates (high- to medium-confidence), corresponding to ~ 10% of the synaptic S-acylated proteome and including both cytosolic and membrane proteins (e.g. G-proteins, ion channels and transporters, endocytic proteins, synaptic adhesion molecules, mitochondrial and lysosomal proteins) (Gorenberg et al., 2020). The authors further proposed that PPT1 is secreted, endocytosed and then retrogradely trafficked to endosomes/lysosomes (Gorenberg et al., 2020) as previously described in non-neuronal cells (Hellsten et al., 1996). Also, following endocytosis, a fraction of PPT1 would escape endosomes/lysosomes allowing deacylation of cytosolic proteins (Gorenberg et al., 2020). Since the study of Gorenberg et al. (2020) identified PPT1 substrates based on their increased S-acylation in PPT1-KO samples (for which protein levels were not affected compared to WT), it was further suggested that other deacylases most likely do not compensate for the absence of PPT1, implying a certain degree of specificity for this deacylase (Gorenberg et al., 2020). As a side note, it is worth mentioning that PPT1 activity has been reported to be decreased by S-acylation at Cys-6 (Segal-Salto et al., 2016).

Independent studies identified two additional thioesterase enzymes, acyl protein thioesterase 1 (APT1/LYPLA1) (Duncan and Gilman, 1998) and acyl protein thioesterase 2 (APT2/LYPLA2) (Toyoda et al., 1999). Although first recognised as lysophospholipases (Sugimoto et al., 1996; Toyoda et al., 1999), APT1 was later shown to have enhanced thioesterase activity (Hirano et al., 2009) and to mediate the deacylation of proteins such as H-Ras and α subunits of G proteins (Duncan and Gilman, 2002, 1998), whereas APT2 was found to be active against the tumour necrosis factor receptor (TNFR) (Zingler et al., 2019) and melanocortin 1 receptor (MC1R) (Chen et al., 2019). Although there is no clear consensus motif, and only a

limited number of substrates have been identified so far, APT1/2 enzymes appear to display some specificity (Won et al., 2018). For instance, APT1 but not APT2 functions against BK potassium channels (Tian et al., 2012) and NCX1 (Gök et al., 2020), whereas APT2 but not APT1 mediates deacylation of zDHHC6 (Abrami et al., 2017), growth associated protein 43 (GAP43) (Tomatis et al., 2010) and the scaffolding protein Scribble (Scrib) (Hernandez et al., 2017). APT1 and APT2 have been mainly studied as cytosolic enzymes, partially localising at the Golgi apparatus and at the plasma membrane of cells (Duncan and Gilman, 1998; Hirano et al., 2009; Kong et al., 2013). Also, dynamic S-acylation on Cys-2 was found to mediate the shuttling of APT1/2 between the Golgi apparatus and the plasma membrane with APT1 further shown to mediate its own deacylation as well as that of APT2 (Kong et al., 2013). However, a recent study suggested that APT1 is predominantly localised and active in mitochondria (Kathayat et al., 2018). In the latter, endogenous APT1, as well as overexpressed myc-tagged APT1, was detected in mitochondria, whereas APT1 tagged with mCitrine, a bulkier tag than myc (used in previous studies (Vartak et al., 2014)), was shown to mis-localise to the cytosol and the plasma membrane, and it was suggested that this accounted for its erroneous annotation. In contrast, APT2 was shown in this study to associate with the Golgi system and the plasma membrane regardless of the tag used. Thus, it was proposed that APT1 and APT2 are responsible for the deacylation of proteins within mitochondria and cytosol, respectively (Kathayat et al., 2018). Nonetheless, it will be important to further investigate the localisation of APT1 as several other studies have shown that APT1 functions as a cytosolic thioesterase (Gök et al., 2020; Kong et al., 2013). It is possible that APT1 localisation may be dependent on cell type, differential splicing or other factors. According to the available crystal structures, APT1 and APT2 are both characterised by a canonical Ser-His-Asp catalytic triad (Ser-199, Asp-174 and His-209 in APT1; Ser-122, Asp-176 and His-210 in APT2). This is enclosed in a rather atypical α/β hydrolase fold, containing seven parallel β sheets ($\beta 2$ – $\beta 8$) intervened with other structural elements (helices, loops and strands). In addition, there are important non-canonical features, including four small antiparallel β strands (S1-S4) also encompassing the

short helix G1, and the $\beta 5$ - $\alpha 2$ loop (Abrami et al., 2020; Wepy et al., 2019; Won et al., 2016). Within the antiparallel β sheets, the S1-G1-S2 loop forms a sub-structure named the β tongue. Together with positively charged regions, the β tongue was shown to promote the association of APT1 and APT2 with cellular membranes (Abrami et al., 2020). The $\beta 5$ - $\alpha 2$ loop and flanking structures (G1 helix, $\beta 8$ - $\alpha 4$ loop and G3 helix) form a relatively long and hydrophobic channel which replaces the canonical cap and lid domains found in other α/β hydrolases and represent the fatty acyl chain binding site. The flexibility of the $\beta 5$ - $\alpha 2$ loop would permit the engagement of various protein substrates (Abrami et al., 2020; Wepy et al., 2019; Won et al., 2016). More in-depth analyses of APT2 suggested that the β tongue mediates the initial interaction with cellular membranes allowing APT2 to sample membranes, while S-acylation of the N-terminal Cys-2 promotes stronger membrane anchorage, in agreement with the study of Kong et al. (2013) (Abrami et al., 2020). Upon encountering an S-acylated substrate, APT2 was proposed to trigger extraction of the acyl chain from the membrane, also facilitated by deforming the lipid bilayer, and capture it into its hydrophobic channel where hydrolysis occurs. Following this, deacylation of APT2 releases the thioesterase enzyme into the cytosol. While this deacylation step resets the system, allowing APT2 to start a new catalytic cycle, it also renders the protein susceptible to degradation: a key lysine within the β tongue (identified with Lys-69) becomes exposed and undergoes ubiquitination, targeting APT2 to the proteasome for destruction (Abrami et al., 2020).

A third set of deacylation enzymes was recently identified as the α/β hydrolase domain (ABHD) family of enzymes, including the members ABHD17A, ABHD17B and ABHD17C (Won et al., 2018). In 2015, Lin and Conibear first reported that deacylation of N-Ras and PSD95 was predominantly mediated by ABHD17 proteins (Lin and Conibear, 2015). Using pulse-chase click chemistry in non-neuronal cells, the S-acyl turnover of N-Ras and PSD95 was found to be enhanced by all three ABHD17A-C enzymes, whereas expression of other thioesterases, such as ABHD16A, ABHD6, or APT1/2 had only a small effect. N-Ras was further shown to be redundantly deacylated by ABHD17A, ABHD17B and ABHD17C in knockdown experiments (Lin and

Conibear, 2015). Concurrently, a study by Yokoi et al. (2016) identified ABHD17A-C, amongst several serine hydrolases, as the specific PSD95 deacylation enzyme in neurons. In this latter report, it was also postulated that ABHD proteins exhibit a significant degree of substrate specificity. For instance, ABHD17B was the most active against PSD95, GAP43 and H-Ras but was inactive towards Fyn, which was instead deacylated by APT2. PSD95 S-acylation was also reduced by ABHD13, which was found to be inactive towards GAP43, Fyn, and H-Ras (Yokoi et al., 2016). ABHD17A-C also controlled dynamic S-acylation of MAP6, a protein involved in the formation and maturation of axons (Tortosa et al., 2017). In COS-7 cells and neurons, ABHD17A and ABHD17B localise at the plasma membrane as well as dendritic shafts and spines; association with Rab5 and Rab11 positive endosomes was also documented (Lin and Conibear, 2015; Yokoi et al., 2016). Although no crystal structure is available for ABHD17 enzymes, the position of the catalytic triad of ABHD17B (residues Ser-170, Asp-235 and His-264) has been predicted and validated by three-dimensional structural modelling and mutagenesis, respectively. Similar to APT1/2, ABHD17 enzymes are S-acylated at their N-termini, within a conserved cysteine-rich domain, and such S-acylation is crucial for both their plasma membrane association and activity (Lin and Conibear, 2015; Yokoi et al., 2016).

Compared to protein acyltransferases (PATs; see below), a smaller number of deacylases have been identified and characterised. Although this is consistent with the finding that dynamic S-acylation/deacylation is restricted to a subset of proteins (Martin et al., 2012), there may be additional deacylation enzymes that are yet to be discovered.

1.4 S-acylation mediated by the zDHHC family of enzymes

In cells, protein S-acylation is determined by the activity of two classes of enzymes: protein S-acyltransferases (PATs), which catalyse the addition of S-acyl chains to substrates, and the acyl protein thioesterases (APTs) discussed above, which mediate the removal of S-acyl moieties.

The first two proteins identified with S-acyltransferase activity were the *S. cerevisiae* Erf2 and Akr1 proteins (Lobo et al., 2002; Roth et al., 2002). Erf2 was initially identified in genetic screen studies as the S-acyltransferase of Ras2 with its ablation (*erf2Δ* strains) resulting in reduced Ras2 S-acylation and protein mis-localisation (Bartels et al., 1999). Likewise, the first hint that Akr1 may function as S-acyltransferase came from genetic studies which identified Akr1 as important for plasma membrane localisation of the yeast protein kinases Yck1 and Yck2 (Feng and Davis, 2000). Erf2 and Akr1 were found to share a conserved 51-amino acid zinc finger cysteine-rich domain containing a DHHC (Asp-His-His-Cys) tetrapeptide and subsequent work showed that there are a total of seven of these so-called “zDHHC” enzymes in *S. cerevisiae* (Lobo et al., 2002; Roth et al., 2006, 2002) and there are twenty-three *ZDHHC* genes in humans (Fukata et al., 2004).

The cysteine-rich domain of zDHHC enzymes resembles a C₂H₂ zinc finger motif (containing two CCHC-type zinc fingers) and has been shown to coordinate two zinc ions (Zn²⁺) (González Montoro et al., 2013; Gottlieb et al., 2015; Putilina et al., 1999; Rana et al., 2018a). Outside the DHHC-CRD, an additional three short motifs are also highly conserved: an Asp-Pro-Gly (DPG) towards the N-terminus, a Thr-Thr-x-Glu (TTxE) and a PaCCT (Palmitoyltransferase Conserved C-terminus) sequence, both of which are located towards the C-terminus (González Montoro et al., 2009; Mitchell et al., 2006). All zDHHC enzymes share a similar membrane topology with most isoforms having a predicted four transmembrane helices. However, zDHHC13, zDHHC17, and zDHHC23 are predicted to have six TMDs, whereas zDHHC4 and zDHHC24 are predicted to have five (Zaballa and van der Goot, 2018). Although the number of transmembrane domains can vary from one isoform to another, the DHHC-CRD is always predicted to lay in the cytoplasm where interaction with and S-acylation of protein substrates take place (Gottlieb and Linder, 2017; Rana et al., 2018b).

Analysis of yeast Erf2 and the mammalian zDHHC2 and zDHHC3 enzymes highlighted that S-acylation by zDHHC enzymes proceeds *via* a two-step ping-pong mechanism (Jennings and Linder, 2012; Mitchell et al., 2010). Specifically, during the first step of

this reaction, a fatty acyl-coenzyme A (acyl-CoA) reacts with the DHHC motif, producing an acyl-enzyme intermediate, in a process known as “autoacylation”. At the molecular level, Asp-153 and His-154 (within the DHHC motif) activate by deprotonation Cys-156, which then reacts with the fatty acyl-CoA. The net result of this first step is autoacylation and release of a reduced CoA-SH molecule. In the second step of the reaction, the fatty acyl group is transferred from the enzyme to a cysteine on a protein substrate. His-154 was suggested to coordinate also this reaction by releasing the extra proton acquired in the first step (Fig. 1.1) (Rana et al., 2018a). Alternatively, in the absence of a suitable substrate, the autoacylated enzyme undergoes spontaneous hydrolysis (Jennings and Linder, 2012; Rana et al., 2018a).

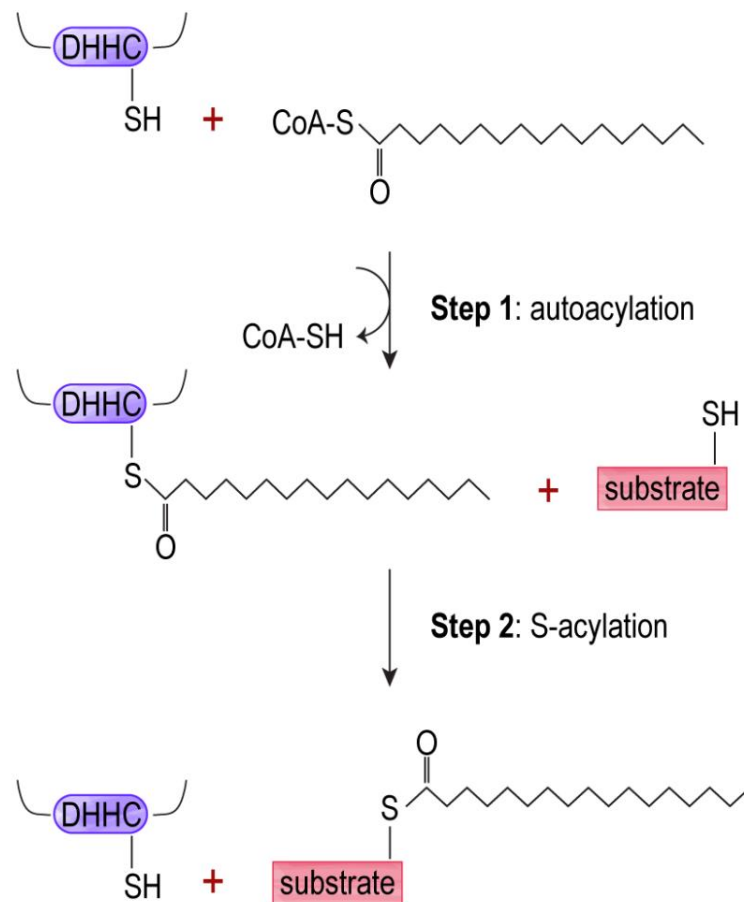


Figure 1.1 Two-step mechanism of action by zDHHC enzymes

After autoacylation of the enzyme (*step 1*), the acyl group is transferred from the autoacylated intermediate to the substrate protein (*step 2*). The catalytic DHHC domain is represented in blue and the substrate protein in pink.

In a seminal study by the Banerjee group, the crystal structure of human zDHHC20 (hDHHC20) and the catalytically inactive form of zebrafish zfDHHS15 were recently solved, providing for the first time extensive insights on the structure as well as the mechanisms of action of this family of enzymes (Rana et al., 2018a). Structurally, the four transmembrane helices of zDHHC20/zfDHHS15 arrange in the lipid bilayer adopting a tepee-like structure with the tip facing the extracellular/luminal side of the membrane while the base opens up at the cytosolic face. The catalytic DHHC-CRD

is found at the membrane-aqueous interface between TM2 and TM3. The structure of the DHHC-CRD consists of three α -helices (α 1, α 2, and α 3) followed by three stacked β hairpins (β 1 to β 6): the two stacks β 2/ β 3 and β 4/ β 5 coordinate two Zn^{2+} ions which ensure the correct positioning of the DHHC active site (contained in β 5/ β 6) (Fig. 1.2a-b). Within the DHHC active site, the aspartic acid (Asp-153) and the first histidine (His-154) activate the catalytic cysteine (Cys-156), while the second histidine (His-155) is involved in Zn^{2+} binding. Together, Asp-153, His-154, and Cys-156 form the catalytic triad of the enzyme (Fig. 1.2c). Interestingly, the second threonine of the C-terminal TTxE motif, Thr-241, directly contacts Asp-153 *via* hydrogen bonds, most likely contributing to the stability of the active site (Fig. 1.2d). Similarly, residues belonging to the PaCCT sequence are engaging in a number of interactions (mainly at the C-terminus) providing additional overall stability (Fig. 1.2e) (Rana et al., 2018a).

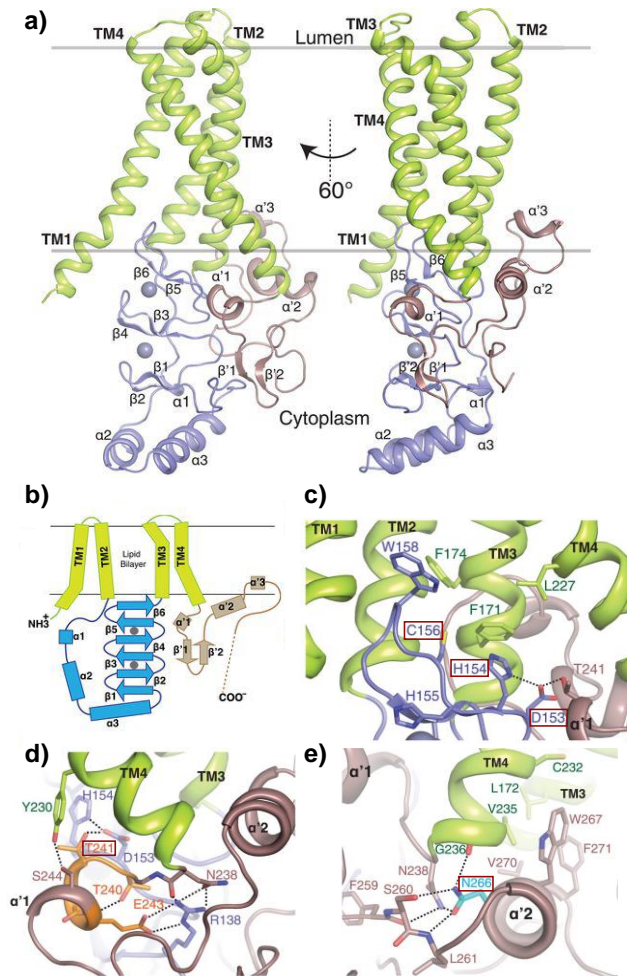


Figure 1.2 Structure of a zDHC enzyme

a) Three-dimensional structure of hDHC20. The four transmembrane helices (TM1-4) are represented in green, the three α -helices (α 1, α 2, and α 3) and the three stacked β hairpins (β 1 to β 6) of the DHC-CRD are in blue, and the C-terminal domain in brown. The two Zn^{2+} ions are represented by grey spheres. **b)** Schematic representation of the structural elements of hDHC20. α -helices are represented as rectangles and β -sheets as arrows. Zn^{2+} ions are shown as circles, whereas the dashed line refers to the unstructured C-terminal domain (not solved in the crystal structure). **c)** Close-up view of the catalytic triad: Asp-153 (D153), His-154 (H154), and Cys-156 (C156). **d)** Close-up view of the C-terminal domain interactions, showing Thr-241 (T241) directly contacting Asp-153 (D153). **e)** Close-up view of the C-terminus PaCCT sequence. Asn-266 (N266) is one of the most conserved residues on the C-terminal domain of zDHC enzymes. All the relevant residues are shown in a dark red box. Figure adapted from (Rana et al., 2018a).

Furthermore, both hDHHC20 and zfDHHC15 contain a hydrophobic cavity stretching from the base to the tip of the tepee-like structure. This cavity is lined with residues belonging to all four TM helices and accommodates the acyl chain in the autoacylated form of the enzyme, which is anchored at the top by the catalytic cysteine (Cys-156 in hDHHC20). Importantly, since the residues within the cavity contact the acyl chain, their nature determines the length of the chain that can be accommodated, thus acting as a “molecular ruler” (Fig. 1.3) (Rana et al., 2018a).

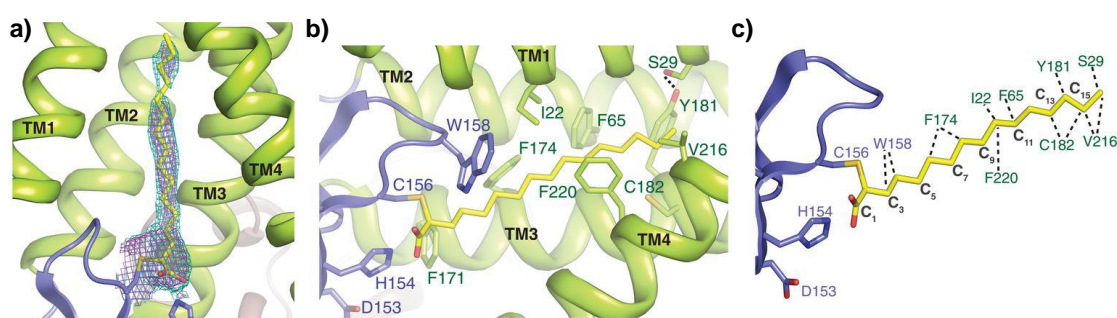


Figure 1.3 S-acylation of zDHHC enzymes

a) Electron density map of a 16-carbon chain (i.e. palmitate chain) covalently attached to Cys-156 (i.e. autoacylated hDHHC20). **b)** Close-up view of the hydrophobic cavity of hDHHC20. The palmitate chain is attached to Cys-156. The residues lining the groove are shown. **c)** Detail of the amino acids that contact the palmitate chain acting as a “molecular ruler”. Figure adapted from (Rana et al., 2018a).

Notably, a previous study by Greaves et al. (2017) showed that the presence of a bulky isoleucine residue from TM3 that lies within the cavity of zDHHC3 limited the ability of this enzyme to incorporate long-chain fatty acids (C18:0), whereas the closely-related zDHHC7 which holds a smaller residue (i.e. serine) at the corresponding position had a greater ability to incorporate C18:0 chains. In this report, fatty acid-analogues (azide/alkyne) and click-chemistry were for the first time

employed to profile the fatty acyl selectivity of a number zDHHC enzymes revealing isoform-specific preferences, summarised in Table 1.1 (Greaves et al., 2017).

zDHHC isoform	Acyl-CoA preference
-3, -5, -7, 11, -15	C14:0/C16:0
-17	C16:0/C18:0
-23	C18:0
-2, -4	None (promiscuous)

Table 1.1 Fatty acyl chain length preference in the zDHHC enzyme family (Greaves et al., 2017)

1.4.1 Subcellular and tissue-distribution of zDHHC enzymes

In a study by Ohno et al. (2006) the intracellular distribution of tagged zDHHC enzymes was analysed in both *S. cerevisiae* and mammalian HEK293T cells. In yeast, most isoforms were found at the endoplasmic reticulum (Erf2, Swf1, and Pfa4) and at the Golgi system (Akr1 and Akr2), whereas one enzyme localised at the plasma membrane (Pfa5), and another one at the vacuole (Pfa3). Likewise, human zDHHC proteins preferentially localised at the ER and Golgi apparatus (most zDHHC isoforms), with a small number detected at the plasma membrane (zDHHC5, zDHHC20, and zDHHC21) (Ohno et al., 2006). Furthermore, the distribution of zDHHC enzymes within the Golgi stacks has also been described: zDHHC3, zDHHC7, zDHHC13, zDHHC17, zDHHC21, and zDHHC22 were reported to predominantly localise at the *cis*-Golgi, whereas zDHHC9, zDHHC11, and zDHHC15 were mainly at the *trans*-Golgi (Ernst et al., 2018). Moreover, zDHHC2 and zDHHC5 have been shown to cycle between the plasma membrane and the endosomal system (Brigidi et al., 2015; Fukata et al., 2013; Greaves et al., 2011). zDHHC17 was also reported to associate with several vesicular structures, including recycling and late endosomes as well as the plasma membrane and dendritic spines (Huang et al., 2004; Singaraja et al., 2002). The intracellular distribution of zDHHC enzymes is summarised in Table

1.2. As can be seen from Table 1.2, some zDHHC enzymes have been found at different intracellular compartments, which might reflect cell type-specific differences or issues associated with the use of specific tags or expression levels in transfection-based experiments.

zDHHC isoform	Subcellular localisation
-1, -2, -4, -6, -9, -10, -11, -12, -14, -16, -19, -21, -22	endoplasmic reticulum (ER)
-1, -2, -3, -4, -7, -8, -9, -12, -13, -14, -15, -17, -18, -21, -22, -23	Golgi apparatus
-3, -7, -9 (low), -13, -17, -21, -22	<i>cis</i> -Golgi
-7, -9, 17	<i>medial</i> -Golgi
-7 (low), -9, 11, -15, -23	<i>trans</i> -Golgi
-2, -5, -8, -11, -14, -17 -18, -20, -21	plasma membrane (PM)
-2, -5, -11, -14, -17, -18	recycling endosomes (REs)
-4	nuclear envelope

Table 1.2 Intracellular distribution of zDHHC S-acyltransferases

Most isoforms have been identified at both the ER and Golgi membranes (Brigidi et al., 2015; Ernst et al., 2018; Fukata et al., 2013; Gorleku et al., 2011; Greaves et al., 2011; Huang et al., 2004; Ohno et al., 2006; Solis et al., 2020; Swarthout et al., 2005; Tian et al., 2012; Zeidman et al., 2011; Zhang et al., 2006). Only small amounts of zDHHC9 and zDHHC7 localise at the *cis*- and *trans*-Golgi, respectively (referred to as “(low)” in the table) (Ernst et al., 2018).

For some zDHHC family members, specific sorting motifs have been recognised to be important determinants for subcellular localisation. For example, the C-terminus of both zDHHC4 and zDHHC6 contains Lys-motifs which are involved in the ER retention/retrieval of these proteins (Gorleku et al., 2011). Two sorting signals in the C-terminus of zDHHC2 were identified that regulate the distribution of this enzyme between the plasma membrane and recycling endosomes (Greaves et al., 2011; Salaun et al., 2017). Also, dynamic phosphorylation of an endocytic C-terminal Tyr-

Asp-Asn-Leu (YDNL) motif was reported to control endocytosis and recycling of zDHHC5 (Brigidi et al., 2015).

Using real time-PCR (RT-PCR), Ohno et al. (2006) investigated the tissue-specific distribution of zDHHC mRNAs, revealing that while most zDHHC isoforms are ubiquitously expressed a few are tissue-specific. Accordingly, *ZDHHC* genes were classified into (i) highly ubiquitous isoforms, including *ZDHHC4*, *ZDHHC5*, *ZDHHC7*, *ZDHHC8*, *ZDHHC10*, *ZDHHC12*, *ZDHHC13*, *ZDHHC17*, and *ZDHHC22*; (ii) nearly ubiquitous, such as *ZDHHC1*, *ZDHHC3*, *ZDHHC6*, *ZDHHC9*, *ZDHHC14*, *ZDHHC16*, *ZDHHC18*, and *ZDHHC21* and; (iii) tissue-specific, *ZDHHC11*, *ZDHHC19*, and *ZDHHC20*. zDHHC11 and zDHHC19 were exclusively detected in testis, and zDHHC20 in testis and placenta only; the expression of zDHHC2 and zDHHC15 could not be determined (Ohno et al., 2006).

Analyses on the abundance of zDHHC enzymes, measured as copy number per cell, revealed that zDHHC S-acyltransferases are low abundance proteins ($< 5 \times 10^2$, in U2OS cells), whereas acyl thioesterases are much more abundant ($> 5 \times 10^4$ for both APT1/2, in U2OS cells) (Beck et al., 2011; Zaballa and van der Goot, 2018).

1.5 Regulation of zDHHC enzymes

How zDHHC enzyme activity might be regulated is still an open question with emerging evidence suggesting that many mechanisms may exist. The activity of zDHHC S-acyltransferases can be modulated at several levels (Chamberlain and Shipston, 2015; Zaballa and van der Goot, 2018).

The activity of some zDHHC enzymes can be constitutively regulated by cofactors or other proteins. This is the case for Erf2 and zDHHC9, which require the cofactors Erf4 and GCP16, respectively, for S-acylation of the yeast Ras2 and mammalian H- and N-Ras (Nadolski and Linder, 2007; Salaun et al., 2020b). Although the physiological roles of Erf4/GCP16 cofactors are not completely understood, experimental evidence suggested that Erf4 is required for both Erf2 stability and enzymatic activity. In fact, lack of Erf4 (Δ *erf4* *S. cerevisiae*) correlated with reduced Erf2 half-life, and increased

ubiquitination and degradation by the ER-associated degradation (ERAD) system. Also, in absence of Erf4, the autoacylated intermediate of Erf2 was shown to undergo rapid hydrolysis, suggesting that Erf4 might shield the active site from water molecules (Lobo et al., 2002; Mitchell et al., 2012). Similar to Erf2-Erf4, in the absence of GCP16, zDHHC9 was found to be inactive, more susceptible to proteolysis (in insect Sf9 cells) and autoacylated zDHHC9 displayed enhanced hydrolysis rates (Mitchell et al., 2014; Swarthout et al., 2005). Despite these similarities, Erf4 and GCP16 are not functionally interchangeable and while in yeast Erf2-Erf4 co-localise at the ER (Zhao et al., 2002), in HEK293 cells, zDHHC9-GCP16 mainly co-localise at the Golgi system (Swarthout et al., 2005).

GCP16 (which is also known as Golga7) also interacts with zDHHC5 and zDHHC8 (Ko et al., 2019; Salaun et al., 2020b). In a study by Woodley and Collins (2019), interaction with Golga7b (which shares 61% identity with GCP16) was suggested to promote plasma membrane association and prevent internalisation of zDHHC5 (Woodley and Collins, 2019). This suggests that the regulatory effects of GCP16/Golga7 may be more widespread in the zDHHC enzyme family.

zDHHC6 activity was reported to be modulated by Selenoprotein K (SelK), which was proposed to act by stabilising the autoacylated enzyme intermediate, similar to that described for Erf4/GCP16 (Fredericks et al., 2018). zDHHC6 is also regulated by S-acylation, mediated by the S-acyltransferase zDHHC16, through an “S-acylation cascade”. Combining site-directed mutagenesis, kinetic analysis and mathematical modelling, it was shown that the activity and half-life of zDHHC6 are both controlled by the degree of S-acylation of three C-terminal cysteine residues: Cys-328, Cys-329 and Cys-343 (Abrami et al., 2017). The regulation of zDHHC6 stability by S-acylation appears to involve an interplay between S-acylation and ubiquitination.

The HTT protein was reported to act as a positive modulator of zDHHC17 (Huang et al., 2011). *In vitro*, GST-SNAP25 S-acylation was enhanced by almost 70% by GST-zDHHC17 in the presence of wild-type, but not a mutant HTT protein containing an expansion of the polyglutamine repeat region (128 glutamines compared to 15 in the

wild-type HTT protein). Furthermore, *hdh*^{+/-} mice, lacking one allele of the *HTT* gene, displayed reduced zDHHC17 S-acylation which was suggested to reflect reduced autoacylation and thus enzyme activity (Huang et al., 2011). Thus, HTT may act to regulate the autoacylated state of zDHHC17, similar to the effects of GCP16 on zDHHC9. However, it is important to note that zDHHC17 is also S-acylated outside of the DHHC catalytic domain and therefore changes in S-acylation status may not be directly correlated with enzyme activity (and S-acylation of the active site cysteine) (Collins et al., 2017).

Other zDHHC enzymes are thought to be regulated by dynamic changes in their intracellular localisation. For example, zDHHC2 and zDHHC5 cycle between recycling endosomes (REs) and post-synaptic membranes, and this cycling controls access to the substrate proteins PSD95 and δ -catenin, respectively (Brigidi et al., 2015; Noritake et al., 2009). Neuronal activity has been shown to be crucial for the dynamic trafficking of both of these enzymes. At steady state, zDHHC2 localises in dendritic shafts, whereas synaptic blockage promotes redistribution of zDHHC2 to synaptic membranes, increasing both PSD95 S-acylation and AMPAR clustering (Noritake et al., 2009). In contrast, under basal conditions, zDHHC5 is found at the plasma (post-synaptic) membranes where it is stabilised by association with both Fyn and PSD95. Upon increased neuronal activity, zDHHC5 dissociates from Fyn and PSD95 to undergo clathrin-mediated endocytosis, through association with AP2 μ protein and trafficking to dendritic shafts. In dendritic shafts, zDHHC5 S-acylates δ -catenin (within 3-10 min post stimulation) and both zDHHC5 and S-acylated δ -catenin recycle back to the plasma membrane (within 3-20 min post stimulation). Ten to twenty min post stimulation zDHHC5 dissociates from δ -catenin, allowing a new cycle to start (Brigidi et al., 2015). In this case, the activity-dependent internalisation of zDHHC5 is mediated by dephosphorylation of a key tyrosine residue within a tyrosine-based endocytic motif, which allows recognition of the motif by the clathrin adaptor AP2 (Brigidi et al., 2015).

In neuronal stem cells (NSCs), zDHHC5 levels were found to be regulated by extracellular growth factors (GFs). When neuronal differentiation was induced in

NSCs using medium lacking EGF (endothelial growth factor), FGF2 (also known as basic fibroblast growth factor, bFGF) and heparin, zDHHC5 levels were shown to decrease by 90% within 1 h, suggesting that degradation mechanisms are triggered following GFs withdrawal. Indeed, zDHHC5 levels could be rescued by treating cells with proteasome inhibitors (e.g. ALLN and MG-132) or adding back GFs, such as EGF and FGF2 (Li et al., 2012). The activity of zDHHC7 was also shown to be responsive to GFs as it was positively regulated by insulin in both HEK293T and 3T3-L1 adipocytes. Following insulin treatment of 3T3-L1 adipocytes, zDHHC7 autoacylation as well as S-acylation of Glut4 (glucose transporter 4) were shown to be increased by ~3 fold (Du et al., 2017).

In neuroblastoma N2a cells, zDHHC3 activity was found to be regulated by phosphorylation at specific tyrosine residues. Specifically, phosphorylation of Tyr-295 and Tyr-297 by Src kinase was reported to negatively regulate zDHHC3 activity, acting as a switch “off” signal. In contrast, phosphorylation of Tyr-18 by activated fibroblast growth factor receptor (FGFR), positively modulated activity (switch “on” signal), increasing the S-acylation of substrates such as the neural cell adhesion molecule NCAM (Lievens et al., 2016).

In addition to changes in phosphorylation, localisation or expression levels, another suggested regulatory mechanism is *via* changes in the oligomeric state of zDHHC enzymes. In this regard, homo- and hetero-multimers have been reported for the *cis*-Golgi enzymes zDHHC3 and zDHHC7 (Fang et al., 2006) as well as for zDHHC2, which cycles between REs and the plasma membrane (as described above) (Lai and Linder, 2013). The active state was suggested to correspond to the monomeric form of the enzymes and the inactive state to the oligomeric one (Lai and Linder, 2013). In support of this proposal, catalytically inactive versions of both zDHHC2 and zDHHC3 were found to self-associate more than the corresponding wild-type pairs in bioluminescence resonance energy transfer (BRET), blue native polyacrylamide gels and co-immunoprecipitation experiments. Synthetic zDHHC2 and zDHHC3 dimers were also found less active when compared to zDHHC2 and zDHHC3 monomers (Lai and Linder, 2013).

1.6 Substrate specificity of zDHHC enzymes

One of the most elusive aspects of the S-acylation field is how zDHHC enzymes achieve substrate recognition and specificity. The paucity of knowledge in this area can be in part linked to the lack of a universal recognition motif. While both N-myristoylation and isoprenylation have well-defined consensus sequences (refer to paragraph 1.1 for more details), the major requirement for S-acylation appears to be the presence of accessible/membrane-proximal cysteine residues (Chamberlain and Shipston, 2015; Lemonidis et al., 2017b; Rana et al., 2018b; Rodenburg et al., 2017; Zaballa and van der Goot, 2018).

Over the years, zDHHC enzymes have been recognised as having a certain degree of functional redundancy and often a single substrate can be modified by multiple zDHHC isoforms in co-expression experiments (e.g. PSD95 can be S-acylated by zDHHC2, zDHHC3, zDHHC7, and zDHHC15). In contrast, other substrates do appear to depend on specific zDHHC enzymes for their modification, for example, calnexin is predominantly S-acylated by zDHHC6 (Fukata et al., 2016; Lynes et al., 2013).

It has been proposed that a first level of substrate “specificity” is conferred by the subcellular localisation of zDHHC enzymes. For example, an ER-resident protein will be more likely to be modified by ER zDHHC enzymes, such as the case of calnexin S-acylation by zDHHC6 described above (Fukata et al., 2016; Philippe and Jenkins, 2019). This idea is also exemplified by the activity-dependent changes in localisation of zDHHC2 and zDHHC5, which facilitate access to and S-acylation of PSD95 and δ -catenin, respectively (Brigidi et al., 2015; Fukata et al., 2013).

In addition to subcellular co-localisation contributing to enzyme-substrate specificity, a number of zDHHC enzymes contain recognised binding domains which can mediate direct interaction with protein substrates, including: (i) zDHHC6 which encompasses an SH3 domain in its C-terminus, (ii) zDHHC3, zDHHC5, zDHHC7, zDHHC8, zDHHC14, zDHHC16, zDHHC17, zDHHC20 and zDHHC21 all containing predicted PDZ-binding

motifs, and (iii) zDHHC13 and zDHHC17 which are characterised by seven N-terminal ankyrin repeats (Gottlieb and Linder, 2017).

A new concept of zDHHC enzyme-substrate specificity has been recently described following studies conducted on the ankyrin repeat (ANK) domain of zDHHC13 and zDHHC17 (Lemonidis et al., 2015a; Verardi et al., 2017). These studies suggest that while for a pool of zDHHC enzymes a weak interaction with the substrates is sufficient to mediate S-acylation, other enzymes require a much stronger interaction with their substrates to mediate S-acylation. Additionally, it has been demonstrated that a strong enzyme-substrate interaction does not always reflect high S-acylation efficiency, which instead is strictly related to the nature of the specific zDHHC isoform and its intrinsic S-acylation activity (Lemonidis et al., 2017b, 2014).

1.6.1 The ankyrin-repeat (ANK) domain of zDHHC17 and zDHHC13 mediates substrate recognition and binding

zDHHC13 and zDHHC17 are unique in the zDHHC enzyme family for the presence of a seven ankyrin repeat (ANK) domain at their N-termini. The importance of the ANK domain as a recruitment module for substrate proteins of these enzymes was highlighted for the first time by studies conducted on HTT and zDHHC17 (Huang et al., 2011). Subsequent research on the four *cis*-Golgi PATs zDHHC3, zDHHC7, zDHHC13 and zDHHC17 and their interplay with SNAP25b and CSP α , better characterised the concepts of specificity of binding and efficiency of S-acylation (Lemonidis et al., 2014). Lemonidis and colleagues reported that while zDHHC3 and zDHHC7 are the most intrinsically active isoforms; zDHHC13 and zDHHC17 mediated the strongest and most specific interaction with both SNAP25b and CSP α . The observed binding was mediated by the ANK domains of zDHHC17 and zDHHC13 and deletion of these regions (17- Δ NAnk and 13- Δ NAnk mutants, respectively) correlated with loss of SNAP25b/CSP α binding, assessed by yeast growth in the split ubiquitin system (SUS) (Lemonidis et al., 2014). In addition, the ANK domain of zDHHC17 was found to be essential for S-acylation of SNAP25b/CSP α , whereas zDHHC13 was

inactive against both SNAP25b and CSP α despite displaying a similar strength of interaction as zDHHC17 with these proteins. This latter aspect was suggested to be linked to the presence of a DQHC motif (instead of a canonical DHHC) uniquely found in zDHHC13 and a different orientation of the ANK domain with respect to the catalytic site in zDHHC13 *versus* zDHHC17 (Lemonidis et al., 2014).

Based on these observations, Golgi-localised zDHHC enzymes were classified into two main groups. The first includes zDHHC enzymes with high S-acylation activity and low substrate specificity (i.e. zDHHC3 and zDHHC7) for which (i) proximity to the substrate proteins and (ii) reactivity of the target cysteine(s) in the substrate are thought to be important for enzyme catalysis. The second comprises zDHHC enzymes with low intrinsic S-acylation activity but high substrate specificity (i.e. zDHHC17 and zDHHC13) which instead recognise specific features and form stable complexes with protein substrates (Greaves et al., 2009a; Lemonidis et al., 2017a, 2015b, 2014). In agreement with this classification, the study of Ernst et al. (2018) also recognised both zDHHC3 and zDHHC7 as highly active isoforms, involved in the bulk S-acylation of anterograde cargo proteins at the Golgi membranes (Ernst et al., 2018).

1.6.2 Identification of a zDHHC-ANK-binding motif (zDABM)

The interaction of zDHHC17 with its substrate proteins has been extensively characterised through mutational and structural analyses. In a first study, Greaves et al. (2009) identified the residue Pro-117 as important for membrane association of SNAP25b, following co-expression with zDHHC17 but not zDHHC7 or zDHHC3 (Greaves et al., 2009a). Follow-up studies found that zDHHC13 and zDHHC17 recognised *via* their ANK domain a specific sequence, known as the zDHHC-ANK domain binding motif (“zDABM”) which includes a critical proline residue (Pro-117 in SNAP25b), in several substrates, including SNAP23, SNAP25b, CSP α , HTT, CLIP3 (also known as ClipR-59) and MAP6 (Lemonidis et al., 2015a). The zDABM has the amino acid consensus sequence $\psi\beta\text{XXQP}$ (where ψ indicates an aliphatic residue, either Val, Ile, Ala, or Pro; β indicates a C-beta branched amino acid, either Val, Ile, or Thr; X

indicates any amino acid), also referred to as either the [VIAP][VIT]XXQP or QP motif. The $\psi\beta$ XXQP sequence needs to be present within an unstructured region to be recognised by zDHH17. Based on the specific amino acids present at the first two positions (i.e. ψ and β), the $\psi\beta$ XXQP motif was further classified into three sub-motifs (i) [VIA][VI]XQP (ii) P[VI][VIL]XQP and (iii) Q[VI]TXXQP (Lemonidis et al., 2015a). For clarity, within this thesis the terms zDABM, [VIAP][VIT]XXQP or QP motif will be used interchangeably, whereas “ $\psi\beta$ XXQP motif” will not be used.

More recently, *in silico* predictions and peptide array experiments were combined to further characterise the requirements for binding between zDABM sequences and the ANK domain of zDHH17 and to identify novel potential zDHH17/zDHH13 binding partners. While the [VIAP][VIT] of the zDABM are quite versatile, the QP dipeptide is always conserved (besides a few exceptions in which Q can be substituted by other amino acids) (Lemonidis et al., 2017a). Also, all members of the SNAP25, Sprouty (SPRY), cornifelin, ankyrin, and SLAIN-motif containing families, as well as several proteins involved in cell communication, signalling and cytoskeletal organisation were validated as putative zDHH17 interactors through their zDABMs (Lemonidis et al., 2017a). It further emerged that more than one zDABM sequence *per* protein may exist, suggesting that zDHH17 might bind to the same substrate at more than one site forming different complexes (Lemonidis et al., 2017a). Wider interactome BioPlex (Biophysical Interactions of ORFeome-derived complexes) analysis, in which affinity purification was coupled to mass spectrometry identification, further confirmed many of the zDHH17 interactions found in the study of Lemonidis and colleagues, including that of zDHH17 with SPRY2 protein, of particular interest for this thesis (Huttlin et al., 2017).

1.6.3 Critical residues for zDHH17 ANK domain - substrate interaction

Recently, Verardi and colleagues solved a high-resolution crystal structure of the ANK domain of zDHH17 (ANK17) in complex with a peptide of SNAP25b containing the zDABM sequence (residues 111-GVVASQPARV-120). This allowed the identification

of the key amino acids involved in the ANK17-SNAP25b interaction (Fig. 1.4). Within ANK17, Trp-130 (W130) and Asn-100 (N100) are the most critical residues for substrate recruitment and binding. The aromatic ring of W130 (Trp-130) forms the most extensive interactions (vdW: van der Waals) with P117 (Pro-117) of SNAP25b, whereas N100 (Asn-100) establishes hydrogen-bonds (H-bonds) with V113 (Val-113). V113 also contacts I99 (Ile-99) in ANK17 *via* van der Waals (vdW) interactions. Moreover, Y67 (Tyr-67) in ANK17 interacts through vdW forces with V112 (Val-112) of SNAP25b, while E89 (Glu-89) and D122 (Asp-122) in ANK17 engage in H-bonds with Q116 (Gln-116) in SNAP25b (Verardi et al., 2017).

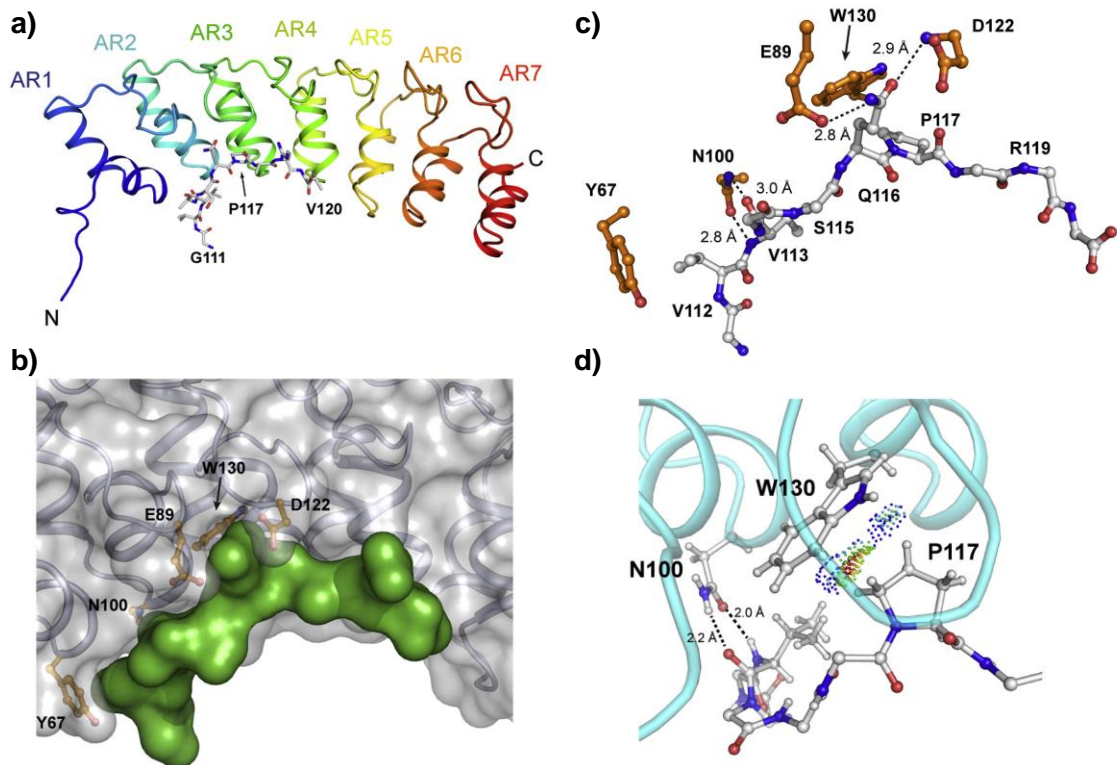


Figure 1.4 Interaction between ANK17 and SNAP25b₁₁₁₋₁₂₀ peptide

a) Cartoon representation of the seven ANK domain of zDHH17 (AR1-AR7) and stick representation of SNAP25b₁₁₁₋₁₂₀ peptide. **b)** ANK17-SNAP25b₁₁₁₋₁₂₀ binding. SNAP25b (in green) interacts with the concave region of ANK17 (in grey). The key interacting residues in ANK17 are also shown (in orange). **c)** Detail of the key amino acids involved in the ANK17-SNAP25b interaction. Y67 contacts V112 (vdW forces), E89 and D122 both interact with Q116 (H-bonds), N100 contacts V113 (H-bonds), and W130 interacts with P117 (vdW forces). SNAP25b peptide is shown in grey and ANK17 residues in orange. **d)** Close up view of W130 and N100 on ANK17 contacting P117 and V113 in SNAP25b peptide, respectively. Figure adapted from (Verardi et al., 2017).

Importantly, within ANK17, mutation of either N100 or W130 to alanine abolished the ability of zDHH17 to bind not only SNAP25 but also Huntingtin protein (HTT), suggesting a broader role of these residues in substrate recruitment. Furthermore, alanine-substitution at P117, V113 or Q116 in SNAP25b reduced the interaction with

ANK17 (Verardi et al., 2017). In agreement with these observations, a recent study in which zDHHC17-MAP2K4 interaction was dissected also identified W130 and Y67 (among other amino acids) as key residues in zDHHC17 for MAP2K4 recruitment (Chen et al., 2020). Although MAP2K4 does not contain a zDABM, this report further highlights the importance of this binding pocket in substrate binding.

1.7 zDHHC17 S-acyltransferase: (patho)physiology

zDHHC17 was originally isolated during yeast two-hybrid screens for novel interactors of huntingtin and identified as Huntingtin Interacting Protein 14 (HIP14). The same study also identified HIP14-like (HIP14L, or zDHHC13), which is the closest paralogue of zDHHC17. Both zDHHC17 and zDHHC13 show significant homology with the two *Saccharomyces cerevisiae* ankyrin-repeat containing proteins Akr1 and Akr2, as well as other transcripts belonging to *Caenorhabditis elegans*, *Drosophila melanogaster*, *Mortierella alpina* and *Schizosaccharomyces pombe* (Singaraja et al., 2002).

In the same study, zDHHC17 was mapped to the human chromosome 12q14-q15 as a single genomic locus of 5272 nucleotides. The canonical form of the protein is produced by a single open reading frame (ORF) of 1902 nucleotides, which is translated into a protein of 632 amino acids. By alternative splicing, three isoforms can be generated with isoform 1 acknowledged as the “canonical” sequence (identifier Q8IUH5-1, UniProtKB) and visible on immunoblotting as a single band of ~70 kDa (Singaraja et al., 2002).

In cells, zDHHC17 mainly localises at the *cis*-Golgi compartment but its presence on cytoplasmic vesicles, the plasma membrane, and dendritic spines has also been documented (Ernst et al., 2018; Huang et al., 2004; Singaraja et al., 2002). Although particularly enriched throughout the brain (e.g. in the cortex, striatum and hippocampus, cerebellum, brainstem and thalamus), zDHHC17 expression has also been detected in several human peripheral tissues, including kidneys, testis, thymus, heart, pancreas and liver. As a consequence, zDHHC17 has been described as a highly ubiquitous zDHHC enzyme (Ohno et al., 2006; Singaraja et al., 2002).

zDHHC17 mediates the S-acylation of several important synaptic proteins, such as CSP α (Ohyama et al., 2007), SNAP25, PSD95, HTT, GAD65, Synaptotagmin-I (Huang et al., 2004), the GluR1 and GluR2 subunits of AMPAR (Huang et al., 2009) and GluNR2B subunits of NMDAR (Kang et al., 2019). In addition, many other neuronal proteins have been reported as zDHHC17 binding partners although S-acylation of most of them has yet to be established (Butland et al., 2014; Huttlin et al., 2017; Lemonidis et al., 2017a).

In addition to functioning as S-acyltransferase enzymes, one study also reported that zDHHC17 and zDHHC13 could mediate membrane transport of Mg²⁺ ions in *Xenopus* oocytes, a function that appears to be regulated by their own S-acyltransferase activity. In COS-7 and MDCK cells extracellular concentrations of Mg²⁺ modulated zDHHC17 transcript as well as protein abundance, besides redistributing the protein to sub-plasma membrane vesicles. Therefore, it was suggested that zDHHC17 acts as a “chanzyme” combining ion transport with enzymatic function (Goytain et al., 2008).

1.7.1 zDHHC17 and Huntington disease

Huntington’s disease (HD), named after George Huntington who first described this condition in 1872, is an autosomal-dominant neurodegenerative disorder characterised by motor, cognitive and behavioural deficits (Bates et al., 2015). Huntingtin protein (HTT) is a 348 kDa protein, which contains an N-terminal polyglutamine (polyQ) region that normally contains between 6-35 glutamines. HD is caused by the expansion of the cytosine-adenine-guanosine (CAG) repeat sequence (encoding polyQ) in the coding region of the *HTT* gene, which results in an increased number of glutamines in the polyQ region of the HTT protein. When the number of glutamines in the polyQ sequence is >40, this leads to the development of Huntington’s disease, a late-onset neurodegenerative disorder (HTT with a pathogenic expansion of the polyQ region is referred to as mutant HTT, mHTT) (Bates et al., 2015). PolyQ expansions are thought to increase protein instability as well as proteolysis which, in turn, lead to intracellular accumulation of protein fragments

(Bates et al., 2015). Aggregation of such HTT-fragments results in the accumulation of visible cytoplasmic and nuclear inclusions that either interfere with the normal function of neurons and other cells in the brain (Davies et al., 1997) or alternatively have a protective role by sequestering otherwise highly-reactive smaller HTT aggregates (Arrasate et al., 2004). HD affects many brain regions but, in particular, leads to apoptosis of medium spiny neurons in the striatum (Rikani et al., 2014).

There is growing interest in the effects that different post-translational modifications have on the function of HTT and the aggregation of mHTT. The effects of phosphorylation and ubiquitination have been studied in detail, however HTT is also dynamically S-acylated at a single site in the N-terminal region (Cys-214) (Yanai et al., 2006). zDHHC17 (HIP14) and zDHHC13 (HIP14L) are the two main zDHHC isoforms active against HTT protein (Huang et al., 2011, 2009). Over the years, the interplay between zDHHC17 and HTT has been extensively studied and characterised. Importantly, mHTT with a 128 polyQ tract (i.e. disease-associated mutation) is characterised by reduced interaction with zDHHC17 (128Q *versus* 15Q) (Singaraja et al., 2002) and, in turn, reduced S-acylation (Yanai et al., 2006). Furthermore, the formation of mHTT nuclear inclusions was enhanced by knockdown of zDHHC17 or by mutation of Cys-214 and indeed wild-type HTT also displayed increased inclusion formation when Cys-214 was replaced by a serine residue (Yanai et al., 2006). In addition to HTT being a substrate of zDHHC17, it has also been suggested that HTT enhances the S-acylation activity of zDHHC17 by stabilising the autoacylated enzyme intermediate (Huang et al., 2011). Intriguingly, this regulatory function is lost when the polyQ region of HTT is increased and zDHHC17 isolated from brain lysates of YAC128 mice (i.e. expressing the 128Q mHTT) is dysfunctional (Singaraja et al., 2011). This has led to the proposal that, in addition to toxic gain-of-function effects, expression of mHTT may also lead to a loss of zDHHC17 activity, which might further exacerbate the pathological process in HD (Huang et al., 2011; Singaraja et al., 2011).

Hip14^{-/-} (Hip14-deficient) mice were generated by gene-trap technology. These mice were shown to be hypomorphic and express zDHHC17 at approximately 10% of the levels of wild-type mice (Singaraja et al., 2011). Interestingly, the gene-trap mice

were suggested to have many similar features seen in HD mouse models such as YAC128 mice (Singaraja et al., 2011), which express a human HTT transgene with 128 CAG repeats (Slow et al., 2003). Specifically, the gene-trap mice displayed deficits in motor coordination, a decrease in the number of excitatory synapses, a reduced striatal volume and decreased number of medium spiny neurons. This evidence was used to support the notion that a loss of zDHHC17 activity (caused by mHTT) is a contributing factor to the pathological features of HD (Singaraja et al., 2011). A number of similar molecular changes were detected in YAC128 and *Hip14*^{-/-} mice models including reduced caspase-6 (CASP6) S-acylation and increased protein activity. CASP6 plays an important role in neuronal apoptosis during other neurodegenerative diseases, including Huntington and Alzheimer's disease (AD), but also in non-neurodegenerative diseases, such as stroke and ischemia (Skotte et al., 2017). A subsequent conditional knockout (KO) *Hip14*^{Δ/Δ} mouse model further highlighted the physiological importance of zDHHC17. After induction of the KO, these mice displayed synaptic and behavioural deficits, depressive and anxiolytic-like phenotypes and within ten weeks, they died due to progressive paralysis (Sanders et al., 2016).

Altogether, these models highlight the potential implications of zDHHC17 in HD (and possibly many other disorders) and the overall importance of this enzyme for both neuronal integrity and neurological function.

1.7.2 zDHHC17 and diabetes mellitus

Diabetes mellitus is a chronic metabolic disorder characterised by high blood sugar levels (hyperglycaemia), two main type of diabetes can be recognised: Type 1 and Type2 (Asmat et al., 2016).

Type 1 diabetes (T1D) is an autoimmune disease characterised by the loss of pancreatic β -cells, the insulin-producing cells in the islets of Langerhans. At the cellular level, this dysfunction involves an inflammatory event (known as insulinitis) which is mainly mediated by the proinflammatory cytokines IL-1 β and INF- γ . Based

on an *in silico* “interactome network analysis”, zDHHC17 was found to be one of the top-scoring candidate proteins linked to Type 1 diabetes. Further analysis established that zDHHC17 is expressed in β -cells where it is involved in important events, including insulin secretion and β -cells survival. Additionally, by interfering with IL-1 β -induced apoptosis, one of the main pathways responsible of pancreatic β -cells death, zDHHC17 may act as an important anti-apoptotic factor in this cell type (Berchtold et al., 2011). Notably, glucose metabolism dysfunctions and diabetes have also been linked and suggested as contributing factors to HD, although the relevance of this remains to be established (Montejo et al., 2017).

Type 2 diabetes (T2D) is characterised by a diminished response to insulin due to systemic cells, mainly adipocytes and muscle cells, failing to respond to this hormone, coupled to insufficient insulin production by pancreatic β -cells to overcome this insulin resistance. At the cellular level, upon insulin stimulation, the glucose transporter 4 (Glut4) translocates from an intracellular storage site to the plasma membrane where it mediates glucose uptake (Asmat et al., 2016). This pathway was shown to be modulated by zDHHC17, in a ClipR-59-dependent manner. Following S-acylation by zDHHC17, ClipR-59 associate with the plasma membrane where it facilitates the recruitment of phospho-Akt (PKB). Phosphorylation of Akt is an important step in the insulin signalling pathway and ClipR-59 mediated recruitment of phospho-Akt to the plasma membrane is important for subsequent Akt-dependent phosphorylation steps and the insulin-stimulated movement of Glut4 to the plasma membrane. Indeed, over-expression of zDHHC17 augmented, whereas expression of zDHHC17 shRNA decreased, plasma membrane levels of Glut4 in 3T3-L1 adipocytes (Ren et al., 2013).

Taken together, these studies established important links between zDHHC17 and insulin secretion and insulin signalling, dysfunction of which can lead to diabetes.

1.7.3 zDHHC17 and other diseases

The role of zDHHC17 has also been investigated, albeit to a limited extent, in cancer. Ducker et al. (2006) undertook a cancer profiling array, in which the expression of zDHHC17 was evaluated in a number of human tumours from a total of 154 patients. This analysis revealed upregulation of zDHHC17 (>50% increase) in colon, stomach, lung, breast and prostate cancers. In contrast, zDHHC17 expression was found to be downregulated (>20% decrease) in liver, thyroid gland, bladder and vulva tumours (Ducker et al., 2006). zDHHC17 was also reported to act as an oncogenic protein in NIH-3T3 fibroblasts and mice, and this was suggested to relate to Ras S-acylation (Ducker et al., 2004). However, it is important to emphasise that to-date, Ras proteins have not been identified as zDHHC17 substrates (Butland et al., 2014; Huang et al., 2011; Lemonidis et al., 2017a). Finally, zDHHC17 was found to be upregulated and promote malignant progression in glioblastoma multiforme (GBM) through activation of JNK and p38 MAPK signalling (zDHHC17-MAP2K4-JNK/p38 signalling module) (Chen et al., 2020).

Finally, the interaction of zDHHC17 with JNK2/3 has been linked to neuronal cell death following acute ischaemic stroke. This pathway was suggested to be independent of the S-acyltransferase activity of zDHHC17 and instead, zDHHC17 was suggested to perform a scaffold function by regulating the MKK7-JNK2/3 signalling module which leads to cell death in response to stress conditions (e.g. excitotoxicity and brain injury) (Yang and Cynader, 2011). This study highlights the importance of discriminating S-acylation-dependent and -independent functions of zDHHC17 as the ANK domain can interact with a large variety of cellular proteins, many of which are not thought to be direct substrates of this enzyme (Lemonidis et al., 2017a).

1.8 The Sprouty (SPRY) family of proteins

Receptor Tyrosine Kinases (RTKs) are cell-surface receptors that bind a range of different growth factors and activate intracellular signalling cascades, such as RAS-ERK, PI3K-AKT, JAK-STAT and PLC γ pathways, ultimately promoting cell proliferation,

differentiation and survival (Lemmon and Schlessinger, 2010). However, as inappropriate activation of growth factor signalling can stimulate excessive cell growth and tumorigenesis, these signalling pathways must be tightly regulated. Sprouty proteins (SPRY) are negative regulators of RAS-ERK signalling *via* a number of proposed mechanisms (Kim and Bar-Sagi, 2004).

SPRY was initially discovered during studies in *Drosophila melanogaster* as an antagonist of FGF signalling. FGF is involved in the development of the tracheal system, and while overexpression of SPRY protein was shown to inhibit tracheal budding, *SPRY*-loss of function (i.e. *SPRY*^{-/-}) resulted in additional tracheal branches in *D. melanogaster* (Hacohen et al., 1998). In a follow-up study, *D. melanogaster* SPRY (dSPRY) was also found able to inhibit the epidermal growth factor receptor (EGFR) during the development of tissues including the eye, the peripheral and central nervous systems, wing veins and ovary (Kramer et al., 1999). Concurrently, Casci and colleagues reported the interaction of SPRY with other RTKs, such as Torso and Sevenless, hence establishing dSPRY as a general regulator of RTK signalling. At the molecular level, dSPRY was shown to bind several members of the Ras-MAPK pathway between activated RTKs and Ras, including Drk (homologue of mammalian Grb2) and Gap1 (a Ras GTPase-activating protein) (Casci et al., 1999). However, in another genetic-based study dSPRY was shown to inhibit the Ras-MAPK signalling downstream of activated Ras, at the level of Raf or MEK (Reich et al., 1999). Notably, these first studies also established that dSPRY expression was induced by the signalling pathways that it acted upon, thereby generating negative feedback loops (Casci et al., 1999; Hacohen et al., 1998; Kramer et al., 1999; Reich et al., 1999).

1.8.1 General domain structure of SPRY proteins

The genome of *D. melanogaster* encodes a single SPRY protein of 591 amino acids and an estimated molecular weight of 63 kDa. At the C-terminus of the protein, there is a characteristic cysteine-rich domain (CRD) of 124-residues, containing 22 cysteines (Hacohen et al., 1998). This unique feature led to the identification of four

mammalian SPRY isoforms (SPRY1-4), which are smaller than the dSPRY (32 to 34 kDa) but that all share the CRD, which was therefore named the “SPRY domain” (De Maximy et al., 1999; Minowada et al., 1999). It is interesting to note that the CRD and the SPRY domain are annotated in UniProtKB as two distinct regions despite their almost perfect overlapping. The terms CRD and SPRY domain will be used interchangeably in this thesis. Outside of the SPRY domain, the homology between *D. melanogaster* and mammalian SPRY proteins (SPRYs) is limited to a short stretch of N-terminal amino acids (NXY*XXXP), also referred to as the Cbl tyrosine kinase-binding (TKB) motif, and encompassing a highly conserved tyrosine residue (indicated by the asterisk): Y201 in dSPRY and Y55 in SPRY2 (the isoform that shares the highest nucleotide and amino acid identity with dSPRY) (Fong et al., 2003; Sasaki et al., 2001). Analyses of mammalian SPRYs reveals the conservation of a third sequence upstream of the CRD: a serine-rich motif (SRM) which is less obvious in dSPRY (Impagnatiello et al., 2001) and contains several serine and threonine residues undergoing dynamic phosphorylation (DaSilva et al., 2006; Lao et al., 2007). A schematic of *D. melanogaster* and mammalian SPRY proteins is depicted in Figure 1.5. Altogether, (i) the cysteine-rich domain, (ii) the highly conserved tyrosine residues and (iii) the serine-rich motif are involved in many protein-protein interactions which, in turn, finely-tune the activity of SPRY proteins (Guy et al., 2009, 2003).

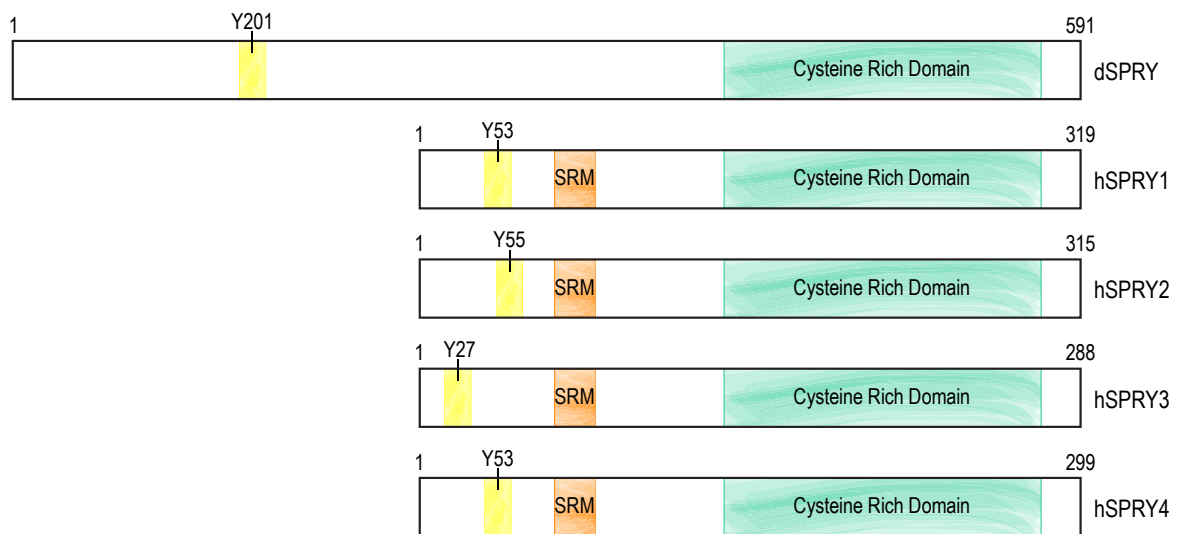


Figure 1.5 Structure of *D. melanogaster* and human SPRY proteins

The N-terminal regions of both *D. melanogaster* and human SPRY proteins contain the highly conserved Tyr (Y) residues, which is located in a conserved motif (depicted in yellow in the figure). The positions of the highly conserved Ser-rich (SRM) and Cys-rich domains (CRD) are depicted in orange and aquamarine boxes, respectively. *D. melanogaster* SPRY (dSPRY) is located on chromosome 3L (Gene ID: 38424) and encodes a protein of 591 residues (63 kDa) (Hacohen et al., 1998). In humans, the four SPRY proteins (SPRY1-4) are the products of four different genes, located on chromosomes 4q28.1 (*SPRY1* - Gene ID: 10252), 13q31.1 (*SPRY2* - Gene ID: 10253), Xq28/Yq12 (*SPRY3* - Gene ID: 10251), and 5q31.3 (*SPRY4* - Gene ID: 81848). As shown in the figure, SPRY1 is 319 amino acids long (UniProtKB entry ID: O43609), SPRY2 is 315 (UniProtKB entry ID: O43597), SPRY3 is 288 (UniProtKB entry ID: O43610), and SPRY4 is 299 (UniProtKB entry ID: Q9C004).

Based on sequence similarities, SPRY proteins have been also identified in several other vertebrates, including chick (four isoforms), the clawed frogs *Xenopus laevis* and *Xenopus tropicalis* (two isoforms) and zebrafish (two isoforms), whereas they have not been found in the nematode *Caenorhabditis elegans* (Mason et al., 2006). Amongst vertebrates, SPRY2 (of particular interest for this thesis) is the most highly conserved isoform and also displays the highest similarity with the *D. melanogaster*

protein with 51% amino acid identity within the CRD (Hacohen et al., 1998). As a consequence, this also represents the best characterised of the mammalian SPRY isoforms. In humans, the *SPRY2* gene encodes a protein of 315 amino acids and a molecular weight of ~ 35 kDa; the SPRY domain encompasses amino acids 177-291, whereas the cysteine-rich domain encompasses residues 178-301 and contains 26 cysteines. Within the amino terminus, the highly conserved tyrosine residue is at position 55 while the SRM covers amino acids 125-131 (Fig. 1.6) (UniProtKB entry ID: O43597). The human *SPRY2* gene contains two exons and one intron and two potential translation start sites (Ding et al., 2003). Within the promoter, binding elements for transcription factors including AP2, Ets-1, CREB, NF-1 and SP1 have been identified and suggested to be responsible for the basal transcription of hSPRY2 (Ding et al., 2003). In addition, the *SPRY2* promoter is a direct target of the FoxO family of transcription factors (Paik et al., 2007).

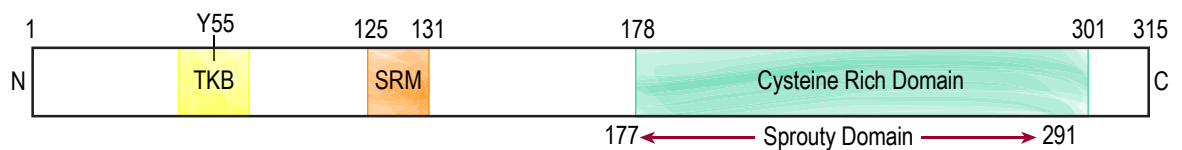


Figure 1.6 Schematic representation of human SPRY2 protein

The highly conserved tyrosine kinase binding (TKB) motif, including Y55, is in yellow; the Ser-rich motif, spanning residues 125-131, in orange; and the Cys-rich domain, encompassing amino acids 178-301, in aquamarine. The position of the Sprouty domain, residues 177-291, is also reported in the figure (UniProtKB ID: O43597).

1.8.2 Subcellular localisation of SPRY proteins

In *D. melanogaster*, SPRY mainly localises to the intracellular face of the plasma membrane and to some intracellular structures containing EGF receptors (EGFRs), possibly endosomes (Casci et al., 1999; Hacohen et al., 1998). A similar distribution was reported for overexpressed human SPRY2 in both COS-1 and HEK293T cells (Lim

et al., 2000). In unstimulated cells, hSPRY2 was reported to localise to the cytosol and to associate with cytoskeletal structures identified as microtubules (i.e. tubulin co-localisation). Following EGF (and to a lesser extent FGF) stimulation, hSPRY2 was seen to exhibit a rapid translocation to plasma membrane ruffles where it co-localised with both actin and ezrin (Lim et al., 2000). This movement of hSPRY2 was reported to be mediated by a region within the CRD, named the SPRY translocation domain (TD) (Lim et al., 2000), that binds phosphatidylinositol 4,5-bisphosphate (PIP₂) and co-localises in cells with the PIP₂-binding pleckstrin homology (PH) domain of phospholipase Cδ (PLCδ) (Lim et al., 2002). In addition, PIP₂ depletion was shown to relocalise the protein to the cytosol, further suggesting a specific interaction of hSPRY2 with this component of the plasma membranes (Lim et al., 2002). Moreover, positively charged amino acids were shown to be important as mutation of a highly conserved arginine residue in the TD (i.e. SPRY2 R252D) resulted in reduced PIP₂ binding and defects in plasma membrane translocation (Lim et al., 2002). However, upon EGF stimulation, SPRY2 R252D was reported to correctly translocate to the plasma membrane by others (Cabrita et al., 2006). Furthermore, in human umbilical vein endothelial cells (HUVECs), endogenous hSPRY1 and overexpressed mSPRY1 and mSPRY2 were found in perinuclear and vesicular structures as well as the leading edge of the plasma membrane. While such localisation related to active proliferating HUVECs, following serum starvation, hSPRY1 could not be observed at the plasma membrane. Conversely, upon FGF2 or VEGF (vascular-growth factor) stimulation, a fraction of both SPRY1 and SPRY2 was shown to translocate to the plasma membrane where they associated with caveolin-1, a component of membrane caveolae. In the same study, mSPRY1 and mSPRY2 were also reported to be S-acylated (Impagnatiello et al., 2001). Translocation from the cytoplasm to the plasma membrane and relocation to intracellular structures was also observed in mouse lung epithelial cells (MLE15) in response to FGF10 (Tefft et al., 2002). It was only in later studies that the nature of the intracellular structures populated by SPRY proteins was characterised. In murine myoblast (C2C12) and COS-1 cells, endogenous and overexpressed hSPRY2, respectively, was shown to co-localise with the early endosomal marker Rab5 upon

EGF stimulation. However, no co-localisation was observed with the late endosomal marker Rab7 neither in COS-1 nor in MDCK cells (Kim et al., 2007). Interestingly, the presence of hSPRY2 in these compartments was suggested to interfere with the trafficking of EGFR from early to late endosomes (Kim et al., 2007). In contrast, in human glioma cells (U87, SF126, and U251) ectopic hSPRY2 was found not only in early (Rab5 positive) but also in late LAMP1/Rab7 positive endosomes/lysosomes as well as in recycling (Rab11 positive) endosomes. In this report, the association with these endosomal compartments was observed regardless of growth factor stimulation. Furthermore, combining super-resolution fluorescence and immunoelectron microscopy, endogenous cytoplasmic SPRY2 was shown to mainly associate with elements of the cytoskeleton such as vimentin (Hausott et al., 2019). Similar observations were also made by Kim and co-workers (2007), which reported endogenous SPRY2 to be enriched in cytoplasmic puncta in both C2C12 and MIAPaCa-2 (human pancreatic tumour cells) cells. Intriguingly, in glioma cells, endogenous hSPRY2 was found to localise to the plasma membrane only following protein overexpression (Hausott et al., 2019). Different cell lines, experimental setup as well as differences in expression levels, might account for the different subcellular localisation detected for endogenous *versus* exogenous SPRY proteins.

In mouse brain, immunohistochemistry analyses revealed SPRY2 staining throughout the brain and in many neuronal structures, including the cell soma, proximal projections and growth cones (Aranda et al., 2008). SPRY2 has been shown to regulate BDNF (brain-derived neurotrophic factor) signalling in neurons and to control neurite outgrowth in both immature cerebellar granule neurons (CGN) (Gross et al., 2007) and PC12 cells, where neuritogenesis can be induced by both NGF and FGF (Gross et al., 2001; Yim et al., 2015).

Altogether, these findings highlight that mammalian SPRY proteins associate with several subcellular compartments and that their localisation can be further modified by growth factor stimulation. Although the role of the CRD in plasma membrane targeting has been well-documented, it is not clear whether this depends upon interaction of SPRYs with caveolin-1 and PIP₂ or S-acylation (Edwin et al., 2009).

Moreover, the subcellular localisation of SPRY proteins can be affected by other proteins. For instance, SPRY2 association with the plasma membrane ruffles was induced by the small GTPase Rac1 (Lim et al., 2002) and reduced by interaction with Tesk1, a protein kinase which constitutively relocates SPRY2 to vesicular structures, including endosomes (Chandramouli et al., 2008).

1.8.3 Regulation of RTK signalling by SPRY proteins

As mentioned before, SPRY proteins modulate RTK functions through negative feedback loops, in both developing and adult tissues (Kim and Bar-Sagi, 2004). Upon growth factor stimulation, RTKs undergo dimerisation, tyrosine autophosphorylation and receptor activation which is followed by the recruitment of several intracellular signalling molecules. These include the adaptor growth factor receptor bound protein-2 (Grb2), which is intrinsically associated to the guanine nucleotide exchange factor son of sevenless (SOS) and induces Ras protein to exchange GDP for GTP. Activated and GTP-bound Ras then relays the signal to the downstream MAPK cascade consisting of the three serine/threonine kinases: Raf1 (MAPKKK), MEK1/2 (MAPKK), and ERK1/2 (MAPK) which activate one another by sequential phosphorylation. This pathway is also referred to as the Ras-ERK or Ras-MAPK (Gschwind et al., 2004; Lemmon and Schlessinger, 2010).

While this signalling cascade relies on Ras proteins for MAPK activation, other highly-conserved signalling pathways independent from Ras also exist, including the PI3K-AKT and PLC γ signalling pathways (Lemmon and Schlessinger, 2010). In the phosphoinositide-3-kinase (PI3K)-AKT/PKB (protein kinase B) cascade, activated RTKs recruit PI3K which mediates the conversion of plasma membrane PIP₂ to phosphatidylinositol (3,4,5)-trisphosphate (PIP₃). PIP₃ is then recognised and bound by the PH domain of AKT (also known as protein kinase B, PKB), which once in plasma membrane undergoes phosphorylation at Thr-308 and Ser-473 (mediated by PDK1 and mTORC2, respectively) before activating numerous downstream targets. These include the mammalian target of rapamycin (mTOR) and the glycogen synthase 3 beta

(GSK3 β) (Hemmings and Restuccia, 2012). Alternatively, growth factor-mediated activation of RTKs leads to intracellular activation of phospholipase C gamma (PLC γ) which hydrolyses PIP₂ in the plasma membrane to generate inositol (1,4,5)-triphosphate (IP₃) and diacylglycerol (DAG). IP₃ then binds to specific receptors on the endoplasmic reticulum to release and increase intracellular levels of calcium ions (Ca²⁺). Together with DAG, Ca²⁺ activates downstream serine/threonine enzymes, including the protein kinase C (e.g. PKC β and PKC δ) family of proteins which directly target and activates Raf1, thus the downstream MAPK cascade (Lemmon and Schlessinger, 2010).

Both Ras-MAPK and PLC γ pathways culminate in the phosphorylation and activation of the kinase ERK. The following steps, common to both signalling pathways, involve the translocation of phospho-ERK to the nucleus, activation of several transcription factors (e.g. Myc and Fos) and regulation of specific growth factor-responsive genes, including *SPRY* (Lemmon and Schlessinger, 2010). Meanwhile, inactive *SPRY* proteins in the cytoplasm undergo activation and plasma membrane recruitment in response to growth factor signalling (Lim et al., 2000; Mason et al., 2004). Over the years, several studies have established mammalian *SPRY*s as negative modulators of FGF (Gross et al., 2001; Impagnatiello et al., 2001; Yusoff et al., 2002), VEGF (Impagnatiello et al., 2001), PDGF (platelet-derived growth factor) (Gross et al., 2001), NGF (Gross et al., 2001; Wong et al., 2002), GDNF (glial-cell line-derived growth factor) (Basson et al., 2005) and BDNF (Gross et al., 2007) signalling. In marked contrast, it is now accepted that *SPRY*s mainly act as positive modulators in the context of EGFR signalling (Rubin et al., 2003; Sasaki et al., 2001; Wong et al., 2002). Regardless of the outcome, *SPRY* proteins have been reported to interact with a myriad of signalling molecules downstream of activated RTKs (Edwin et al., 2009), thus complicating our understanding of their molecular mode of action which appears to be as varied as the cascade pathways they act upon (Fig. 1.7) (Cabrita and Christofori, 2008; Mason et al., 2006).

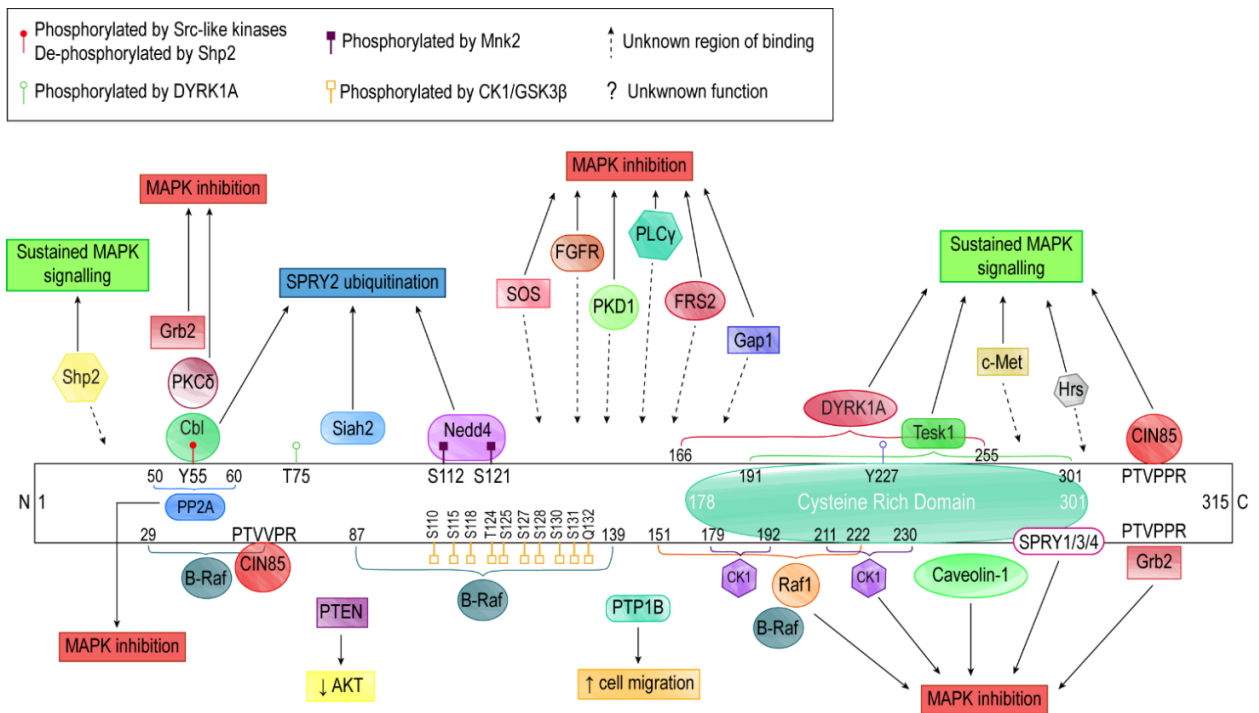


Figure 1.7 Schematic representation of hSPRY2 interactors

Schematic representation of the proteins that interact with hSPRY2 and the corresponding regions of binding. Raf1 (Sasaki et al., 2003), B-Raf (Brady et al., 2009), CIN85 (Haglund et al., 2005), Grb2 (Hanafusa et al., 2002; Lao et al., 2006) and CK1 (Yim et al., 2015) bind to more than one site on SPRY2. Siah2 (Nadeau et al., 2007) and Caveolin-1 (Cabrita et al., 2006) bind to the C- and N-termini of the protein, respectively, but their exact region(s) of binding is unclear. Therefore, in the figure, they are in proximity of their presumed binding site but no sequence is specified. Similarly, SPRYs (Ozaki et al., 2005) can form homo- as well as heterodimers *via* their CRD but the precise regions involved in these interactions are unknown, thus not specified in the figure. The interaction sites of proteins such as Shp2, SOS, FGFR, FRS2, Gap1 (Tefft et al., 2002), PKD1 (Chow et al., 2009), PLCγ (Akbulut et al., 2010), c-Met (Saini et al., 2018) and Hrs (Kim et al., 2007) are not known and thus indicated by dashed arrows. Although involved in SPRY2 function, the physical interaction between SPRY2 and PTEN (Edwin et al., 2006) or PTP1B (Yigzaw et al., 2003) has not been observed. The functional consequence of each interaction is represented as coloured boxes and indicated by solid arrows. The known phosphorylation sites are also represented, and the different colours refer to the different kinases and phosphatases that modify these sites (refer to the figure legend). Figure adapted from (Edwin et al., 2009).

(i) FGF signalling

Following FGF receptor activation, SPRY1 and SPRY2 (Hanafusa et al., 2002), but not SPRY4 (Mason et al., 2004), rapidly undergo phosphorylation at their highly conserved N-terminal tyrosine residue mediated by kinases belonging to the Src-family of proteins (Hanafusa et al., 2002; Mason et al., 2004), including Src itself (Li et al., 2004). Notably, this residue is found in a larger region, containing other conserved amino acids and resembling an SH2-binding motif (Fong et al., 2003; Hanafusa et al., 2002; Sasaki et al., 2001). In agreement with this, phosphorylation of Y53 in *Xenopus* SPRY1 (xSPRY1) or Y55 in mSPRY2 generates a docking site for the SH2 domain of Grb2, thereby interfering with the binding of Grb2 to either FGF-receptor substrate-2 (FRS2) or Shp2 phosphatase (SH2 domain-containing protein tyrosine phosphatase-2). *In vitro*, a phosphopeptide, mimicking Y55 phosphorylation and encompassing mSPRY2 residues 52-59, competed with FRS2, Shp2 and full-length mSPRY2 for binding to Grb2. The same phosphopeptide was also able to inhibit ERK activation in C2C12 and COS-7 cells (Hanafusa et al., 2002). Since FRS2 and Shp2 are required for the recruitment of Grb2-SOS complex to FGFR and downstream activation of Ras, it was suggested that by sequestering Grb2, SPRY1/2 would directly prevent downstream activation of Ras (Hanafusa et al., 2002). The importance of the highly conserved tyrosine residue in both FGF and EGF signalling is further highlighted by the observation that mutation of Y53 and Y55 in SPRY1/4 and SPRY2, respectively, blocked their ability to inhibit FGFR signalling while leaving the EGFR cascade unaffected (Hanafusa et al., 2002; Li et al., 2004; Mason et al., 2004; Sasaki et al., 2001).

SPRY2 harbours a Pro-rich domain (PXXPXR motif) in its C-terminus that binds the N-terminal SH3 motif of Grb2 and is not conserved in other SPRY isoforms, perhaps accounting for the observation that SPRY2 is a stronger antagonist of FGF signalling than either SPRY1 or SPRY4 (Lao et al., 2006; Martínez et al., 2007; Yusoff et al., 2002). In unstimulated cells, the Pro-rich motif is cryptic and only becomes accessible following FGFR activation (Lao et al., 2006) and PP2A (protein phosphatase 2A)-mediated dephosphorylation of specific serine residues within the SRM of SPRY2,

including Ser-112 and Ser-115 (Lao et al., 2007). Binding of PP2A to a region surrounding Y55 (residues 50-60) was shown to directly compete with c-Cbl (further discussed later) and possibly SOS binding, thereby preventing Ras activation (Lao et al., 2006, 2007). SPRY2-Grb2 binding is also positively regulated by casein kinase 1 (CK1), which binds to regions 179-192 and 211-230 in a phosphorylation-dependent manner, and also phosphorylates SPRY2. CK1 has been suggested to act in concert with PP2A to activate SPRY2 in the FGF-ERK pathway (Yim et al., 2015). Conversely, dephosphorylation of serine residues, including Ser-115 is prevented by testicular protein kinase 1 (Tesk1) by directly interfering with SPRY2-PP2A binding. Irrespective of its kinase activity, Tesk1 also blocks Grb2 recruitment by SPRY2. Therefore, Tesk1 was suggested to act as negative regulator of SPRY2 by preventing ERK inactivation (Chandramouli et al., 2008).

It is important to note that there are some controversies regarding the interaction between SPRY and Grb2. For instance, one study reported that the SPRY2-Grb2 complex is constitutive rather than inducible, not dependent on Y55 phosphorylation and also not required for ERK inhibition following FGF treatments. This study used acute FGF stimulation (i.e. short-term FGFR signalling), whereas all previous studies discussed above used overexpressed FGFR (i.e. long-term FGFR signalling) which may account for the discrepancies (Martínez et al., 2007). Another report found that upon FGF2 and EGF stimulation, only SPRY1 (and not SPRY2, SPRY3 or SPRY4) bound to Grb2 (Ozaki et al., 2005), whereas others have not observed an interaction between SPRY1 and Grb2 (Gross et al., 2001; Lao et al., 2006). Furthermore, SPRY4 but not the other isoforms were reported to interact with SOS (Ozaki et al., 2005), whereas Tefft et al. (2002) reported binding between SPRY2 and SOS. Association between SPRY proteins and SOS was not observed by others (Gross et al., 2001; Hanafusa et al., 2002). Moreover, mSPRY2-FRS2 interaction was documented by Tefft et al. (2002), whereas both Yusoff et al. (2002) and Lao et al. (2006) could not detect such binding. SPRY proteins can also form homo- as well as hetero-oligomers by interacting through their CRDs (Hanafusa et al., 2002; Ozaki et al., 2005). It has been shown that interaction between SPRY1 and SPRY4 (FGF2-mediated) generates hetero-oligomers

that inhibit ERK activation more potently than other combinations. This highest inhibitory effect was suggested to relate to the ability of SPRY1-SPRY4 to sequester the Grb2-SOS complex hence efficiently suppressing FRS2 association and Ras activation (Ozaki et al., 2005).

SPRY proteins have also been suggested to exert their inhibitory effects at the level of Raf (Tefft et al., 2002; Yusoff et al., 2002), PLC γ (Akbulut et al., 2010) and PKC δ (Chow et al., 2009). As briefly mentioned above, mSPRY2-Raf binding is increased upon FGF10 stimulation (Tefft et al., 2002). In another study, the interaction of endogenous SPRY2 and SPRY4 with endogenous Raf1 was found to involve a specific region within the CRD, encompassing amino acids 151-222 and referred to as the "Raf-binding motif" (RBM). Intriguingly, this region is conserved from *D. melanogaster* to mammalian SPRY, suggesting that all isoforms can potentially bind Raf1 (Sasaki et al., 2003). Peptide-array experiments which employed B-Raf (a different isoform of Raf1), revealed the presence of two additional Raf binding domains in mSPRY2 (for a total of three, RBD1-3) located at positions 29-61 and 87-139, respectively. Also, the mSPRY2-B-Raf interaction was reported to be reduced by phosphorylation of Ser-111 and Ser-120, and to a lesser extent by phosphorylation of other four serine residues (i.e. Ser-7, Ser-42, Ser-140 and Ser-167) (Brady et al., 2009). Intriguingly, SPRY2 was found phosphorylated on all of these six serine residues in melanoma cells that harbour the oncogenic form of B-Raf V600E (Brady et al., 2009). As a consequence, SPRY2-B-Raf binding is disrupted leading to sustained B-Raf signalling and MAPK activation (Brady et al., 2009; Tsavachidou et al., 2004). In line with this, upon FGF treatments, a SPRY2 6A mutant (in which all of the six serine residues were simultaneously mutated to alanines) inhibited ERK activation more potently than wild-type protein (Brady et al., 2009). It was further proposed that at later time points from FGF stimulation, SPRY2 may undergo phosphorylation on specific residues in order to attenuate its own (inhibitory) activity (Brady et al., 2009). The interaction of SPRYs with PLC γ was initially documented by Akbulut et al. (2010). Similar to Grb2, phosphorylation of Y53 in SPRY1 or Y55 in SPRY2, promotes SPRY engagement with the SH2 domain of PLC γ (PLC γ 1 and PLC γ 2). Also, SPRY1-PLC γ

binding is induced by FGF and PDGF in HEK293T cells, and by hepatocyte growth factor (HGF) in IMCD3 cells (Akbulut et al., 2010). At a functional level, the association of SPRY1/2 with PLC γ correlated with reduced PLC γ phosphorylation and activity, decreased IP $_3$ and DAG production as well as reduced Ca $^{2+}$ mobilisation. This resulted in reduced NFAT activity, one of the main transcription factors modulated by Ca $^{2+}$ -mediated signalling. Upon SPRY1 overexpression, reduced PKC δ phosphorylation was also observed, which was suggested to relate to the reduced PLC γ activity (Akbulut et al., 2010).

In PC-3 cells and upon FGF2 stimulation, SPRY2 was reported to bind endogenous PKC δ in a phospho-Y55-dependent manner. However, instead of recognising Y55 or surrounding motifs, PKC δ interaction is promoted by conformational changes (induced by Y55 phosphorylation) (Chow et al., 2009). Furthermore, by forming a trimeric complex with both PKC δ and its substrate protein PKD1 (protein kinase D1), SPRY2 was shown to directly interfere with the transfer of phosphate groups from PKC δ to PKD1. This ultimately results in reduced phospho-PKD1. In the same study, neither SPRY1 nor SPRY4 were found able to bind PKC δ (Chow et al., 2009).

Altogether, these findings highlight the existence of several mechanisms through which SPRY proteins modulate FGF receptor signalling, which may act in concert, separately or even in parallel. A summary is provided in Figure 1.8.

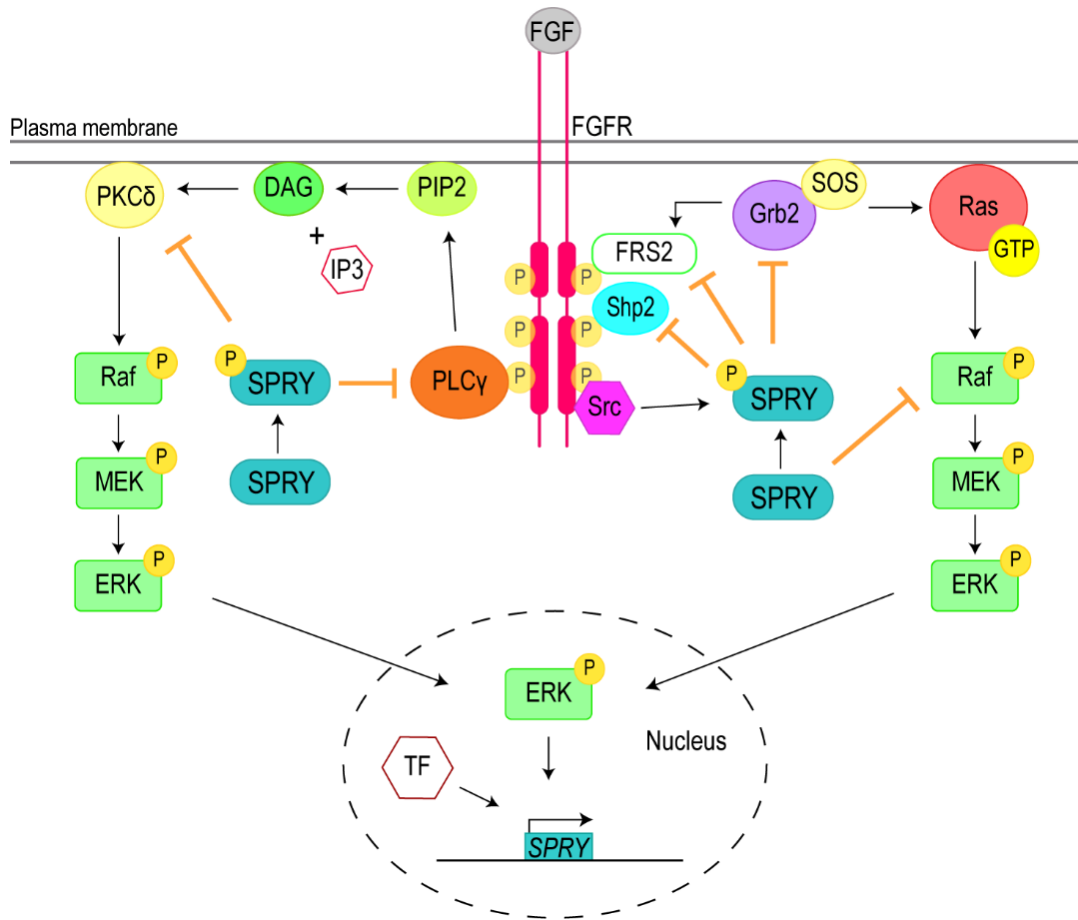


Figure 1.8 Modulation of FGF signalling by SPRY proteins

Schematic representation of the molecular events triggered downstream of activated FGF receptors. Both PLCγ (*on the left*) and Ras-MAPK (*on the right*) signalling cascades result in ERK activation (i.e. phospho-ERK) and transcriptional upregulation of target *SPRY* genes. In the cytoplasm, following phosphorylation of the highly conserved tyrosine, SPRY proteins inhibit a number of signalling molecules. Raf inhibition is independent of phospho-Tyr. SPRY outcomes are represented by orange arrows.

(ii) EGF signalling

Like FGFR, stimulation of EGFR leads to phosphorylation of the highly conserved tyrosine residue in both SPRY1 and SPRY2 (Hall et al., 2003; Hanafusa et al., 2002; Rubin et al., 2003). However, in the context of EGF signalling, this event leads to the interaction of SPRY2 with the SH2 domain of the E3 ubiquitin ligases c-Cbl and b-Cbl (Fong et al., 2003; Rubin et al., 2003; Wong et al., 2001). Physiologically, c-Cbl promotes polyubiquitination and subsequent degradation of activated EGF receptors, thereby downregulating the Ras-MAPK cascade pathway. The binding of SPRY2 to c-Cbl directly competes with the binding of c-Cbl to EGFR, leading to inhibition of EGFR internalisation/degradation and therefore sustained EGF-mediated signalling (Egan et al., 2002; Rubin et al., 2003; Wong et al., 2002). The association between SPRY2 and c-Cbl was suggested to be constitutive and to involve two binding domains on both proteins. In unstimulated cells, the amino terminal region of SPRY2 (residues 36-53 of hSPRY2) weakly binds to the RING-finger domain of c-Cbl (Wong et al., 2001). Following growth factor stimulation, this interaction becomes tighter because of phosphorylation of Tyr-55 (Fong et al., 2003), which is specifically recognised by the TKB domain of c-Cbl (Ng et al., 2008), resulting in SPRY2 polyubiquitination and subsequent degradation by the 26S proteasome (Hall et al., 2003).

The mechanism by which SPRY2 prevents EGFR internalisation has been suggested to involve the protein CIN85 (Cbl-interacting protein of 85 kDa). CIN85 is an endocytic adapter that mediates endocytosis and degradation of activated EGF receptors together with c-Cbl. In a study by Haglund et al. (2005), two Pro-rich motifs in SPRY2, located at the amino and carboxyl-terminal ends of the protein (the latter being the same motif that mediates Grb2 interaction) were shown to bind two SH3 domains in CIN85. This resulted in the formation of a ternary complex which also included c-Cbl, bound to both SPRY2 and CIN85, and inhibition of EGFR endocytosis. In the same study, SPRY4 which cannot bind CIN85 was found unable to sustain EGF signalling (Haglund et al., 2005). A later study described that hSPRY2 also specifically interferes with the trafficking of activated EGFR from early to late endosomes through a

mechanism independent from c-Cbl and involving the interaction of hSPRY2 with Hrs (hepatocyte growth factor-regulated tyrosine kinase substrate). The binding of hSPRY2 to Hrs was shown to prevent the interaction of Hrs with Tsg101 (tumour-susceptibility gene 101) which is directly implicated in the sorting of EGFR from early to late endosomes. As a result, activated EGFR was retained in early endosomes and accumulation of active ERK in late endosomes was also prevented, thus resulting in sustained ERK signalling (Kim et al., 2007).

It is currently unclear how SPRY proteins distinguish between activated FGF and EGF receptors. In one report, Tyr-227 in SPRY2 was found to undergo phosphorylation following FGF, but not EGF, stimulation. Phosphorylation at this site, and possibly also at Tyr-269 and Tyr-283, was shown to be important for MAPK inhibition, potentially providing a molecular mechanism by which SPRY2 can effectively differentiate between FGFR and EGFR signalling pathways (Rubin et al., 2005). Intriguingly, hSPRY1 and hSPRY2 were found to act as positive as well as negative regulators in the context of EGFR signalling. While the N-terminal end (residues 1-172 of hSPRY2) of the protein would enhance EGF signalling by c-Cbl sequestration, the C-terminus (residues 176-315 of hSPRY2) would repress the same pathway *via* unidentified mechanisms (Egan et al., 2002).

In this context, it is also worth noting that hSPRY2 has been reported to inhibit AKT (also known as protein kinase B, PKB) *via* a mechanism involving PTEN (tumour suppressor phosphatase and tensin homologue deleted on chromosome 10) in response to EGF. The PI3K-AKT signalling pathway acts downstream of activated EGFR and directly regulates cellular proliferation (Kawazoe and Taniguchi, 2019). PTEN inhibits the PI3K-AKT cascade by converting PIP₃ back to PIP₂. In both HeLa cells and primary mouse embryonic fibroblasts (PMEF), expression of hSPRY2 reduced the amount of phosphorylated PTEN (corresponding to the inactive form of the protein) while increasing the overall intracellular levels of PTEN, thereby antagonising the PI3K-AKT signalling cascade (Edwin et al., 2006). A summary is provided in Figure 1.9.

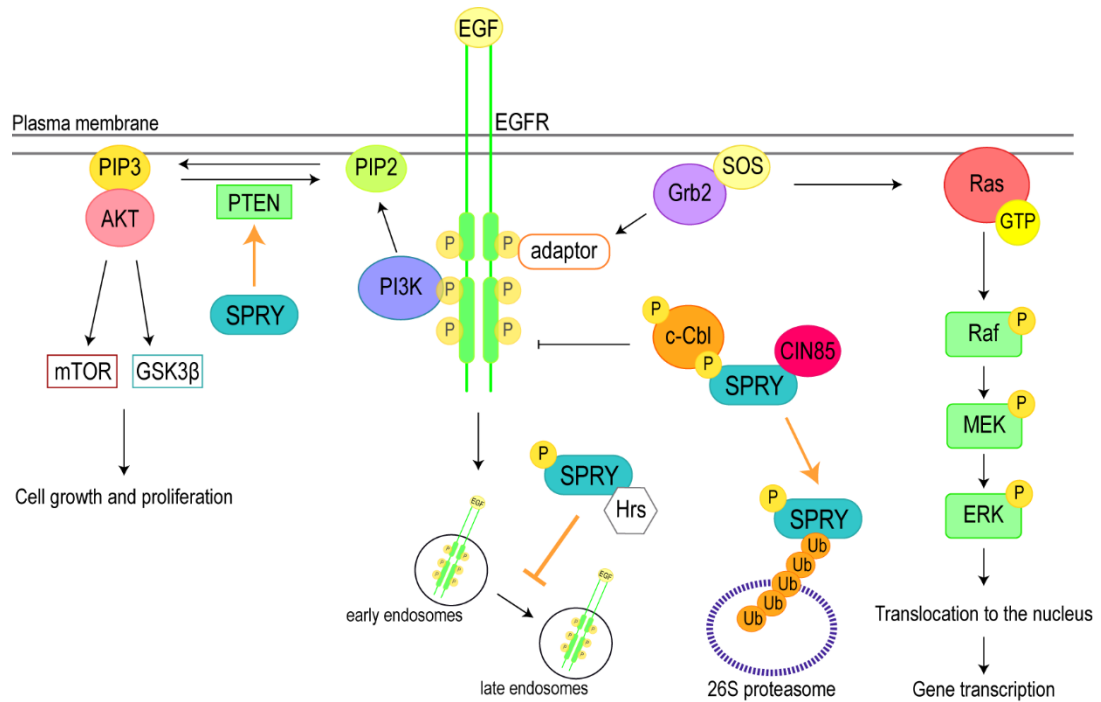


Figure 1.9 Modulation of EGF signalling by SPRY proteins

Schematic representation of the molecular events triggered downstream of activated EGFR. Following phosphorylation of the highly conserved tyrosine, SPRY directly competes with EGFR for binding to c-Cbl. By interacting with c-Cbl, SPRY undergoes polyubiquitination and subsequent degradation by the proteasome. Inhibition of EGFR internalisation also involves the interaction of SPRY with CIN85 and the formation of a c-Cbl-SPRY-CIN85 ternary complex. SPRY-Hrs binding interferes with the trafficking of activated EGFR from early to late endosomes. The net result of these events is sustained EGF signalling (*on the right*). In contrast, following EGFR activation SPRY antagonises PI3K-AKT signalling *via* a mechanism involving PTEN (*on the left*). SPRY outcomes are represented by orange arrows.

(iii) VEGF signalling

In endothelial cells, binding of VEGF to the corresponding VEGF receptors can lead to Ras-independent activation of Raf1 *via* the PLC γ signalling cascade (Cabrita and Christofori, 2008; Kim and Bar-Sagi, 2004; Mason et al., 2006). Inhibition of this pathway by SPRY proteins occurs through mechanisms that are independent of the highly conserved N-terminal tyrosine residue. In fact, a SPRY4 Y53A mutant, as well as a protein lacking the first 80 amino terminal residues (SPRY4 Δ N80), retained the ability to antagonise VEGF-mediated signalling, whereas the same mutants failed to inhibit either FGF or EGF-mediated activation of ERK. In marked contrast, a SPRY4 Δ CR (i.e. lacking the CRD) could not antagonise VEGF-dependent activation of ERK and this domain was required for SPRY4-Raf1 binding. Furthermore, endogenous SPRY2 and SPRY4 interact with endogenous Raf1 in response to VEGF, interfering with Raf1 phosphorylation and thus blocking MAPK signalling at this point (Sasaki et al., 2003) (Fig. 1.10).

Altogether, these observations highlight the overall complexity of SPRYs mode of action which is coordinately regulated by intricate intermolecular interactions and post-translational modifications (Edwin et al., 2009; Kim and Bar-Sagi, 2004).

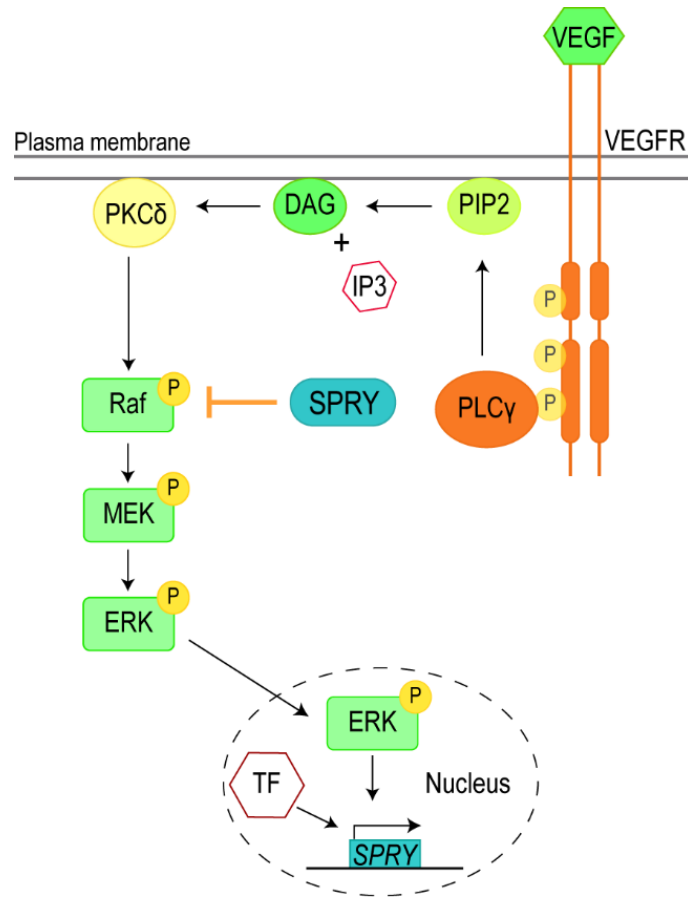


Figure 1.10 Modulation of VEGF signalling by SPRY proteins

Schematic representation of the molecular events triggered downstream of activated VEGFR. SPRY inhibits VEGF signalling by binding to Raf and *via* mechanisms independent of phosphorylation of the highly conserved N-terminal tyrosine. The inhibition of Raf by SPRY is represented by an orange arrow.

1.8.4 Regulation of SPRY proteins by post-translational modifications (PTMs)

As highlighted in the previous section, the activity of SPRY proteins is controlled by several proteins, many of which are linked to post-translational modifications, including E3 ubiquitin ligases (Wong et al., 2001), protein kinases (Sasaki et al., 2003; Tefft et al., 2002) and phosphatases (Lao et al., 2007).

Besides c-Cbl mediated ubiquitination and degradation (discussed in the context of the EGFR signalling), SPRYs are recognised by other ubiquitin ligases, such as seven-in-absentia homolog-2 (Siah2) (Nadeau et al., 2007) and Nedd4 (Edwin et al., 2010). For instance, SPRY2 interacts with the RING finger domain of Siah2 (residues 66-153) through its N-terminal domain and independently of phosphorylation at Tyr-55. Overexpression of Siah2 in COS-7 cells results in proteasomal degradation of SPRY1, SPRY2 and to a lesser extent of SPRY4 (Nadeau et al., 2007). SPRY1 and SPRY2, but not SPRY3 and SPRY4, were found to constitutively associate with Nedd4, a HECT domain-containing E3 ubiquitin ligase. Endogenous Nedd4 ubiquitinates and regulates the cellular content of SPRY2; phosphorylation of Ser-112 and Ser-121 in hSPRY2 is absolutely required for the interaction of hSPRY2 with the WW domains of this ligase and serine-to-alanine substitutions at these sites completely abolished SPRY2-Nedd4 binding (Edwin et al., 2010). As phosphorylation at Ser-112/121 was previously reported to negatively affect binding of SPRY2 to B-Raf (Brady et al., 2009), it was further suggested that upon phosphorylation of these serines, SPRY2 would switch its interaction from B-Raf to Nedd4 (Edwin et al., 2010). Furthermore, phosphorylation at Ser-112/121 interferes with c-Cbl binding by negatively regulating phosphorylation at Tyr-55. In the same study, the protein kinase Mnk1 (mitogen-activated protein kinase-interacting kinase 1) was identified as important for phosphorylation of Ser-112/121 (DaSilva et al., 2006). However, a later study by Edwin et al. (2010) argues that the isoform involved is Mnk2 and not Mnk1 as only silencing Mnk2 (using specific siRNA) results in reduced SPRY2-Nedd4 interaction.

Interestingly, phosphorylation of hSPRY2 on Ser-112 and Ser-121 correlates with a band-shift, which can be detected as a slower migrating band in SDS-PAGE (DaSilva et al., 2006). In addition to these residues, phosphorylation at Ser-110, Ser-115, Ser-

118, Thr-124, Ser-125, Ser-127, Ser-128, Ser-130, Ser- 131 and Glu-132 also contributes to the band-shifting of SPRY2. Most of these residues were shown to be phosphorylated in resting cells, most likely by kinases such as CK1/2 or GSK3 β , and to undergo growth-factor mediated dephosphorylation (as shown for Ser-112/115) by specific phosphatases (e.g. PP2A), thereby promoting SPRY2 activation. However, the individual physiological relevance of most of these sites remains to be established (Lao et al., 2007).

The activity of SPRY2 can also be regulated by the protein kinase DYRK1A (dual specificity tyrosine phosphorylation regulated kinase 1A). SPRY2-DYRK1A interaction was mapped at region 166-255 of SPRY2 and amino acids 600-616 in DYRK1A and resulted in phosphorylation of Thr-75 in SPRY2. Following FGFR activation, phosphorylation of Thr-75 by DYRK1A attenuated the inhibitory effects of SPRY2 on MAPK signalling (Aranda et al., 2008). Similarly, the kinase Tesk1 was suggested to act as a negative regulator of SPRY2 by preventing its interaction with Grb2 (Chandramouli et al., 2008). In contrast, the activity of CK1 was suggested to promote SPRY2 activation in the context of both FGF and NGF signalling and binding of CK1 to SPRY2 was mapped at two distinct regions in SPRY2 (amino acids 179-192 and 211-230 for CK1 ϵ and CK1 δ) (Yim et al., 2015). Thus, it was suggested that while DYRK1A and Tesk1 phosphorylate the inactivation sites in SPRY2, CK1 (and maybe CK2 and GSK3 β) is responsible for phosphorylation of the activation sites (Lao et al., 2007; Yim et al., 2015).

Shp2 has been shown to mediate de-phosphorylation of the conserved tyrosine residues (Y53 and Y55) in SPRY1 and mSPRY2, thereby returning SPRY proteins to their unphosphorylated and inactive state (Hanafusa et al., 2004). Although the interaction between SPRY2 and Shp2 was reported to be decreased upon FGF10 stimulation in lung epithelial cells (Tefft et al., 2002), another study showed that SPRY1-Shp2 interaction was instead increased by activated FGFR3 in HEK293 cells (Jarvis et al., 2006). Whether these discrepancies arise from different experimental setup or whether they reflect the different behaviour of SPRY1 *versus* SPRY2 is unclear. In contrast to Shp2, the phosphatase PP2A was shown to augment SPRY2

activity by directly competing with c-Cbl binding (Lao et al., 2007). Thus, it is possible that the intracellular levels of Shp2 and PP2A dynamically modulate the on/off status of SPRY proteins in the context of FGF signalling.

Moreover, hSPRY2 was shown to increase the amount of soluble protein tyrosine phosphatase 1B (PTP1B), resulting in decreased tyrosine phosphorylation of cellular proteins while promoting the anti-migratory effects of SPRY2. However, SPRY2-PTP1B interaction has not been directly observed and the molecular mechanism by which SPRY2 increases the cytosolic content of PTP1B remains unknown (Yigzaw et al., 2003).

Furthermore, both SPRY1 and SPRY2 were shown to be S-acylated, and S-acylation was further suggested to account for the membrane localisation of SPRY proteins reported by (Impagnatiello et al., 2001) as well as by others (Tefft et al., 2002). However, whether S-acylation of SPRY proteins is a dynamic process that can be further modulated by growth factors is currently unknown.

1.9 SPRY proteins and development

The same studies that established *D. melanogaster* SPRY as a general inhibitor of the RTKs also recognised a key role for dSPRY in branching morphogenesis and development (Hacohen et al., 1998; Minowada et al., 1999).

Likewise, during vertebrate organogenesis SPRY proteins play a crucial role by regulating temporal and spatial activation of RTK signalling cascades. In both mouse and chick embryos, from gastrulation to mid-gestation, *SPRY1*, *SPRY2*, and *SPRY4* transcripts could be detected in highly restricted clusters, corresponding to bud-forming regions and characterised by high levels of FGF (Minowada et al., 1999). At later development stages, *SPRY* expression was found in almost all adult tissues, including the brain, heart, lung, kidney and skeletal muscles (Minowada et al., 1999). In contrast, *SPRY3* expression was restricted to adult brain and testis, with no transcripts detected in embryos (Minowada et al., 1999). Furthermore, different growth factors can modulate *SPRY* expression in distinct tissues. For instance, FGF8

induced *SPRY2* expression within the neuronal tube in chick embryos (Chambers et al., 2000), whereas in mouse embryonic lung explant culture, FGF10 upregulated the expression of *mSPRY2* mRNA in adjacent epithelial tips (Mailleux et al., 2001).

The importance of SPRY proteins in development and branching morphogenesis is further underscored by several mouse models, in which *SPRY* genes have been either mutated or deleted. *SPRY1*^{-/-} mice embryos are characterised by supernumerary ureteric buds and develop extra ureters and kidneys. These phenotypes can be rescued by reducing GDNF dosage (*SPRY1*^{-/-}; *Gdnf*^{+/-} mice) highlighting that during genitourinary development, SPRY1 regulates GDNF related pathways (e.g. GDNF-Ret-Wnt11) (Basson et al., 2006, 2005). Interestingly, SPRY1 knock-in mice, bearing a tyrosine-to-alanine substitution at position 53, display developmental deficits identical to those of *SPRY1*-null mice, suggesting that the SPRY1 Y53A mutation also inactivates SPRY1 *in vivo* (Vaquero et al., 2019).

SPRY2^{-/-} mice are characterised by severe hearing impairment due to abnormalities in the organ of Corti where a Deiter's cell is transformed into a pillar cell, resulting in an additional tunnel of Corti. These phenotypes are partially rescued by reducing *FGF8* gene dosage, linking SPRY2 to this pathway during ear development (Shim et al., 2005). A different *SPRY2*-null mouse displayed gastrointestinal defects and enteric nerve hyperplasia, suggesting aberrant activation of the GDNF-Ret pathway, similar to *SPRY1*^{-/-} mutants (Taketomi et al., 2005). Furthermore, *SPRY2* knockout is accompanied by reduced lifespan with mice usually dying within six weeks (Shim et al., 2005; Taketomi et al., 2005). Also, SPRY1 and SPRY2 are essential for normal development of external genitalia and *SPRY1*^{-/-}; *SPRY2*^{-/-} embryos lack internal tubular urethra and show abnormal urethral epithelium. Interestingly, these defects only occur in males, suggesting that SPRY proteins might play a key role in sexual dimorphism (Ching et al., 2014). Moreover, loss of function of either *SPRY2* (i.e. *SPRY2*^{-/-}) or *SPRY4* (i.e. *SPRY4*^{-/-}), resulted in supernumerary teeth in a region usually toothless (called the diastema) and susceptible to FGF4/FGF9 signalling (Klein et al., 2006). Furthermore, double *SPRY2*^{-/-}; *SPRY4*^{-/-} mutations are embryonically lethal with embryos displaying severe craniofacial, limb and lung abnormalities (Taniguchi

et al., 2007). In addition, *SPRY2* deficient mice also exhibited cleft palate and expressed higher levels of FGF target genes, such as *Msx1*, *Etv5* and *Ptx1* (Matsumura et al., 2011). In *SPRY1-SPRY2* double knockout mice, specific mandibular structures (e.g. glenoid fossa) are absent and this was shown to relate to hyperactivation of FGFR4 signalling (Purcell et al., 2012). Interestingly, overexpression of *SPRY2* during specific developmental stages in chick embryos also resulted in craniofacial defects, such as cleft palate and facial clefting, suggesting that overexpression of *SPRY2* may mimic *SPRY* deficiency (Goodnough et al., 2007). Similar facial abnormalities were found in *SPRY1; Wnt1-Cre* mouse embryos in which *SPRY1* expression was specifically forced in the neuronal crest resulting in disrupted patterning of key craniofacial marker genes, including *Msx1*, *Msx2*, *Dlx5* and *Dlx6*. *SPRY1; Wnt1-Cre* mice also displayed serious cardiac defects, suggesting an important role for *SPRY1* in both craniofacial and cardiac morphogenesis (X. Yang et al., 2010).

SPRY4-null mice were shown to be characterised by growth retardation and defects in digits and forelimbs (fused and duplicated, polysyndactyly), resembling the hyperactivation of FGF signalling (Taniguchi et al., 2007). To date, no *SPRY3* knockout mouse has been generated.

1.10 *SPRY2* and tumorigenesis

As inappropriate activation of growth factor signalling can stimulate excessive cell growth and tumorigenesis, it is not surprising that deregulation of *SPRY* proteins has been reported in a wide range of malignancies (Masoumi-Moghaddam et al., 2014).

SPRY2 has a well-established function as a tumour suppressor protein and indeed, its expression is reduced in several tumours. These include renal cell carcinoma, hepatocellular carcinoma, gastric cancer, non-small-cell lung carcinoma, B-cell lymphoma and chronic lymphocytic leukaemia, epithelial ovarian cancer, breast cancer and prostate cancer. Furthermore, low expression of *SPRY2* also correlates with poorer prognosis in some of these malignancies. Interestingly, there is also evidence that *SPRY2* has oncogenic activity, and its upregulation is associated with

poor prognosis in glioblastoma patients. Furthermore, the role of SPRY2 in colorectal cancer is still controversial with some findings reporting protein upregulation and others downregulation (Table 1.3) (Kawazoe and Taniguchi, 2019; Masoumi-Moghaddam et al., 2014).

Cancer type	SPRY2 expression
Renal cell carcinoma	↓ (Wang et al., 2017)
Hepatocellular carcinoma	↓ (Fong et al., 2006; Sirivatanauksorn et al., 2012)
Pancreatic cancer	↓ (Zhao et al., 2018)
Gastric cancer	↓ (Xu et al., 2018)
Colorectal cancer	↓ (Feng et al., 2011); ↑ (Holgren et al., 2010)
Prostate cancer	↓ (Fritzsche et al., 2006)
Breast cancer	↓ (Lo et al., 2004)
Epithelial ovarian cancer	↓ (Masoumi-Moghaddam et al., 2015)
Endometrial carcinoma	↓ (Velasco et al., 2011)
Melanoma	↓ (Tsavachidou et al., 2004); ↑ (Bloethner et al., 2005)
Non-small-cell lung carcinoma	↓ (Sutterlüty et al., 2007)
Sarcoma tumours	↑ (Baird et al., 2005; Lito et al., 2008; Saini et al., 2018; Schaaf et al., 2010); ↓ and ↑ (Rathmanner et al., 2013)
B-cell lymphoma	↓ (Frank et al., 2009)
Chronic lymphocytic leukaemia	↓ (Shukla et al., 2016)
Multiple myeloma	↓ (Wang et al., 2015)
Glioblastoma multiforme	↓ (Kwak et al., 2011); ↑ (Walsh et al., 2015)

Table 1.3 Expression of SPRY2 in various human cancer types

1.10.1 SPRY2 and prostate cancer (PC)

Prostate cancer (PC) is one of the most common types of tumour in men and the implication of SPRY proteins in this malignancy has been known for almost fifteen years. Metastatic prostate cancer is often treated by surgical or medical castration to reduce the androgen levels (androgen deprivation therapy, ADT) that drive tumour

growth. However, the majority of patients subsequently develop castration-resistant prostate cancer (CRPC), a lethal stage of the disease involving molecular pathways both dependent and independent of androgen receptors (AR) (Patel et al., 2018).

Early studies by McKie et al. (2005) revealed that *SPRY2* mRNA expression is reduced in both invasive prostate cancer cell lines (e.g. LNCaP and the PC3 derivative lines PC-3M, PC-3MLN4 and PC-3MPRO4) and high-grade clinical prostate cancer, compared to benign prostatic hyperplasia (BPH) as well as better differentiated tumours. *SPRY2* expression is increasingly reduced passing from low- to moderate- to high-grade prostate cancer. Furthermore, in 76-82% of high-grade prostate cancers, the *SPRY2* promoter was found to be extensively hypermethylated and treatments of PC cells with agents that relieve DNA methylation (5-aza-2'-deoxycytidine) restored *SPRY2* expression. Therefore, epigenetic inactivation was suggested to be one of the mechanisms implicated in *SPRY2* downregulation in PC (McKie et al., 2005). Subsequent analysis of microarray containing micro-dissected prostate carcinoma specimens found downregulation of both *SPRY1* and *SPRY2* genes. However, no hypermethylation of the *SPRY2* CpG islands was observed in any of the PC cell lines investigated and *SPRY2* downregulation was suggested to occur independently of DNA methylation (Fritzsche et al., 2006). Genomic profiling of 218 prostate tumours further revealed that (i) *SPRY2* levels are either decreased or lost in 18% of primary tumours and 74% of metastatic cancers, (ii) PTEN is inactivated in 4% of primary and 42% of invasive cancers, and (iii) Ras-ERK and PI3K-AKT pathways are also altered in 42-43% of primary and 90-100% of metastatic tumours (Taylor et al., 2010).

The role of SPRY proteins in the development and progression of prostate cancer has been further corroborated by *in vivo* studies. Concomitant deletion of *SPRY1* and *SPRY2* in mouse prostate epithelium resulted in hyperactivation of Ras-ERK signalling (increased phospho-MEK) which occasionally caused prostatic intraepithelial neoplasia (PIN); a pre-malignancy of the prostate. Further inactivation of *Pten* (in addition to *SPRY1* and *SPRY2*-loss of function) accelerated PIN and promoted transition to a more invasive phenotype through modulation of both Ras-ERK and PI3K-AKT pathways (Schutzman and Martin, 2012). In another report, *Pten*^{+/-}; *SPRY2*^{+/-}

mice were shown to develop metastatic prostate cancer and to be characterised by PI3K-AKT hyperactivation. Importantly, targeting of this pathway with PI3K inhibitors (e.g. PI103), inhibited the development of nodal metastasis *in vivo*. At the molecular level, loss of SPRY2, accompanied by partial inactivation of PTEN, was shown to correlate with sustained RTK signalling (e.g. EGFR and HER2) and nuclear accumulation of MAPK p38, ultimately promoting tumour survival. However, following complete loss of PTEN, RTKs, such as EGFR and HER2, underwent proteasomal degradation with this event leading to EGFR/HER2 resistant tumours (Gao et al., 2012). More recently, SPRY2 deficiency has been also implicated in castration-resistant phenotypes. In this case, hyperactivation of the HER2-p38 cascade resulted in an increase of interleukin 6 (IL6) at both tumour and systemic level. IL6 increases cholesterol biosynthesis and lipolysis at the systemic level, whereas in tumour cells the content of cholesterol receptors SRB1 (an HDL receptor) and androgen biosynthetic enzymes (i.e. HSD3B1) are augmented. These events result in increased androgen biosynthesis. Thus, loss of SPRY2 and subsequent activation of HER2-IL6 pathways are particularly relevant in the context of AR-dependent castration-resistant prostate cancer (which depend upon androgen). However, anti-IL6 treatments correlate with increased metastases in mouse models. In marked contrast, reducing circulating cholesterol (by statins) or its cellular uptake (by specific targeting of SRB1 receptors) have been suggested to be far more promising approaches (Patel et al., 2018).

In an elegant study, Patel et al. (2013) further elucidated the key role played by SPRY2, PTEN and PP2A in determining prostate cancer progression. Using a combination of *in vivo* and *in vitro* experiments, it was shown that while knockdown (KD) of SPRY2 leads to the activation of both Ras-ERK and PI3K-AKT signalling pathways, this event *per se* is not sufficient to drive tumorigenesis. In fact, loss of SPRY2 activates several downstream tumour suppressor proteins, including PTEN, PP2A, GSK3 β , TP53 (tumour protein p53) and ROS (reactive oxygen species) resulting in growth arrest. Briefly, lack of SPRY2 results in nuclear accumulation of PTEN, which interacts with and stabilises TP53 to arrest cells at G1. In parallel, hyperactivation of

RTK also increases intracellular ROS, leading to the activation of PP2A. PP2A mediates GSK3 β -dependent phosphorylation of PTEN, promoting its nuclear accumulation. As a consequence, PP2A downregulation drives tumour progression when SPRY2 levels are reduced. In agreement with this, 19% of primary prostate cancers were reported to exhibit decreased expression of PP2A-A subunit (which is the one involved in GSK3 β binding). Such a complex network also suggests that loss of SPRY2 might represent an early event in prostate cancer, whereas inactivation of PTEN, PP2A and TP53 might occur at later stages to allow invasive carcinogenesis (Patel et al., 2013).

Taken together, these studies highlight that SPRY2 plays a central role during prostate cancer progression and also support a potential role as early prognostic marker.

1.10.2 SPRY2 and glioblastoma multiforme (GBM)

Glioblastoma multiforme (GBM) is the most common brain tumour in adults and is characterised by high invasiveness. Once diagnosed, the available treatments often combine surgical removal with radiotherapy and chemotherapy. However, the average survival remains extremely low with a life expectancy of just 12 to 15 months. Despite early findings suggesting a tumour suppressor function for SPRY2 in malignant gliomas, accumulating evidence indicates that SPRY2 may instead promote GBM proliferation and progression, thus acting as an oncogene (Hausott and Klimaschewski, 2019).

In initial studies, SPRY2 levels were found to be decreased in 79.7% of invasive (World Health Organisation grades II-IV) human gliomas, but not in non-invasive (World Health Organisation grade I) gliomas and normal tissues. This was suggested to relate to post-transcriptional downregulation of SPRY2 by the microRNA miR-21 in U87MG glioma cells as well as in glioma tissues (in which SPRY2 levels inversely correlate with miR-21). Therefore, SPRY2 was suggested to act as tumour suppressor in malignant gliomas and to play an important role in tumour progression (Kwak et al., 2011).

The oncogenic activity of SPRY2 was reported for the first time by Walsh and colleagues who observed functionally meaningful levels of SPRY2 protein in both

glioblastoma primary samples and cell lines (Walsh et al., 2015). Intriguingly, depletion of SPRY2 in those GBM cells characterised by high levels of SPRY2 (e.g. U251, U118MG, and U87MG cells), resulted in reduced proliferation and colony formation as well as increased sensitivity to drugs that inhibit EGFR and c-MET (the receptor for EGF and HGF, respectively). It was suggested that SPRY2 might somehow act in concert with both MAPK p38 and JNK to promote cell proliferation, invasion and drug resistance (Walsh et al., 2015). The importance of SPRY2 expression *in vivo* was further validated by mouse xenograft models. Mice injected with GBM cells (U87MG-L) with SPRY2 knockdown developed smaller tumours than mice injected with wild-type GBM cells (i.e. expressing SPRY2) (Walsh et al., 2015). Further analyses of human glioblastoma tissues revealed that SPRY2 is expressed in both EGFR variant III (EGFRvIII)-positive and EGFRvIII-negative tumours, the two most common types of glioblastoma tumours (Walsh et al., 2015). Interestingly, *SPRY2* mRNA was found to be upregulated in EGFRvIII tumours (the most aggressive type) and to positively correlate with reduced patient survival (Walsh et al., 2015). Conversely, patients with low *SPRY2* mRNA have a better clinical outcome and prolonged survival rates (Park et al., 2018; Walsh et al., 2015).

High expression of SPRY isoforms (SPRY1, SPRY2 and SPRY4) and low expression of PTEN and neurofibromin 1 (NF1) are also associated with diffuse gliomas and reduced overall survival (Zhang et al., 2016). High SPRY2 expression has been further observed by Park et al. (2018) in GBM microarray gene expression profiles as well as in transcriptomic analysis of 19 different cancers. Among the analysed tumours GBM expressed the highest levels of *SPRY2*. The high mRNA expression was shown to positively correlate with protein levels (Park et al., 2018). In agreement with the study of Walsh et al. (2015), depletion of SPRY2 in GBM cells (KD U87) or in patient-derived GBM stem cells (KD GSC), inhibited cell proliferation while increasing cell death, compared to normal astrocytes. These phenotypes were suggested to relate to increased activation of both ERK and AKT, leading to DNA damage and cells entering S-phase prematurely (Park et al., 2018). Furthermore, xenograft mouse models in which SPRY2 expression can be dampened through a doxycycline-inducible SPRY2-

shRNA displayed reduced tumour volume and longer survival than control animals in which SPRY2 is steadily expressed (Park et al., 2018). On the other hand, *in vivo* overexpression of SPRY2 (U251 SPRY2 OE mice) resulted in increased tumour growth formation, larger tumours and reduced survival. Interestingly, mice transplanted with the SPRY2 mutant S121A (U251 SPRY2 S121A OE mice) did not develop any discernible tumour and their survival rate were significantly increased. Altogether, these observations further highlight that SPRY2 drives GBM proliferation also *in vivo* (Park et al., 2018).

Although the exact mechanisms by which SPRY2 augments GBM tumorigenesis are yet to be ascertained, these studies agree on the potential benefits of targeting/downregulating SPRY2 in GBM patients (Hausott and Klimaschewski, 2019).

1.11 Aims of the thesis

Based on the available literature, SPRY proteins represent a novel class of interactors and potential substrates of zDHH17 (Huttlin et al., 2017; Lemonidis et al., 2017a). zDHH17 is active towards a plethora of proteins, including neuronal substrates involved in synaptic function, plasticity and neuronal development (El-Husseini and Brecht, 2002; Fukata and Fukata, 2010). Given their key role as regulators of the MAPK/ERK pathway, SPRY proteins play a crucial role in development and organogenesis and their deregulation has been correlated to a large number of diseases, such as cancer, neurological disorders and cardiovascular dysfunction (Cabrita and Christofori, 2003; Hausott and Klimaschewski, 2019; Kawazoe and Taniguchi, 2019; Masoumi-Moghaddam et al., 2014). Therefore, a better understanding of the mechanisms and outcomes of S-acylation on SPRY proteins is of great interest. Among the four isoform, SPRY2 appears to be the most relevant. Therefore, the aims of this thesis are to:

(i) Establish whether SPRY2 undergoes S-acylation mediated by zDHH17 and whether other zDHH family members, such as zDHH7 and zDHH3, which are characterised by a higher activity and lower specificity of action, are also active

against SPRY2. Different activity levels will be evaluated using palmitic acid azide and click chemistry assays.

(ii) Identify the key features required for efficient S-acylation of SPRY2. This will include a detailed mutagenesis analysis to pin-point where, and to what extent, S-acylation mediated by zDHHC17 occurs within the cysteine-rich domain of SPRY2. In addition, the existence of other elements important for S-acylation will be considered and further analysed using structural prediction tools.

(iii) Investigate if SPRY2 stability and subcellular localisation are affected and/or modulated by S-acylation. These analyses will employ cell-based assays and confocal immunofluorescence imaging.

(iv) Determine the sequence requirements for SPRY2-zDHHC17 interaction and their importance in the context of S-acylation. To this end, the previously identified zDHHC17 ANK domain binding pocket, which includes Asp-100 and Trp-130, as well as the zDABM of SPRY2 (encompassing the key Pro-154) will be thoroughly examined using both cell-based and cell-free techniques.

(v) Characterise other functions of the ANK domain of zDHHC17, such as its role as a potential homo- and hetero-dimerisation/oligomerisation module and consider the functional significance of dimerisation.

Chapter 2 Materials and Methods

All reagents were purchased from Sigma-Aldrich UK (Poole, UK) unless otherwise stated.

2.1 Cellular Biology

2.1.1 Mammalian Cell Culture

Human Embryonic Kidney 293 cells (HEK293T), purchased from ATCC (ATCC, England, UK), were cultured in DMEM+GlutaMAX™-I media (Gibco, LifeTechnologies™ Ltd., Paisley, UK) supplemented with 10% Fetal Bovine Serum (Gibco, LifeTechnologies™ Ltd., Paisley, UK) and incubated at 37°C, 5% CO₂. Cells were split and replated at the desired density every 7 days. After removing the old media, cells were briefly washed in pre-heated Phosphate-Buffered Saline (1X PBS) and incubated for 2 min at 37°C in 2 ml TrypLE™ Express (Gibco, LifeTechnologies™ Ltd., Paisley, UK). Cells were detached from the surface by tapping the flask and 8 ml of fresh DMEM was added. Cells were seeded for maintenance at a dilution ratio of 1:10 with a final volume of 10 ml for 75 cm² flasks (Corning® Sigma-Aldrich Company Ltd., Dorset, UK) or at a dilution ratio of 1:5 on poly-D-lysine-coated 24-well plates for experimental analysis (Corning™ Sigma-Aldrich Company Ltd., Dorset, UK).

Rat adrenal pheochromocytoma PC12 cells (PC12), purchased from ATCC (ATCC, England, UK) were maintained in Advanced RPMI-1640 media (Gibco, LifeTechnologies™ Ltd., Paisley, UK) supplemented with 10% Horse Serum (HS) (Gibco, LifeTechnologies™ Ltd., Paisley, UK), 5% Fetal Bovine Serum (FBS) (Gibco, LifeTechnologies™ Ltd., Paisley, UK), and 1% L-glutamine (Gibco, LifeTechnologies™ Ltd., Paisley, UK), grown at 37°C in a humidified atmosphere containing 5% CO₂. Every 7 days, cells were collected and transferred to a centrifuge tube and centrifuged at 800 xg for 3 min at RT. After discarding the supernatant, the obtained cell pellet was resuspended in 4 ml TrypLE™ Express (Gibco, LifeTechnologies™ Ltd., Paisley, UK) and incubated for 4 min at 37°C. Fresh RPMI (6 ml) was then added and cells were centrifuged once more at 800 xg for 3 min at RT. After discarding the supernatant, the cell pellet was resuspended in 10 ml of RPMI and cells were thoroughly

resuspended and seeded for maintenance at a dilution ratio of 1:5 with a final volume of 10 ml for 75 cm² flasks (Corning® Sigma-Aldrich Company Ltd., Dorset, UK). For fractionation experiments, cells were plated at a dilution ratio of 1:4 on poly-D-lysine-coated 24-well plates (Corning™ Sigma-Aldrich Company Ltd., Dorset, UK). For immunofluorescence analysis cells were used at a dilution ratio of 1:10 and 1:5 and seeded on poly-D-lysine coverslips (Corning® Sigma-Aldrich Company Ltd., Dorset, UK) in non-coated 24-well plates (Starlab, Blakelands, UK).

2.1.2 Plasmids

zDHHC enzymes: Murine zDHHC17 (encoding amino acids 11-632), zDHHC13 (encoding amino acids 1-622), zDHHC7 (encoding amino acids 1-308) and zDHHC3 (encoding amino acids 1-299) cloned in pEFBOS-HA vectors were provided by Professor Masaki Fukata (Fukata et al., 2004).

zDHHC17 mutants encoding W130A and N100A were obtained through site-direct mutagenesis PCR using the zDHHC17 pEFBOS-HA plasmid as a DNA template (see below for details). The mutant zDHHC17 C467A (referred to as zDHHA17) was previously generated by Dr Christine Salaun (University of Strathclyde) using the same DNA template. From the original pEFBOS-HA zDHHC17, the constructs zDHHC17, zDHHC17 ΔN (encoding amino acids 54-632), zDHHC17 ΔNANK17 (encoding amino acids 287-632), zDHHC17 ΔC (encoding amino acids 11-569) were generated by Gateway® Technology (Invitrogen Ltd., Paisley, UK) by our group (Lemonidis et al., 2014). The pEGFP-N1 zDHHC17 was also cloned from the original pEFBOS-HA zDHHC17 by Dr Kimon Lemonidis (University of Strathclyde) by Gateway® Technology (Invitrogen Ltd., Paisley, UK).

SPRY2: EGFP-tagged wild-type (WT) and P154A mutants SPRY2 (encoding amino acids 1-315 of mouse sequence) cloned in pEGFP-C2 vector through Gateway® Technology (Invitrogen Ltd., Paisley, UK) were previously generated by Dr Kimon Lemonidis (University of Strathclyde) and the final sequence confirmed by sequencing (GATC service by Eurofins Genomics, Wolverhampton, UK). All the SPRY2 mutants

(schematically listed below) were obtained through site-direct mutagenesis PCR using pEGFP-C2 SPRY2 WT or EGFP-SPRY2 P154A as DNA template, unless otherwise specified. The validity of the final clones was confirmed (GATC service by Eurofins Genomics, Wolverhampton, UK).

SPRY2 tyrosine-55 mutants: SPRY2 Y55A and SPRY2 Y55F. The codon for the highly conserved tyrosine at position 55 was substituted with codons for either alanine (A) or phenylalanine (F) residues.

SPRY2 serine mutants: S111A; S111D; S120A; S120D. The codons for serine residues at positions 111 and 120 were individually mutated either to codons for alanine or aspartic acid (D).

SPRY2 cysteine mutants: C178/181A; C184/186/189A; C201/205/207A; C218/220/221A; C229A; C237A; C242/244A; C249/250A; C265/268A; C275/279/282A; C291/293A; C300/301A. Codons for all cysteine residues in the cysteine-rich domain (CRD) of SPRY2 (amino acids 177-301) were mutated to codons for alanine in blocks of one, two, or three amino acids. These mutants were generated by Irina Lousa (University of Porto).

C265A and C268A mutants: the single cysteine mutants C265A and C268A were generated by mutation of cysteine codons to alanine codons at position 265 or 268 of the SPRY2 sequence.

SPRY2 alanine mutants: KSEL-4A (155-158); KPGD-4A (159-162); VKPL-4A (163-166); SKDD-4A (167-170); LGLH-4A (171-174); AYR-3A (175-177); TYPR-4A (190-193); PLPS-4A (194-197); DWI-3A (198-200); SAQNV-5A (208-212); IDYGT-5A (213-217); VKGL-4A (222-225); FYH-3A (226-228). This set of mutants covers the amino acid sequence 155-228, excluding cysteine residues and all amino acids in between them.

SPRY2 single alanine mutants: S208A; Q210A; N211A; V212A; I213A; D214A; Y215A; G216A; T217A; V222A; K223A; G224A; L225A. The codon for each amino acid from position 208 to position 225, excluding cysteine residues and the amino acids in between them, was mutated to codons for alanine.

SPRY2 NDK mutants: using SPRY2 K223A mutant as a DNA template, specific primers were designed to simultaneously mutate codons for asparagine and aspartic acid at positions 211 and 214 of the corresponding amino acid sequence into alanine codons. The resulting SPRY2 NDK was also used as a DNA template to generate a SPRY2 P154A NDK mutant.

SPRY2 QP mutants: SPRY2 P13A; SPRY2 P96A; SPRY2 P154A; SPRY2 P13/91/96/154A. Codons for proline (P) residues belonging to the SPRY2 QP motifs were mutated to codons for alanine (A) residues. The QP at position 91 which is not conserved in the human genome was also included in the study.

SPRY2 C-terminus truncated mutants: SPRY2 G148X; SPRY2 R177X; SPRY2 I200X; SPRY2 S230X; SPRY2 S260X; SPRY2 G290X. An identical second series of truncated SPRY2 versions were generated using pEGFP-C2 SPRY2 P154A as a template. This P154A series does not include the mutant G148X. For these truncated versions, primers were designed to insert a premature stop codon into the coding sequence of SPRY2.

SPRY2 N-terminus truncated mutants: SPRY2 100-315 (encoding amino acids 100-315 of mouse SPRY2), SPRY2 120-315 (encoding amino acids 120-315 of mouse SPRY2), SPRY2 140-315 (encoding amino acids 140-315 of mouse SPRY2), and SPRY2 155-315 (encoding amino acids 155-315 of mouse SPRY2). This set of mutants, cloned into pcDNA3.1(+) N-eGFP vectors (N-terminal tagged), was synthesised and purchased from GenScript company (GenScript Biotech, HK).

Cherry-SPRY2 WT: SPRY2 WT was sub-cloned in mCherry-C2-GW vector using Gateway® Technology system (Invitrogen Ltd., Paisley, UK). Other plasmids: EGFP-tagged CSP α (bovine) and SNAP25b (rat) were cloned into pEGFP-C2 vectors (Greaves et al., 2009a; Greaves and Chamberlain, 2006). EGFP-HTT (encoding amino acids 1-550 of human HTT) was originally synthesized by Life Technologies Inc. and cloned into a pEGFP-C2 vector. EGFP-tagged cDNA including EVL-I (human, isolated from human embryonic cDNA brain library), SLAIN 1 (human), SPRED 1 (murine), SPRED 2 (murine, provided by Akihiro Yoshimura), JNK1 α 2 (human), JNK3 α 2 (human), PAI-

RBP1 (human) were all cloned in pEGFP-C2 vector through Gateway® Technology (Invitrogen Ltd., Paisley, UK) by our group (Lemonidis et al., 2017a) and the validity of entry clones was confirmed by sequencing (GATC service, Constance, Germany).

2.1.3 DNA Transfection

HEK293T and PC12 cells were transfected using Polyethylenimine (PEI) and Lipofectamine 2000 reagent (Invitrogen Ltd., Paisley, UK), respectively. In both cases, the reagents were used at a ratio to the plasmid DNA of 2:1.

HEK293T cells were grown on 24-well plates and transfected at 90% confluence with different amounts of plasmid DNA depending on the assay.

- For click chemistry, co-immunoprecipitation (Co-IP) assays (excluding Chapter 5 Co-IP experiments), and cycloheximide experiments, for a single transfection, the DNA concentrations were optimised at 0.33 µg of pEGFP-SPRY2 constructs and 0.66 µg of pEF-BOS HA constructs per well of a 24-well plate. The two DNA plasmids (substrate and enzyme) were added together into 100 µl of pre-heated serum-free DMEM+GlutaMAX™-I. PEI was added at the above-mentioned ratio directly into the 100 µl and the mixes were vortexed and incubated for 20 min at RT before being added to the cells. Transfected cells were returned to the incubator and used after 24 h.
- For zDHHC co-immunoprecipitation assays (Chapter 5) cells were co-transfected as described above. For a single transfection, the DNA concentrations were optimised at 0.5 µg of pEF-BOS HA constructs and 0.5 µg of pEGFP-N1 plasmids per well of a 24-well plate. Cells were used after 24h.
- For pull-down assays, cells were transfected using 1 µg of each construct per well of a 24-well plate. Cells were used after 24 h.

PC12 cells were grown on 24-well plates and transfected at confluences of 70% for fractionation experiments and 20/30% for confocal imaging. Different amounts of plasmid DNA were used depending on the assay.

- For confocal imaging, for a single transfection, 0.2 µg of mCherry-SPRY2 WT, and 0.2 µg of EGFP-SPRY2 constructs (SPRY2 WT, SPRY2 NDK, or SPRY2 C265/268A) were used per well of a 24-well plate. The plasmids were added together into 50 µl of pre-heated serum-free DMEM+GlutaMAXTM-I. Lipofectamine 2000 was added at the above-mentioned ratio into 50 µl of DMEM+GlutaMAXTM-I and incubated for 5 min at RT. Plasmids and Lipofectamine mixes were combined, incubated for a further 20 min at RT, and then added to the cells. Cells were used after 48 h.
- For fractionation and “click-on-beads” experiments, transfections were performed following the same protocol and using 1 µg of each plasmid DNA. Cells were used after 48 h.

2.1.4 Cycloheximide experiments

Cycloheximide (CHX) is a eukaryotic protein synthesis inhibitor. Since it blocks the translation of new proteins, cycloheximide is used to study the half-life (i.e. rate of degradation) of specific proteins of interest over time (Buchanan et al., 2016).

24 h post-transfection, HEK293T cells were incubated with 50 µg/ml of cycloheximide (CHX) per well of a 24-well plate and returned to 37°C and 5% CO₂. After 0, 2, 4, 6, or 8 h incubation, cells were washed once in PBS and lysed using 100 µl of 1X Laemmli sample buffer containing 25 mM DTT. Each cell lysate was transferred in a fresh tube and boiled at 95°C for 5 min. Samples were resolved by SDS-PAGE; HA and EGFP-tagged proteins were revealed by immunoblotting.

2.2 Molecular Biology

2.2.1 Site-Directed Mutagenesis

Site-directed mutagenesis (SDM) is commonly used to generate specific changes in a double-stranded DNA plasmid using specific primers in a PCR reaction. All primers

were designed using the online software “QuickChange Primer Design” from Agilent (Agilent, Santa Clara, USA).

SDM PCR was used to generate zDHHC17 W130A and N100A mutants starting from pEFBOS-HA zDHHC17 WT as a DNA template. The sequences of the used primers are shown in Table 1. PCR reaction mixes were prepared on ice and contained 2 μ l of KOD Hot-Start DNA polymerase (Novagen[®] EMD Millipore Corp., Billerica, USA), 5 μ l of 10X KOD polymerase buffer (Novagen[®] EMD Millipore Corp., Billerica, USA), 3 μ l of 25 mM MgSO₄ (Novagen[®] EMD Millipore Corp., Billerica, USA), 5 μ l of 2 mM dNTP_s (Novagen[®] EMD Millipore Corp., Billerica, USA), 2 μ l Dimethyl Sulfoxide - DMSO (Sigma-Aldrich, St. Louis, USA), 10 μ M of each primer (forward and reverse), 50 ng cDNA and dH₂O added to a final volume of 50 μ l. The reaction consisted of an initial polymerase activation step at 95°C for 2 min followed by 18 cycles of a denaturation step at 95°C for 20 s, an annealing step in the range of 50-60°C for 14 min, and an extension step at 68°C for 8 min. The final products were stored at 4°C until analysis.

To generate EGFP-SPRY2 mutants, SDM PCR was performed using as DNA templates either EGFP-SPRY2 WT or EGFP-SPRY2 P154A. SPRY2 NDK mutant was derived using SPRY2 K223A as a DNA template. The sequences of the employed primers are listed in Table 1. PCR reaction mixes were prepared on ice and contained 1 μ l of Pfu DNA polymerase (Promega Corp., Madison, USA), 5 μ l of Pfu DNA polymerase 10X Reaction buffer (Promega Corp., Madison, USA), 1 μ l of 10 mM dNTP_s (Promega Corp., Madison, USA), 10 μ M of each primer (forward and reverse), 75 ng of cDNA and dH₂O to a final volume of 50 μ l. The reaction was designed with an initial denaturation step at 95°C for 2 min followed by 18 cycles of a denaturation step at 95°C for 1 min, an annealing step in the range of 50-60°C, accordingly to the primers, and an extension step at 72°C for 14 min. The final products were stored at 4°C until analysis.

Either a 2720 Thermal Cycler or a Veriti[®] Thermal Cycler, both from AB Applied Biosystem was used for SDM PCR.

Primer Name	Sequence (5' - 3')
<i>zDHHC17:</i>	
zDHHC17 W130A_F	GAATTCAACTCCGTTGCACGCGGCCACAAGACAAGGCC
zDHHC17 W130A_R	GGCCTTGTCTTGTGGCCGCGTGCAACGGAGTTGAATTC
zDHHC17 N100A_F	CTTCTTCATTGGGCTGCCATCGCTAACAGAATAGATTTAGTC
zDHHC17 N100A_R	GACTAAATCTATTCTGTTAGCGATGGCAGCCCAATGAAGAAG
<i>SPRY2 tyrosine mutants:</i>	
SPRY2 Y55A_F	CAGTAGGGCCCTCTGTGGCCTCATTGGTGTTCGGA
SPRY2 Y55A_R	TCCGAAACACCAATGAGGCCACAGAGGGCCCTACTG
SPRY2 Y55F_F	AGTAGGGCCCTCTGTGAACTCATTGGTGTTCG
SPRY2 Y55F_R	CGAAACACCAATGAGTTCACAGAGGGCCCTACT
<i>SPRY2 serine mutants:</i>	
SPRY2 S111A_F	CTGTCCAGGTCCATCGCCACTGTCAGCTCAGG
SPRY2 S111A_R	CCTGAGCTGACAGTGGCGATGGACCTGGACAG
SPRY2 S111D_F	CCCTGAGCTGACAGTGTTCGATGGACCTGGACAGA
SPRY2 S111D_R	TCTGTCCAGGTCCATCGACACTGTCAGCTCAGGG
SPRY2 S120A_F	GGTACTTGTCTTGTAGCGCTCCGAGACCCTGAG
SPRY2 S120A_R	CTCAGGGTCTCGGAGCGCTACAAGGACAAGTACC
SPRY2 S120D_F	TGGTACTTGTCTTGTATCGCTCCGAGACCCTGAGC
SPRY2 S120D_R	GCTCAGGGTCTCGGAGCGATAACAAGGACAAGTACCA
<i>SPRY2 cysteine mutants:</i>	
SPRY2 C265A_F	GCTGGAAGGTAACACCATAAAGCAGGCCAAAAGAGAGACATGAC
SPRY2 C265A_R	GTCATGTCTCTCTTTTTGCCTGCTTTATGGTGTACCTTCCAGC
SPRY2 C268A_F	ACCCTTGGCTGGAAGGTAAGCCATAAACAAGGCCAAAAG
SPRY2 C268A_R	CTTTTTGCCTTGTATGGGCTTACCTTCCAGCCAAGGGT
<i>SPRY2 alanine mutants:</i>	
KSEL-4A_F	GGCTTAACGTCACCAGGCTTGGCCGCGCTGCAGGCTGCACTCGGATTATTCC
KSEL-4A_R	GGAATAATCCGAGTGCAGCCTGCAGCGGCGGCCAAGCCTGGTGACGTTAAGCC
KPGD-4A_F	CTTGCTCAGTGGCTTAACGGCAGCAGCCGCGAGCTCCGATTTAGGCTGC
KPGD-4A_R	GCAGCCTAAATCGGAGCTCGCGGCTGCTGCCGTTAAGCCACTGAGCAAG
VKPL-4A_F	AGACCCAAATCATCTTGTCTCGCTGCCGAGCGTACCAGGCTTGAGCTCCG
VKPL-4A_R	CGGAGCTCAAGCCTGGTGACGCTGCGGCAGCGAGCAAGGATGATTTGGGTCT

SKDD-4A_F	CTGTAGGCATGCAGACCCAAAGCAGCCGCGGCCAGTGGCTTAACGTCACCAGG
SKDD-4A_R	CCTGGTGACGTTAAGCCACTGGCCGCGGCTGCTTTGGGTCTGCATGCCTACAG
LGLH-4A_F	AGTCCTCACACCTGTAGGCAGCCGCAGCCGCATCATCCTTGCTCAGTGGCTTAACGTC
LGLH-4A_R	GACGTTAAGCCACTGAGCAAGGATGATGCGGCTGCGGCTGCCTACAGGTGTGAGGACT
AYR-3A_F	GGATGATTTGGGTCTGCATGCAGCCGCGTGTGAGGACTGCGGCAAGTG
AYR-3A_R	CACTTGCCGCGAGTCTCACACGCGGCTGCATGCAGACCCAAATCATCC
TYPR-4A_F	AGTCCGACGGCAGGGGCGCCGCGGCGGCGCACTCCTTACACTTGC
TYPR-4A_R	GCAAGTGTAAGGAGTGCGCCGCCGCGGCGCCCTGCCGTGCGACT
PLPS-4A_F	CACAGATCCAGTCCGCCGCCGCGGCCCTCGGGTAGGTGCA
PLPS-4A_R	TGCACCTACCCGAGGGCCGCGGCGGCGGACTGGATCTGTG
DWI-3A_F	GGCACTGCTTGTGCAGGCGCGGCCGACGGCAGGGGCGCTC
DWI-3A_R	GAGGCCCTGCCGTGCGCCGCCGCGCTGTGACAAGCAGTGCC
SAQNV-5A_F	CACACAAGTCCCATAGTCAATGGCGCCGCTGCTGCGCAGAGGCACTGCTTGTACAG
SAQNV-5A_R	CTGTGACAAGCAGTGCCTCTGCGCAGCAGCGGCCGCACTTACTATGGGACTTGTGTG
IDYGT-5A_F	ACCTTTCACACAGCACACACAAGCCGCGAGCGGCAGCGACGTTCTGGGCTGAGCAGAGGC
IDYGT-5A_R	GCCTCTGCTCAGCCCAGAACGTCGCTGCCGCTGCGGCTTGTGTGTGCTGTGTGAAAGGT
VKGL-4A_F	ATCGTCATTGGAGCAGTGATAGAAGGCAGCTGCCGCACAGCACACACAAGTCCCATAGTC
VKGL-4A_R	GACTATGGGACTTGTGTGTGCTGTGCGGCAGCTGCCTTCTATCACTGCTCCAATGACGAT
FYH-3A_F	CAATTGTCCTCATCGTCATTGGAGCAGGCAGCGGCGAGACCTTTCACACAGCACACACAAGT
FYH-3A_R	ACTTGTGTGTGCTGTGTGAAAGGTCTCGCCGCTGCCTGCTCCAATGACGATGAGGACAATTG
<i>SPRY2 single alanine mutants:</i>	
SPRY2 S208A_F	ACGTTCTGGGCTGCGCAGAGGCACTGC
SPRY2 S208A_R	GCAGTGCCTCTGCGCAGCCCAGAACGT
SPRY2 Q210A_F	CATAGTCAATGACGTTGCGGCTGAGCAGAGGCACT
SPRY2 Q210A_R	AGTGCCTCTGCTCAGCCGCGAACGTCATTGACTATG
SPRY2 N211A_F	CCCATAGTCAATGACGGCCTGGGCTGAGCAGAGG
SPRY2 N211A_R	CCTCTGCTCAGCCCAGGCCGTCATTGACTATGGG
SPRY2 V212A_F	GTCCCATAGTCAATGGCGTTCTGGGCTGAGC
SPRY2 V212A_R	GCTCAGCCCAGAACGCCATTGACTATGGGAC
SPRY2 I213A_F	CACAAGTCCCATAGTCAGCGACGTTCTGGGCTGAGC
SPRY2 I213A_R	GCTCAGCCCAGAACGTCGCTGACTATGGGACTTGTG
SPRY2 D214A_F	CACACAAGTCCCATAGGCAATGACGTTCTGGGC

SPRY2 D214A_R	GCCCAGAACGTCATTGCCTATGGGACTTGTGTG
SPRY2 Y215A_F	CAGCACACACAAGTCCCAGCGTCAATGACGTTCTGGGC
SPRY2 Y215A_R	GCCCAGAACGTCATTGACGCTGGGACTTGTGTGTGCTG
SPRY2 G216A_F	CACAGCACACACAAGTCGCATAGTCAATGACGTTTC
SPRY2 G216A_R	GAACGTCATTGACTATGCGACTTGTGTGTGCTGTG
SPRY2 T217A_F	CACACAGCACACACAAGCCCCATAGTCAATGACGT
SPRY2 T217A_R	ACGTCATTGACTATGGGGCTTGTGTGTGCTGTGTG
SPRY2 V222A_F	GATAGAAGAGACCTTTTCGCACAGCACACACAAGTC
SPRY2 V222A_R	GACTTGTGTGTGCTGTGCGAAAGGTCTCTTCTATC
SPRY2 K223A_F	GCAGTGATAGAAGAGACCTGCCACACAGCACACACAAGTC
SPRY2 K223A_R	GACTTGTGTGTGCTGTGTGGCAGGTCTCTTCTATCACTGC
SPRY2 G224A_F	TGTGTGCTGTGTGAAAGCTCTCTTCTATCACTGCT
SPRY2 G224A_R	AGCAGTGATAGAAGAGAGCTTTACACAGCACACA
SPRY2 L225A_F	ATTGGAGCAGTGATAGAAGGCACCTTTACACAGCACACA
SPRY2 L225A_R	TGTGTGCTGTGTGAAAGGTGCCTTCTATCACTGCTCCAAT
<i>SPRY2 NDK and P154A NDK mutants:</i>	
SPRY2 NDK_F	CACACAAGTCCCATAGGCAATGACGGCCTGGGCTGAGCAGAGG
SPRY2 NDK_R	CCTCTGCTCAGCCCAGGCCGTCATTGCCTATGGGACTTGTGTG
<i>SPRY2 QP mutants:</i>	
SPRY2 P13A_F	GTCTGCAGCAAAGCCTGCGACCCGTTG
SPRY2 P13A_R	CAACGGGTGCGCAGGCTTTGCTGCAGAC
SPRY2 P91A_F	GGAGCCTAGGAGCCTGGCGGTGCTC
SPRY2 P91A_R	GAGCACCGCCAGGCTCCTAGGCTCC
SPRY2 P96A_F	GACCTGCGAGGCCTGGAGCCTGG
SPRY2 P96A_R	CCAGGCTCCAGGCCTCGCAGGTC
SPRY2 P154A_F	CTTGAGCTCCGATTTAGCCTGCACTCGGATTATTC
SPRY2 P154A_R	GAATAATCCGAGTGCAGGCTAAATCGGAGCTCAAG
<i>SPRY2 WT or P154A truncated versions:</i>	
SPRY2 G148X_F	TGCACTCGGATTATTCAATCAGCAGCAGCAGGC
SPRY2 G148X_R	GCCTGCTGCTGCTGATTGAATAATCCGAGTGCA
SPRY2 R177X_F	GGTCTGCATGCCTACTAGTGTGAGGACTGCGG
SPRY2 R177X_R	CCGCAGTCTCACACTAGTAGGCATGCAGACC

SPRY2 I200X_F	CCTGCCGTCGGACTGGTAATGTGACAAGCAGTGCC
SPRY2 I200X_R	GGCACTGCTTGTTCACATTACCAGTCCGACGGCAGG
SPRY2 S230X_F	CACAATTGTCCTCATCGTCATTTTTAGCAGTGATAGAAGAGACCTTT
SPRY2 S230X_R	AAAGGTCTCTTCTATCACTGCTAAAATGACGATGAGGACAATTGTG
SPRY2 S260X_F	CATAACAAGGCCAAAAAGAGTTACATGACTCCCATCGCTGAC
SPRY2 S260X_R	GTCAGCGATGGGAGTCATGTAACCTTTTTGCCTTGTTTATG
SPRY2 G290X_F	TGTATTTGAGTTTTTACAACGACATTACGGCCTGTTCACTCGGTCATAAC
SPRY2 G290X_R	GTTATGACCGAGTGAACAGGCCGTAATGTCGTTGTAAAAACTCAAATACA

Table 2.1 Sequences of oligonucleotide primers used to generate zDHC17 and SPRY2 mutants by site-direct mutagenesis PCR

For zDHC17, primers were designed to substitute tryptophan (W) at position 130 and asparagine (N) at position 100 to alanine (A) (the primers introduced the following mutations: TTG→GCG for Trp→Ala and AAT→GCG for Asp→Ala, respectively). For SPRY2 mutants, primers were designed to substitute a number of amino acids usually with alanine (A) residues but also with phenylalanine (F), or aspartic acid (D). Other constructs were generated by inserting premature stop codons (refer to section 2.1.2 for more details regarding each set of mutants).

2.2.2 Agarose Gel electrophoresis

Amplicons from PCR reactions were visualized by agarose gel electrophoresis. An electric field is applied to the DNA fragments which are negatively charged and therefore will migrate towards the positive electrode. As a consequence, the DNA is separated by size through the agarose matrix. A concentration of 1% (w/v) agarose (Biolone, London, UK) in 1X TAE buffer [Stock 50X: 2M Tris, 50 mM EDTA, Acetic Acid to pH 8] was used to make gels, supplemented with SYBR Safe® (Life Technologies™ Ltd., Paisley, UK) at a dilution 1:10,000. Gels were immersed in 1X TAE buffer. Samples were prepared adding loading buffer (Fisher BioReagents™, Geel, Belgium) at a dilution ratio of 1:5 and were run at 80 V constant (PowerPac™ Basic from BioRad, USA) alongside HyperLadder™ 1 Kb or HyperLadder™ 100 bp (Biolone, London, UK) as a marker of DNA size. After electrophoresis, the DNA samples were

visualized under UV light by an Ingenius-Syngene Bio UV illuminator and associated camera.

2.2.3 Purification of the PCR products

Depending on the PCR product, clones were either purified from agarose gel or treated with restriction enzymes before any other downstream application.

2.2.3.1 DNA extraction from agarose gel

PCR products relative to zDHC17 mutants were recovered from agarose gels using PureLink™ Quick gel extraction kit (Invitrogen, Löhne, Germany) according to the manufacturer's protocol. A minimal area of the gels containing the DNA fragments of interest was excised under UV light using Transilluminator 4000 (Stratagene, Carlsberg, USA) and placed in 1.5 ml tubes. 500 µl of Gel Solubilisation Buffer L3 (Invitrogen, Löhne, Germany) was added to the tubes containing the DNA slices and placed into a 50°C heat block (FisherScientific FB15101 DryBath) until gel dissolution. The dissolved gels containing the DNA were loaded onto Quick Gel Extraction Columns and centrifuged at 13,000 *xg* for 1 min. After discarding the flow-through, 500 µl of Wash Buffer (W1) was added and two centrifugations, the first at 13,000 *xg* for 1 min and the second at maximum speed (corresponding to 13,200 *xg*) for 2 min were performed. For DNA recovery, 50 µl of Elution Buffer (E5) was added followed by centrifugation at 13,000 *xg* for 1 min. Eluted DNA was stored either at 4°C or at -20°C.

2.2.3.2 DpnI treatment

The restriction enzyme DpnI specifically recognizes and cleaves methylated sequences on a target DNA (recognition site GA^{m6}TC) and it is therefore used after a PCR reaction to eliminate the cDNA template, the only methylated DNA present in the final PCR mix.

All the PCR products corresponding to SPRY2 clones were DpnI treated (Thermo Scientific™, UK). For each 9 µl of PCR product, 1 µl of DpnI was added and mixes were incubated at 37°C for 1 h in a Clifton water bath (Clifton, Nickel-Electro Ltd., UK).

2.2.4 Gateway Cloning System

The Gateway System is a widely-used method for cloning DNA of interest. DNA fragments, flanked by recombination sequences known as the “att sites” are cloned into “entry clone” plasmids (pDONR). Using a specific mix of “BP” or “LR Clonase” enzymes, the DNA in an entry clone can be easily transferred to a vast array of Gateway (GW) expression vectors.

To sub-clone mouse SPRY2 wild-type (encoding amino acids 1-315) into mCherry-C2-GW vector (Cherry tag is expressed at N-terminus of the protein) 150 ng of both mCherry-C2-GW and pDONR-SPRY2 WT (Dr Kimon Lemonidis, University of Strathclyde) were mixed. 1 µl of LR Clonase II mix (Invitrogen Ltd., Paisley, UK), 2 µl of TE buffer was added to a final volume of 5 µl and the mix was incubated overnight at 25°C. The final product was used to transform competent TOP10 *E. Coli* cells (see below).

2.2.5 Production of competent TOP10 *E. Coli* cells

50 µl of competent TOP10 *E. Coli*, stored at -80°C, was thawed on ice for 10-15 min. 200 µl of Luria Broth (LB) media [1% Tryptone; 0.5% yeast extract; 1% NaCl] was added under sterile conditions and cells were grown for 30 min, 250 rpm at 37°C with continuous shaking (Thermo scientific MAXQ4000). Bacteria were streaked onto two agar plates (without antibiotics) and after an ON incubation at 37°C, a single bacterial colony was used to inoculate 2 ml of LB (without antibiotics) which was incubated ON, at 250 rpm and 37 °C. 1 ml of the ON culture was used to inoculate 100 ml of fresh LB and bacterial cells were incubated for 1.5-2h, 250 rpm at 37 °C until OD₆₀₀ reached a value of 0.2-0.4 (POLARstar Omega, BMG Labtech). After chilling the culture on ice for 15 min, cells were separated in two 50 ml tubes and centrifuged at 3,300 *xg* for 10 min at 4°C. After discarding the supernatant, each bacterial pellet was resuspended in 10 ml of 0.1 M CaCl₂ sterile and ice-cold. Cells were incubated on ice for an additional 30 min before being centrifuged at 3,300 *xg* for 10 min at 4°C. After

discarding the supernatant, each pellet was resuspended in 3 ml of 0.1 M CaCl₂ containing 15% glycerol. The obtained 6 ml were snapped-frozen into 50 µl, 100 µl, and 250 µl aliquots and stored at -80°C for 3 to 6 months. Transformation efficiency was determined as colony forming unit (cfu) per µg of DNA used (µg of DNA).

2.2.6 Bacterial transformation and culture for plasmid DNA amplification

Competent TOP10 *E. Coli* cells (produced in-house) were transformed with purified plasmids of interest. These included DNA products of site-direct-mutagenesis (sdm) PCR, Gateway cloning, or GenScript constructs.

50 µl or 100 µl *E. Coli* TOP10 aliquots, stored at -80°C, were thawed on ice for 10-15 min. Transformation was performed at a ratio of 1:10 (vol/vol) plasmid:bacteria for sdm PCR products. Alternatively, 5-10 µl of DNA deriving from cloning reactions and 0.1-0.5 µl of GenScript plasmids were used. In all cases, DNA transformation was followed by 30 min of incubation on ice, 30 s at 42°C and a further 2 min on ice. 250 µl of Luria Broth (LB) media [1% Tryptone; 0.5% yeast extract; 1% NaCl] was added under sterile conditions and the cultures were incubated for 45-60 min, 250 rpm at 37°C with continuous shaking (Thermo scientific MAXQ4000). After growth, cells were plated onto agar plates [1% Tryptone; 0.5% yeast extract; 1% NaCl; 1.5% agar] supplemented with selective antibiotic (100 µg/ml of Ampicillin or 30 µg/ml of Kanamycin) to selectively grow transformed cells. Bacteria were grown overnight at 37°C in a Heraeus incubator (Thermo Scientific, Loughborough, UK). Single bacterial colonies were used to inoculate 5 ml of Luria Broth (LB) and grown for approximately 16 h at 37°C and 250 rpm. If grown colonies were found to contain the expected plasmid (see below), 2ml of the Miniprep pre-culture were used to inoculate 150 ml of LB for Midiprep plasmid purifications and grown overnight with continuous shaking at 250 rpm at 37°C.

2.2.7 Plasmid DNA purification

Pure Link™ Quick Plasmid Miniprep kit (Invitrogen, Löhne, Germany) and NucleoBond® Xtra Midi Plus (Macherey-Nagel GmbH&Co.KG., Düren, Germany) were used respectively for miniprep and midiprep plasmid DNA purifications. The resulting purified plasmid DNA was used for protein expression and purification (see below), to transfect HEK293T and PC12 cells. Plasmid purification followed the manufacturer's instructions and all buffers used were provided with the kit.

2.2.7.1 Miniprep plasmid purification

After overnight shaking, 1-5 ml of the bacterial culture was sedimented at >12,000 xg for 10 min and the supernatant discarded. The cell pellet was completely resuspended in 250 μ l of Resuspension Buffer (R3), previously supplemented with 100 μ g/ml of RNAase. 250 μ l of Lysis Buffer (L7) was added, and the mix inverted 5 times and incubated for 5 min at RT. The precipitation step occurred using 350 μ l of Precipitation Buffer (N4), mixing and centrifuging the lysate at >12,000 xg for 1 min. The supernatant was then loaded onto a Spin Column in a 2 ml Wash Tube and centrifuged at 12,000 xg for 1 min. After discarding the supernatant, 700 μ l of Wash Buffer (W9) was added to the column and centrifugation took place twice at 12,000 xg for 1 min. Plasmid DNA was eluted by adding 50-75 μ l of pure H₂O and incubating the tube for 1 min at RT, followed by DNA recovery by centrifugation at 12,000 xg for 2 min. Plasmid yield was determined by spectrophotometry at A260 nm using NanoDrop™ 2000/2000c (Thermo Scientific™) and stored at -20°C.

2.2.7.2 Restriction Enzyme digestion

After isolating the plasmid DNA, mCherry-SPRY2 WT was digested to assess if the sub-cloning was successful. The restriction enzymes (RE) BglIII (recognition site A^VGATCT) and BamHI (recognition site G^VGATCC) were both used. Digested cDNAs were resolved on agarose gel electrophoresis and the samples containing the insert were sent for sequencing (refer to the section below).

2.2.7.3 Sequencing

To confirm the clones, zDHHC17 mutants, all SPRY2 mutants as well as mCherry-SPRY2 WT plasmid were sent for sequencing to GATC Biotech Company (Eurofins & GATC). The outputs were analysed and aligned with the corresponding wild-type DNA of reference using ApE software.

2.2.7.4 Midiprep plasmid purification

After overnight growth, bacterial cells were harvested by centrifugation at 4,000 xg for 20 min and 4°C (Sigma 4K15 Centrifuge - Rotor 12256). The cell pellet was completely resuspended in 8 ml of Resuspension Buffer (RES) containing RNAase. 8 ml of Lysis Buffer (LYS) was added, and the mix inverted 5 times and incubated for 5 min at RT. The lysate was then neutralized with 12 ml of Neutralization Buffer (NEU) and loaded onto the NucleoBond® Xtra Column Filter, previously equilibrated with 12 ml of Equilibration Buffer (EQU). The Column Filter was washed with an additional 5 ml of EQU buffer to remove the remaining lysate. After discarding the Filter, the NucleoBond® Xtra Column was washed with 8 ml of Wash Buffer (WASH) and the plasmid DNA eluted by Elution Buffer (ELU) into a fresh tube. 3.5 ml of isopropanol was added to precipitate the eluted plasmid DNA and centrifuged at 4,000 xg for 45-60 min at 4°C. The pellet was washed with 2 ml of 70% ethanol and centrifuged at 3,000 xg for 15 min at RT. The resulting pellet was dried at RT and reconstituted in 300 μ l of dH₂O both pipetting up and down and vortexing. The plasmid DNA yield was determined by spectrophotometry at A260 nm using a NanoDrop™ 2000/2000c (Thermo Scientific™) and then stored at -20°C.

2.2.8 Protein Expression and Purification

ANK17 wild-type (WT) was cloned into pET28B (amino acids 54-288) and PET303 (amino acids 51-288) vectors through Gateway® System (Invitrogen Ltd., Paisley, UK) to obtain ANK17 N- and C-terminally His₆-tagged proteins, respectively (Lemonidis et al., 2015a). 10 to 50 ng of His₆-ANK17 WT (either into pET28B-GW or pET303-GW) was used to transform *E. Coli* BL21(DE3)pLysS (Promega, Southampton, UK) following

the same protocol described above for TOP10 cells. ANK17 W130A was obtained by site-directed mutagenesis using ANK17 WT (cloned in pET28B) as a DNA template. After transformation, the bacterial cells were plated onto LB agar plates (previously described) supplemented with selective antibiotics: 30 µg/ml of Kanamycin plus 25 µg/ml of Chloramphenicol for pET28B, and 100 µg/ml of Ampicillin plus 25 µg/ml of Chloramphenicol for pET303. A single colony was used to inoculate 5 ml of LB (previously described) containing the appropriate antibiotics and cells were grown with continuous shaking @200-250 rpm for 3-6 h at 37°C until the OD₆₀₀ reached 0.3-0.5. This pre-culture was used to inoculate 500 ml of sterile supermedia [1.5% Tryptone; 2.5% Yeast extract; 150mM NaCl] containing antibiotics. Cells were grown overnight with continuous shaking at 200-250 rpm at 37°C, which resulted in an OD₆₀₀ of approximately 1.2. 500µl of this *Uninduced fraction* (U Fraction) was kept at -20°C for subsequent analysis. The overnight culture was diluted 1:2 with 500 ml of fresh supermedia supplemented with antibiotics and induced with 1 mM IPTG (Isopropyl βD1 Thiogalactopyranoside) for 4-6 h at 37°C with continuous shaking at 200-250 rpm. 500µl of this *Induced fraction* (I Fraction) was kept at -20°C for subsequent analysis. After induction, cells were harvested in 250 ml centrifuge tubes (Nalgene®-Sigma, UK) and centrifuged at 6,000 *xg* for 10 min at 4°C (Sigma 4K15 Centrifuge - Rotor 12256). The supernatant was discarded, and the pellet stored at -20°C or -80°C overnight. Each pellet, derived from the same litre of overnight culture, was resuspended in 25 ml of Binding Buffer [20mM Tris pH8; 150mM NaCl; 10mM Imidazole] and transferred into a fresh 50 ml tube. 1 mg/ml of chicken egg lysozyme was added (fresh stock solution at 40 mg/ml in H₂O) and tubes were incubated for 30 min on ice. Resuspended cells were then sonicated in a Branson Sonifier Sonicator 250 (Fisher Scientific) on ice using first 3 cycles of 20 s ON and 20 s OFF at output 2 and then 3 cycles of 20 s ON and 20 s OFF at output 3. 75 µl of the sonicate was collected and separated into *Supernatant* (S) and *Pellet* (P) *fractions* for subsequent analysis. The remainder was centrifuged in 30 ml round-bottom tubes (Thermo Scientific Nalgene®, UK) at 20,000 *xg* for 40-60 min at 4°C (Sigma 4K15 Centrifuge - Rotor 12166_H). Pellets were discarded and cleared lysates were incubated overnight

at 4°C by end-over-end rotation with 1 ml bed volume of Ni²⁺-NTA agarose (QIAGEN®, Hilden, Germany), previously washed with 10 volumes of dH₂O and equilibrated with 15 volumes of Tris Buffer [20mM Tris pH8; 300mM NaCl]. After centrifugation at 2,000 *xg* for 3 min at 4°C, the resin was washed 3 times with 10 volumes of Tris Buffer supplemented with 50 mM Imidazole (AlfaAesar®, Heysham, UK). For each wash, tubes were incubated by end-over-end rotation for 15 min at 4°C, centrifuged at 2,000 *xg* for 3 min at 4°C and the supernatant was discarded. The protein was finally eluted from the resin using 3 ml of Tris Buffer supplemented with 0.5 M Imidazole. Incubation took place by end-over-end rotation for 10 min at RT followed by a final centrifugation at 2,000 *xg* for 3 min at 4°C. The supernatant, containing purified His₆-proteins, was recovered, and 15 µl was collected as *Eluate Fraction* (E Fraction). All the collected fractions (U, I, P, S, E) were supplemented with 4X Laemmli sample buffer, resolved on a 12% acrylamide SDS gel and stained with Coomassie Instant Blue™ (Expedeon Ltd., Cambridge, UK) to assess the presence and purity of the recovered protein. The rest of the *Eluate fraction* was dialyzed, using Slide-A-Lyzer™ G2 Dialysis Cassette (Thermo Scientific, Rockford, UK) against 5 L of 1X PBS [Stock 10X: 13M NaCl, 1M NaH₂PO₄ in dH₂O] overnight at 4°C, under slow stirring. The amount of total protein eluted was estimated both by spectrophotometry at A₂₈₀ using NanoDrop™ 2000/2000c (ProtParam used parameter: Molecular Weight and Ext. coefficient assuming all cysteine residues reduced) and by using a BSA standard curve, running several volumes of the dialysed sample (10 µl, 5 µl, 2 µl) and several known amounts of BSA (1 µg, 0.5 µg, 0.25 µg, 0.125 µg, 0.0625 µg) side-by-side on a 12% SDS-PAGE. The concentration of the purified protein was estimated by densitometry analysis of the corresponding Coomassie-stained bands relative to the BSA bands.

2.2.9 Pull-down assay using His₆-tagged protein immobilised on Ni²⁺-NTA

A pull-down assay is a type of affinity purification in which a “bait” protein is used to pull-down “prey” interacting proteins to (i) reveal predicted protein-protein interactions or (ii) identify novel protein-protein interactions.

Twenty-four h post-transfection, HEK293T cells expressing HA or EGFP-tagged proteins in 24-well plates were washed once with PBS. 150 μ l of Lysis Buffer were added [20 mM Tris pH 8; 150 mM NaCl; 1% Triton X-100; 20 mM Imidazole] and cells were mechanically scraped from the surface of the plate. The content of 3 or 4 replicates wells was combined into a single tube. The lysate was clarified by centrifugation at 13,200 xg for 10 min at 4°C. 75 μ l was collected as *Input Fractions*, mixed with 25 μ l of 4X Laemmli sample buffer and stored at -20°C. 150 μ l of the lysate was diluted in 1 ml of Binding Buffer [20 mM Tris pH 8; 150 mM NaCl; 20 mM Imidazole], mixed with 25 μ l bed volume of Ni²⁺-NTA agarose resin and either 40 μ g of His₆-ANK17 WT, His₆-ANK17 W130A or no His₆-tagged proteins (a corresponding PBS volume was used as negative control). Ni²⁺-NTA resin was previously washed with 10 volumes of H₂O and equilibrated with 15 volumes of Binding Buffer. The amount of His₆-tagged protein to use was calculated based on the corresponding protein concentration and the volumes were adjusted to be equal in all samples. Mixes were incubated for 2 h by end-over-end rotation at 4°C. After incubation, centrifugation at 2,000 xg for 3 min at 4°C occurred. Pellets containing resin and bound proteins were washed 3 times with Washing Buffer [20 mM Tris pH 8; 300 mM NaCl; 1% Triton X-100; 40 mM Imidazole]. For each wash, the resin was either incubated by end-over-end rotation for 5 min at 4°C or mixed by hand, centrifuged at 2,000 xg for 3 min at 4°C and the supernatant discarded. The resin was resuspended in 50 μ l of 1X Laemmli sample buffer and bound proteins were eluted by boiling the samples at 95°C for 10 min. Samples were centrifuged at 2,000 xg for 3 min and supernatants were collected in fresh tubes as *Bound Fractions*. 7.5% of the total input samples and 30% or 40% of bound fractions were loaded on 10% or 12% SDS-PAGE. Bound His₆-ANK17 proteins (WT or W130A) were detected by Ponceau S staining. HA and EGFP-tagged proteins were revealed by immunoblotting.

2.3 Protein Biochemistry

2.3.1 Click Chemistry

The term click chemistry refers to labelling assays that use reporter molecules for the identification, localisation, and characterisation of biomolecules. In the S-acylation field, a sample of interest is metabolically labelled using modified fatty acids (alkyne or azide-palmitic acid probes) which zDHHC enzymes use as substrates for S-acylation of proteins. Once the probes are incorporated into the substrates they can be revealed by Western blotting, fluorescent or radioactive methods based on the molecule (azide or alkyne modified) that was reacted or “clicked” with the azide/alkyne fatty acid (Gao and Hannoush, 2018).

For metabolic labelling, 24 h after transfection, HEK293T cells in 24-well plates were washed once using 500 μ l of PBS per well and then incubated with 500 μ l/well of fresh serum-free DMEM+GlutaMAX-I containing 1 mg/ml of fatty acid-free BSA and 100 μ M of palmitic-acid (C16:0) azide (stock solution at 50 mM in DMSO) for 4 h at 37°C and 5% CO₂. After washing with PBS, cells were lysed on ice using 100 μ l/well of Lysis Buffer [50mM Tris pH 8; 0.5% SDS; 1X protease inhibitor cocktail] and transferred into fresh tubes. For each 100 μ l of cell lysate, 80 μ l of fresh click reaction mix containing 2.5 μ M of alkyne dye-IR800, 2 mM of CuSO₄ (Copper (II) Sulphate), and 0.2 mM of TBTA (Tris[(1-benzyl-1H-1,2,3-triazole-4yl) methyl]), were added. 20 μ l of 4 mM ascorbic acid (AlfaAesar®, Heysham, UK) was added to start the reaction. The total final volume of 200 μ l, including the cell lysate, was vortexed and incubated for 1 h with end-over-end rotation at RT. 67 μ l of 4X Laemmli sample buffer, containing 100 mM of DTT, were added to each sample and boiled at 95°C for 5 min. Samples were resolved by SDS-PAGE; HA and EGFP-tagged proteins were revealed by immunoblotting.

2.3.2 Co-Immunoprecipitation assay

Similar to a pull-down assay, co-immunoprecipitation is used to study protein-protein interactions. Generally, a specific antibody is used to immunoprecipitate a protein of

interest from cell lysates or other solutions. As long as the binding is sufficiently strong and buffer conditions not too stringent, the binding partners of the immunoprecipitated protein are also precipitated (co-immunoprecipitated) and they can be characterised (Phizicki and Fields, 1995).

For co-immunoprecipitation assays, HEK293T cells expressing HA or EGFP-tagged proteins in 24-well plates were used 24 h post-transfection. After removing the culture media, cells were mechanically scraped from the surface of the plate in 300 μ l/well of PBS. At this stage, the content of 3 replicate wells was combined in a single tube. Cells were centrifuged at 500 xg for 4 min at 4°C. After discarding the supernatant, the pellet was washed with 500 μ l of PBS, and cells were collected by centrifugation at 500 xg for 5 min at 4°C. After discarding the supernatant, the pellet was thoroughly resuspended in 200 μ l of Lysis Buffer [PBS, 0.5% Triton X-100, 1X protease inhibitors] and incubated on ice for 30 min pipetting to disrupt any clumps every 10 min. The lysate was clarified at 20,000 xg for 10 min at 4°C and supernatant from this step was collected in fresh tubes, supplemented with 300 μ l of PBS to a final volume of 500 μ l. 50 μ l were kept as *Input* sample and the remaining 450 μ l of cell lysate was mixed with 5 μ l bed volume of GFP-Trap beads (Chromotek, Munich, DE). GFP beads were previously washed with 20 volumes of H₂O and equilibrated with 25 volumes of PBS. Mixes were incubated for 1 h by end-over-end rotation at 4°C. After incubation, centrifugation at 2,500 xg for 2 min at 4°C occurred. The pellet containing the beads and bound proteins was washed twice with 1 ml of PBS. For each wash, the beads were briefly vortexed, centrifuged at 2,500 xg for 2 min at 4°C and the supernatant discarded. 50 μ l of 2X Laemmli sample buffer containing 50 mM DTT was added. Bound proteins were eluted by boiling the beads at 95°C for 10 min. Following centrifugation at 2,500 xg for 2 min at 4°C, supernatants were collected in fresh tubes as *Bound* samples and resolved by SDS-PAGE. HA and EGFP-tagged proteins were revealed by immunoblotting.

2.3.3 Click Chemistry coupled with immunoprecipitation

To improve the detection of S-acylated proteins that might be expressed at low levels, click chemistry was coupled with immunoprecipitation assay in a “click-on-beads” approach. In this modified protocol, following metabolic labelling, cell lysates were affinity-purified for the enrichment of the proteins of interest before being subsequently clicked.

PC12 cells expressing EGFP-tagged proteins, in 24-well plates, were used 48 h post-transfection. Cells were metabolically labelled as described in section 2.3.1 (i.e. 1 mg/ml of fatty acid-free BSA + 100 μ M of palmitic-acid in serum-free RPMI media). After 4 h at 37°C and 5% CO₂, the content of 4 replicate wells was combined in a single tube, and cells were centrifuged at 500 *xg* for 5 min at 4°C. After discarding the supernatant, the pellet was washed once with 500 μ l of PBS, and cells were collected by centrifugation at 500 *xg* for 5 min at 4°C. After discarding the supernatant, each pellet was lysed as described for co-immunoprecipitation (section 2.3.2). 500 μ l of cell lysate was mixed with 5 μ l bed volume of pre-washed GFP-Trap beads (Chromotek, Munich, DE). Mixes were incubated for 1 h (or overnight) by end-over-end rotation at 4°C. Following centrifugation at 3,000 *xg* for 3 min at 4°C, the supernatant was discarded, and the pellet washed twice with 1 ml of PBS. The pellet containing the beads and binding proteins was resuspended in 100 μ l of PBS supplemented with 0.2% Triton X-100. 80 μ l of click reaction plus 20 μ l of ascorbic acid were added as described in section 2.3.1. The final volume of 200 μ l (bound proteins plus click mix) was vortexed and incubated for 1 h with end-over-end rotation at RT. After incubation, centrifugation at 3,000 *xg* for 3 min at 4°C occurred. The pellet (containing beads and clicked bound proteins) was washed once with 1 ml of PBS, and the supernatant was discarded. Bound proteins were eluted by adding 50 μ l of 2X Laemmli sample buffer containing 50 mM DTT and boiling the beads for 10 min at 95°C. Following centrifugation at 3,000 *xg* for 3 min, supernatants were collected in fresh tubes and resolved by SDS-PAGE. EGFP-tagged proteins were revealed by immunoblotting.

2.3.4 Subcellular fractionation by ultracentrifugation

Analytical ultracentrifugation represents a widely used biochemical tool that uses g -force to isolate subcellular components (i.e. cytosol, membranes, organelles) as well as macromolecules such as proteins or nucleic acids. Ultracentrifugation also allows the analysis of the distribution of proteins of interest (Ohlendieck and Harding, 2017).

48 h post-transfection, PC12 cells in 24-well plates were first washed and then detached in 400 μ l of PBS per well. At this stage, the content of four wells was combined into a fresh tube. After centrifugation at 1,000 xg for 10 min at 4°C, each cell pellet was resuspended in 500 μ l of Dounce Buffer [50 mM Tris pH 7.4, 150 mM NaCl, 1X protease inhibitor cocktail] and cells were disrupted with 40 strokes. Cell lysates were transferred into fresh tubes, centrifuged at 250 xg for 5 min at 4°C and supernatants were recovered as 'post-nuclear supernatant' (PNS). The PNS was centrifuged at 100,000 xg for 1 h at 4°C in Beckman ultracentrifuge. The supernatant was collected as 'cytosolic' fraction and the pellet as 'membrane' fraction. Membrane fractions were resuspended in 100 μ l of 1X Laemmli sample buffer and kept at RT. Cytosolic fractions were acetone-precipitated using 3 vol of 100% ice-cold acetone, thoroughly vortexed, and incubated for 30 min at -80°C. Samples were centrifuged at 13,200 xg for 10 min at 4°C. The resulting pellet was washed twice with 500 μ l of 70% ice-cold acetone and resuspended in 100 μ l of 1X Laemmli sample buffer containing 25 mM DTT. Cytosolic and membrane fractions were boiled for 5 min and resolved by SDS-PAGE. Proteins were revealed by immunoblotting. GAPDH and Syntaxin1a were used as control proteins for the cytosolic and membrane fractions, respectively.

2.3.6 Sodium Dodecyl Sulphate-Polyacrylamide Gel Electrophoresis (SDS-PAGE)

On SDS-PAGE, protein samples are treated with sodium dodecyl sulfate, an anionic detergent that denatures and imparts an overall negative charge to the proteins. Once an electric field is applied, proteins (negatively charged) migrate toward the anode (positively charged) and are separated accordingly to their molecular weight.

Gels were cast by pouring two different solutions (i) a resolving (bottom) mix and (ii) a stacking (top) mix between two glass plates clamped in a casting stand. Appropriate combs were used to make the wells. (i) The resolving gel is responsible for protein separation. Based on the amount of acrylamide, the gel can vary in pore size allowing the optimal separation according to the molecular weights of the proteins of interest. 12%, 10%, and 8% resolving gels were routinely used mixing the appropriate volumes of 2X Resolving Buffer [0.2% (w/v) SDS; 4 mM EDTA Poole, UK); 750 mM Tris; pH adjusted at 8.9 using HCl 12 N], 30% acrylamide/bis-acrylamide, H₂O, 10% APS (Ammonium Persulfate) and TEMED (Tetramethylethylenediamine). APS generates free radicals which react with acrylamide monomers. These, in a cascade reaction, react with each other and with bis-acrylamide for polymerization into a gel. TEMED is an essential catalyst accelerating the rate of formation of free radicals from APS. (ii) The stacking gel is responsible for concentrating the proteins present in the samples at the top of the resolving gel. This allows homogeneous and better-resolved electrophoresis. Stacking solution was prepared at 4.5% acrylamide concentration mixing 4 ml of 2X Stacking Buffer [0.2% (w/v) SDS; 4 mM EDTA; 250 mM Tris; pH adjusted at 6.8 using HCl 12 N], 2.8 ml of 30% acrylamide/bis-acrylamide, 1.2 ml H₂O, 200 µl of 10% APS and 10 µl TEMED. Protein samples were prepared in 4X or 1X Laemmli sample buffer depending on sample concentration (Stock 4X: 0.4% Bromophenol Blue (AlfaAesar®, Heysham, UK); 200 mM Tris pH 8.0; 40% Glycerol (AlfaAesar®, Heysham, UK); 8% SDS (Fisher Bioscientific, Leics, UK)) supplemented with 100 mM or 25 mM of 1 M DTT (dithiothreitol) (Fisher BioReagents™, Geel, Belgium) and boiled at 95°C for 5 min to enhance protein denaturation. Subsequently, gels were unclamped from the casting stand and clamped into running modules, placed into the tank and filled with Running Buffer (25 mM Tris, 250 mM Glycine, 0.1% SDS). Alongside the samples, pre-Stained Protein Marker (Fisher BioReagents™, Geel, Belgium), with a separation range of 20-118 kDa, was also loaded. A constant voltage of 80 V was applied for protein migration through the stacking gel and 150 V for migration through the resolving gel.

2.3.7 Immunoblotting

After SDS-PAGE, proteins were transferred onto a nitrocellulose membrane of 0.45 μm pore size (GE Healthcare Life Sciences, Germany). Starting from the black side of the cassette the sandwich was assembled as follows: Whatman paper 3 mm, gel, nitrocellulose membrane, and Whatman paper 3 mm. Whatman papers and nitrocellulose were previously soaked in Transfer Buffer [48 mM Tris; 39 mM Glycine; 1.3 mM SDS; 20% of MeOH]. The sandwich was tightly closed and placed into a Bio-Rad Trans-Blot[®] cell filled with transfer buffer. 120 mA constant current was applied overnight to allow protein migration from the gel to the membrane.

The day after, each membrane was briefly rinsed in PBS-Tween (PBS-T) [PBS was supplemented with 0.1% (v/v) Tween-20]. Depending on the experiment, membranes were stained for total protein content (refer to section 2.3.8) before being incubated in 5% (w/v) milk in PBS-T for 1 h at RT to prevent non-specific binding of antibodies. Following a brief wash with PBS-T, each membrane was incubated with the appropriate primary antibody for 1 h at RT, or overnight at 4°C with constant agitation.

Each membrane was washed 3 times in PBS-T for 5 min at RT and probed with a secondary antibody (refer to section 2.3.9 for details) for 1 h at RT with constant agitation. Finally, each membrane was washed 3 times with PBS-T for 5 min at RT with constant agitation and scanned using a Licor[®] Odyssey infrared scanner (LI-COR[®] Inc., USA).

2.3.8 Total Protein Stain

In a total protein stain, all the sample proteins are modified reversibly and detected according to the used staining strategy. Total protein stain is one of the most accurate and reliable methods for normalization of Western Blot (Biosciences, 2015).

After overnight transferring, total proteins were detected using REVERT[™] Total Protein Stain kit (LI-COR Biosciences UK Ltd., Cambridge, UK) accordingly to the manufacturer's protocol. Membranes were briefly rinsed in H₂O and incubated for 5

min at RT in 5 ml of REVERT Total Protein Stain solution, with constant agitation. After washing twice for 30 s in 5 ml of REVERT Wash solution (6.7% (v/v) Glacial Acetic Acid, 30% (v/v) Methanol, in H₂O) membranes were rinsed with H₂O and scanned in the 700 nm channel of a LI-COR Odyssey 9120 IR Imager (LI-COR® Inc., USA). After scanning membranes were incubated for 5-10 min in 5 ml of REVERT Reversal solution [0.1M Sodium Hydroxide, 30% (v/v) Methanol, in H₂O] at RT with constant agitation until staining was no longer visible. Membranes were then rinsed in H₂O, blocked, and used for immunodetection.

2.3.9 Antibodies

The following primary antibodies (Ab) were used for Western blotting:

- Living Colors® A. v. GFP monoclonal antibody (Clontech Laboratories Inc., California USA) also called JL-8 was generated in mice (isotype IgG2a) from hybridoma cells against full-length *Aequorea victoria* green fluorescent protein (GFP). This antibody was used in immunoblotting at a dilution of 1:3,000.
- High-Affinity anti-HA monoclonal antibody (Roche Diagnostic Ltd., West Sussex, UK) was generated in rat and used in immunoblotting at a dilution of 1:1,000.
- Monoclonal mouse anti-Syntaxin1a antibody (clone HPC-1 S0664) (Sigma, Poole, UK) was generated in rat from hybridoma cells (isotype IgG1) and used in immunoblotting at a dilution of 1:1,000.
- Rabbit monoclonal anti-GAPDH antibody (Abcam, Cambridge, UK) was used in immunoblotting at a dilution of 1:1,000.
- Mouse monoclonal anti-6X histidine tag antibody 18184 (Abcam, Cambridge, UK) was derived from tissue culture supernatant. In immunoblot it was used at a dilution of 1:1,000.

The secondary antibodies (DyLight™, Thermo Scientific) were used on a species-specific basis at a dilution of 1:10,000 or 1:20,000. They are conjugated with an infrared dye (IR680 nm or IR800 nm) which allowed protein detection by image scanning.

2.3.10 Peptide Array and Far Western blotting

The term peptide array refers to a collection of peptides spotted on a support surface (a membrane, glass, or plastic). The peptides that are displayed on the surface are incubated with a protein, peptide, or enzyme of interest in a classic “Far Western blotting” to detect protein-protein interactions (Hall, 2004).

Peptide arrays were synthesized by the Baillie lab (University of Glasgow, Glasgow, UK). The entire human SPRY2 sequence (from amino acid at position 1 to 315), was spotted on a nitrocellulose membrane in a total of 59 peptides. Each peptide covered a sequence of 25 amino acids with 20 amino acids overlapping between one peptide and the next one (e.g. if peptide 1 covers residues 1-25, peptide 2 covers residues 6-30).

In all steps, the membrane was kept under constant agitation and at RT using an orbital shaker or a tube roller, unless otherwise specified. The nitrocellulose membrane was first activated in 5 ml of absolute ethanol for 10 min (Fisher Scientific, Loughborough, UK) and then washed twice with 5 ml of TBS-Tween (TBT-T) [Tris-buffer-saline supplemented with 0.1% of Tween-20, pH was adjusted to 7.6 with HCl 12 N] for 10 min. The array was incubated with 5% BSA (w/v) in 5 ml TBS-T for 3 h and subsequently overlaid with 0.5 μ M of His₆-tagged ANK17 WT (encoding amino acids 51-288 of ANK17) in 5 ml TBS-T, overnight and at 4°C. The day after, the membrane was washed 3 times in 5 ml TBS-T for 10 min, probed with a histidine antibody for 2 h, and further washed 3 times for 10 min in TBS-T. Finally, the array was probed with a secondary antibody, washed 3 times for 10 min in TBS-T, and bound peptides were revealed using a Licor® scanner as described above for Immunoblotting (section 2.3.7).

2.4 Confocal microscopy

Confocal microscopy provides a key tool for the direct observation of tissues, cells, subcellular structures and localisation of proteins. Biological samples can be treated, or proteins conjugated with fluorescent dyes returning a visible image.

For immunofluorescence and confocal experiments PC12 cells, plated on poly-D-lysine-coated coverslips, were used 48 h post-transfection. Each coverslip was washed twice in PBS and cells were fixed in 500 μ l of 4% Formaldehyde (16% Formaldehyde was diluted in PBS) (Pierce™, Thermo Fisher Scientific, UK) and incubated for 30 min at RT. After a first wash in 1ml of PBS and a second wash in 1 ml of distilled H₂O, coverslips were air-dried for 1 h and subsequently mounted on glass slides using Mowiol mounting agent. Cells were imaged the following day. All images were acquired as z-stacks using an SP8 confocal microscope (Leica Microsystems) in Lightning mode (Microsystems Leica, 2018).

2.5 Bioinformatics tools

Secondary Structure Prediction. To predict the secondary structure of human SPRY2, PSIPRED 4.0 Protein Analysis Workbench software, from the UCL Department of Computer Science was used (Buchan and Jones, 2019; Jones, 1999). Outputs from different platforms (i.e. PSI-BLAST) are taken into account to provide a prediction accuracy of 84.2% (Buchan and Jones, 2019). The amino acid sequence of human SPRY2 protein was obtained from UniProtKB in FASTA format (identifier O43597) and uploaded on PSIPRED 4.0 which returned the predicted secondary structure.

Helical wheel projections. NetWheels software was used to generate helical wheel projections. The regions of SPRY2 predicted as α -helices using PSIPRED 4.0, were used as input sequences to draw helical wheel projections in which each amino acid is shown on the perimeter of a circle (representing the helix) and the angle of rotation of every three residues is fixed to 100° (Mól et al., 2018).

SPRY2 multiple sequence alignment. Protein sequences of *SPRY Drosophila melanogaster* (Fruit fly) and *Danio rerio* (Zebrafish), *Xenopus tropicalis* (Xenopus), *Gallus gallus* (Chicken), *Bos taurus* (Bovine), *Homo sapiens* (Human), *Rattus norvegicus* (Rat), and *Mus musculus* (Mouse) *SPRY2* were aligned using Clustal Omega software (EMBL-EBI) (Sievers et al., 2011). Also in this case, the input sequences, in FASTA format, were all obtained from UniProtKB and directly uploaded on the program.

2.6 Data quantification and statistical analysis

Quantification of band intensity obtained from Immunoblots and Coomassie-stained gel was done using Odyssey® Infrared Imaging System Data Quantification (LI-COR® Inc., USA). S-acylation and protein expression levels, amount of pulled-down, immunoprecipitated, and fractionated proteins, as well as the extrapolation of protein concentration from BSA standard curves, were all calculated using Excel software 2017 (Microsoft®, Office system). Colocalisation values (i.e. Pearson's coefficient) and *SPRY2* distribution at the plasma membrane were calculated using Fiji-ImageJ software (NIH).

All statistical analyses were performed in GraphPad Prism 7.0 (San Diego, CA, USA). Differences were analysed either with one-way ANOVA followed by Tukey's multiple comparison test, two-way ANOVA, or Unpaired Student t-test, as indicated in figure legends.

All the presented graphs were generated with GraphPad Prism 7.0. Mean values with standard error of the mean (SEM) were plotted, and the number of replicates was indicated in the figure legends. For significant results **** denotes $P < 0.0001$, *** $P < 0.001$, ** $P < 0.01$, * $P < 0.05$. All figures were created and edited using Adobe Illustrator CC 2014 and/or Fiji ImageJ software.

Quantification of overall S-acylation: for each biological sample, the click signal was normalised against the protein expression level (GFP signal), after subtracting the relative background. The background was calculated on an area identical to that of

GFP and click signal. Equation used: $(X-Y)/(A-B)$. (X-Y) refers to the click signals minus their corresponding backgrounds, whereas (A-B) refers to the GFP signals minus their corresponding backgrounds.

Quantification of SPRY2 protein levels: for each biological sample, SPRY2 expression level (GFP signal) was normalised against the total protein stain (TPS), after subtracting the relative background. An area of fixed dimensions was used for the TPS across all experiments. Equation used: $(A-B)/TPS$. (A-B) refers to the SPRY2 signals minus their corresponding backgrounds. TPS refers to the signal of the total protein stain, relative to the lane of the analysed sample.

Quantification of pull-down assay experiments: for each biological sample, the amount of protein pulled down by His₆-ANK17 WT, or by His₆-W130A, took into account the volume (i.e. μ l) loaded for input (i.e. 7.5%) and bound fractions (i.e. 30%). Used equation: $[(\text{signal of fraction bound to His}_6\text{-ANK17}/4) - (\text{negative control signal}/4)] / \text{input signal}$.

Quantification of immunoprecipitation (IP) experiments: for each sample, after background subtraction, the amount of co-immunoprecipitated protein (expressed in percentage) was calculated as a ratio between co-immunoprecipitated (Co-IP'd) and immunoprecipitated (IP'd) samples in the immunoprecipitate only. Used equation: $\text{Co-IP'd}/\text{IP'd}$. To evaluate protein expression levels, input fractions were collected prior to immunoprecipitation, run on agarose gels and revealed by immunoblotting. These fractions were not considered for quantification.

Quantification of SPRY2 in fractionation experiments: for each biological sample and membrane fractions, the amount of SPRY2 was calculated as $\text{Tot SPRY2} = B + U$. B refers to the intensity of SPRY2 fast-migrating band (i.e. bottom band, B), whereas U refers to the intensity of SPRY2 slow-migrating band (i.e. upper band, U). For each species (i.e. fast- or slow-migrating SPRY2), relative amounts were derived as a ratio against the Tot SPRY2. Equations used: $(B/\text{Tot SPRY2})$ or $(U/\text{Tot SPRY2})$.

Intracellular distribution of SPRY2: To measure the intracellular distribution of mCherry-SPRY2 WT and EGFP-SPRY2 proteins, Pearson's coefficient (R_{tot}) was

calculated using Fiji software (NIH). The co-localization threshold function (Coloc 2) was used to analyse different images on both channels (eight images for SPRY2 WT, NDK, and C265/268A; four images for SPRY2 WT and P154A, three images for 155-315).

Quantification of SPRY2 at the plasma membrane: To compare the SPRY2 localization at the plasma membrane (PM) between mCherry-SPRY2 WT and EGFP-SPRY2 constructs WT, NDK, and C265/268A a single slice was chosen for each image, preferably at the centre of the cells. The fluorescence intensity associated with the PM (PM IntDen) and the whole cell (Tot IntDen) was calculated for identical regions of interest (ROI) for both mCherry and EGFP signal. The amount of SPRY2 at the PM was then derived as a ratio of the fluorescence intensity at the PM against the fluorescence intensity of the whole cell (PM IntDen/Tot IntDen).

Chapter 3 Identification of key features required for efficient S-acylation and plasma membrane targeting of SPRY2 protein

3.1 Introduction

The role of SPRY2 in growth factor signalling has been shown in many studies, in species ranging from *Drosophila* to humans (Kim and Bar-Sagi, 2004; Mason et al., 2006). Furthermore, several protein interactions have been identified (Edwin et al., 2009) and the important roles described for phosphorylation and ubiquitination in controlling the levels of SPRY2 in cells (Guy et al., 2003). In addition, SPRY2 was reported to undergo S-acylation (Impagnatiello et al., 2001), the attachment of fatty acids onto cysteine residues (Chamberlain and Shipston, 2015) but the effects of this post-translational modification on the localisation, stability and function of SPRY2 are unclear. All Sprouty proteins (SPRYs) contain a signature cysteine-rich domain (CRD) with twenty-six cysteines in the human and mouse SPRY2 isoforms (UniProtKB-O43597 and UniprotKB-Q9QXV8, respectively). Interestingly, S-acylation of other proteins with cysteine-rich domains has been shown to have a range of regulatory effects. For example, S-acylation of the four-cysteine cluster in the SNARE protein SNAP25b regulates membrane binding, plasma membrane targeting and endosomal cycling (Greaves et al., 2010; Greaves and Chamberlain, 2011a). In addition, the extent of S-acylation of SNAP25b has also been suggested to regulate targeting to cholesterol-rich membrane domains, affecting the function of this SNARE protein in exocytosis (Salaün et al., 2005b, 2005a).

S-acylation of SPRY proteins was reported for the first time almost 20 years ago by Impagnatiello and colleagues. In this first and only report, HUVEC cells, infected with either SPRY1 or SPRY2 constructs, were metabolically labelled using either $^3\text{[H]}$ palmitate or $^{35}\text{[S]}$ methionine/cysteine (Impagnatiello et al., 2001). Selective incorporation of $^3\text{[H]}$ palmitate, coupled with the observation that hydroxylamine treatment could revert $^3\text{[H]}$ labelling (hydroxylamine is known to hydrolyse the thioester bonds characteristic of S-acylation) led to the conclusion that both SPRY1

and SPRY2 are S-acylated (Impagnatiello et al., 2001). Despite S-acylation of SPRY1 and SPRY2 being reported long ago, it is still unclear whether S-acylation, binding to PIP₂, or association with caveolin-1 is the mechanism responsible of plasma membrane (PM) recruitment.

In mammalian cells, S-acylation is mediated by a family of 23 S-acyltransferase “zDHHC” enzymes. S-acylation is a two-step process with the first step being autoacylation of the enzyme, and the second step being the transfer of the acyl chain from the enzyme to the substrate (Jennings and Linder, 2012; Mitchell et al., 2010). Within cells, zDHHC enzymes mainly localise to the Golgi and endoplasmic reticulum, with a few isoforms found at the plasma membrane or at recycling endosomes (Greaves and Chamberlain, 2011b; Ohno et al., 2006). At the Golgi, where most S-acylation events are thought to take place, certain zDHHC enzymes have been classified as low-selectivity/high-activity or high-selectivity/low-activity (Lemonidis et al., 2014). Low-selectivity/high-activity isoforms include zDHHC7 and zDHHC3, which are active against a plethora of proteins and do not appear to recognise specific features of their substrates to mediate S-acylation (Chamberlain and Shipston, 2015). The ability of these enzymes to S-acylate proteins most likely depends on other factors such as co-localisation and proximity of reactive cysteines in the substrate to the DHHC active site (Lemonidis et al., 2017b). High-selectivity/low-activity enzymes include zDHHC17 and zDHHC13, which require specific recognition of their substrate proteins for successful S-acylation. The key substrate-recognition site of zDHHC17 and zDHHC13 is their N-terminal ankyrin-repeat (ANK) domain which recognises a conserved [VIAP][VIT]XXQP (X: any amino acid) sequence, also known as the zDABM (zDHHC ANK Binding Motif) in their substrates (Lemonidis et al., 2015a). This zDABM sequence was initially identified through a detailed mutagenic analysis of interactions of zDHHC17 with the multiply S-acylated proteins SNAP25b and cysteine-string protein (CSP α) (Lemonidis et al., 2015a).

Interestingly, SPRY2 was shown to contain a zDABM (149-IIRVQP-154) and a peptide encompassing this region of the protein bound to the ANK domain of zDHHC17 in peptide array experiments (Lemonidis et al., 2017a). Indeed, a proteome-wide

BioPlex study showed that zDHHC17 and SPRY2 form a complex that can be isolated from HEK293 cells by immunoprecipitation (Huttlin et al., 2017), suggesting that this enzyme may be involved in the S-acylation pathway of SPRY2. However, there is currently no evidence that SPRY2 is a substrate of zDHHC17 and indeed several other proteins that contain a zDABM and interact with zDHHC17 do not undergo S-acylation (Lemonidis et al., 2017a).

The aim of this chapter was to investigate in more detail the mechanisms and outcomes of SPRY2 S-acylation, testing the hypotheses that specific zDHHC enzymes mediate SPRY2 S-acylation and that this post-translational modification affects the level and localisation of SPRY2.

3.2 Results

3.2.1 SPRY2 is S-acylated by zDHHC17 promoting protein stability

The CRD in SPRY2 contains an abundance of cysteine residues that are thought to be modified by S-acylation (Impagnatiello et al., 2001). Recent works showed that SPRY2 contains a recognition site for zDHHC17 enzyme (Lemonidis et al., 2017a) and these proteins also co-immunoprecipitate from cells (Huttlin et al., 2017).

To examine if zDHHC17 is able to S-acylate SPRY2, HEK293T cells were transfected with EGFP-SPRY2 together with either pEFBOS-HA (control), or HA-zDHHC17. Cells were labelled with C16:0-azide, and click chemistry with alkyne-IR800, SDS-PAGE and immunoblotting were performed as described in Chapter 2. Figure 3.1 shows that S-acylation of SPRY2 was increased upon zDHHC17 co-expression. Furthermore, the increase in S-acylation was accompanied by a marked enhancement in expression levels of the SPRY2 fast-migrating (i.e. lower) immunoreactive band (Fig. 3.1).

To test whether the increase in the amount of SPRY2 seen when it is co-expressed with zDHHC17 is dependent on S-acylation, SPRY2 was also co-expressed with a catalytically dead version of zDHHC17 in which the cysteine of the 'DHHC' motif (i.e. Cys-467) was mutated to alanine. This "zDHHA17" mutant retains the principal

binding site for SPRY2 (i.e. the ankyrin repeat domain). As expected, in the presence of this inactive zDHHA17 mutant, S-acylation of SPRY2 was not increased above that of the negative control (i.e. pEFBOS-HA) (Fig. 3.1). Notably, SPRY2 expression was also not increased by this catalytically dead mutant of zDHHC17, suggesting that the observed enhancement in SPRY2 levels is mediated by S-acylation *per se* rather than binding of SPRY2 to zDHHC17 or other effects of protein co-expression.

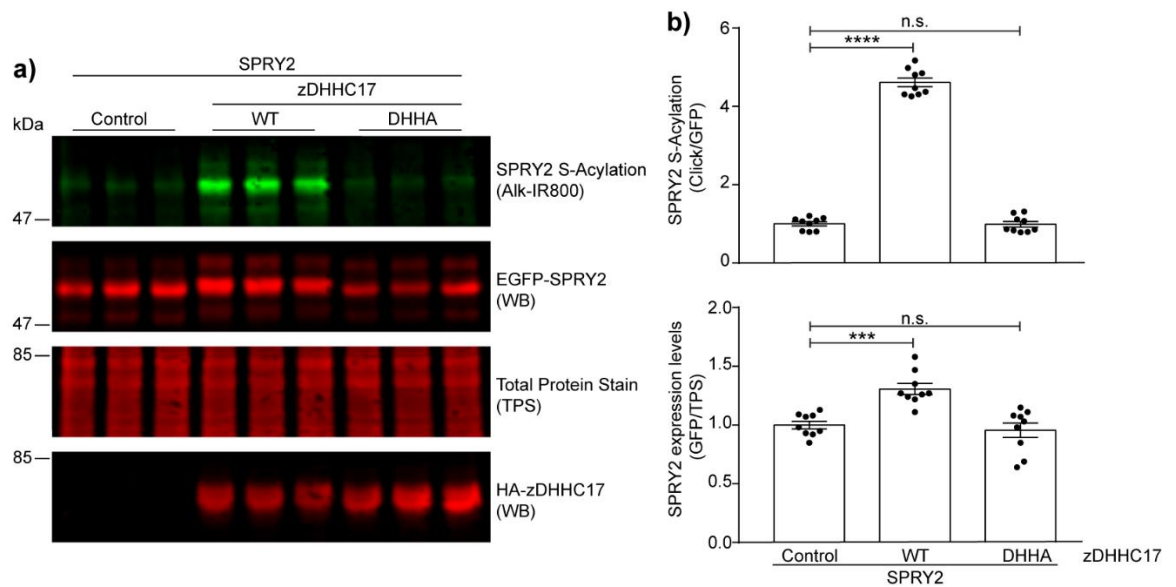


Figure 3.1 S-acylation of SPRY2 by zDHHC17 enhances protein levels

HEK293T cells were transfected with EGFP-tagged SPRY2 together with pEFBOS-HA (referred to as “control” in the figure), or HA-tagged zDHHC17 WT, or zDHHA17. Cells were incubated with 100 μ M C16:0 azide for 4 h and labelled proteins reacted with alkyne IRdye-800 using click chemistry. Before performing immunoblotting, membranes were incubated with a total protein stain (TPS) and the signal was detected at 700 nm. S-acylation was revealed at 800 nm, GFP and HA signals were detected at 700 nm. **a)** Representative image showing SPRY2 S-acylation (*top*), SPRY2 expression levels (*middle top*) and total protein stain (TPS, *middle bottom*) detected on the same immunoblot. For zDHHC17, HA (*bottom*) was revealed for the same samples on a different immunoblot. The positions of the molecular weight markers are shown on the left. **b)** Graphs showing SPRY2 S-acylation and expression levels after normalisation. Each bar shows mean values \pm SEM; filled circles represent individual samples. Differences were analysed by one-way ANOVA (**** denotes $P < 0.0001$, *** $P < 0.001$, n.s. not significant compared with control, $n=9$).

As mentioned above, the increase in S-acylation correlated with enhancement in the levels of the SPRY2 fast-migrating (i.e. lower) immunoreactive band (Fig. 3.1). The slow- (i.e. upper) and fast- (i.e. bottom) migrating bands of SPRY2 have been previously suggested to represent different populations of phosphorylated protein with the slower migration of the upper band linked to phosphorylation of residues

including Ser-112, and Ser-121 in the human protein (DaSilva et al., 2006; Lao et al., 2007).

To confirm that this was the case also in our experiments, the corresponding serine residues in mouse SPRY2 sequence (i.e. Ser-111 and Ser-120, respectively) were substituted with alanines. The resulting SPRY2 S111A and S120A mutants were used to transfect HEK293T cells. Cells were lysed and immunoblotting was performed as described in Chapter 2. Mutation of either Ser-111 (S111A), or Ser-120 (S120A) led to a loss of the upper immunoreactive band of SPRY2 (Fig. 3.2), in agreement with previous work (DaSilva et al., 2006).

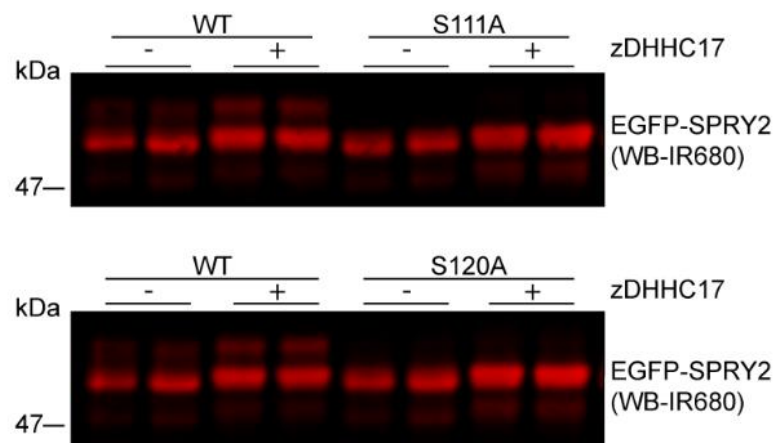


Figure 3.2 Loss of the slower migrating band of SPRY2 after replacement of either Ser-111 or Ser-120 with alanine residues

HEK293T cells were transfected with either EGFP-tagged SPRY2 WT, SPRY2 S111A (*top panel*), or SPRY2 S120A (*bottom panel*) together with either pEFBOS-HA (referred to as “-” in the figure) or HA-tagged zDHHC17 (referred to as “+” in the figure). To reveal SPRY2 levels, membranes were probed using an anti-GFP antibody (*WB-IR680*). The positions of the molecular weight markers are shown on the left.

3.2.2 The increase in SPRY2 levels following S-acylation is independent of the highly conserved Tyr-55 (Y55)

Previous work has shown that phosphorylation of the highly conserved Tyr-55 (Y55) in SPRY2 is linked to protein stability via a c-Cbl-dependent pathway (Kim and Barsagi, 2004). Under EGF stimulation, phosphorylation at this residue enhances the interaction of SPRY2 with c-Cbl, which in turn determines its proteolytic degradation *via* a ubiquitination-dependent pathway (Fong et al., 2003; Sasaki et al., 2001). To investigate if the increased expression of SPRY2 following S-acylation by zDHHC17 is linked to this pathway, we blocked Y55 phosphorylation by substituting Tyr-55 with either an alanine or a phenylalanine residue (i.e. SPRY2 Y55A and Y55F mutants) (Fong et al., 2003; Sasaki et al., 2001).

HEK293T cells were transfected with EGFP-SPRY2 WT, Y55A, or Y55F mutant together with pEFBOS-HA (control) or HA-zDHHC17. Cells were labelled with C16:0-azide, and click chemistry with alkyne-IR800, SDS-PAGE and immunoblotting were performed as described in Chapter 2. As shown in Figure 3.3, both SPRY2 Tyr-55 mutants were used as substrates by zDHHC17 and showed S-acylation levels similar to wild-type SPRY2 suggesting that the phosphorylated state of this residue is not important for zDHHC17-mediated S-acylation. Furthermore, expression levels of both SPRY2 Y55A and Y55F were also increased to a similar level as wild-type SPRY2 when zDHHC17 was co-expressed. These data suggest that the observed S-acylation-dependent enhancement in SPRY2 levels occurs independently of the phosphorylation status of Tyr-55 and therefore occurs through a different process to the characterised c-Cbl-dependent degradation pathway.

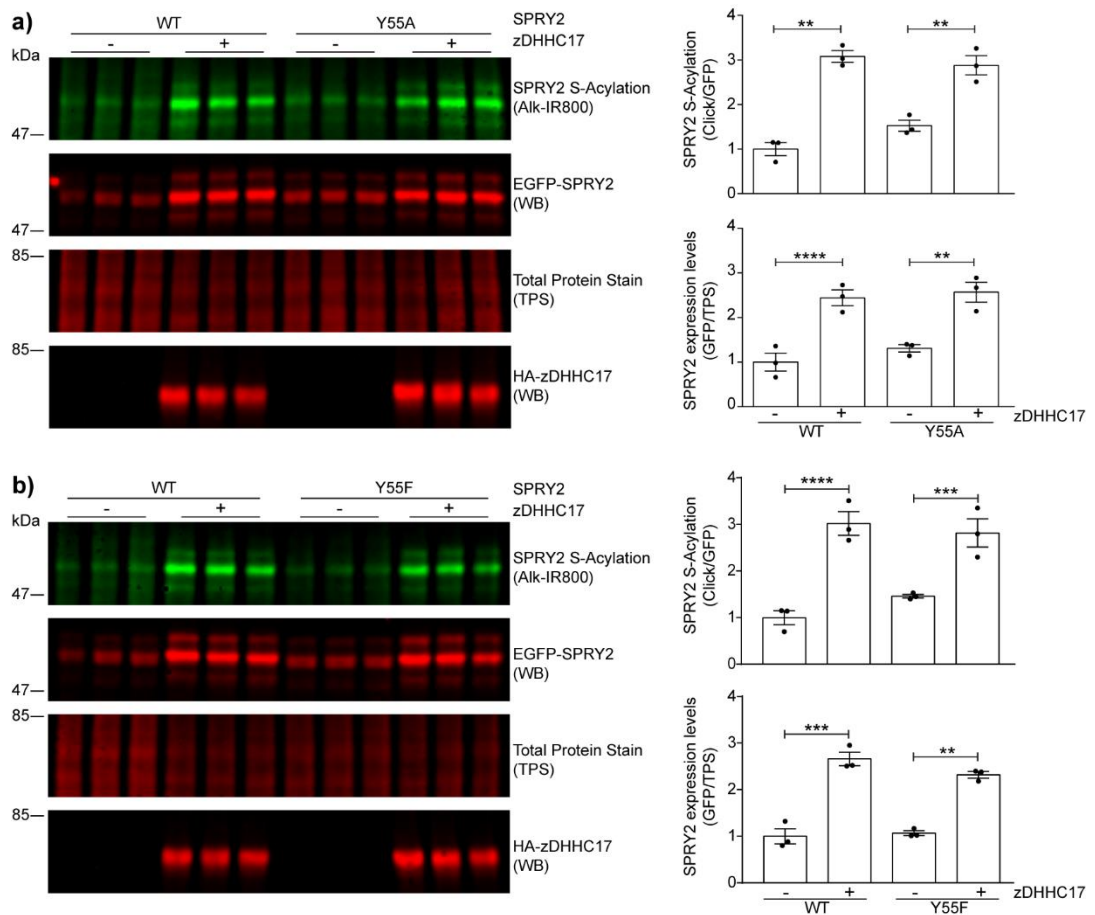


Figure 3.3 S-acylation-dependent increase in SPRY2 levels is independent of phosphorylation at the highly conserved Tyr-55

HEK293T cells were transfected with EGFP-tagged SPRY2 WT, Y55A, or Y55F, together with pEFBOS-HA (referred to as “-” in the figure), or HA-zDHHC17 (referred to as “+” in the figure). Cells were incubated with 100 μ M C16:0-azide for 4 h and labelled proteins reacted with alkyne IRdye-800 using click chemistry. Before performing immunoblotting, membranes were incubated with a total protein stain (TPS) and signal was detected at 700 nm. S-acylation was revealed at 800 nm, GFP and HA signals were detected at 700 nm. **a-b) On the left:** Images showing SPRY2 S-acylation (*top*), SPRY2 expression levels (*middle top*) and total protein stain (TPS, *middle bottom*) detected on the same immunoblot. For zDHHC17, HA (*bottom*) was revealed for the same samples on a different immunoblot. The positions of the molecular weight markers are shown on the left. **a-b) On the right:** graphs showing SPRY2 S-acylation and expression levels after normalisation. Each bar shows mean values \pm SEM; filled circles represent individual samples. Differences were analysed by one-way ANOVA (****

denotes $P < 0.0001$, *** $P < 0.001$, ** $P < 0.01$, comparing conditions containing zDHHC17 with the corresponding conditions without zDHHC17, $n=3$).

3.2.3 Region 260-290, within the CRD of SPRY2, is important for zDHHC17-mediated stability

Since the S-acylation-dependent increase in SPRY2 levels did not appear to be linked to Tyr-55, we investigated if the SPRY domain of SPRY2 (encompassing amino acids 177-291) was playing a role. Thus, truncated versions containing different regions of this domain were generated by inserting premature stop codons into the coding sequence of SPRY2 wild-type. The resulting EGFP-SPRY2 constructs I200X (encoding amino acids 1-200), S230X (encoding amino acids 1-230), S260X (encoding amino acids 1-260), and G290X (encoding amino acids 1-290) (Fig. 3.4a) were used to transfect HEK293T cells. SDS-PAGE, total protein stain, and immunoblotting analyses were performed as described in Chapter 2.

As shown in Figure 3.4b-c, co-expression of zDHHC17 (i) correlated with decreased expression of SPRY2 I200X, (ii) had no effects on levels of SPRY2 S230X or S260X mutants, and (iii) was associated with increased expression levels of SPRY2 G290X mutant. These results might suggest that region 260-290 is important for zDHHC17-mediated stability of SPRY2.

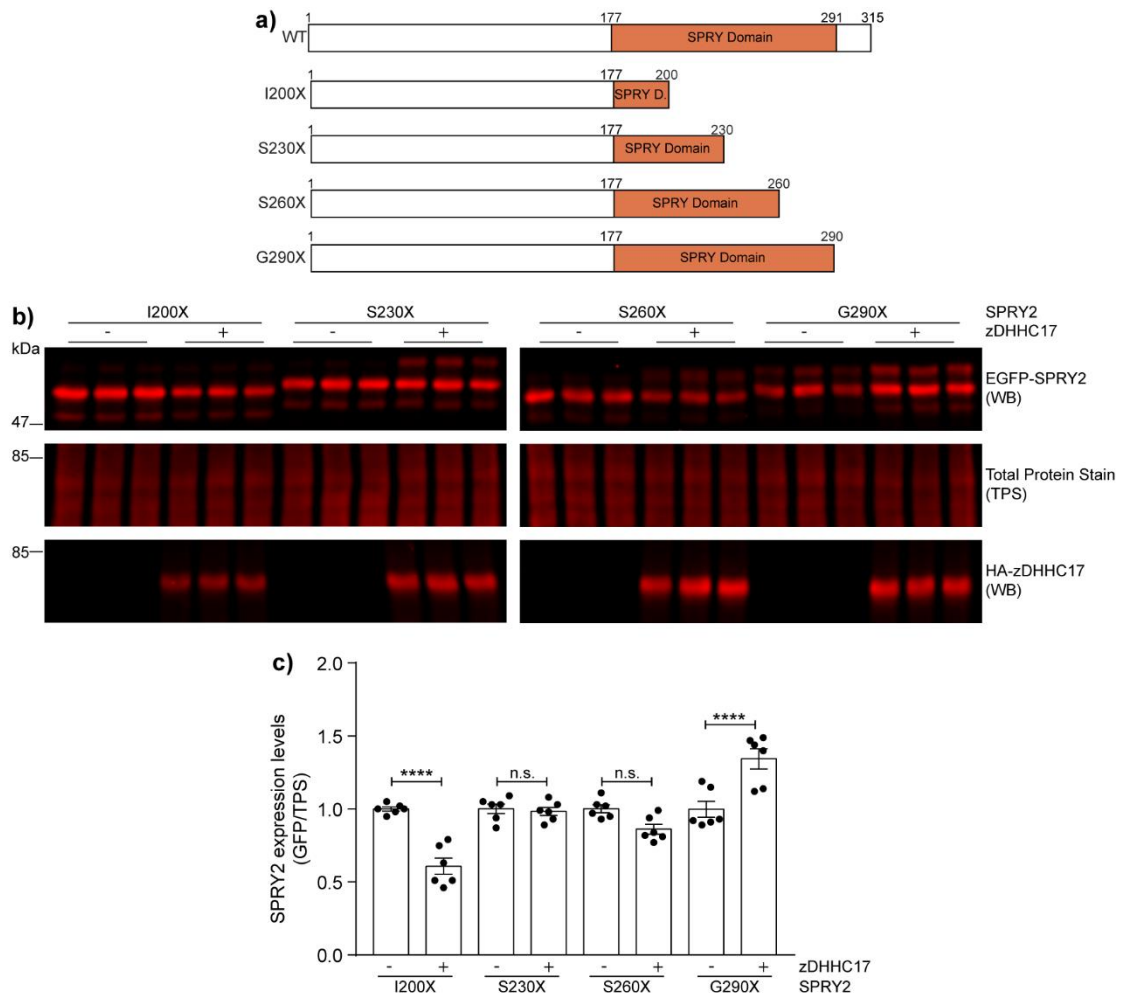


Figure 3.4 SPRY2 region 260-290 is important for the zDHHC17-mediated increase in SPRY2 levels

a) EGFP-tagged SPRY2 I200X, S230X, S260X, and G290X were generated by inserting a premature stop codon in frame with the protein sequence, using EGFP-tagged SPRY2 wild-type as the DNA template. **b)** HEK293T cells were transfected with EGFP-tagged SPRY2 I200X, S230X, S260X, or G290X, together with pEFBOS-HA (referred to as “-” in the figure), or HA-zDHHC17 (referred to as “+” in the figure). Cells were lysed and run on an 8% SDS-PAGE, total protein stain (TPS), GFP and HA were revealed at 700nm. Representative immunoblots showing SPRY2 levels (*top*) and total protein stain (TPS, *middle*) detected on the same immunoblot. For zDHHC17, HA (*bottom*) was revealed for the same samples on a different immunoblot. The positions of the molecular weight markers are shown on the left. **c)** Graph showing SPRY2 expression levels after normalisation. Each condition expressing zDHHC17 was normalised against the corresponding negative control (pEFBOS-HA). Each bar shows

mean values \pm SEM; filled circles represent individual samples. For clarity, only relevant statistical analysis is shown. Differences were analysed by one-way ANOVA (**** denotes $P < 0.0001$, n.s. not significant, $n=6$).

3.2.4 SPRY2 is differentially S-acylated by zDHHC17, zDHHC7, and zDHHC3 enzymes

Certain Golgi-localised zDHHC enzymes have been classified as either high-selectivity/low-activity or low-selectivity/high-activity. zDHHC17 is a high-selectivity/low-activity zDHHC enzyme that requires direct interaction with its substrates for effective S-acylation (Lemonidis et al., 2014). However, this enzyme co-localises at the Golgi with more promiscuous zDHHC enzymes, including the low-specificity/high-activity zDHHC3 and zDHHC7 (Lemonidis et al., 2014; Ohno et al., 2006). To investigate if these more promiscuous enzymes can also modify SPRY2 and to what extent, EGFP-SPRY2 was co-expressed with HA-zDHHC17, HA-zDHHC7 or HA-zDHHC3 in HEK293T cells. Cells were labelled with C16:0-azide, and click chemistry with alkyne-IR800, SDS-PAGE and immunoblotting were performed as described in Chapter 2.

Expression of either zDHHC7 or zDHHC3 resulted in a substantial increase in SPRY2 S-acylation, far greater than that seen with zDHHC17 (Fig. 3.5). Despite this substantially different level of S-acylation, SPRY2 expression was similarly increased by all three zDHHC enzymes (Fig. 3.5b). This latter observation, that zDHHC3, zDHHC7, and zDHHC17 enhance the levels of SPRY2 by the same extent, implies that the increased S-acylation signal associated with zDHHC3 and zDHHC7 reflects the modification of a larger number of cysteines in the CRD by these enzymes, rather than the modification of more SPRY2 molecules. It further suggests that S-acylation of a smaller number of cysteines, mediated by zDHHC17, is sufficient to enhance SPRY2 levels.

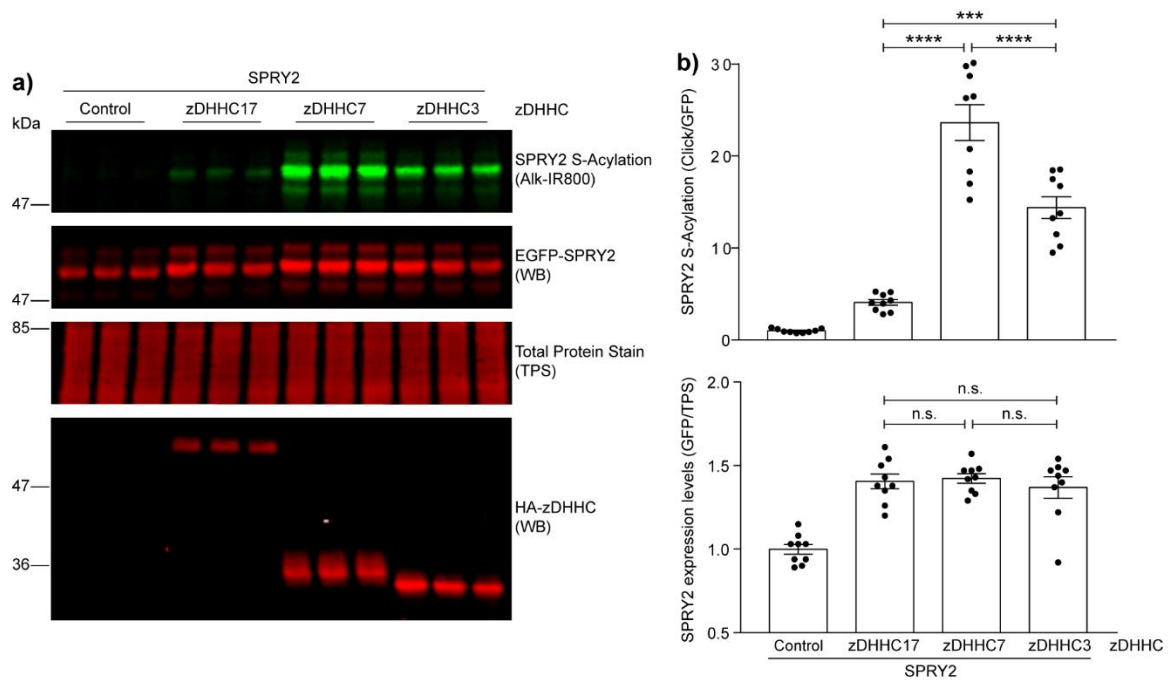


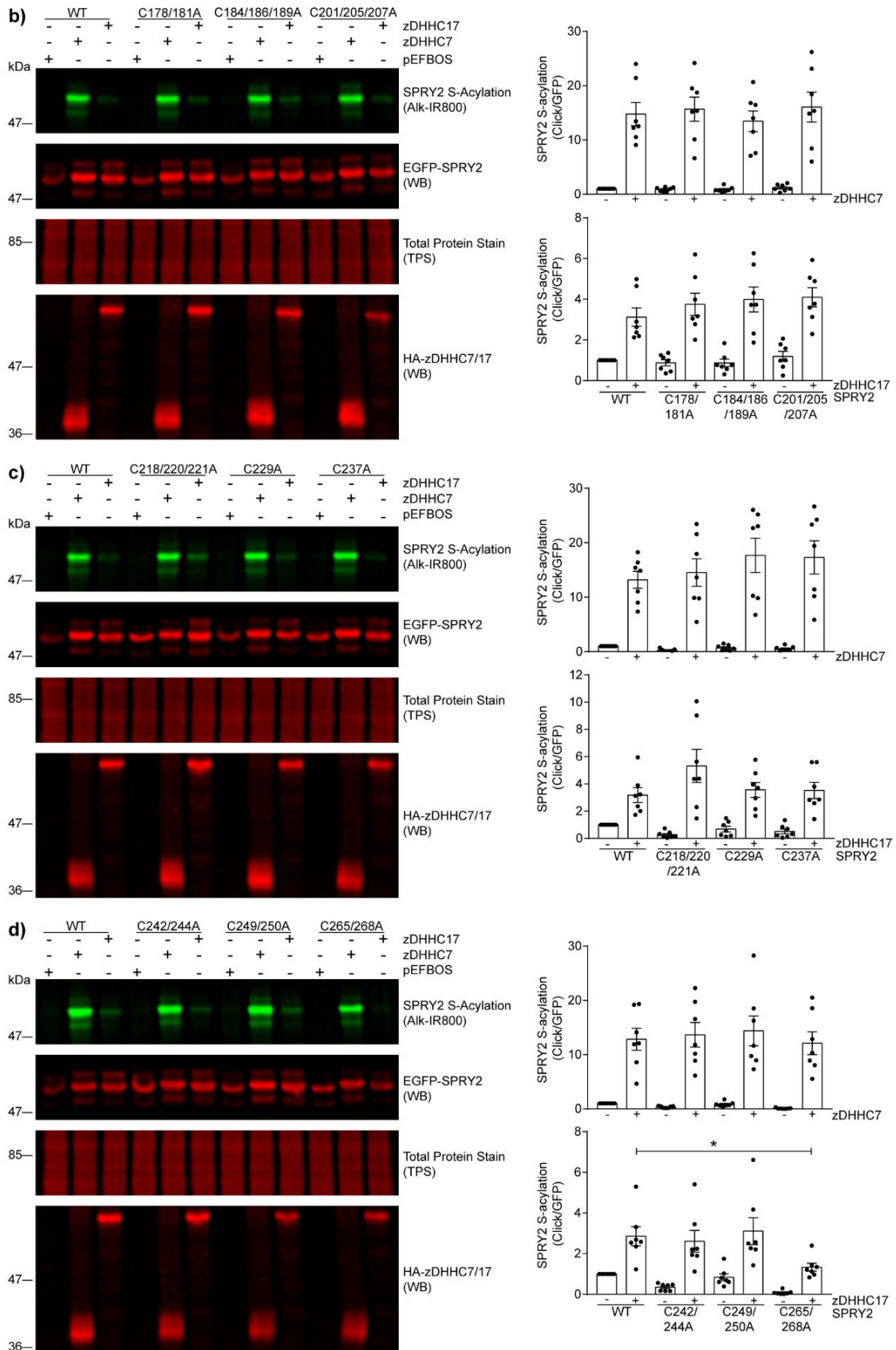
Figure 3.5 SPRY2 is S-acylated by zDHHC17, zDHHC7 and zDHHC3 enzymes

HEK293T cells were transfected with EGFP-tagged SPRY2 together with pEFBOS-HA (referred to as “control” in the figure), or HA-tagged zDHHC17, zDHHC7, or zDHHC3. Cells were incubated with 100 μ M C16:0 azide for 4 h and labelled proteins reacted with alkyne IRdye-800 using click chemistry. Before performing immunoblotting, membranes were incubated with a total protein stain (TPS) and signal was detected at 700 nm. S-acylation was revealed at 800 nm, GFP and HA signals were detected at 700 nm. **a)** Representative image showing SPRY2 S-acylation (*top*), SPRY2 expression levels (*middle top*) and total protein stain (TPS, *middle bottom*) detected on the same immunoblot. For zDHHC17, HA (*bottom*) was revealed for the same samples on a different immunoblot. The positions of the molecular weight markers are shown on the left. **b)** Graphs showing SPRY2 S-acylation and expression levels after normalisation. Each bar shows mean values \pm SEM; filled circles represent individual samples. Differences were analysed by one-way ANOVA (**** denotes $P < 0.0001$, $n=9$).

3.2.5 S-acylation of SPRY2 by zDHHC17 requires cysteines 265 and 268

The results described above suggest that zDHHC17 targets a small subset of cysteines in the CRD of SPRY2, whereas zDHHC7/3 modify a larger number of these residues. To narrow down the cysteines targeted by zDHHC17, we performed alanine mutagenesis of all the putative S-acylation sites. All the cysteines within the CRD of SPRY2 were mutated in blocks of one, two, or three residues (Fig. 3.6a). The resulting EGFP-SPRY2 C178/181A, C184/186/189A, C201/205/207A, C218/220/221A, C229A, C237A, C242/244A, C249/250A, C265/268A, C275/C279/C282A, C291/293A, and C300/301A mutants were co-expressed with either pEFBOS-HA, HA-zDHHC7, or HA-zDHHC17 in HEK293T cells. Cells were labelled with C16:0-azide, and click chemistry with alkyne-IR800, SDS-PAGE and immunoblotting were performed as described in Chapter 2.

Figure 3.6b-e shows that SPRY2 S-acylation by zDHHC17 was significantly decreased (compared with WT SPRY2) only by mutation of Cys-265 and Cys-268 (referred to as C265/268A in Fig. 3.6d) suggesting that these are preferred S-acylation sites. On the other hand, none of the SPRY2 cysteine mutants (including the Cys-265/268 mutant) showed significantly reduced S-acylation when co-expressed with zDHHC7, in agreement with the more promiscuous activity of this enzyme. It is interesting to note that the S-acylation of the C265A/C268A mutant was also reduced in the absence of zDHHC co-expression (compared with WT SPRY2; Fig. 3.6d), suggesting that this mutant is also a poorer substrate for endogenous zDHHC enzymes in HEK293T cells.



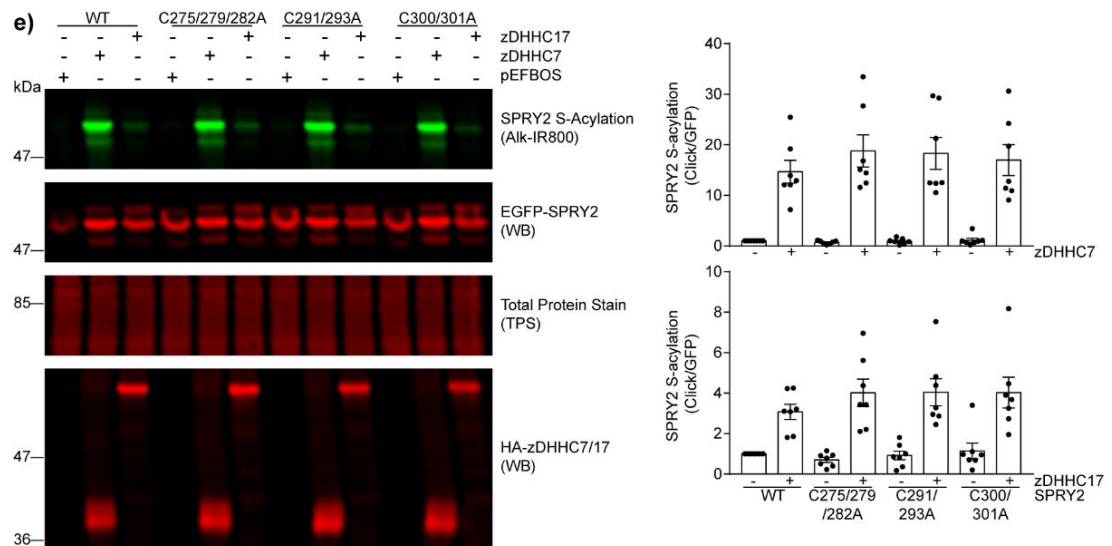
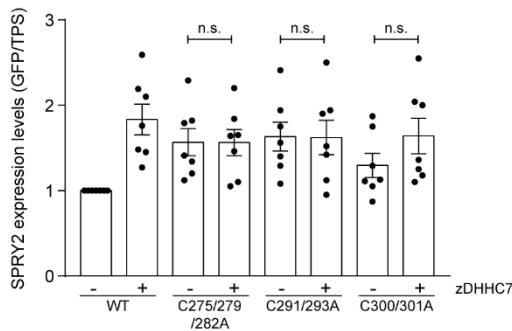
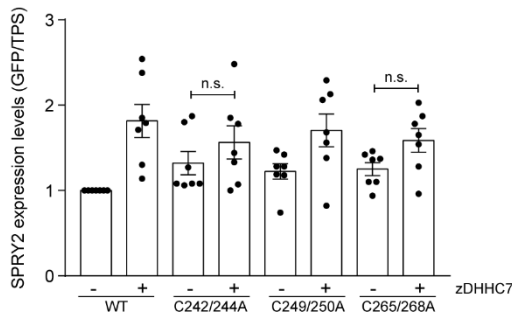
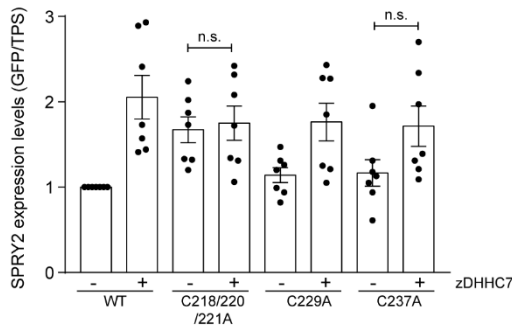
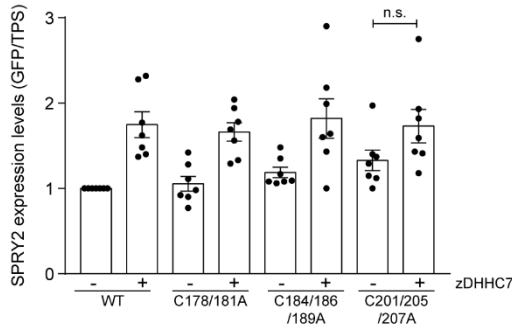


Figure 3.6 Efficient S-acylation by zDHHHC17 requires Cys-265 and Cys-268 within the CRD of SPRY2

a) Amino acid sequence of SPRY2 C-terminal region 178-315 containing the CRD (amino acids 178-301) with all cysteines mutated to alanine, highlighted in red. Among these, C265 and C268 are shown in bold. **b-e)** HEK293T cells were transfected with either EGFP-tagged SPRY2 WT, or one of the 12 cysteine to alanine mutants, together with either pEFBOS-HA (referred to as “-” in the figure), HA-tagged zDHHHC17, or HA-tagged zDHHHC7 (referred to as “+”, zDHHHC17/zDHHHC7 in the figure). Cells were incubated with 100 μ M C16:0 azide for 4 h and labelled proteins reacted with alkyne IRdye-800 using click chemistry. Before performing immunoblotting, membranes were incubated with a total protein stain (TPS) and signal detected at 700 nm. S-acylation was revealed at 800 nm, GFP and HA signals were detected at 700 nm. **b-e)** *On the left*, representative images showing SPRY2 S-acylation (*top*), SPRY2 expression levels (*middle top*) and total protein stain (TPS, *middle bottom*) detected on the same immunoblot, HA (*bottom*) was revealed for the same samples on a different immunoblot. The positions of the molecular weight markers are shown on the left. *On the right*, graphs showing SPRY2 S-acylation after normalisation. Each bar shows mean values \pm SEM; filled circles represent individual samples. For clarity, only relevant statistical analysis is shown in the figure. S-acylation of SPRY2 WT and all cysteine mutants were significantly increased upon zDHHHC17/7 expression compared to the corresponding controls (pEFBOS-HA). The S-acylation of all mutants in the presence of zDHHHC7/17 co-expression was not significantly different from SPRY2 WT, with the exception of C265A/C268A. Differences were analysed by Unpaired t-test (* P < 0.05, n=7).

The expression levels of SPRY2 cysteine mutants were also analysed. As expected, mutation of Cys-265/268 prevented the increase in SPRY2 levels when co-expressed with zDHHC17 (Fig 3.7). In addition, there was no significant increase in levels of this mutant when co-expressed with zDHHC7. Interestingly, Cys-265/268 are within region 260-290, important for zDHHC17-mediated enhancement of SPRY2 (Fig. 3.4). However, the overall effects of cysteine mutagenesis on SPRY2 levels were complex as several other cysteine mutants showed little enhancement in levels upon co-expression of zDHHC7 or zDHHC17, despite undergoing efficient S-acylation (Fig. 3.7). This latter observation highlights a complex association between the cysteine-rich domain, S-acylation and protein levels, which was not further investigated due to time constraints.

SPRY2 cysteine mutants, protein expression levels + zDHHC7



SPRY2 cysteine mutants, protein expression levels + zDHHC17

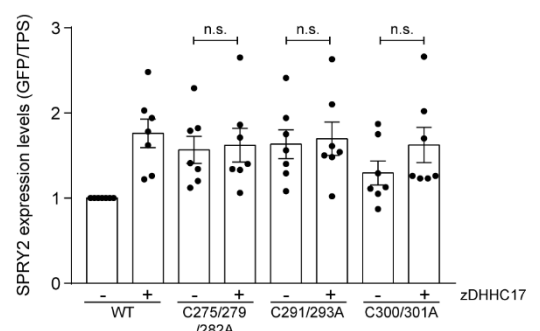
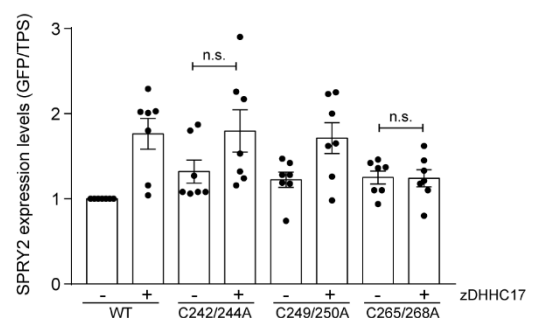
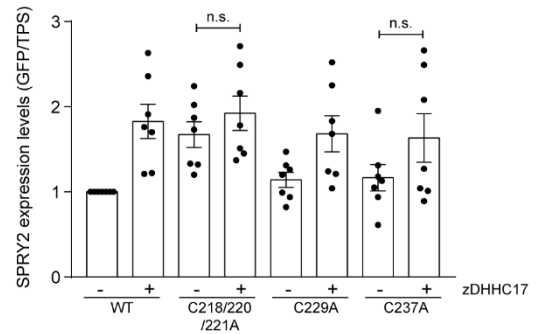
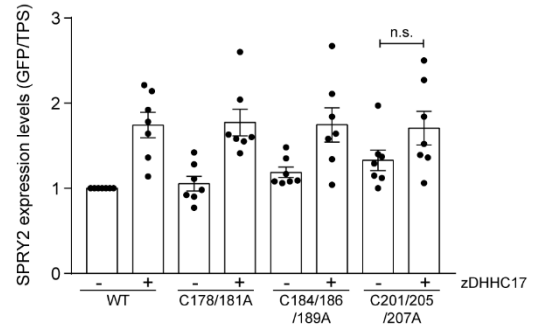


Figure 3.7 Analysis of the effects of cysteine substitutions on the level of SPRY2

Graphs showing SPRY2 levels after normalisation. In all cases, each bar shows mean values \pm SEM; filled circles represent individual samples. For clarity, only relevant statistical analysis is shown in the figure. S-acylation and expression for SPRY2 WT or cysteine mutants were increased upon zDHHC17/7 expression compared to the corresponding controls (pEFBOS-

HA) unless otherwise specified. Differences were analysed by Unpaired t-test (n.s. not significant, n=7).

To examine more closely the requirement for cysteines at positions 265 and 268, these residues were also substituted with alanine individually, and the corresponding SPRY2 mutants C265A and C268A were obtained. HEK293T cells were transfected with EGFP-SPRY2 WT, SPRY2 C265A, SPRY2 C268A, or SPRY2 C265/268A mutant together with either pEFBOS-HA or HA-zDHHC17. Cells were labelled with C16:0-azide, and click chemistry with alkyne-IR800, SDS-PAGE and immunoblotting were performed as described in Chapter 2.

The results presented in Figure 3.8 show that the S-acylation of the C265A mutant by zDHHC17 was significantly reduced compared with wild-type SPRY2. In contrast, SPRY2 C268A mutant did not show a loss of S-acylation. While Cys-265 appears to be the preferential S-acylation site, there was still a substantial level of S-acylation of this mutant and the biggest reduction was observed when both Cys-265 and Cys-268 were mutated simultaneously (i.e. SPRY2 C265/268A) (Fig. 3.8). Rearrangements in the secondary structure of the protein might account for the residual S-acylation observed with SPRY2 C265A mutant. For instance, S-acylation of Cys-268 may be enhanced when S-acylation of Cys-265 is blocked. Similarly, mutation of Cys-268 might result in zDHHC17 modifying not only Cys-265, but also some of the surrounding cysteines, thus accounting for the increased S-acylation observed with the SPRY2 C268A mutant.

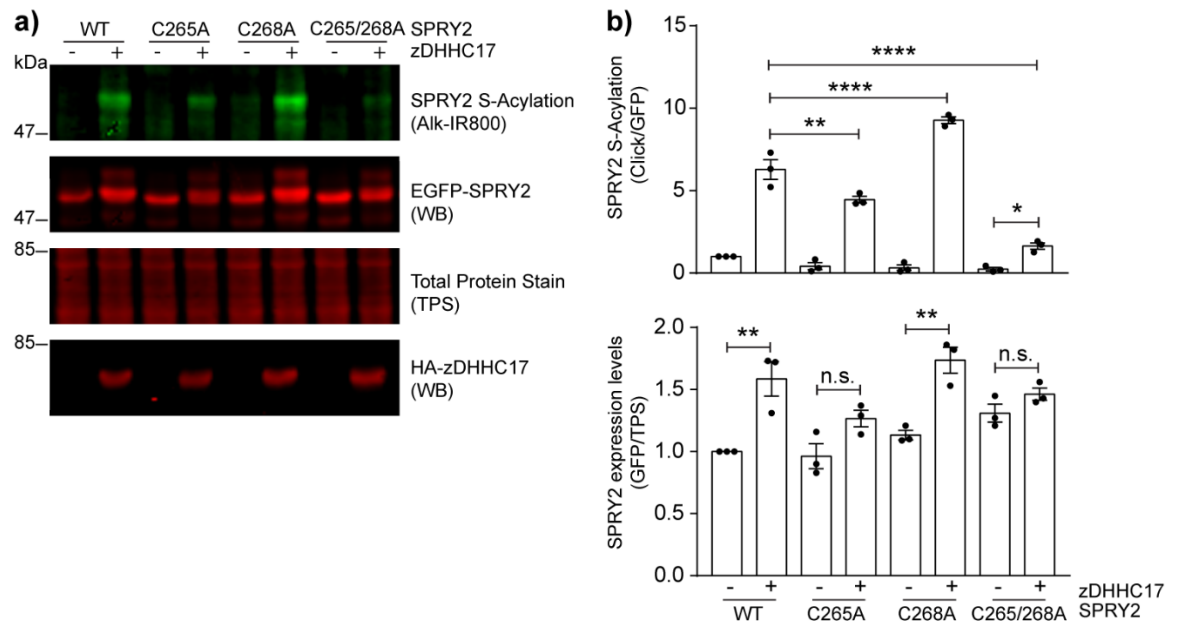


Figure 3.8 S-acylation of SPRY2 mutants with substitutions of Cys-265 and Cys-268

HEK293T cells were transfected with plasmids encoding EGFP-tagged SPRY2 WT, SPRY2 C265A, SPRY2 C268A, or SPRY2 C265/268A double mutant, together with pEFBOS-HA (referred to as “-” in the figure), or a plasmid encoding HA-tagged zDHHC17 (referred to as “+” in the figure). Cells were incubated with 100 μ M C16:0 azide for 4 h and labelled proteins reacted with alkyne IRdye-800 using click chemistry. Before performing immunoblotting, membranes were incubated with a total protein stain (TPS) and signal detected at 700 nm. S-acylation was revealed at 800 nm, GFP and HA signals were detected at 700 nm. **a)** Representative image showing SPRY2 S-acylation (*top*), SPRY2 expression levels (*middle top*) and total protein stain (TPS, *middle bottom*) detected on the same immunoblot. For zDHHC17, HA (*bottom*) was revealed for the same samples on a different immunoblot. The positions of the molecular weight markers are shown on the left. **b)** Graphs showing SPRY2 S-acylation and expression levels after normalisation. Error bars represent mean values \pm SEM; each replicate is shown with filled circles. Differences were analysed by one-way ANOVA (**** denotes $P < 0.0001$, ** $P < 0.01$, * $P < 0.05$, n.s. not significant, $n=3$).

3.2.6 Cys-265 and Cys-268 are located in a hydrophobic patch within an α -helical region of the CRD of the protein

The results above highlight how zDHHC17 can finely “discriminate” between Cys-265 and Cys-268, and preferentially modify only one of them (i.e. Cys-265). To give insight to this data, the secondary structure of SPRY2 was considered. There is currently no crystal structure available for SPRY2 and therefore its secondary structure (amino acids 1-315 of human sequence) was predicted using the software PSIPRED 4.0 (Buchan and Jones, 2019; Jones, 1999). As shown in Figure 3.9, two main regions within the cysteine-rich domain of SPRY2 are predicted to fold into α -helices (pink residues): the first encompassing amino acids 209-227, and the second amino acids 249-286, hence containing both Cys-265 and Cys-268.

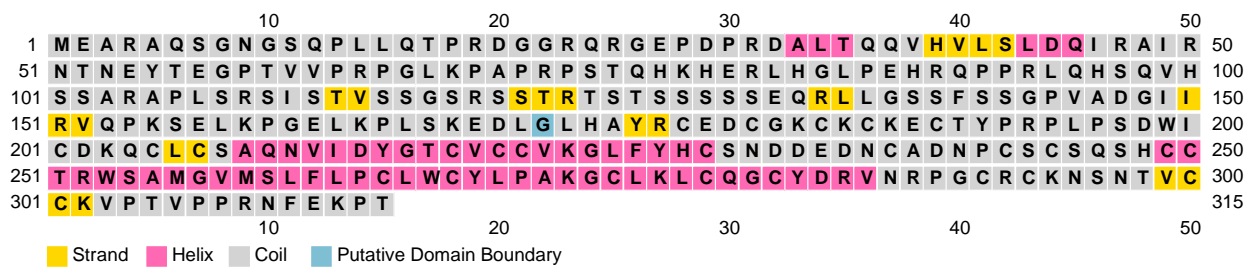


Figure 3.9 Cys-265 and Cys-268 are predicted to lie within an α -helical region

The entire human SPRY2 secondary structure (residues 1-315) was predicted using PSIPRED 4.0 software. The pink residues in the figure are predicted to fold into α -helices and correspond to amino acids 209-227 and 249-286, respectively.

Previous work has shown the importance of hydrophobicity for the efficient S-acylation of other cysteine-rich proteins, including SNAP25 and cysteine-string protein (Greaves et al., 2009a; Greaves and Chamberlain, 2006). Analysis of the hydrophobicity associated with the CRD of SPRY2 (amino acids 178-301 of human SPRY2) revealed that both Cys-265 and Cys-268 are present in a 10-amino acid hydrophobic patch region, 261-LFLPCLWCYL-270 (Fig. 3.11, Cys-265/268 are in bold). This is particularly interesting as this hydrophobic patch may have an underlying membrane affinity enhancing the S-acylation potential of these two cysteine residues by zDHHC17.

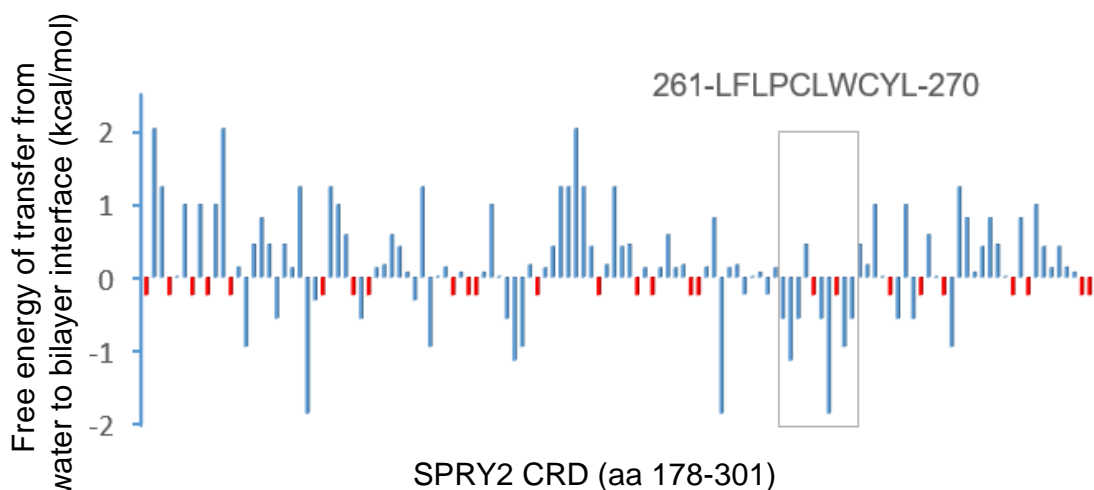


Figure 3.11 Analysis of the hydrophobicity of the cysteine-rich domain (CRD) of SPRY2

Hydrophobicity analysis of the CRD of SPRY2 (encompassing residues 178-301 of human SPRY2 protein). The Y-axis shows experimentally determined free energies of transfer ΔG (kcal/mol) from water to a phosphobilayer (POPC) interface. Cysteine residues are shown in red and the grey box highlights amino acids 261-270 (Wimley and White, 1996).

3.2.7 Specific regions in the CRD are required for efficient S-acylation of SPRY2

Identification of the key features that determine the specificity of cysteine S-acylation is one of the most elusive aspects of the field (Zaballa and van der Goot, 2018). Other than the presence of a striking number of cysteines, no information exists on other elements that might contribute to SPRY2 S-acylation. To investigate such specific features, we examined the amino acid region 155-229. The reason for focusing on this region is that it is immediately downstream of the zDHHC17 recognition site (Pro-154) and includes a conspicuous helical region between amino acids Ala-209 and Cys-229 (Fig. 3.9). To begin, amino acid substitutions were made in this region, focusing on short stretches of residues lacking cysteines. The majority of non-cysteine residues in this region were therefore mutated to alanine in blocks of 3 to 5 amino acids, giving a total of 13 mutants. In particular, we focused on residues that occurred in stretches that lacked intervening cysteines (Fig. 3.12a).

HEK293T cells were transfected with these SPRY2 mutants together with zDHHC17; SPRY2 WT was used as control. Cells were labelled with C16:0-azide, and click chemistry with alkyne-IR800, SDS-PAGE and immunoblotting were performed as described in Chapter 2. Analysis of the zDHHC17 S-acylation and level of each one of these mutants is shown in Figure 3.12. This analysis revealed the presence of three SPRY2 mutants for which both S-acylation and levels were reduced: SAQNV-5A (mutation of amino acids 208-212), IDYGT-5A (mutation of amino acids 213-217), and VKGL-4A (mutation of amino acids 222-225) (Fig. 3.12e and 3.12f).

This finding suggests that there are key non-cysteine residues in the amino acid sequence 208-225, within the CRD of SPRY2, that are required for efficient S-acylation by zDHHC17 (shown in bold red in Fig. 3.12a).

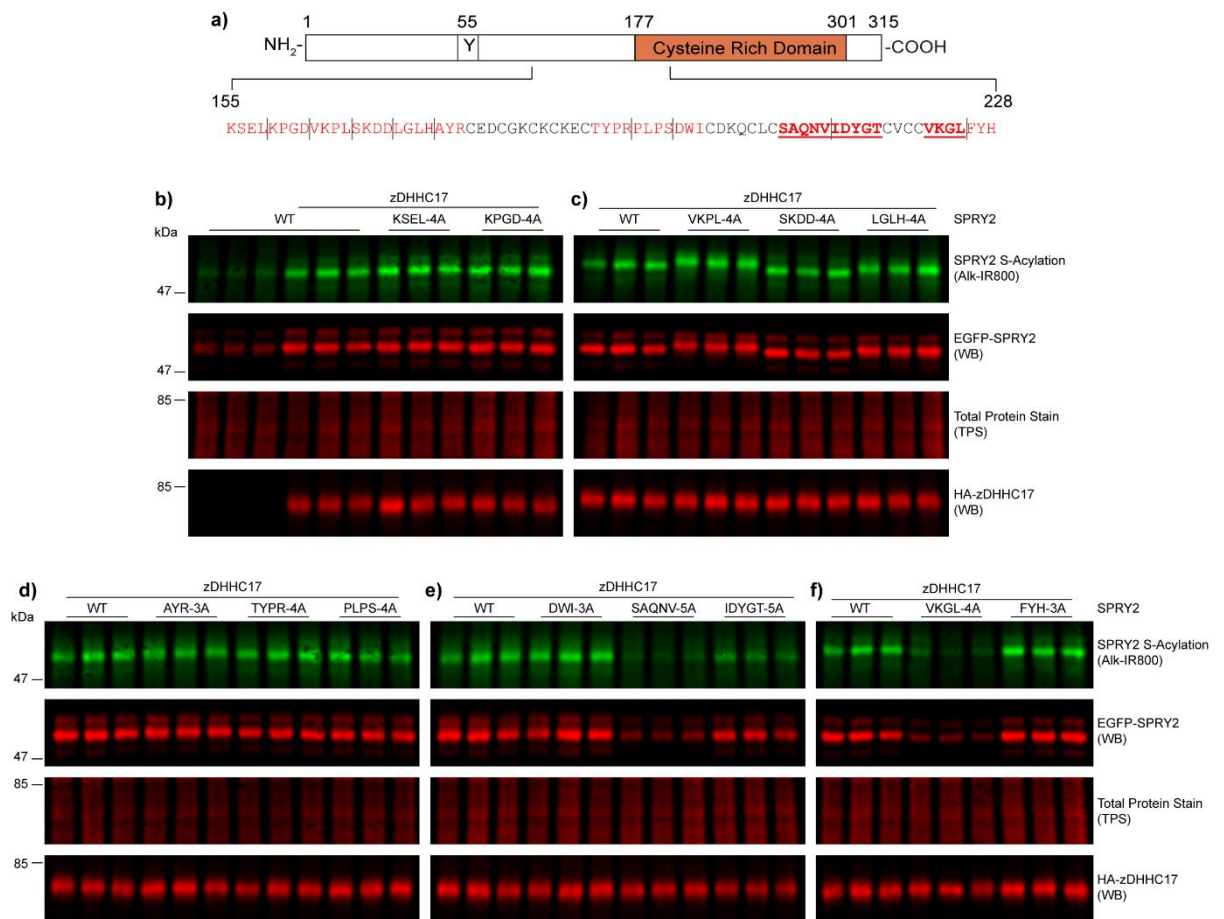


Figure 3.12 SPRY2 S-acylation by zDHHHC17 requires the presence of specific regions within the CRD

a) Schematic representation of SPRY2 protein. The conserved Y55 is shown and the CRD is in orange. The amino acid sequence 155-228 is shown: mutated residues are shown in red, residues that when mutated reduce SPRY2 S-acylation by zDHHHC17 are additionally shown in bold and underlined. **b-f)** HEK293T cells were transfected with plasmids encoding EGFP-SPRY2 alanine mutants and HA-zDHHHC17; plasmids encoding EGFP-SPRY2 WT together with HA-zDHHHC17 was used as a positive control. Cells were incubated with 100 μ M C16:0 azide for 4 h and labelled proteins reacted with alkyne IRdye-800 using click chemistry. Before performing immunoblotting, membranes were incubated with a total protein stain (TPS) and signal was detected at 700 nm. S-acylation was revealed at 800 nm, GFP and HA signals were detected at 700 nm. Each Western blot shows SPRY2 S-acylation (*top*), SPRY2 expression levels (*middle top*) and total protein stain (TPS, *middle bottom*) detected on the same

immunoblot. For zDHHC17, HA (*bottom*) was revealed for the same samples on a different immunoblot. The positions of the molecular weight markers are shown on the left.

To better understand the importance of the sequences 'SAQNV' (residues 208-212), 'IDYGT' (residues 213-217), and 'VKGL' (residues 222-225) for SPRY2 S-acylation in a quantitative manner, the corresponding mutants were analysed in click-chemistry assays using zDHHC17. HEK293T cells were then transfected with EGFP-tagged SPRY2 mutants SAQNV-5A, IDYGT-5A or VKGL-4A together with pEFBOS-HA (control) or HA-zDHHC17. Cells were labelled with C16:0-azide, and click chemistry with alkyne-IR800, SDS-PAGE and immunoblotting were performed as described in Chapter 2.

As shown in Figure 3.13, upon zDHHC17 expression, S-acylation of SAQNV-5A, IDYGT-5A and VKGL-4A mutants was substantially decreased compared to wild-type SPRY2. Accordingly, SAQNV-5A and VKGL-4A expression levels were found to be decreased (Fig. 3.13a and 3.13c), whereas IDYGT-5A expression levels were not affected (Fig. 3.13b and 3.12e). This latter observation suggests that the residual S-acylation associated with this mutant may be sufficient to enhance protein expression. In addition, the S-acylation detected in the absence of zDHHC17 (pEFBOS-HA) was decreased in all the mutants compared to the controls (WT pEFBOS-HA), implying that endogenous S-acylation of these mutants is also reduced.

These quantitative analyses support the conclusion that there are multiple residues within the sequence 'SAQNVIDYGT----VKGL' that are required for efficient S-acylation of SPRY2 by zDHHC17.

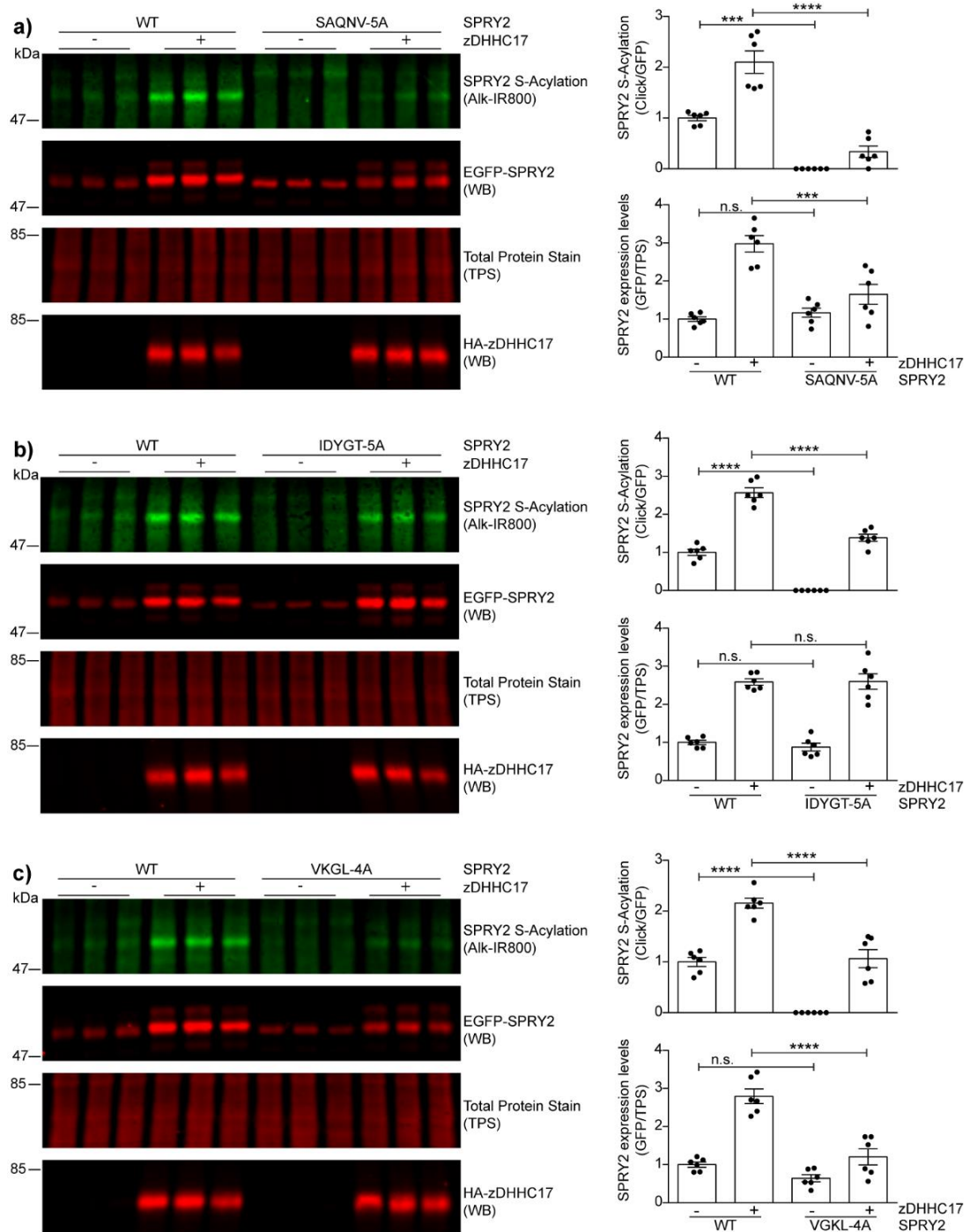


Figure 3.13 Residues within the SPRY2 region 208-225 are important for S-acylation by zDHHC17

HEK293T cells were transfected with EGFP-SPRY2 SAQNV-5A, IDYGT-5A or VKGL-4A mutants together with pEFBOS-HA (referred to as “-” in the figure), or HA-zDHHC17 (referred to as “+” in the figure). Cells were incubated with 100 μ M C16:0 azide for 4 h and labelled proteins

reacted with alkyne IRdye-800 using click chemistry. Before performing immunoblotting, membranes were incubated with a total protein stain (TPS) and signal was detected at 700 nm. S-acylation was revealed at 800 nm, GFP and HA signals were detected at 700 nm. **a-c)** *on the left:* Representative images showing SPRY2 S-acylation (*top*), SPRY2 expression levels (*middle top*) and total protein stain (TPS, *middle bottom*) detected on the same immunoblot. For zDHHC17, HA (*bottom*) was revealed for the same samples on a different immunoblot. The positions of the molecular weight markers are shown on the left. *On the right:* Graphs showing SPRY2 S-acylation and expression levels after normalisation. Error bars represent mean values \pm SEM; each replicate is shown with filled circles. Differences were analysed by one-way ANOVA (**** denotes $P < 0.0001$, *** $P < 0.001$, n.s. not significant, $n=6$).

Next we questioned if the same sequences are also important for zDHHC7-mediated S-acylation of SPRY2. HEK293T cells were transfected with SPRY2 WT, SAQNV-5A, IDYGT-5A, or VKGL-4A mutant together with pEFBOS-HA (control) or HA-zDHHC7. Following labelling, click-chemistry and immunoblotting their corresponding S-acylation was analysed as described in Chapter 2.

Upon zDHHC7 expression, S-acylation of SPRY2 SAQNV-5A and IDYGT-5A mutants was decreased (Fig. 3.14a and 3.14b), whereas that of VKGL-4A mutant was not affected (Fig. 3.14c) compared to wild-type SPRY2. However, substantial residual S-acylation was observed in all cases with none of the mutants showing reduced expression. Overall, this analysis suggests that this region of SPRY2 is also important for efficient S-acylation by zDHHC7 but that the effects are less pronounced than seen with zDHHC17.

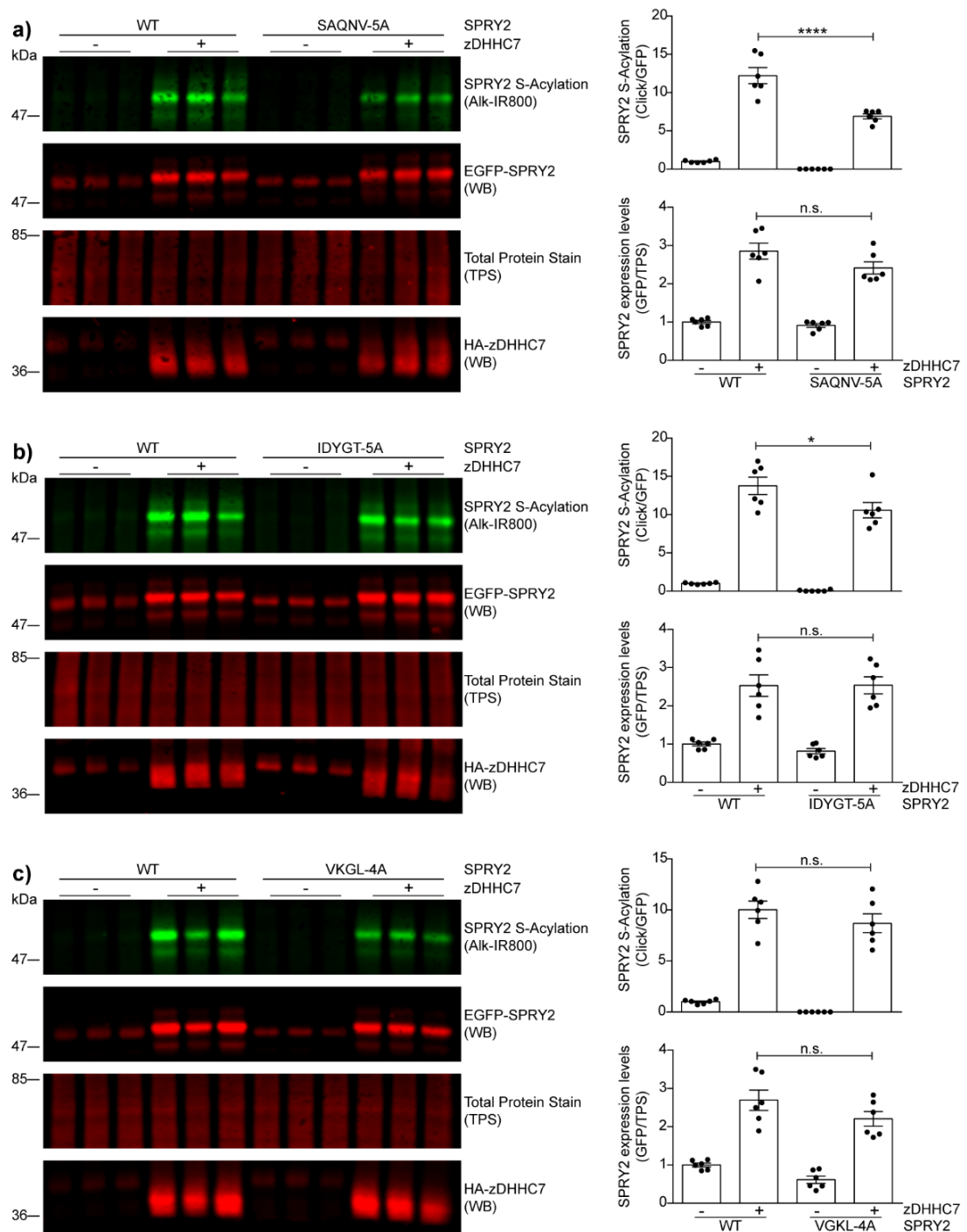


Figure 3.14 Residues within the SPRY2 region 208-225 are important for S-acylation by zDHHC7

HEK293T cells were transfected with EGFP-SPRY2 SAQNV-5A, IDYGT-5A or VKGL-4A mutants together with pEFBOS-HA (referred to as “-” in the figure), or HA-zDHHC7 (referred to as “+” in the figure). Cells were incubated with 100 μ M C16:0 azide for 4 h and labelled proteins reacted with alkyne IRdye-800 using click chemistry. Before performing immunoblotting,

membranes incubated with a total protein stain (TPS) and signal was detected at 700 nm. S-acylation was revealed at 800 nm, GFP and HA signals were detected at 700 nm. **a-c)** *on the left*: Representative images showing SPRY2 S-acylation (*top*), SPRY2 expression levels (*middle top*) and total protein stain (TPS, *middle bottom*) detected on the same immunoblot. For zDHHC17, HA (*bottom*) was revealed for the same samples on a different immunoblot. The positions of the molecular weight markers are shown on the left. *On the right*: Graphs showing SPRY2 S-acylation and expression levels after normalisation. Error bars represent mean values \pm SEM; each replicate is shown with filled circles. Differences were analysed by one-way ANOVA (**** denotes $P < 0.0001$, * $P < 0.05$, n.s. not significant, $n=6$).

3.2.8 Identification of the key residues within the sequence 'SAQNVIDYGT----VKGL' important for SPRY2 S-acylation by zDHHC17

To narrow down the residues directly involved in SPRY2 S-acylation, we subsequently undertook additional site-directed mutagenesis where each amino acid within the SAQNV, IDYGT and VKGL sequences was individually substituted by alanine. These mutants were then co-expressed with HA-zDHHC17 in HEK293T cells. Cells were labelled with C16:0-azide, and click chemistry with alkyne-IR800, SDS-PAGE and immunoblotting were performed as described in Chapter 2.

Although mutation of the whole region 208-SAQNV-212 caused a loss of S-acylation (Fig. 3.12), none of the single mutations introduced in this region was sufficient to cause a significant decrease in this parameter (Fig. 3.15). This suggests that the reduced S-acylation seen with mutation of the entire region likely reflects small additive effects of multiple amino acids. However, mutation of Asn-211 (N211) did have a variable effect on S-acylation, and indeed this mutant did not show a significant increase in S-acylation mediated by zDHHC17 when compared with the control sample (Fig. 3.15c).

Analysis of the single mutants from the IDYGT and VKGL regions gave clearer results, and D214A and K223A mutants both showed a significant reduction in zDHHC17-mediated S-acylation (Fig. 3.16 and 3.17). Furthermore, reduced S-acylation of the SPRY2 D214A and K223A mutants was also associated with decreased protein levels

(Fig. 3.16b and 3.17b). Although no other mutants affected S-acylation of SPRY2 by zDHHC17, mutation of Tyr-215 (Y215A), and Leu-225 (L225A) did affect the ability of zDHHC17 to enhance SPRY2 levels (Fig. 3.16c and 3.17d).

These data identify Asp-214 (D214), and Lys-223 (K223), within the cysteine-rich domain (CRD) as the key residues required for efficient S-acylation of SPRY2 by zDHHC17, with a possible role also for Asn-211 (N211).

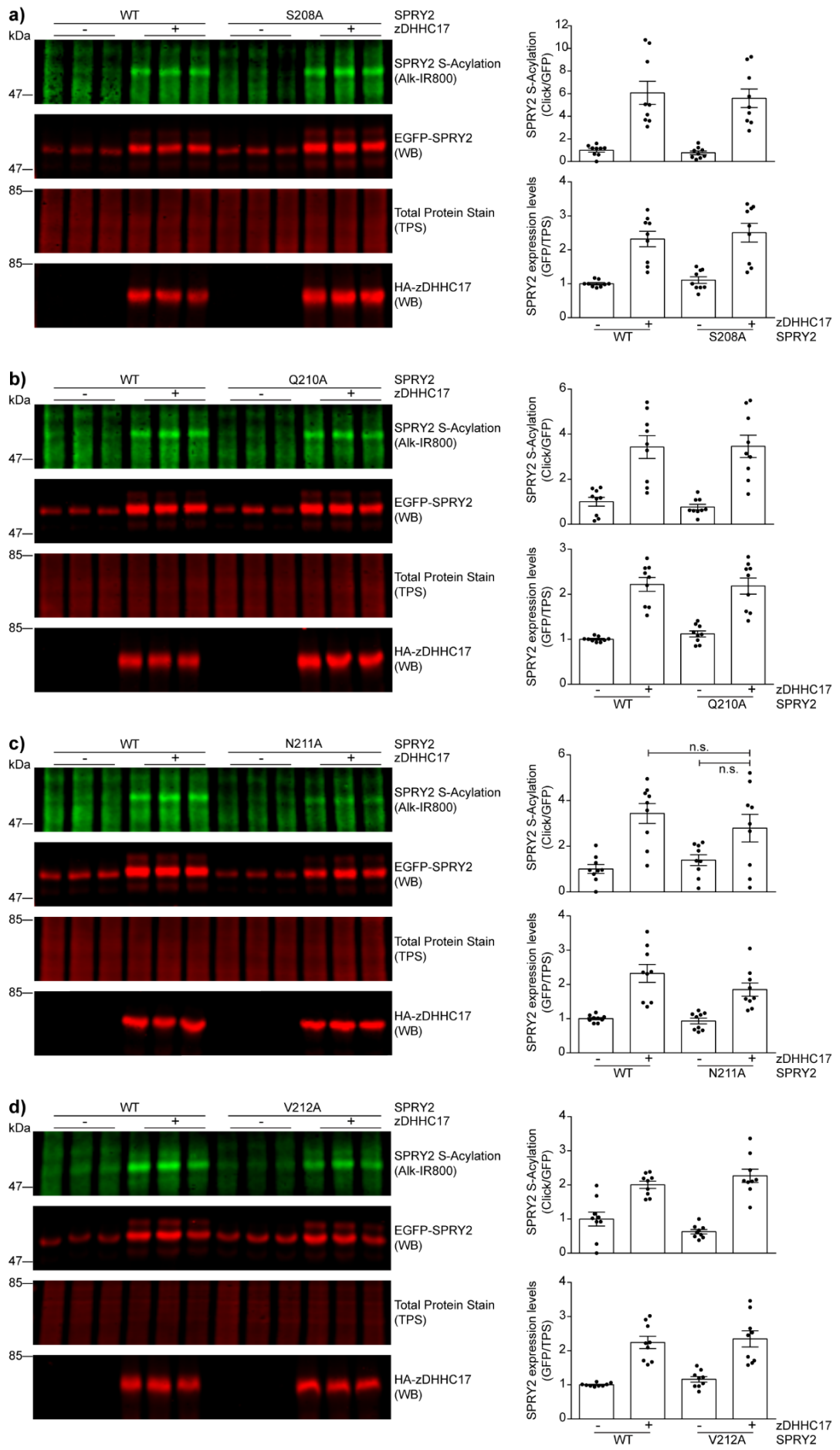


Figure 3.15 Analysis of SPRY2 mutants S208A, Q210A, N211A, and V212A S-acylation by zDHHC17

HEK293T cells were transfected with EGFP-SPRY2 mutants S208A, Q210A, N211A, or V212A together with pEFBOS-HA (referred to as “-” in the figure), or HA-zDHHC17 (referred to as “+” in the figure). Cells were incubated with 100 μ M C16:0 azide for 4 h and labelled proteins reacted with alkyne IRdye-800 using click chemistry. Before performing immunoblotting, membranes incubated with a total protein stain (TPS) and signal was detected at 700 nm. S-acylation was revealed at 800 nm, GFP and HA signals were detected at 700 nm. **a-d)** *On the left:* Representative images showing SPRY2 S-acylation (*top*), SPRY2 levels (*middle top*) and total protein stain (TPS, *middle bottom*) detected on the same immunoblot. For zDHHC17, HA (*bottom*) was revealed for the same samples on a different immunoblot. The positions of the molecular weight markers are shown on the left. *On the right:* Graphs showing SPRY2 S-acylation and expression levels after normalisation. Error bars represent mean values \pm SEM; each replicate is shown with filled circles. For clarity, only relevant statistical analysis is shown in the figure, specifically where S-acylation of mutant protein with zDHHC17 was not different from that without zDHHC17. Differences were analysed by one-way ANOVA (n.s. not significant, n=9).

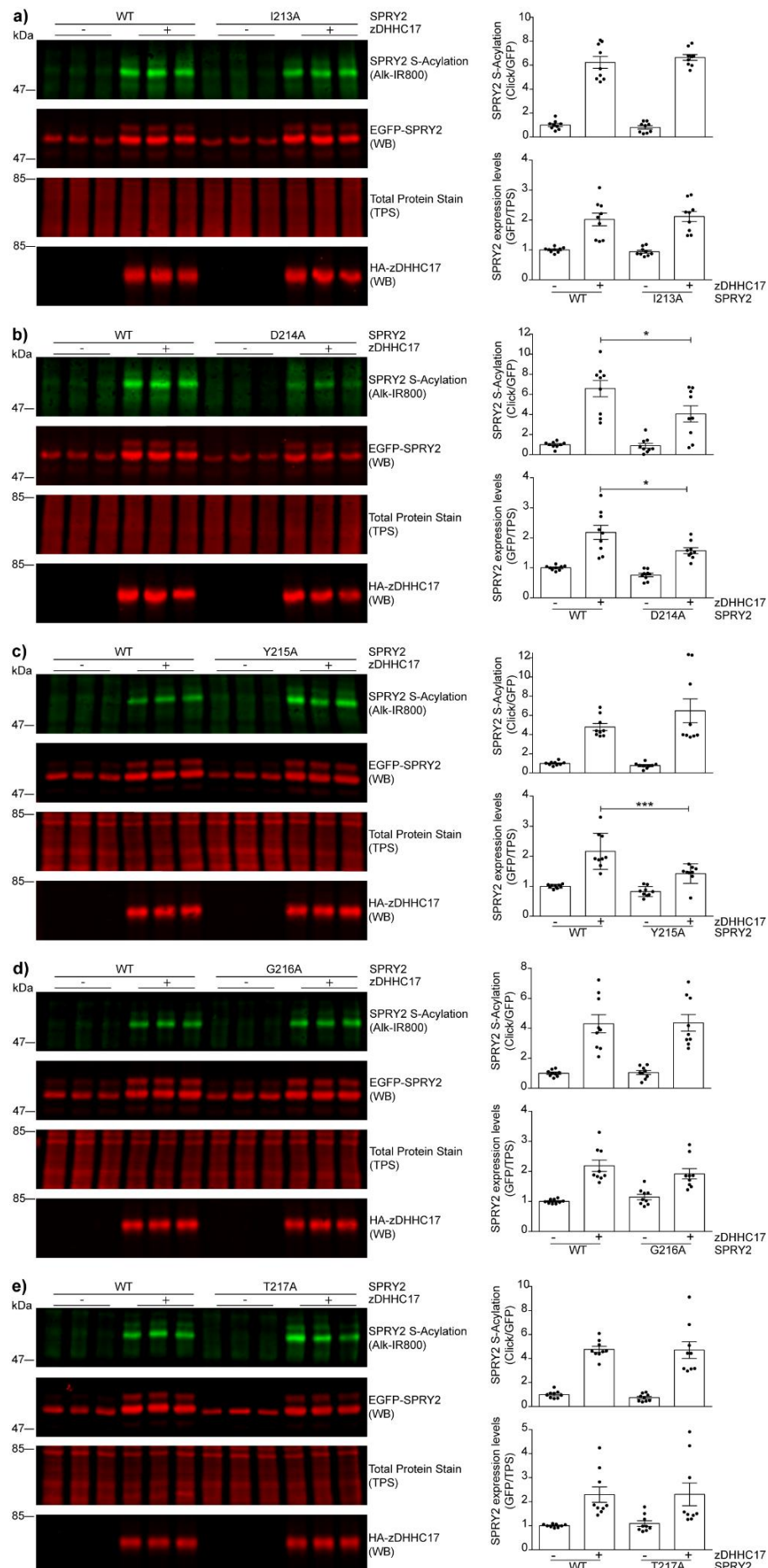


Figure 3.16 Analysis of SPRY2 mutants I213A, D214A, Y215A, G216A, and T217A S-acylation by zDHHC17

HEK293T cells were transfected with EGFP-SPRY2 mutants I213A, D214A, Y215A, G216A, or T217A together with pEFBOS-HA (referred to as “-” in the figure), or HA-zDHHC17 (referred to as “+” in the figure). Cells were incubated with 100 μ M C16:0 azide for 4 h and labelled proteins reacted with alkyne IRdye-800 using click chemistry. Before performing immunoblotting, membranes incubated with a total protein stain (TPS) and signal was detected at 700 nm. S-acylation was revealed at 800 nm, GFP and HA signals were detected at 700 nm. **a-e)** *On the left:* Representative images showing SPRY2 S-acylation (*top*), SPRY2 levels (*middle top*) and total protein stain (TPS, *middle bottom*) detected on the same immunoblot. For zDHHC17, HA (*bottom*) was revealed for the same samples on a different immunoblot. The positions of the molecular weight markers are shown on the left. *On the right:* Graphs showing SPRY2 S-acylation and expression levels after normalisation. Error bars represent mean values \pm SEM; each replicate is shown with filled circles. For clarity, only relevant statistical differences are shown in the figure, specifically where S-acylation of mutant protein with zDHHC17 was less than that of the WT protein with zDHHC17. Differences were analysed by one-way ANOVA (***) denotes $P < 0.001$, * $P < 0.05$, $n=9$).

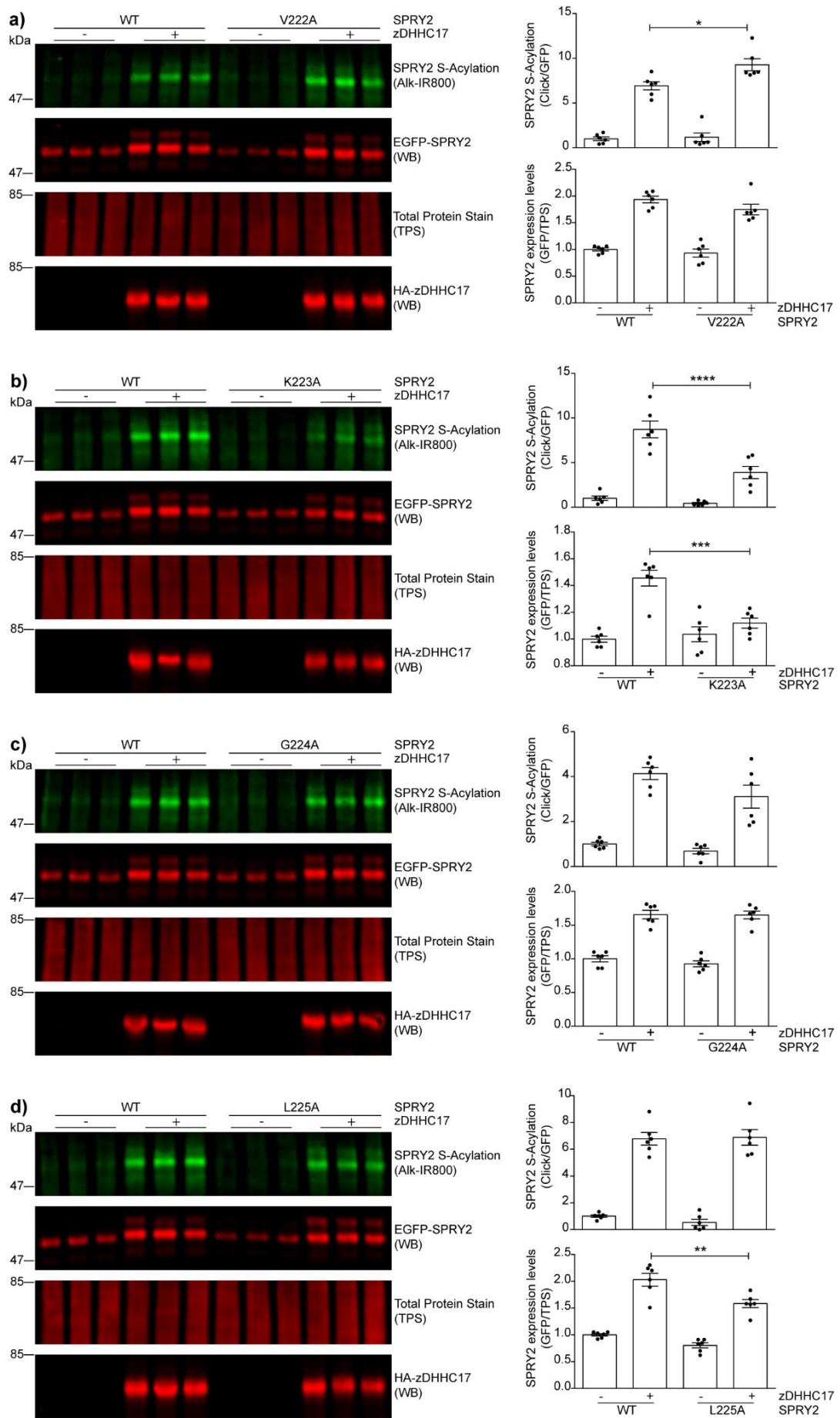


Figure 3.17 Analysis of SPRY2 mutants V222A, K223A, G224A, and L225A S-acylation by zDHHC17

HEK293T cells were transfected with EGFP-SPRY2 mutants V222A, K223A, G224A, or L225A together with pEFBOS-HA (referred to as “-” in the figure), or HA-zDHHC17 (referred to as “+” in the figure). Cells were incubated with 100 μ M C16:0 azide for 4 h and labelled proteins reacted with alkyne IRdye-800 using click chemistry. Before performing immunoblotting, membranes incubated with a total protein stain (TPS) and signal was detected at 700 nm. S-acylation was revealed at 800 nm, GFP and HA signals were detected at 700 nm. **a-d)** *On the left:* Representative images showing SPRY2 S-acylation (*top*), SPRY2 levels (*middle top*) and total protein stain (TPS, *middle bottom*) detected on the same immunoblot. For zDHHC17, HA (*bottom*) was revealed for the same samples on a different immunoblot. The positions of the molecular weight markers are shown on the left. *On the right:* Graphs showing SPRY2 S-acylation and expression levels after normalisation. Error bars represent mean values \pm SEM; each replicate is shown with filled circles. For clarity, only relevant statistical differences are shown in the figure, specifically where S-acylation of mutant protein with zDHHC17 was less than that of the WT protein with zDHHC17. Differences were analysed by one-way ANOVA (**** denotes $P < 0.0001$, *** $P < 0.001$, ** $P < 0.01$, * $P < 0.05$, $n=6$).

3.2.9 Combined substitutions of Asn-211 (N211), Asp-214 (D214) and Lys-223 (K223) block S-acylation of SPRY2 by both zDHHC17 and zDHHC7

The results above clearly show that Asp-214 (D214), Lys-223 (K223), and possibly Asn-211 (N211) are directly involved in S-acylation of SPRY2 by zDHHC17. To better understand the importance of these residues, their conservation was evaluated across a number of species (Fig. 3.18). The corresponding regions of interest from *Drosophila melanogaster* (Fruit fly), *Danio rerio* (Zebrafish), *Xenopus tropicalis* (Xenopus) *Gallus gallus* (Chicken), *Bos taurus* (Bovine), *Homo sapiens* (Human), *Rattus norvegicus* (Rat), and *Mus musculus* (Mouse) were aligned using CLUSTAL Omega software (Sievers et al., 2011).

Interestingly, both Asp-214 (D214) and Lys-223 (K223) are highly conserved from *Drosophila* to humans. On the other hand, Asn-211 (N211) is only partially conserved, further suggesting that this residue might have a minor role.

```

sp|O44783|SPY_DROME      WVCNKTCLCSAESVTDYASCLCCAKALFYHCARDNDLDCDDGNGTPCVDNPCSCGPKYKRTQRWGWLGALSIFLPCPLWIFYWP 479
tr|F1QU39|F1QU39_DANRE  WMCGRRCVCSATSAMDYVTCVCCVKCLFYHCSNDDDED-----VCADKPFSCCTQSHCCMRWSAISVLALFLPCLLCYLP 272
tr|Q5PRF7|Q5PRF7_XENTR  WICDKQCLCSAQEVVDYGTCCVCKKCLFYHCSNDDDED-----NCADNPCSCSQSHCCTRWSAIGVMALFLPCLWICYLP 270
tr|F1NZG9|F1NZG9_CHICK  WICDKQCLCSAQNVVDYGTCCVCKKGLFYHCSNDDDED-----NCADNPCSCSQSHCCTRWSAMGVVSLFLPCLWICYLP 269
sp|Q08E39|SPY2_BOVIN    WICDKQCLCSAQNVVDYGTCCVCKKGLFYHCSNDDDED-----NCADNPCSCSQSHCCTRWSAMGVMSLFLPCLWICYLP 271
sp|O43597|SPY2_HUMAN    WICDKQCLCSAQNVVDYGTCCVCKKGLFYHCSNDDDED-----NCADNPCSCSQSHCCTRWSAMGVMSLFLPCLWICYLP 271
sp|Q9QXV8|SPY2_MOUSE   WICDKQCLCSAQNVVDYGTCCVCKKGLFYHCSNDDDED-----NCADNPCSCSQSHCCTRWSAMGVMSLFLPCLWICYLP 271
tr|Q5HZA2|Q5HZA2_RAT   WICDKQCLCSAQNVVDYGTCCVCKKGLFYHCSNDDDED-----NCADNPCSCSQSHCCTRWSAMGVMSLFLPCLWICYLP 270
*:.:.*:*** ..:* : * **.* *****: *::          *.*:* ** : ** .:..:***** * *

```

Figure 3.18 Asp-214 (D214) and Lys-223 (K223) are highly conserved across species

CLUSTAL multiple sequence alignment of SPRY2 protein across species. Both D214 and K223 (red rectangles in the figure) are highly conserved, whereas N211 (yellow rectangle in the figure) is only partially conserved. Compared species: *Drosophila melanogaster* (Fruit fly), *Danio rerio* (Zebrafish), *Xenopus tropicalis* (Xenopus) *Gallus gallus* (Chicken), *Bos taurus* (Bovine), *Homo sapiens* (Human), *Rattus norvegicus* (Rat), and *Mus musculus* (Mouse).

Asn-211 (N211), Asp-214 (D214), and Lys-223 (K223) are in a region predicted to fold into an α -helix (encompassing amino acids 209-227) (Fig. 3.9). In a helical wheel projection, the charged residues Asp-214 (D214) and Lys-223 (K223) are positioned on opposite sides of the helix (red asterisks in Fig. 3.19) suggesting a broader role of these amino acids in the context of SPRY2 S-acylation, i.e. facilitating appropriate membrane-interaction rather than interaction with a specific zDHHC enzyme.

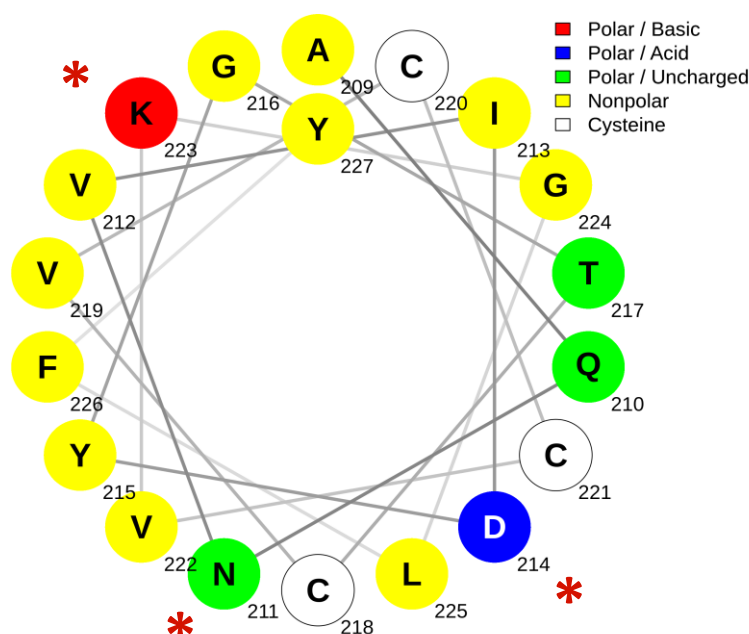


Figure 3.19 Asp-214 and Lys-223 are positioned on opposite sides of the same α -helix

Helical wheel projection of SPRY2 region encompassing amino acids 209-227 using NetWheels software. The positions of Asn-211, (N211), Asp-214 (D214), and Lys-223 (K223) are marked by red asterisks. For the SPRY2 secondary structure prediction refer to Figure 3.9.

To examine if these residues do indeed play a broader role in SPRY2 S-acylation rather than allowing specific S-acylation by zDHHC17, a combined mutant in which both D214 and K223 were replaced by alanine was generated. In addition, N211 was also replaced by an alanine as this residue consistently showed a visual reduction in S-acylation (refer to Fig. 3.15). The resulting SPRY2 “NDK” mutant was then co-expressed in HEK293T cells with pEFBOS-HA (control) and either zDHHC17 or zDHHC7.

Cells were labelled with C16:0-azide, and click chemistry with alkyne-IR800, SDS-PAGE and immunoblotting were performed as described in Chapter 2. As shown in Figure 3.20, the combined substitution of all three amino acids in the NDK mutant with alanines dramatically reduced both SPRY2 S-acylation and expression compared to wild-type protein. While SPRY2 NDK S-acylation and expression levels were not enhanced at all by zDHHC17 co-expression (Fig. 3.20a), co-expression of zDHHC7 did have a partial effect on these parameters even though still substantially less than seen with wild-type SPRY2 (Fig. 3.20b). These results strongly support that the NDK residues may play a more general role in SPRY2 S-acylation.

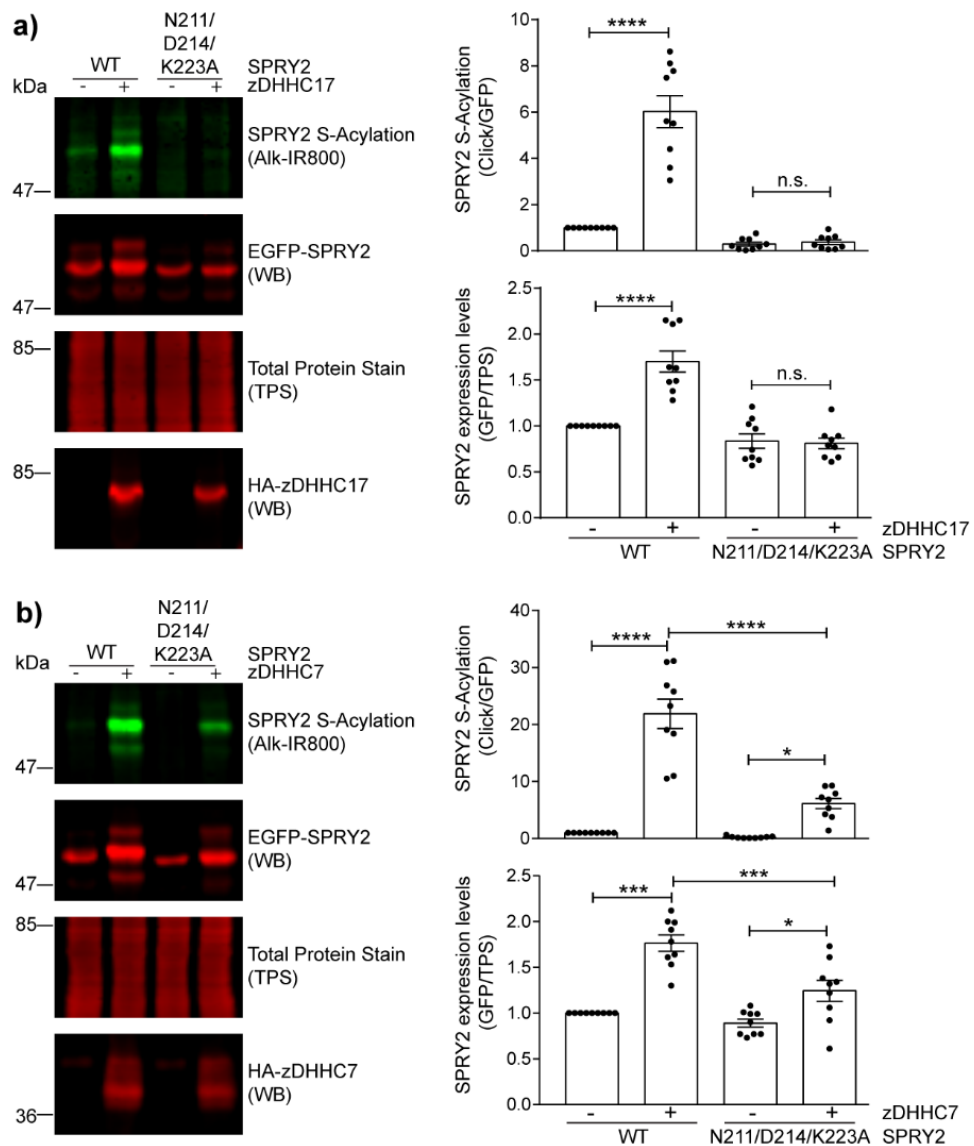


Figure 3.20 Combined alanine substitution of Asn-211, Asp-214, and Lys-223 in the CRD leads to a loss of SPRY2 S-acylation by both zDHHC17 and zDHHC7

HEK293T cells were transfected with either EGFP-tagged SPRY2 WT, or SPRY2 NDK mutant together with pEFBOS-HA (referred to as “-” in the figure), HA-tagged zDHHC17, or zDHHC7 (referred to as “+” in the figure). Cells were incubated with 100 μ M C16:0 azide for 4 h and labelled proteins reacted with alkyne IRdye-800 using click chemistry. Before performing immunoblotting, membranes were incubated with a total protein stain (TPS) and signal detected at 700 nm. S-acylation was revealed at 800 nm, GFP and HA signals were detected at 700 nm. **a-b)** *On the left:* Representative images showing SPRY2 S-acylation (*top*), SPRY2 levels (*middle top*) and total protein stain (TPS, *middle bottom*) detected on the same

immunoblot. For zDHHC17, HA (*bottom*) was revealed for the same samples on a different immunoblot. The positions of the molecular weight markers are shown on the left. *On the right*: Graphs showing SPRY2 S-acylation and expression levels after normalisation. Each bar shows mean values \pm SEM; filled circles represent individual samples. Differences were analysed by one-way ANOVA. Importantly, both S-acylation and expression of SPRY2 NDK + DHHC17 (or zDHHC7) were markedly decreased compared to SPRY2 WT + DHHC17 (or zDHHC7) (**** denotes $P < 0.0001$, *** $P < 0.001$, * $P < 0.05$, n.s. not significant, n=9).

3.2.10 The NDK mutant undergoes more rapid degradation than wild-type SPRY2

The results presented in paragraphs 3.2.1-3.2.3 clearly suggest a link between S-acylation of SPRY2 and protein expression levels. Indeed, S-acylation has previously been shown to modulate the stability of some proteins (Chamberlain and Shipston, 2015). Based on this, we further investigated if this was also the case for SPRY2 and employed the S-acylation deficient SPRY2 NDK mutant in cycloheximide-block experiments. Thus, HEK293T cells were transfected with either SPRY2 wild-type or SPRY2 NDK together with HA-tagged zDHHC17. After overnight incubation, cells were treated using 50 $\mu\text{g/ml}$ of cycloheximide (CHX) for 0, 2, 4, 6 or 8 h to inhibit protein synthesis and then analysed by immunoblotting.

As shown in Figure 3.21, the SPRY2 NDK mutant had a significantly faster rate of degradation than the wild-type protein further supporting a role for S-acylation in mediating SPRY2 stabilisation.

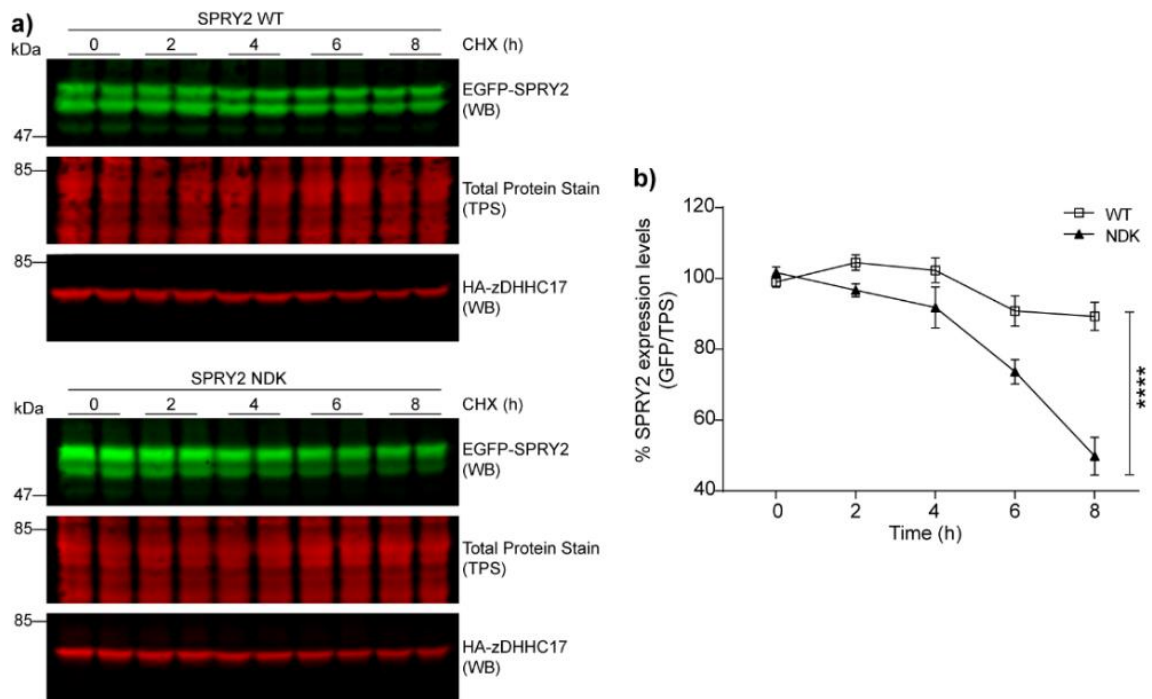


Figure 3.21 Cycloheximide-block experiments reveal a shorter half-life for the S-acylation-deficient NDK mutant

HEK293T cells were transfected with plasmids encoding either EGFP-tagged SPRY2 WT or NDK mutant together with HA-tagged zDHHC17. After approximately 24 h, cells were treated with 50 μ g/ml cycloheximide (CHX) for 0, 2, 4, 6, or 8 hours. Cells were lysed in 1X Laemmli buffer and resolved by SDS-PAGE. Before performing immunoblotting, membranes were incubated with a total protein stain (TPS) and signal detected at 700 nm. GFP and HA signals were detected at 800 and 700 nm, respectively. **a)** Representative images showing SPRY2 expression levels (*top*), total protein stain (TPS, *middle*), and HA levels (*bottom*). The positions of the molecular weight markers are shown on the left. **b)** Graph showing SPRY2 WT (open squares) and SPRY2 NDK (black triangles) levels after normalisation at the indicated time points. Symbols represent mean values \pm SEM. Results were analysed by two-way ANOVA (**** denotes $P < 0.0001$, $n=6$).

3.2.11 S-acylation-deficient mutants are membrane-associated and display a distinct migration pattern on SDS-PAGE

So far, two distinct SPRY2 mutants, NDK and C265/268A have been shown to have a marked inhibitory effect on SPRY2 S-acylation. As this modification is known to regulate trafficking and membrane binding of other S-acylated proteins (Chamberlain and Shipston, 2015; Greaves and Chamberlain, 2007), we investigated if these mutants have an altered distribution compared with wild-type SPRY2. These experiments were performed in neuroendocrine PC12 cells, as these express transfected proteins at lower levels than HEK293T cells. This lower expression limits issues with protein mis-targeting. Furthermore, other substrates of zDHHC17, such as the SNARE protein SNAP25b and cysteine-string protein (CSP α), are efficiently S-acylated and trafficked in PC12 cells without zDHHC17 co-expression (implying that endogenous expression of this enzyme is sufficient to mediate effective S-acylation of transfected proteins) (Greaves et al., 2009a; Salaun et al., 2020a). Thus, EGFP-tagged SPRY2 WT, SPRY2 NDK and SPRY2 C265/268A mutants were transfected into PC12 cells and localisation was initially assessed by fractionation analysis. Cytosol and membrane fractions were separated by cell disruption followed by ultracentrifugation (see Chapter 2).

Figure 3.22 shows that the fractionation protocol successfully enriched cytosol and membrane proteins based on the distribution of GAPDH (soluble) and syntaxin (transmembrane). Interestingly, all SPRY2 constructs were found exclusively associated with the membrane fractions, implying that S-acylation is not essential for membrane association of this protein. Strikingly, an inverse correlation between the slow- (i.e. upper) and fast- (i.e. bottom) migrating bands of SPRY2 was also found when SPRY2 WT was compared to either SPRY2 NDK or SPRY2 C265/268A mutant, with the S-acylation-deficient mutants displaying increased levels of the slow-migrating (i.e. upper) band (Fig. 3.22c). As previously discussed, the different SPRY2 bands are thought to reflect different phosphorylated species (see Fig. 3.2), suggesting that the S-acylation-deficient mutants may have enhanced phosphorylation at certain serine residues.

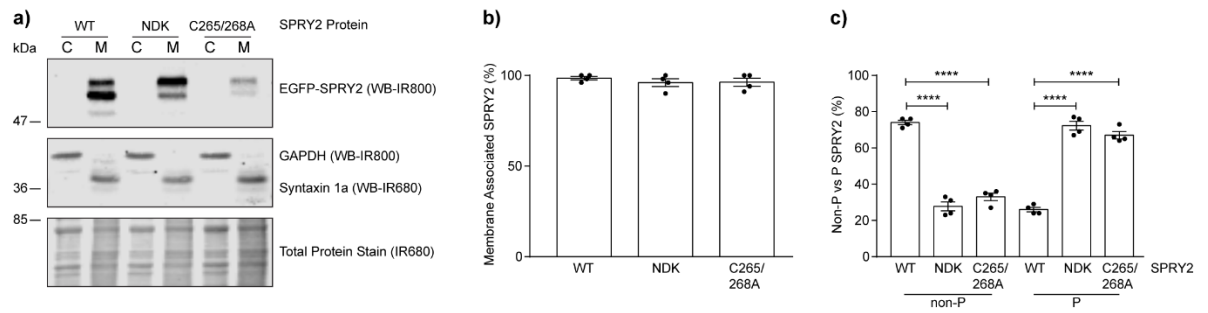


Figure 3.22 Membrane localisation and electrophoretic properties of S-acylation-deficient mutants of SPRY2

PC12 cells were transfected with either EGFP-SPRY2 WT, NDK, or C265/268A. Cells were fractionated into cytosol (C) and membrane (M) fractions and samples were analysed by immunoblotting. **a)** Representative images for SPRY2 (*top IR800*); GAPDH and Syntaxin 1a (*middle IR800 and IR680*) were used as cytosolic and membrane markers, respectively. Total protein stain (*TPS, bottom IR680*) was performed before probing the membranes. **b)** Graph showing membrane-associated SPRY2. Each bar shows mean values ± SEM; filled circles represent individual samples (n=4). **c)** Graph showing the amount of non-phosphorylated (non-P: fast/bottom-migrating SPRY2) and phosphorylated (P: slow/upper-migrating SPRY2) SPRY2 WT, NDK, or C265/268A in the membrane fractions. Each bar shows mean values ± SEM; filled circles represent individual samples. Differences were analysed by one-way ANOVA (**** denotes P < 0.0001, n=4).

3.2.12 Disruption of S-acylation leads to mis-localisation of SPRY2 and loss of plasma membrane association

To further investigate the role of S-acylation in controlling the subcellular localisation of SPRY2, protein distribution of wild-type and S-acylation-deficient mutants of SPRY2 was examined by confocal microscopy. For this purpose, the localisation of EGFP-tagged SPRY2 WT was compared with that of SPRY2 C265/268 and NDK, in PC12 cells. Such analysis showed that both the C265/268A and NDK mutants displayed a loss of plasma membrane localisation compared with wild-type SPRY2 (Fig. 3.23).

In order to compare the localisation of the mutant and wild-type proteins in the same cell, PC12 cells were also co-transfected with EGFP-SPRY2 WT, SPRY2 NDK, or SPRY2 C265/268A mutant, together with mCherry-SPRY2 WT. As shown in Figure 3.23c-e, mCherry-SPRY2 WT co-localised with EGFP-SPRY2 WT, whereas there was a clear visual loss of EGFP-SPRY2 NDK and EGFP-SPRY2 C265/268A expression at the plasma membrane compared with the WT mCherry construct. This different localisation was confirmed quantitatively by calculating (i) the Pearson's coefficient of correlation, determined for the fluorescence intensity co-variance of the EGFP constructs with the co-expressed mCherry WT construct (Fig. 3.23f) and (ii) the fluorescence intensity of SPRY2 at the plasma membrane (Fig. 3.23g). For this analysis, the fluorescence intensity at the PM was expressed as a ratio against the total fluorescence intensity (PM IntDen/Tot IntDen), within the same cell and for both EGFP (WT, NDK, or C265/268A) and co-expressed mCherry WT constructs. As predicted, both EGFP-SPRY2 NDK and C265/268A mutants had a marked decrease in plasma membrane localisation compared to mCherry-SPRY2 WT expressed in the same cells, whereas there was no significant difference in plasma membrane fluorescence of co-expressed EGFP and mCherry-tagged WT proteins (Fig. 3.23g).

Taken together, these results clearly show that mutations that perturb/disrupt SPRY2 S-acylation lead to a loss of plasma membrane targeting of this protein.

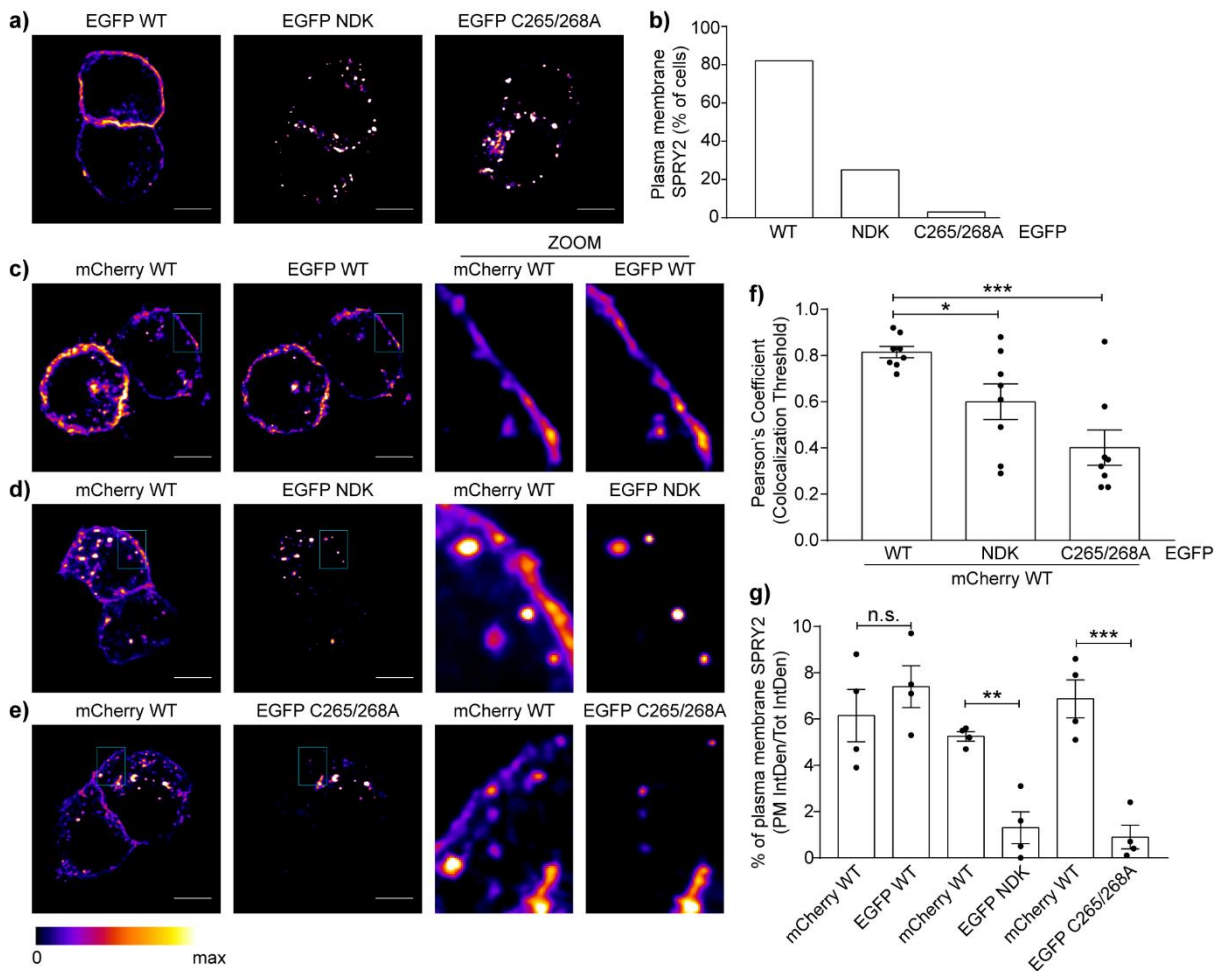


Figure 3.23 Analysis of localisation of SPRY2 WT and SPRY2 S-acylation defective mutants NDK, and C265/268A

a) Confocal imaging of PC12 cells transfected with plasmids encoding EGFP-SPRY2 WT, NDK, or C265/268A. Representative images are shown in the figure. Scale bars represent 5 μm. **b)** Graph showing the percentage (%) of cells showing clear PM staining for each EGFP construct. A total of 73 cells was counted for each condition. **c-e)** Confocal imaging of PC12 cells co-transfected with plasmids encoding EGFP-SPRY2 WT, NDK, or C265/268A together with plasmid encoding mCherry-SPRY2 WT. Representative images are shown in the figure for mCherry and EGFP, and a magnified view of the indicated area for both channels is shown as “ZOOM”. Scale bars represent 5 μm. **f)** Graph showing Pearson's coefficient (Rtot). Each bar shows mean values of Rtot ± SEM; filled circles represent individual images. Results were analysed by Unpaired t-test (***) denotes P < 0.001, * P < 0.05, n=8). **g)** Graph showing percentage (%) of SPRY2 at the plasma membrane (PM) calculated as the ratio of the PM fluorescence intensity (PM IntDen) against the total fluorescence intensity (Tot IntDen) in the

same cell, for both EGFP and mCherry. Each bar shows mean values \pm SEM; filled circles represent individual cells. Results were analysed by Unpaired t-test (***) denotes $P < 0.001$, ** $P < 0.01$, n.s. not significant, $n=4$).

3.3 Discussion

Sprouty proteins (SPRY) are major players in maintaining cell homeostasis (Kim and Bar-Sagi, 2004) and their deregulation has been linked to a number of malignancies, developmental disorders, and neurological diseases (Hausott and Klimaschewski, 2019; Kawazoe and Taniguchi, 2019; Masoumi-Moghaddam et al., 2014). SPRY2, the focus of this study, is the most highly conserved of the SPRY proteins and its CRD was reported to undergo S-acylation almost 20 years ago (Impagnatiello et al., 2001). However, the specific zDHHC enzymes involved in SPRY2 S-acylation, or the cellular consequences of this modification, are not known. The ANK domain of zDHHC17 binds to SPRY2 through its zDABM centred at Pro-154 (Lemonidis et al., 2017a). Furthermore, zDHHC17 co-immunoprecipitated SPRY2 from HEK293 cells in interactome studies (Huttlin et al., 2017). Based on this evidence, this study aimed to identify (i) the specific zDHHC enzymes mediating SPRY2 S-acylation (ii) the specific cysteines within the CRD of the protein that are modified (iii) other features, different from cysteines, required for S-acylation and (iv) the importance of S-acylation in the context of SPRY2 localisation and intracellular targeting.

In HEK293T cells, SPRY2 was shown to be differentially S-acylated by zDHHC17, zDHHC7, and zDHHC3, although all enzymes promoted an increase in SPRY2 levels. Moreover, these effects were found to be independent of phosphorylation at its highly conserved Tyr-55, which has been shown to mediate a c-Cbl-ubiquitination-dependent degradation process (Fong et al., 2003; Wong et al., 2002, 2001). Click chemistry-based experiments further revealed that within the CRD of SPRY2, containing 26 cysteine residues, zDHHC17 displays selectivity for Cys-265/268, while zDHHC7 revealed no such cysteine selectivity. Using a site-directed mutagenesis approach, within the CRD of SPRY2, the highly conserved residues Asp-214 (D214) and Lys-223 (K223) were shown to be required residues for efficient S-acylation by

both zDHHC17 and zDHHC7. Secondary structure predictions coupled with helical wheel projections show that the region encompassing these residues forms an α -helix and that D214 and K223 are positioned at opposite sides of this helix. In neuroendocrine PC12 cells, fractionation assays revealed that SPRY2 is membrane-associated regardless of S-acylation status and the migration of the S-acylation mutants on SDS gels may indicate possible interplay between S-acylation and phosphorylation of SPRY2. Finally, confocal imaging analysis suggested that S-acylation is required for efficient localisation of SPRY2 at the plasma membrane.

In agreement with the hypothesis of zDHHC17 being a putative S-acyltransferase of SPRY2, co-expression of the two proteins in HEK293T cells promoted S-acylation, but also increased protein levels of SPRY2. This increase in SPRY2 levels specifically required S-acylation as a catalytic dead version of zDHHC17 failed to enhance SPRY2 levels. Moreover, S-acylation-deficient mutants of SPRY2 (i.e. NDK and C265/268A) displayed reduced levels compared to the WT protein. In cycloheximide-block experiments, the S-acylation-deficient NDK mutant is degraded more quickly than the wild-type counterpart.

The most plausible explanation for these findings is that S-acylation stabilises SPRY2, increasing the protein half-life. Indeed, S-acylation has been previously shown to affect the stability of several substrate proteins, including the chemokine receptor CCR5 (Percherancier et al., 2001), the anthrax toxin receptor (TEM8) (Abrami et al., 2006), and the *S. cerevisiae* SNARE protein Tlg1 (Valdez-Taubas and Pelham, 2005). In many cases, this results from direct competition of S-acylation with ubiquitination. One example is represented by the yeast SNARE protein Tlg1, and its zDHHC enzyme Swf1. Blockage of S-acylation, by either deleting *Swf1* gene, or mutating the specific S-acylated cysteines, results in increased Tlg1 ubiquitination and vacuole-mediated degradation (Valdez-Taubas and Pelham, 2005). A similar mechanism has been suggested for the anthrax toxin receptor TEM8. Indeed, S-acylation defective receptors have a shorter half-life than wild-type counterparts and are characterised by increased internalisation, and degradation (Abrami et al., 2006). Thus, it is possible that S-acylation protects SPRY2 from ubiquitination and degradation *via* similar

pathways. Nonetheless, analysis of the levels of truncated versions of SPRY2, lacking different portions of the SPRY domain (i.e. I200X, S230X, S260X, and G290X) also suggested that region 260-290 may be required for zDHHC17-mediated stabilisation. This finding is consistent with the observation that substitution of Cys-265/268 prevented S-acylation and stabilisation by zDHHC17. Although not presented in the thesis, it was noted that these SPRY2 truncated mutants had higher protein levels than full-length SPRY2, perhaps suggesting that the C-terminal end (residues 291-315) of SPRY2 might also play a role in protein stability. One possibility is that S-acylation of Cys-265/268 by zDHHC17 leads to the masking of a degron sequence in this C-terminal region of SPRY2. It will be interesting in future work to explore how S-acylation affects the ubiquitination status of SPRY2, or whether mutation of ubiquitination sites affects increased levels of SPRY2 on co-expression with zDHHC enzymes. This analysis could focus initially on the C-terminus of SPRY2 as Lys-313 was identified in a protein-wide study of ubiquitination sites (Udeshi et al., 2013). How might S-acylation affect degradation of SPRY2? S-acylation might induce conformational changes in SPRY2 that mask specific degron sequences. This could be achieved by inducing tighter interaction of SPRY2 with the membrane that precludes association of factors to sequences/residues involved in SPRY2 turnover. Previous studies suggest that degrons are usually found in unstructured regions of proteins, usually characterised by rapid turnover, and either at the C- or the N-terminus (Erales and Coffino, 2014). This is interesting given the fact that SPRY2 is highly unstructured, and exerts its function with a quick turnover (Mason et al., 2006). Overall, S-acylation is promoting SPRY2 stabilisation through a mechanism not yet identified, and further characterisation of the interplay between S-acylation and stabilisation was not possible within this study. The effects of S-acylation on expression levels are important as SPRY2 is down-regulated, even transcriptionally silenced, in several malignancies (Kawazoe and Taniguchi, 2019). Therefore, a better understanding of the diverse mechanisms that physiologically regulate the intracellular levels of SPRY2 is important.

In click chemistry experiments, the increased levels associated with SPRY2 S-acylation appeared to be most prominent for the fast-migrating immunoreactive band of SPRY2, while the slower-migrating band of the protein was less affected. Interestingly, the slower-migrating band of SPRY2 correlates with phosphorylation at specific residues, including Ser-111/120 (mouse SPRY2 sequence) (DaSilva et al., 2006; Lao et al., 2007) (Fig. 3.2). This observation might suggest that the phosphorylation status of specific residues (e.g. Ser-111/120) play a role in S-acylation. Phosphorylation of the highly conserved Tyr-55 (Y55) is known to regulate levels of SPRY2 *via* c-Cbl-mediated proteasomal degradation (Kim and Bar-Sagi, 2004). However, mutation of this site had no effect on S-acylation-dependent stabilisation of SPRY2, implying that S-acylation effects are independent of the c-Cbl-mediated degradation pathway. Beside c-Cbl, intracellular SPRY2 levels can be regulated by other E3 ubiquitin ligases, including Siah2 (Seven-in-absentia homolog-2) (Nadeau et al., 2007) and Nedd4 (Edwin et al., 2010). Binding and proteasome targeting of SPRY2 by both Siah2 and Nedd4 was suggested to occur independently of phosphorylation of Tyr-55 (Y55) (Edwin et al., 2010), or Tyr-227 (Y227) (Nadeau et al., 2007). Particularly, while the interaction of Nedd4 with SPRY2 was shown not to depend on Tyr-55, phosphorylation of other key residues including Ser-112/121 was essential (Edwin et al., 2010). Interestingly, analysis of Nedd4 sequence reveals the presence of a favourable zDABM which could potentially interact with the ANK domain of zDHHC17 thus raising a number of questions. Can zDHHC17 and Nedd4 bind simultaneously (or exclusively) to SPRY2? Could S-acylation be preventing SPRY2 ubiquitination and its proteasomal degradation by interfering with Nedd4 pathway? Does phosphorylation at Ser-112/121 play a role?

Besides zDHHC17, we show that expression of other *cis*-Golgi localised zDHHC enzymes, such as zDHHC7 and zDHHC3 also induced SPRY2 S-acylation. However, in contrast to zDHHC7 and zDHHC3, zDHHC17 appeared to modify a restricted subset of cysteines in the CRD of SPRY2 (i.e. Cys-265/268). While zDHHC17 requires prior binding to substrates for successful S-acylation, zDHHC7/3 show a very weak or undetectable binding to their substrates (Greaves et al., 2010; Lemonidis et al.,

2017b, 2014). The ANK domain of zDHHC17 binds a zDABM sequence in its substrates, which in SPRY2 is centred at Pro-154 (P154) (Lemonidis et al., 2017a). Following this binding, the catalytic DHHC domain of zDHHC17 mediates cysteine S-acylation. It is possible that this necessary interaction with the ANK domain physically restricts the cysteines within the CRD of SPRY2 that are accessible to the catalytic DHHC domain of zDHHC17. In support of this idea, the length and flexibility of the linker region between the zDABM and the CRD of SNAP25b were recently found to be important parameters for the efficient S-acylation of SNAP25b by zDHHC17 (Salaun et al., 2020a). Specifically, it was shown that reducing the length of the flexible linker or introducing structure into this region perturbed S-acylation of the CRD of SNAP25b (Salaun et al., 2020a). Another interesting observation was that Cys-265 and Cys-268 are present in a hydrophobic patch of the CRD. Previous work has shown that hydrophobicity of the CRD of SNAP25b and cysteine-string protein (CSP α) is essential for the S-acylation of these proteins (Greaves et al., 2009a, 2008; Greaves and Chamberlain, 2006). Indeed, replacement of certain cysteines in the CRD of SNAP25b with less hydrophobic residues (e.g. serine, alanine) perturbed S-acylation of the remaining cysteines, whereas more hydrophobic residues (e.g. leucine) did not interfere with S-acylation of the remaining cysteines (Greaves et al., 2009a). It was proposed that this relates to the requirement for transient membrane association of the hydrophobic CRD of proteins such as SNAP25b and CSP α for S-acylation by zDHHC17 (Greaves et al., 2009a, 2008; Greaves and Chamberlain, 2006). Thus, it is possible that the hydrophobic patch of SPRY2 (residues 261-270 in the mouse protein) facilitates the S-acylation of Cys-265 and Cys-268 by moving these residues close to the membrane and therefore into proximity of the membrane-associated catalytic DHHC motif of zDHHC17 (Rana et al., 2018a). The intrinsically low activity of zDHHC17 might require cysteines that are targeted by this enzyme to have a longer membrane residency time in their non-acylated state to facilitate efficient S-acylation. On the other hand, the higher activity of zDHHC7 and zDHHC3, coupled with the lack of structural constraints imposed by a substrate recruitment domain,

are two factors that may allow these highly promiscuous enzymes to modify any cysteines that are in proximity to the membrane.

In addition to the cysteine residues important for SPRY2 S-acylation by zDHHC17, we also found that Asp-214 (D214) and Lys-223 (K223), within the CRD of SPRY2, are key residues for correct S-acylation by both zDHHC17 and zDHHC7. An NDK mutant, in which these residues together with Asn-211 (N211) were replaced by alanines, completely abolished and greatly reduced SPRY2 S-acylation by both zDHHC17 and zDHHC7, respectively, suggesting that integrity in this region is required for S-acylation in general. Sequence conservation across a number of species including *Drosophila*, *Xenopus*, Zebrafish, mouse and human, further supports the importance of these residues. D214 and K223 were found to be the most highly conserved, whereas N211 is substituted by serine residues in *Drosophila* (S411) and Zebrafish (S212), and by a glutamic acid (E210) in *Xenopus*. In our assays, single mutation at D214 (D214A) or at K223 (K223A) affected SPRY2 S-acylation by zDHHC17 more than the single mutation at N211 (N211A) (refer to Fig. 3.15-3.17), further suggesting that D214 and K223 might be more important than N211 for S-acylation. Structural prediction software suggested that these NDK residues are in a predicted α -helix region and the negatively charged D214 orientates opposite to the positively charged K223. If this prediction is correct, then it is probably unlikely that these residues are part of a protein recognition sequence. Positively charged amino acids can interact with negative charges in membrane phospholipids (e.g. PIPs), whereas negatively-charged amino acids are generally excluded from contact with the membrane. Thus, one possibility is that D214 and K223 play a role in membrane interactions of SPRY2 that are important for S-acylation for example, by positioning the helix at the membrane interface. Nonetheless, fractionation experiments in PC12 cells showed that the NDK mutant was still tightly membrane associated, and therefore these amino acids may facilitate spatial proximity with relevant zDHHC enzymes (e.g. by targeting SPRY2 to the Golgi) or orientate the CRD to facilitate S-acylation, rather than being a membrane binding domain *per se*.

Using PC12 cells in fractionation experiments, it was shown that both SPRY2 C265/268A and SPRY2 NDK localised almost exclusively in the membrane fractions. While tight membrane association of SPRY1/2 proteins was previously reported (Impagnatiello et al., 2001), this result suggests that S-acylation is not required for stable membrane association of SPRY2. This is different from other proteins containing CRDs, such as SNAP25b and CSP α , which strongly depend upon S-acylation to move from the cytosol to membranes (Greaves et al., 2009a, 2008). One possible explanation is that the high number of cysteines within the CRD of SPRY2 provides a stronger intrinsic membrane-affinity as cysteine is a hydrophobic amino acid (Wimley and White, 1996). Indeed, the hydrophobic CRD of both SNAP25b and CSP α plays an important role in initial membrane binding of these proteins prior to S-acylation by providing a weak membrane affinity that brings the proteins into proximity of membrane-associated zDHHC enzymes (Greaves et al., 2009a; Greaves and Chamberlain, 2006). The more extensive CRD of SPRY2 could perhaps provide an even stronger membrane affinity than seen for the CRDs of SNAP25b and CSP α .

One of the key roles played by S-acylation is the trafficking of soluble proteins from the Golgi to the plasma membrane (Chamberlain and Shipston, 2015; Ernst et al., 2018; Greaves et al., 2009b; Linder and Deschenes, 2007) and S-acylation of SPRY1 and SPRY2 was previously suggested to represent the molecular basis for their membrane association in HUVEC cells (Impagnatiello et al., 2001). We found that S-acylation is a prerequisite for correct targeting of SPRY2 to the plasma membrane. In PC12 cells, SPRY2 WT localised both at the plasma membrane and on intracellular vesicles or puncta, whereas the C265/268A and NDK mutants displayed a marked loss of plasma membrane levels. Interestingly, both SPRY2 WT and S-acylation deficient mutants (either C265/268A or NDK) showed a partial intracellular co-localisation, while they rarely co-localised at the plasma membrane. Homo- and hetero-dimerisation of SPRY proteins has been previously reported (Chen et al., 2013; Ozaki et al., 2005). Therefore, it is possible the formation of mixed oligomers (i.e. formed by mCherry-tagged SPRY2 WT and EGFP-tagged C265/268A or NDK) which could allow S-acylation deficient mutants to act as dominant-negative forms of the protein.

This would interfere with appropriate plasma membrane trafficking, retaining wild-type SPRY2 in intracellular structures. However, this scenario does not affect the overall conclusion that S-acylation is important for plasma membrane targeting of SPRY2. Future work should look in more detail at the intracellular localisation of wild-type and S-acylation-deficient mutant of SPRY2. CRISPR-Cas9 approaches can also be used to introduce relevant mutations into endogenous SPRY2 and thereby rule out any effects linked to over-expression or the use of protein tags.

Also, we noticed that SPRY2 is not homogeneously distributed in the cytosol but rather found in unknown spots/punctate structures. Interestingly, a similar distribution was recently observed in glioblastoma cells in which these “small spots” were identified by the authors as early, late, and recycling endosomes (Hausott et al., 2019). In the present study, there are no indications of the nature of these intracellular structures. However, it will be interesting to investigate whether the reduced PM association of the SPRY2 S-acylation deficient mutants (i.e. SPRY2 NDK and C265/268A) correlates with increased retention in specific sub-cellular compartments (e.g. Golgi or ER).

Finally, there was also a striking difference in the electrophoretic mobility of SPRY2 wild-type and the S-acylation deficient proteins, with the mutants having higher levels of the slower-migrating band that is suggested to have an altered mobility due to serine phosphorylation (DaSilva et al., 2006). Cross-talk between S-acylation and phosphorylation has been reported for a number of proteins, including the STREX subunit of the large-conductance BK channel where they regulate both surface expression and channel activity (Shipston, 2014a, 2014b). The interplay between these modifications and also ubiquitination of SPRY2 is an area that warrants detailed analysis in future work.

The results presented in this chapter provide the first detailed analysis of SPRY2 S-acylation and demonstrates that this PTM plays a key role in regulating many features of SPRY2. S-acylation by both high- and low-activity zDHHC enzymes promoted protein stability. Interestingly, an NDK motif was required for correct S-acylation by both zDHHC17 and zDHHC7. In addition, S-acylation and phosphorylation at specific

sites appeared to be mutually exclusive with possible important implications on SPRY2 stability and activity. Finally, our data demonstrate that S-acylation is required for correct localisation of SPRY2 at the plasma membrane. While some of the important pending questions have been answered, many more arise. Future works will be important to address whether and how SPRY2 S-acylation is dynamically regulated by growth factors. Also, it is not clear how S-acylation promotes SPRY2 stability, analysis of the C- and N-termini of SPRY2 will be required to find out putative degrons at these sites. Given the key role of SPRY2 as a tumour suppressor, a better understanding of the physiological consequences of its S-acylation will provide new insight that may have therapeutic relevance.

Chapter 4 Characterisation of SPRY2 interactions with the ankyrin-repeat domain of zDHHC17

4.1 Introduction

How zDHHC enzymes achieve specific substrate recognition is one of the most elusive aspects of the S-acylation field. Nevertheless, mechanisms involved in substrate recruitment have emerged for a small number of enzymes. Among the 23 mammalian zDHHC enzymes, zDHHC17 and zDHHC13 are the only two family members to contain an N-terminal ankyrin repeat (ANK) domain which has been shown to mediate recognition and binding of a number of substrates (Greaves and Chamberlain, 2010; Huang et al., 2009; Lemonidis et al., 2014; Verardi et al., 2017). The importance of this ANK domain for substrate recognition was first reported for S-acylation of huntingtin protein (HTT) by zDHHC17 (Singaraja et al., 2002; Yanai et al., 2006). Subsequent studies demonstrated that the ANK domain of zDHHC17, and the related zDHHC13 enzyme, was also crucial for binding to SNAP25b and CSP α . Interestingly, although this ANK domain-mediated interaction is essential for the S-acylation of both SNAP25b and CSP α by zDHHC17, zDHHC13 interaction with these proteins does not result in their S-acylation (Lemonidis et al., 2014). Further analyses of the interaction of SNAP25b, CSP α , HTT and other substrates with zDHHC17, identified a conserved consensus [VIAP][VIT]XXQP motif which binds to the ANK domain of zDHHC17, with the proline residue playing a crucial role in recognition. This consensus sequence was named the “zDHHC ankyrin-repeat binding motif” (zDABM) and it needs to be present in an unstructured cytosolic region of substrates to mediate binding to zDHHC17 and zDHHC13 (Lemonidis et al., 2015a).

A high-resolution crystal structure of the ANK domain of zDHHC17 (ANK17) in complex with a peptide fragment containing the zDABM of SNAP25b (sequence 111-GVVASQPARV-120; zDABM is underlined) was recently solved. With this, the specific residues involved in the ANK17-SNAP25b interaction were identified (Verardi et al., 2017). Within ANK17, Trp-130 (W130) and Asn-100 (N100) were shown to be critical

for substrate recruitment and binding. Through its aromatic ring, W130 establishes crucial contacts with the highly conserved proline residue (P117) of the zDABM of SNAP25b, whereas N100 forms hydrogen bonds with Val-113 (V113). Furthermore, Tyr-67 (Y67) on ANK17 interacts *via* van der Waals forces with Val-112 (V112) in SNAP25b, whereas Glu-89 and Asp-122 (E89/D122) in the ANK domain establish hydrogen bonds with Gln-116 (Q116) in the SNAP25 peptide (Verardi et al., 2017). By identifying proteins that contain a cytosolic and unstructured zDABM, and subsequently validating interactions with ANK17 in peptide arrays, a large number of potential novel interactors of zDHHC17 were identified (Lemonidis et al., 2017a). These novel interactors included SNARE proteins, all family members of the Sprouty (SPRY) and SPRED, cornifelin, ankyrin, and SLAIN-motif containing proteins, as well as several proteins involved in cell communication, signalling, proliferation, and cytoskeletal organisation (Lemonidis et al., 2017a). Interestingly, the interaction of SPRY and SPRED proteins with zDHHC17 has been previously reported in a yeast two-hybrid screen (Butland et al., 2014), and SPRY2 and zDHHC17 were further shown to interact in HEK293 cells in a BioPlex interactome study (Huttlin et al., 2017).

The results presented in Chapter 3 show that SPRY2 is S-acylated by zDHHC17 on specific cysteine residues and that this regulates both expression levels and plasma membrane association of this substrate. The aim of this chapter was to investigate the zDHHC17-SPRY2 interaction further and to determine (i) whether the zDABM of SPRY2 mediates interaction with the ANK domain of zDHHC17 and (ii) whether this is important for subsequent S-acylation.

4.2 Results

4.2.1 Alanine substitution of Trp-130 (W130A) within the ANK domain of zDHH17 severely impairs the binding of SPRY2 and several other proteins that contain zDABM sequences

The study of Verardi *et al.* (2017) uncovered the key amino acids within the ANK domain of zDHH17 that mediate the interaction with the zDABM of SNAP25b and HTT. Among these, Trp-130 (W130) contacts several residues including the highly conserved proline of the zDABM of these substrates. Another study identified ANK17-binding zDABM peptides in a large number of proteins including SPRY2 (Lemonidis *et al.*, 2017a). To confirm that SPRY2 interacts with the ANK domain of zDHH17 *via* the same mechanism previously described for SNAP25b and HTT, we tested the binding of this protein, together with a sub-set of other proteins containing validated zDABM sequences (Lemonidis *et al.*, 2017a) to immobilised His₆-ANK17 wild-type or a mutant in which W130 was substituted by alanine (W130A). In addition to SPRY2, the tested proteins included (i) the Receptor Tyrosine Kinase (RTK) inhibitors SPRED1 and SPRED2 (Sprouty-related proteins), (ii) the mitogen-activated Ser/Thr protein kinases (MAPK) JNK1 α 2 and JNK3 α 2, (iii) the nuclear protein PAI-RBP1 (plasminogen activator inhibitor RNA-binding protein-1), (iv) the vesicle-trafficking proteins CSP α and SNAP25b, (v) the microtubule-associated HTT and SLAIN1 (SLAIN motif containing protein 1) and, (vi) the actin-associated EVL-I protein (Ena/VASP-like).

His₆-ANK17 WT or His₆-ANK17 W130A were expressed and purified in *E. Coli* and then used in pull-down assay experiments. All the above-mentioned proteins (EGFP-tagged at the N-terminus) were expressed in HEK293T cells and corresponding cell lysates incubated with His₆-ANK WT, His₆-ANK W130A or PBS (negative control), and their capture on Ni²⁺-NTA resin was examined. Figure 4.1 shows that SPRY2 as well as all the other tested proteins were efficiently pulled down by ANK17 WT, whereas there was a substantial loss of binding to the ANK17 W130A mutant. This observation suggests that Trp-130 is crucial for efficient recruitment not only of SNAP25b and HTT but also of many other substrates and interactors of zDHH17, including SPRY2.

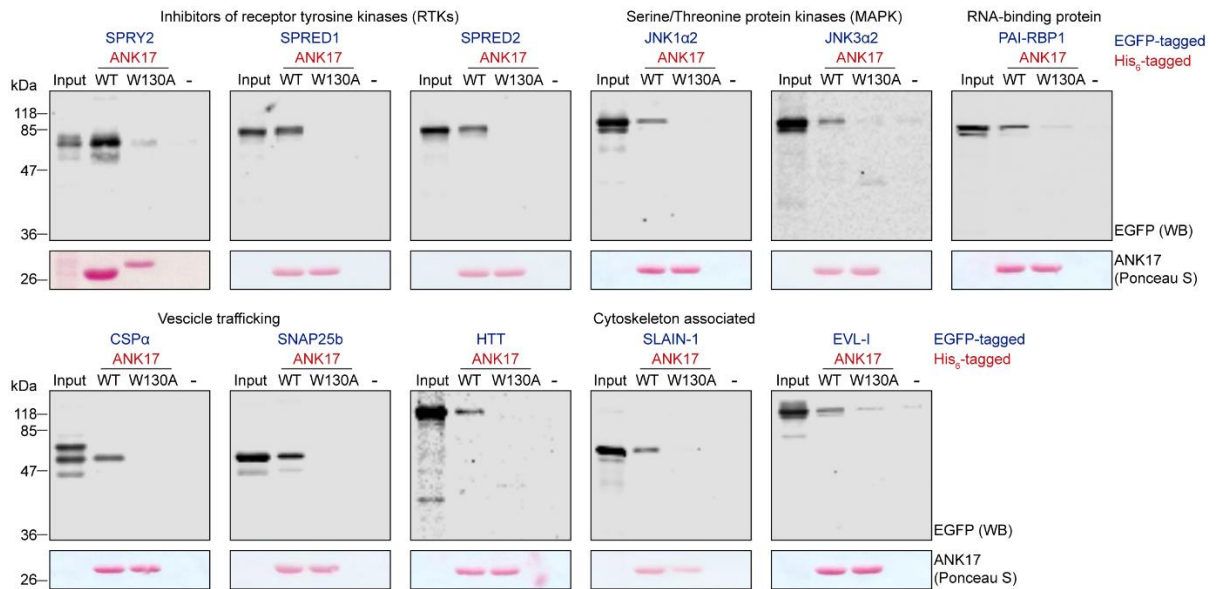


Figure 4.1 Effect of the W130A substitution of the ANK domain on substrate binding by zDHHC17

Plasmids encoding EGFP-tagged CSP α , SNAP25b, HTT, SLAIN1, EVL-1, SPRED1, SPRED2, SPRY2, JNK1 α 2, JNK3 α 2, and PAI-RBP1 were transfected into HEK293T cells. The corresponding lysates were incubated with His₆-ANK17 WT or W130A mutant (the ANK domain encompassed amino acids 54-288 of zDHHC17 with the exception of ANK WT used for SPRY2 pulldown, which encompassed amino acids 51-288), and captured on Ni²⁺-NTA agarose. The negative control samples (referred to as “-” in the figure) indicate where substrate proteins were incubated with Ni²⁺-NTA agarose beads in the absence of His₆-ANK17. 7.5% of the total input and 40% of the total bound fraction were run on 12% polyacrylamide gels and resolved by SDS-PAGE. After transfer to nitrocellulose, the membranes were stained by Ponceau S solution and probed with a GFP antibody. The positions of molecular weight markers are shown on the left side of all immunoblots.

4.2.2 N100A and W130A substitutions have no effect on S-acylation of SPRY2 by zDHHC17

The results above build on the study of Verardi *et al.* (2017) by showing that Trp-130 (W130) is critical for the binding of ANK17 to a broad range of proteins, including SPRY2, most likely by establishing key contacts with their zDABM sequences. In addition to W130, Asn-100 (N100) was shown to make important contacts (H-bonds) with the main chain of Val-113, present at the second position of the zDABM of SNAP25b. Supporting the key role of W130 and N100 in substrate binding, alanine-substitutions at these positions in ANK17 were shown to block SNAP25b S-acylation by zDHHC17 (Verardi *et al.*, 2017). In a similar way, alanine substitution of Pro-117 (key proline at position 6 of the zDABM) in SNAP25b, severely impairs its binding to and S-acylation by zDHHC17 (Greaves *et al.*, 2009a; Lemonidis *et al.*, 2015a).

To determine if S-acylation of SPRY2 occurs *via* the same mechanism described for SNAP25b, we investigated the importance of N100 and W130 of ANK17 for SPRY2 S-acylation. HEK293T cells were co-transfected with EGFP-tagged SPRY2 together with pEFBOS-HA (control), or plasmids encoding HA-zDHHC17 WT, HA-zDHHC17 W130A, or HA-zDHHC17 N100A. The cells were labelled with C16:0-azide, and click chemistry with alkyne-IR800, SDS-PAGE and immunoblotting were performed as described in Chapter 2.

Unexpectedly, SPRY2 was efficiently S-acylated not only by zDHHC17 WT, but also by zDHHC17 W130A and zDHHC17 N100A (Fig. 4.2a). To confirm that the introduced mutations in zDHHC17 were having the expected effect, the ability of these mutants to S-acylate SNAP25b was also examined. As predicted, under the same conditions, neither zDHHC17 W130A nor N100A mutant was active against SNAP25b (Fig. 4.2b). Taken together, this data suggests that the canonical substrate binding pocket in the ANK domain of zDHHC17 is likely not required for S-acylation of SPRY2. In marked contrast, the same binding pocket is crucial for correct S-acylation of SNAP25b, as previously reported by Verardi and colleagues (Verardi *et al.*, 2017).

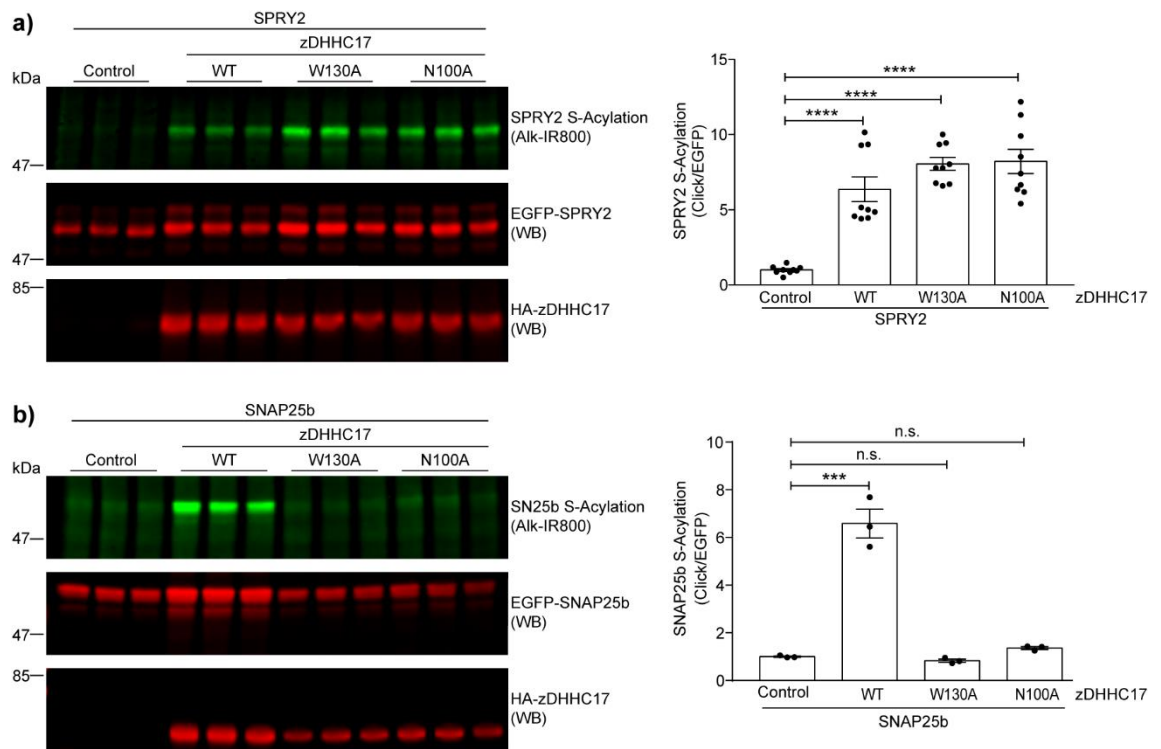


Figure 4.2 S-acylation of SPRY2 by zDHHC17 does not require Trp-130 or Asn-100

HEK293T cells were transfected with plasmids encoding either EGFP-tagged SPRY2, or SNAP25b together with either pEFBOS-HA (referred to as “control” in the figure), HA-tagged zDHHC17 WT, zDHHC17 W130A, or zDHHC17 N100A. Cells were incubated with 100 μ M of palmitic acid azide (C16:0-azide) for 4h and labelled proteins reacted with alkyne IRdye-800 nm. EGFP and HA signals were detected at 700 nm. **a) Left panel**, representative images showing SPRY2 S-acylation (*top*) and SPRY2 levels (*middle*) detected on the same immunoblot. For zDHHC17, HA (*bottom*) was revealed for the same samples on a different immunoblot. The positions of the molecular weight markers are shown on the left of all immunoblots. **Right panel**, graph showing mean SPRY2 S-acylation levels after normalisation. Error bars represent \pm SEM; each replicate is shown with filled circles. Differences were analysed by one-way ANOVA (**** denotes $P < 0.0001$, $n=9$). **b) Left panel**, image showing SNAP25b S-acylation (*top*), SNAP25b levels (*middle*), and zDHHC17 levels (*bottom*). The positions of the molecular weight markers are shown on the left of all immunoblots. **Right panel**, graph showing mean SNAP25b S-acylation levels after normalisation. Error bars represent \pm SEM; each replicate is shown with filled circles. Differences were analysed by one-way ANOVA (***) denotes $P < 0.001$, n.s. not significant, $n=3$).

4.2.3 Mutation of the zDABM sequence(s) in SPRY2 has no effect on S-acylation mediated by zDHHC17

The results in Figure 4.2a suggest that the interaction of the zDABM sequence of SPRY2 (also referred to as the “QP” motif) with the ANK domain of zDHHC17 may not be required for S-acylation. To confirm this directly, we tested if mutation of the zDABM of SPRY2 affected its S-acylation by wild-type zDHHC17. In peptide-array studies, the identified zDABM motif of SPRY2, which binds to the ANK domain of zDHHC17, was shown to include Pro-154 (P154) (Lemonidis et al., 2017a). As proline residues in zDABM sequences appear to be critical for interaction with ANK17 (Verardi et al., 2017), we generated a SPRY2 P154A mutant. In addition to this zDABM sequence, there are an additional three other QP sequences in SPRY2 which include Pro-13, Pro-91, and Pro-96 (Fig. 4.3a). Although none of these QP dipeptides are present in sequences that conform to canonical zDABM consensus, proline to alanine substitutions were nevertheless generated at these sites (SPRY2 P13A, SPRY2 P91A, and SPRY2 P96A mutants). Furthermore, a SPRY2 P13/91/96/154A mutant, in which all the prolines in QP dipeptides were simultaneously substituted by alanines, was also generated.

These EGFP-tagged SPRY2 proline mutants were co-expressed in HEK293T cells with HA-tagged zDHHC17, whilst EGFP-tagged SPRY2 WT was expressed together with either pEFBOS-HA or HA-tagged zDHHC17. Cells were labelled with C16:0-azide, and click chemistry with alkyne-IR800, SDS-PAGE and immunoblotting were performed as described in Chapter 2. Figure 4.3b-d shows that all the tested proline mutants were efficiently modified by zDHHC17, implying that S-acylation is indeed independent of zDABM sequences in SPRY2 (and the N100/W130 binding pocket in zDHHC17 ANK domain). Upon zDHHC17 expression, both P154A and P13/91/96/154A mutants displayed slightly increased S-acylation levels, compared to wild-type SPRY2. Taken together, these results are consistent with results obtained with the zDHHC17 W130A and N100A mutants, and further support that interaction of zDABM sequences with the N100/W130 binding pocket in ANK17 is dispensable for SPRY2 S-acylation.

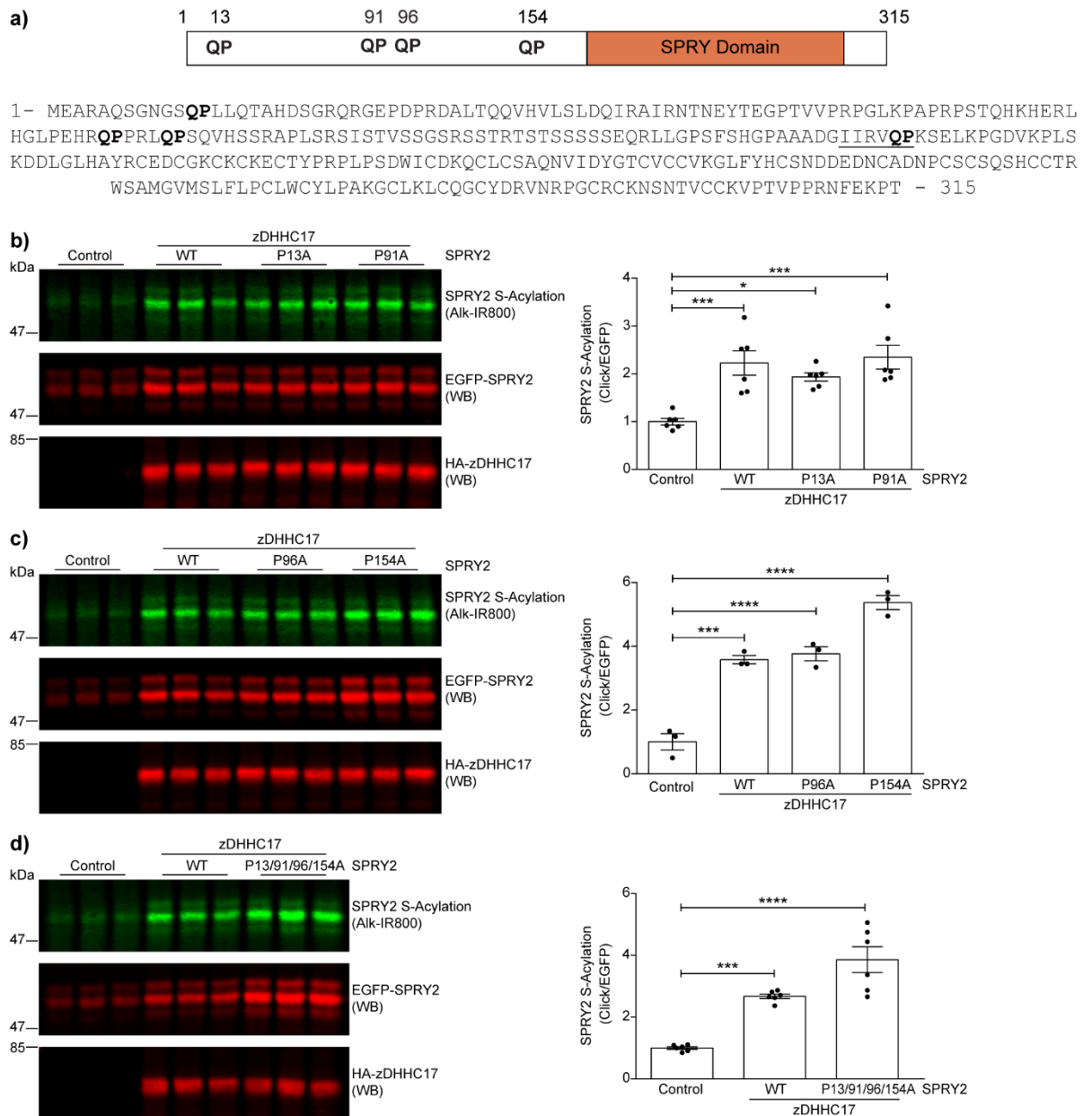


Figure 4.3 S-acylation of SPRY2 by zDHHC17 does not require zDABM sequences

a) Schematic representation of mouse SPRY2 protein and complete amino acid sequence (residues 1-315). All the QP dipeptides which were mutated into “QA” are shown in bold. **b-d)** HEK293T cells were transfected with a plasmid encoding EGFP-tagged SPRY2 WT together with either pEFBOS-HA (referred to as “control” in the figure) or HA-tagged zDHHC17. Plasmids encoding EGFP-tagged SPRY2 P13A, SPRY2 P91A, SPRY2 P96A, SPRY2 P154A, and SPRY2 P13/91/96/154A mutants were co-transfected with HA-tagged zDHHC17. Cells were incubated with 100 μ M of palmitic acid azide (C16:0-azide) for 4h and labelled proteins reacted with alkyne IRdye-800 nm. EGFP and HA signals were detected at 700 nm. *Left panels,*

representative images showing SPRY2 S-acylation (*top*) and SPRY2 levels (*middle*) detected on the same immunoblot. For zDHHC17, HA (*bottom*) was revealed for the same samples on a different immunoblot. The positions of the molecular weight markers are shown on the left side of all immunoblots. *Right panels*, graphs showing mean SPRY2 S-acylation levels after normalisation. Error bars represent \pm SEM; each replicate is shown with filled circles. For clarity, only relevant statistical analysis is shown in the figure. Differences were analysed by one-way ANOVA (**** denotes $P < 0.0001$, *** $P < 0.001$, * $P < 0.05$). Not shown in the figure: S-acylation of SPRY2 P13A, P91A, or P96A vs. SPRY2 WT was not significant (i.e. $P > 0.05$), whereas S-acylation of the two SPRY2 P154A mutants vs. SPRY2 WT was different (e.g. P154A was $P < 0.01$ and P13/91/96/154A was $P < 0.05$). **b and d**) $n=6$; **c**) $n=3$.

4.2.4 Disruption of the zDABM sequence in SPRY2 diminishes but does not abolish interaction with ANK17 in pull-down assays

The results described so far show that the conventional zDABM interaction with the N100/W130 pocket in ANK17 is not required for SPRY2 S-acylation. However, the results in Figure 4.1 suggests that SPRY2 interaction with ANK17 is reduced when a W130A substitution is introduced. To rule out that the ANK17 W130A mutant is behaving anomalously in pull-down assays, we also examined the binding of ANK17 WT to proline mutants of SPRY2.

Thus, HEK293T cells were transfected with EGFP-tagged SPRY2 wild-type, P154A, or P13/91/96/154A mutants (Fig. 4.4a). The corresponding lysates were incubated with His₆-ANK17 or PBS (negative control), and their capture on Ni²⁺-NTA resin examined. As shown in Figure 4.4b, full-length SPRY2 WT was efficiently pulled down by ANK17, whereas both P154A and P13/91/96/154A mutants displayed a marked loss in binding to ANK17. However, mutant SPRY2 binding was not completely abolished, in agreement with Figure 4.1 (SPRY2 panel). Thus, while the characterised zDABM of SPRY2, including Pro-154, is the main binding site to the ANK domain of zDHHC17, the observed residual binding suggests that SPRY2 may have an additional (lower affinity) binding site on ANK17. It is also interesting to note that in this set of

experiments the slow-migrating (i.e. bottom) band of SPRY2 was preferentially captured by ANK17.

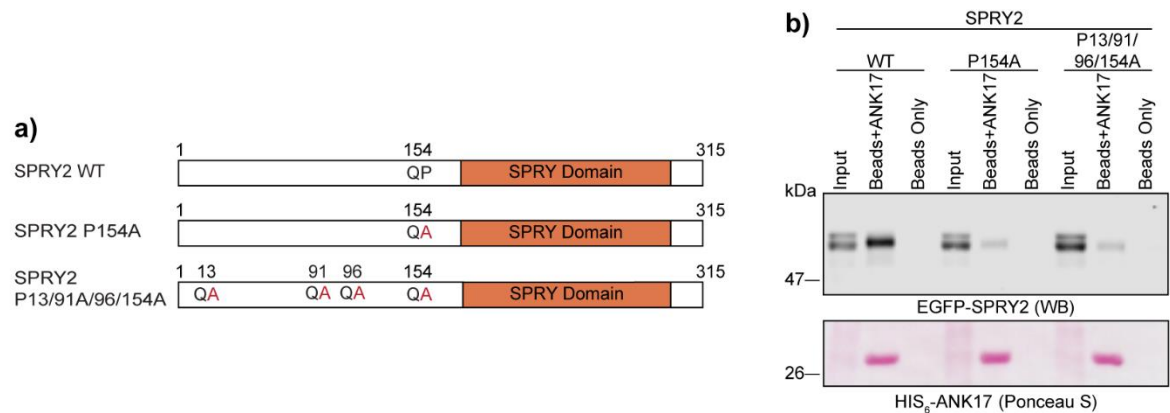


Figure 4.4 Mutation of Pro-154 within the zDABM of SPRY2 reduces but does not abolish binding to ANK17

a) Schematic of the SPRY2 constructs employed in pulldown assay experiments: EGFP-tagged SPRY2 wild-type (WT), SPRY2 P154A and SPRY2 P13A/91A/96A/154A. **b)** Pulldown assay experiments. The EGFP-tagged SPRY2 proteins depicted in panel a) were expressed in HEK293T cells, and the corresponding lysates incubated with His₆-ANK17 (the ANK domain encompassed amino acids 51-288 of zDHHC17) and captured on Ni²⁺-NTA agarose beads. The negative control samples (referred to as “Beads Only” in the figure) indicate where substrate proteins were incubated with Ni²⁺-NTA agarose beads in the absence of His₆-ANK17. 7.5% of the total input and 30% of the total bound fraction were run on 10% polyacrylamide gels and resolved by SDS-PAGE. After transfer to nitrocellulose, the membranes were stained by Ponceau S solution and probed with a GFP antibody. The positions of molecular weight markers are shown on the left side of all immunoblots.

4.2.5 Mutation of Pro-154 in SPRY2 leads to reduced but not abolished interaction with full-length zDHHC17

To ascertain that the pull-down experiments using ANK17 faithfully report on interactions of full-length zDHHC17, we assessed the ability of SPRY2 wild-type or SPRY2 P154A mutant to bind full-length zDHHC17 in immunoprecipitation (IP) experiments. In addition, we investigated whether Asn-211 (N211), Asp-214 (D214), and Lys-223 (K223) of SPRY2, which were shown in Chapter 3 to be important for SPRY2 S-acylation, were involved in the binding of zDHHC17. Hence, the SPRY2 NDK mutant was included in this series of experiments as well as a SPRY2 P154A NDK construct. The binding of these mutants to zDHHC17 was assessed using a zDHHC17 C467A mutant (referred to as “zDHHA17”), in which the catalytic Cys-467 of the DHHC motif was mutated to alanine. This approach was taken to prevent S-acylation of SPRY2, which increases protein stability (Chapter 3) and therefore could complicate interpretation of IP experiments.

HEK293T cells were transfected with plasmids encoding EGFP (control), EGFP-tagged SPRY2 WT, P154A, NDK, or P154A NDK together with HA-tagged zDHHA17. The corresponding lysates were incubated with beads conjugated to a GFP antibody, and the amount of zDHHA17 bound by SPRY2 proteins was analysed. In agreement with the pull-down assays, proline to alanine substitution at position 154 of SPRY2 (P154A and P154A NDK mutants) resulted in diminished, but not abolished, binding to zDHHA17. Moreover, the SPRY2 NDK mutant did not show any loss of binding to zDHHA17 (and indeed binding appeared to be increased), ruling out that these residues participate in zDHHC17 binding (Fig. 4.5).

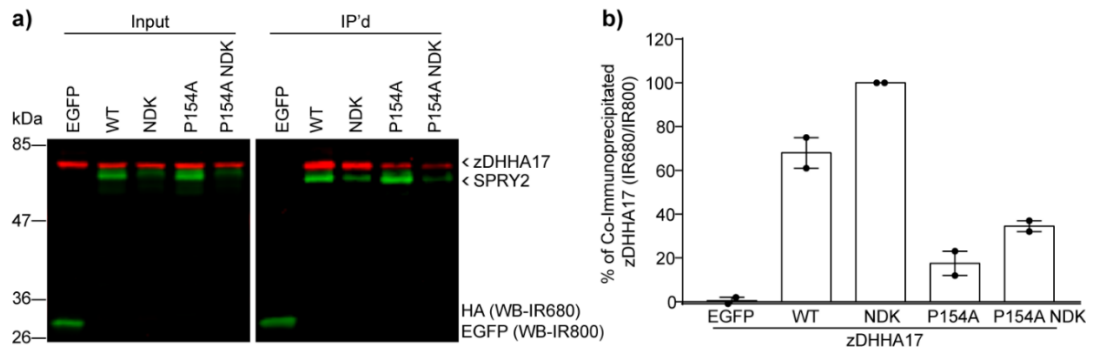


Figure 4.5 Mutation of Pro-154 in SPRY2 diminishes but does not abolish interaction with full-length zDHHC17

HEK293T cells were transfected with plasmids encoding EGFP (control) or EGFP-tagged SPRY2 WT, SPRY2 NDK, SPRY2 P154A, and SPRY2 P154A NDK together with HA-tagged zDHHC17 C467A (referred to as “zDHHA17” in the figure). Cell lysates were incubated with agarose beads conjugated to a GFP antibody. Bound proteins were collected, run on 10% polyacrylamide gels and resolved by SDS-PAGE. After transfer to nitrocellulose, the membranes were probed with a GFP antibody to reveal SPRY2 proteins (IR800) and with a HA antibody to reveal zDHHA17 (IR680). **a)** *Left immunoblot*, representative image showing SPRY2 and zDHHA17 expression levels in input samples before immunoprecipitation experiments. *Right immunoblot*, representative image showing immunoprecipitated (IP'd) EGFP-SPRY2 proteins and co-immunoprecipitated zDHHA17. The positions of the molecular weight markers are shown on the left of the immunoblots. **b)** Graph showing mean zDHHA17 co-immunoprecipitated by each SPRY2 protein, calculated as the ratio between HA and GFP signals (IR680/IR800) in the immunoprecipitated (IP'd) samples (*right immunoblot*). Error bars represent \pm SEM; each replicate is shown with filled circles (n=2).

4.2.6 Truncation analysis suggests that the SPRY domain is sufficient for S-acylation of SPRY2 by zDHHC17

As shown above, SPRY2 S-acylation does not require interaction between its characterised zDABM sequence and the ANK17 N100/W130 binding pocket. Indeed, our data (Fig. 4.4 and 4.5) also suggest the presence of an additional ANK17 binding site in SPRY2, possibly linked to S-acylation. Because the C-terminal domain (i.e. residues 177-291) of SPRY2 contains Cys-265/268 and the NDK motif, both shown to be key elements for S-acylation by zDHHC17 (Chapter 3), we focused on the N-terminus of the protein. Thus, the ability of a series of truncated versions of SPRY2, lacking either 100, 120, 140, or 155 amino terminal residues (Fig. 4.6a) to undergo zDHHC17-mediated S-acylation was evaluated in click chemistry experiments.

HEK293T cells were co-transfected with EGFP-tagged SPRY2 100-315, 120-315, 140-315, or 155-315 together with either pEFBOS-HA (control) or HA-tagged zDHHC17. Following incubation with C16:0-azide, click chemistry, SDS-PAGE and immunoblotting were performed as described in Chapter 2. As shown in Figure 4.6b, all SPRY2 constructs were efficiently S-acylated by zDHHC17. Notably, the fact that the SPRY2 155-315 mutant was used as a substrate implies that the SPRY domain, plus a few amino acids up- and down-stream of it, is *per se* sufficient for SPRY2 S-acylation by zDHHC17.

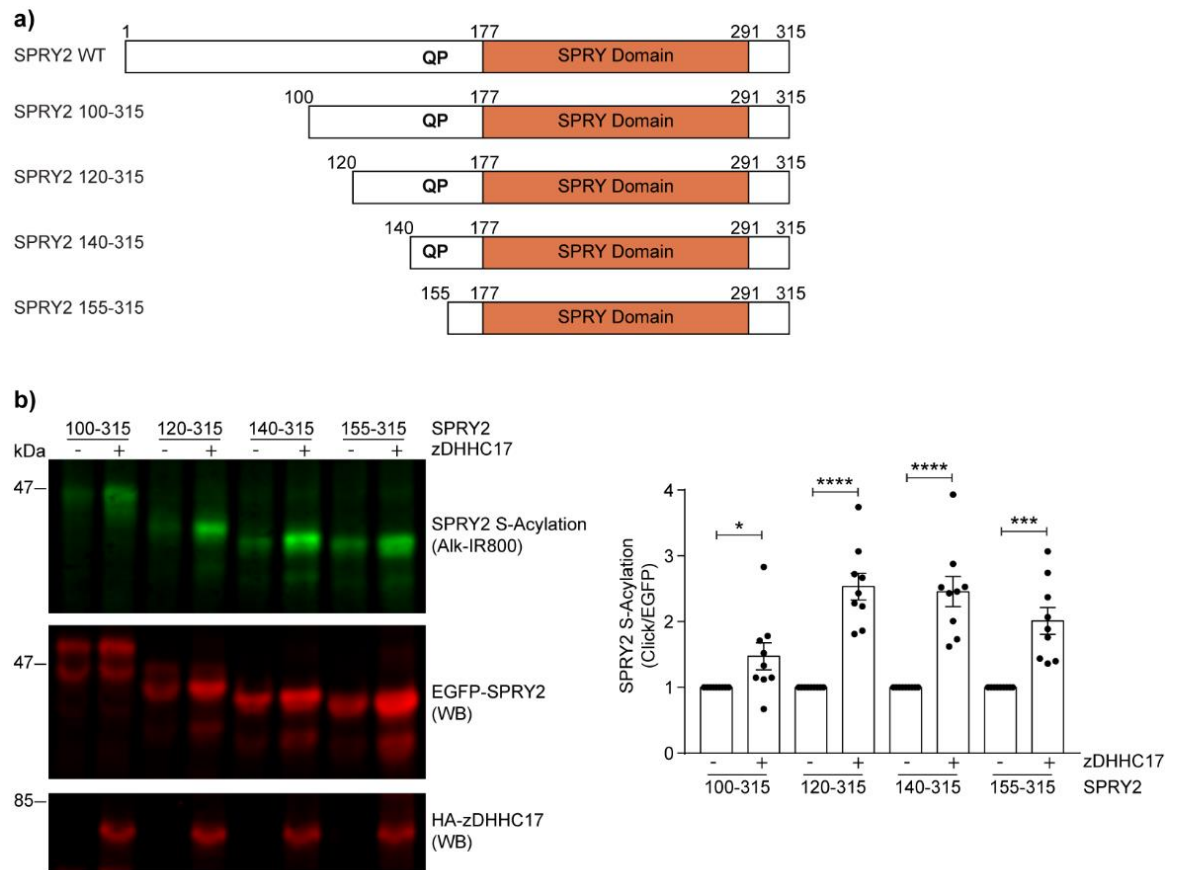


Figure 4.6 Residues 155-315 of SPRY2, encompassing the SPRY domain, are sufficient for S-acylation by zDHHC17

a) Schematic of the SPRY2 constructs employed in click chemistry assay experiments: SPRY2 100-315, 120-315, 140-315, and 155-315 of mouse sequence (UniprotKB-Q9QXV8). All constructs have EGFP tags appended at the N-terminus. **b)** HEK293T cells were transfected with plasmids encoding EGFP-tagged SPRY2 100-315, SPRY2 120-315, SPRY2 140-315, or SPRY2 155-315 together with either pEFBOS-HA (referred to as “-” in the figure) or HA-zDHHC17 (referred to as “+” in the figure). Cells were incubated with 100 μ M of palmitic acid azide (C16:0-azide) for 4h and labelled proteins reacted with alkyne IRdye-800 nm. *Left panel*, representative images showing SPRY2 S-acylation (*top*), SPRY2 levels (*middle*) and zDHHC17 levels (*bottom*), detected on the same immunoblot. The positions of the molecular weight markers are shown on the left side of all immunoblots. *Right panel*, graph showing mean SPRY2 S-acylation levels after normalisation against the corresponding control samples (pEFBOS-HA). Error bars represent \pm SEM; each replicate is shown with filled circles. Differences were analysed by Unpaired t-test (**** denotes $P < 0.0001$, *** $P < 0.001$, ** $P < 0.01$, * $P < 0.05$, $n=9$).

Region 155-315 of SPRY2, which is sufficient for S-acylation by zDHHC17 (Fig. 4.6), also includes the C-terminus of the protein (i.e. amino acids 292-315 - UniProtKB-Q9QXV8), previously shown to mediate important protein interactions, including that of SPRY2 with Grb2 (Lao et al., 2006) and CIN85 (Haglund et al., 2005). To evaluate whether this domain was interacting with zDHHC17, thus accounting for the observed S-acylation, a SPRY2 protein lacking residues 291-315 (SPRY2 G290X) was employed in click chemistry assays. In addition, a SPRY2 P154A G290X construct, in which the P154A mutation was introduced, was also included (Fig. 4.7a).

HEK293T cells were transfected with either pEFBOS-HA or HA-tagged zDHHC17 together with plasmids encoding EGFP-tagged SPRY2 G290X with or without the P154A substitution. Following incubation with C16:0-azide, click chemistry, SDS-PAGE and immunoblotting were performed as described in Chapter 2. Upon zDHHC17 co-expression, the S-acylation of both SPRY2 G290X WT and G290X P154A was increased, compared to control samples (pEFBOS-HA) (Fig. 4.7b). Therefore, the C-terminal domain of SPRY2 is not required for zDHHC17-mediated S-acylation, and most likely not involved in its binding. Together with Figure 4.6, this observation further indicates that amino acids 155-290 of SPRY2 are sufficient to sustain S-acylation by zDHHC17 also raising the question of whether an additional binding site (linked to S-acylation) exist within this region.

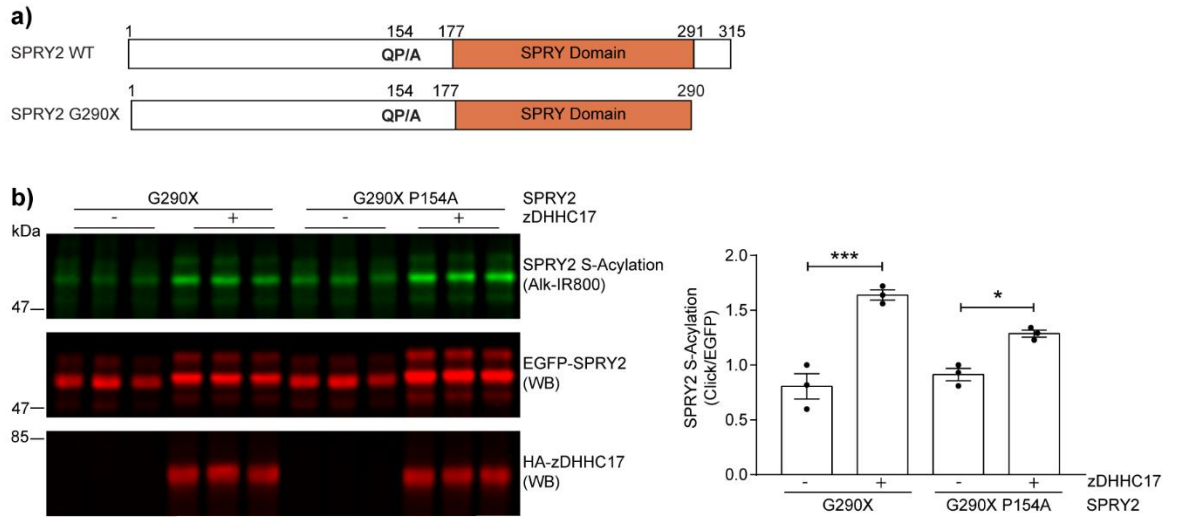


Figure 4.7 SPRY2 S-acylation by zDHHC17 does not require its C-terminal domain

a) Schematic representation of SPRY2 WT (or P154A) full-length and SPRY2 G290X mutants. G290X truncated versions were generated by inserting a premature stop codon in frame with the protein sequence, using as DNA template either EGFP-tagged SPRY2 WT or P154A mutant. **b)** HEK293T cells were transfected with either pEFBOS-HA (referred to as “-” in the figure) or plasmids encoding HA-zDHHC17 (referred to as “+” in the figure) together with EGFP-SPRY2 G290X deletion constructs either without (WT) or with the P154A substitution. Cells were incubated with 100 μ M of palmitic acid azide (C16:0-azide) for 4h and labelled proteins reacted with alkyne IRdye-800 nm. GFP and HA signals were detected at 700 nm. *Left panel*, representative images showing SPRY2 S-acylation (*top*) and SPRY2 levels (*middle*) detected on the same immunoblot. For zDHHC17, HA (*bottom*) was revealed for the same samples on a different immunoblot. The positions of the molecular weight markers are shown on the left side of all immunoblots. *Right panel*, graphs showing mean SPRY2 S-acylation levels after normalisation; the conditions containing zDHHC17 were normalised against the corresponding controls samples (pEFBOS-HA). Error bars represent \pm SEM; each replicate is shown with filled circles. Differences were analysed by one-way ANOVA (***) denotes $P < 0.001$, * $P < 0.05$, $n=3$).

4.2.7 The ANK domain is required for zDHHC17-mediated S-acylation of SPRY2

To confirm that S-acylation of SPRY2 by zDHHC17 requires interaction with the ANK domain, a series of zDHHC17 truncation mutants were assessed for their ability to modify SPRY2 by click chemistry experiments. These constructs included: HA-tagged zDHHC17- Δ N, lacking the N-terminus upstream of the ANK domain (encoding residues 54-632); (ii) zDHHC17- Δ NANK17, lacking both the N-terminus and the ANK domain (encoding residues 287-632) and, (iii) zDHHC17- Δ C, lacking the cytosolic C-terminal region downstream of the sixth transmembrane domain (encoding residues 11-569) (Fig. 4.8a).

HEK293T cells were co-transfected with EGFP-tagged SPRY2 wild-type together with pEFBOS-HA (control), or plasmids encoding HA-zDHHC17 WT, Δ N, Δ NANK17, or Δ C. The cells were labelled with C16:0-azide, and click chemistry with alkyne-IR800, SDS-PAGE and immunoblotting were performed as described in Chapter 2. Figure 4.8b shows that both zDHHC17- Δ NANK17 and zDHHC17- Δ C mutations led to a marked loss of SPRY2 S-acylation, whereas the zDHHC17- Δ N mutant effectively modified SPRY2. Inactivity of the Δ C mutant towards SNAP25b has been previously reported (Lemonidis et al., 2014), and indeed the latest crystallographic data reveal that the C-terminus of zDHHC enzymes is crucial for both enzyme stability and catalytic activity (Rana et al., 2018a). On the other hand, the loss of activity observed with zDHHC17- Δ NANK17 suggests that this domain is required for efficient S-acylation of SPRY2, although it is possible that the ANK domain is also important for the overall structural integrity of zDHHC17 and its removal interferes indirectly with enzymatic activity.

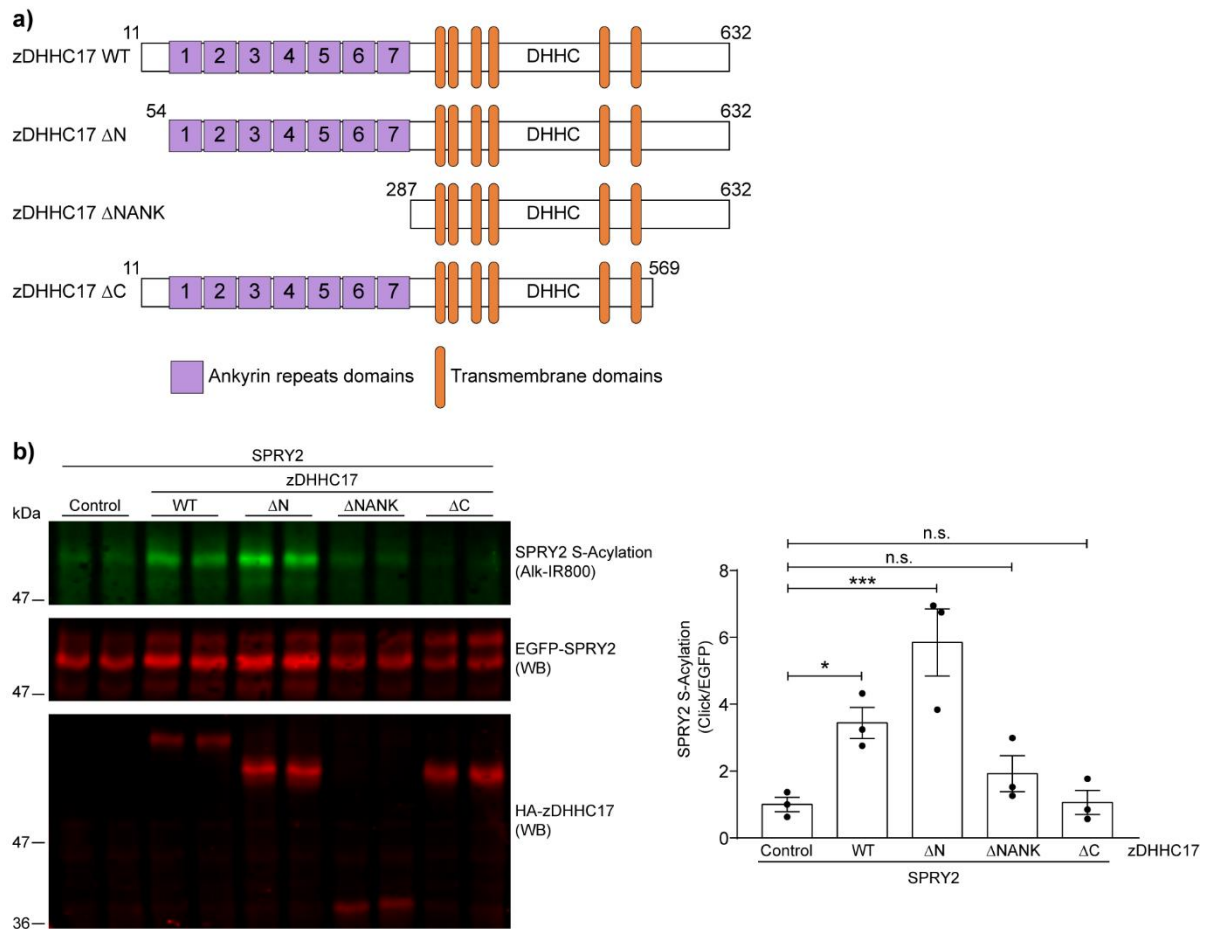


Figure 4.8 Deletion of ANK17 or the C-terminal tail of zDHHC17 prevents SPRY2 S-acylation

a) Schematic of the HA-tagged zDHHC17 constructs employed in click chemistry assay experiments: zDHHC17-ΔN encodes for amino acids 54-632 (lacks the N-terminal region upstream of the ANK domain); zDHHC17-ΔNANK17 encodes for amino acids 287-632 (lacks the N-terminus plus the ANK domain); zDHHC17-ΔC encodes for amino acids 11-569 (lacks the cytosolic C-terminal region downstream of the sixth transmembrane domain). **b)** HEK293T cells were transfected with plasmids encoding EGFP-tagged SPRY2 WT together with pEFBOS-HA (referred to as “control” in the figure), HA-zDHHC17 WT, zDHHC17-ΔC, zDHHC17-ΔNANK, or zDHHC17-ΔC. Cells were incubated with 100 μM of palmitic acid azide (C16:0-azide) for 4h and labelled proteins reacted with alkyne IRdye-800 nm. *Left panel*, representative images showing SPRY2 S-acylation (*top*) and SPRY2 levels (*middle*) detected on the same immunoblot. For zDHHC17 WT and mutant proteins, HA (*bottom*) was revealed for the same samples on a different immunoblot. The positions of the molecular weight markers are shown on the left side of all immunoblots. *Right panel*, graph showing mean SPRY2 S-acylation levels after normalisation. Error bars represent ± SEM; each replicate is

shown with filled circles. Differences were analysed by one-way ANOVA (***) denotes $P < 0.001$, * $P < 0.05$, n.s. $P > 0.05$, $n=3$).

4.2.8 Peptide array experiments suggest the presence of a second binding site upstream of the zDABM of SPRY2

The results presented so far are consistent with the presence of an additional ANK17 binding site in SPRY2 that is linked to S-acylation. The truncation analyses imply that this binding site is present in the SPRY domain (i.e. residues 155-290). Therefore, to pinpoint the exact location of the additional ANK17 binding site in SPRY2, we undertook peptide array experiments (arrays were synthesised by the Baillie lab, at the University of Glasgow). For completeness, the arrays were prepared to cover the entire amino acid sequence of human SPRY2 protein (amino acids 1-315): a total of 59 peptides were spotted on nitrocellulose membranes and screened for binding to the ANK domain of zDHHC17. Each peptide covered a sequence of 25 amino acids with 20 residues overlapping between one peptide and the next one (e.g. if peptide 1 covers residues 1-25, peptide 2 covers residues 6-30) (Fig. 4.9a). Following overlay of the array with His₆-ANK17, immunoblotting was performed as described in Chapter 2 and the results are shown in Figure 4.9b.

The strongest binding of ANK17 occurred at positions 27-30 of the array, corresponding to peptides encompassing the zDABM sequence of SPRY2 149-IIRVQP-154. Consistent with the results shown thus far, this motif represents the major ANK17 binding site. It is interesting to note that the peptide at position 31, containing the QP dipeptide of the zDABM but not the upstream isoleucine residues (at positions 1 and 2 of the zDABM), did not interact with His₆-ANK17. This latter observation highlights that the integrity at the zDABM is an important requirement for correct recruitment and binding of substrates by zDHHC17. In agreement with this, mutation of Val-113, at position 2 of the zDABM of SNAP25b was shown to reduce ANK17 binding (Verardi et al., 2017).

Another series of less intense positive spots were revealed on the array, from position 18 to position 24, with signal peaking for peptides 20-22 (Fig. 4.9b). Analyses of the corresponding peptides led to the identification of the sequence 106-PLSRSISTVSSGSRS-120, which may contain a second ANK17 binding site. Surprisingly, this region lays within the N-terminus of SPRY2, upstream of both the consensus zDABM sequence and the SPRY domain. It further appears to be a lower affinity interaction site than the zDABM sequence. This sequence falls within the serine-rich motif of SPRY2 (SRM, residues 108-132 in human SPRY2) which is conserved across mammalian SPRY proteins (Guy et al., 2009) and encompasses several serine residues with those at positions 112, 115, 116, and 118 previously reported to undergo dynamic phosphorylation (Brady et al., 2009; Lao et al., 2007; Sweet et al., 2008). Interestingly, no binding was readily apparent to peptides in the region 155-290 despite the finding that this region of SPRY2 was efficiently S-acylated by zDHHC17 (Fig. 4.6 and 4.7).

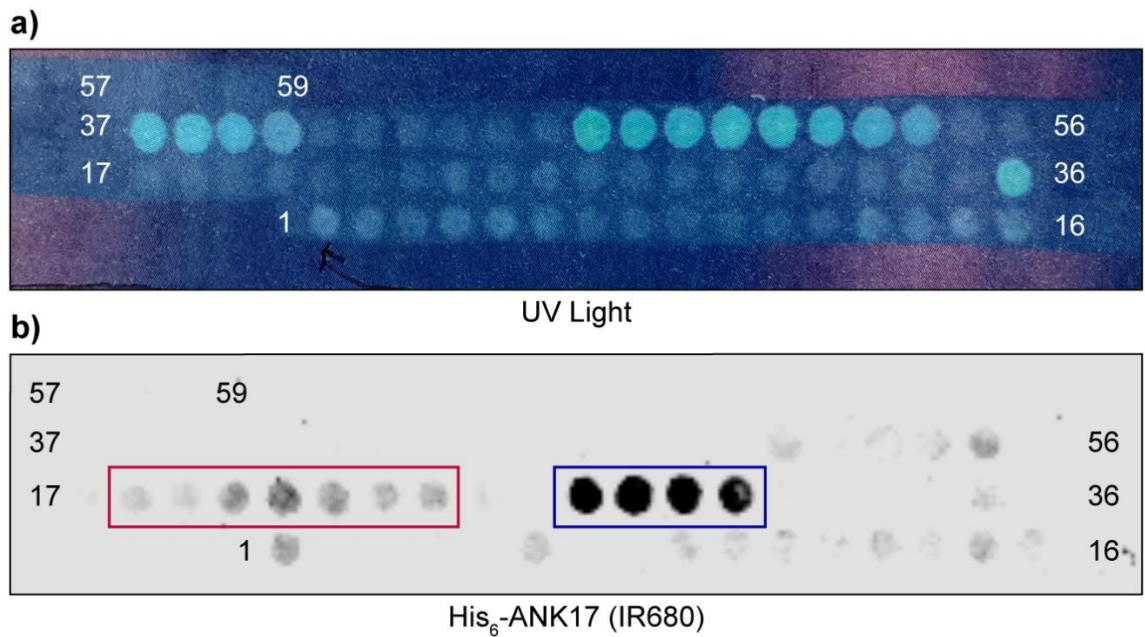


Figure 4.9 A potential second ANK17 binding domain is present at position 106-120 of human SPRY2

Human SPRY2 protein, amino acids 1-315, was spotted on nitrocellulose membranes in 59 peptides. Each peptide had a length of 25 amino acids with 20 amino acids overlapping between one peptide and the next one. The position of the first and last spot for each column is shown in the figure. **a)** The position of all peptides was revealed by UV light. The brightest spots represent peptides containing residues with aromatic rings (phenylalanine, tryptophan, and tyrosine). Dimmer peptides do not contain aromatic amino acids. **b)** Peptide array experiment. SPRY2 peptide array was incubated with 0.5 μ M of purified His₆-ANK17 protein (the ANK domain encompassed amino acid 51-288 of zDHHC17) and probed with a histidine antibody to reveal the peptides bound by ANK17 (IR680). Peptides recognised by His₆-ANK17 are boxed in the figure: red box refers to the putative novel ANK17 binding motif, blue box to the recognised zDABM sequence. Relative positions on the array are annotated.

4.2.9 In PC12 cells, SPRY2 P154A and SPRY2 155-315 are efficiently S-acylated by endogenous enzymes and targeted to the plasma membrane similar to wild-type SPRY2. As both SPRY2 P154A and SPRY2 155-315 mutants were efficiently modified by overexpressed zDHHC17 in HEK293T cells, we next investigated whether they can be endogenously S-acylated in neuroendocrine PC12 cells and whether they display a similar localisation as wild-type SPRY2. Although not directly demonstrated, the data presented in Chapter 3 (section 3.2.12), suggests that in this cell line SPRY2 may be modified by endogenous zDHHC17.

Therefore, PC12 cells were transfected with plasmids encoding EGFP-SPRY2 wild-type, SPRY2 P154A or SPRY2 155-315 mutants and the S-acylation levels associated with these proteins were evaluated. Following incubation of cells with C16:0-azide, the resulting cell lysates were incubated with beads conjugated to GFP antibodies and EGFP-tagged SPRY2 proteins were purified. The corresponding samples were subsequently processed by click chemistry, SDS-PAGE and immunoblotting as described in Chapter 2. Figure 4.10 shows that both SPRY2 P154A and 155-315 mutants were efficiently S-acylated, implying that in PC12 cells these mutants are correctly used as substrates by endogenous zDHHC enzymes.

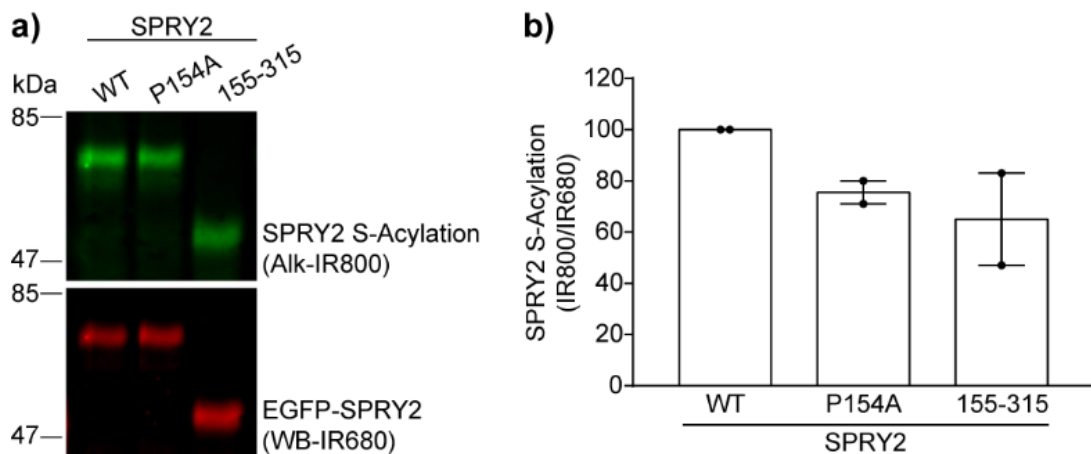


Figure 4.10 SPRY2 P154A and 155-315 mutants are endogenously S-acylated in PC12 cells

PC12 cells were transfected with either EGFP-SPRY2 WT, SPRY2 P154A, or SPRY2 155-315 mutant. Cells were incubated with 100 μ M of palmitic acid azide (C16:0-azide) for 4h. After cell lysis, labelled proteins were incubated 1h (or over-night) with agarose beads conjugated to a GFP antibody and later reacted with alkyne IRdye-800 nm. **a)** Representative images showing SPRY2 S-acylation (*top panel; IR800*) and SPRY2 expression levels (*bottom panel; IR680*) detected on the same immunoblot. The positions of the molecular weight markers are shown on the left side of all immunoblots. **b)** Graph showing mean SPRY2 S-acylation levels after normalisation. Error bars represent \pm SEM; each replicate is shown with filled circles (n=2).

Since both SPRY2 P154A and SPRY2 155-315 were efficiently S-acylated in PC12 cells (Fig. 4.10), we next examined their subcellular distribution by confocal microscopy. To do this, PC12 cells were co-transfected with EGFP-SPRY2 WT, SPRY P154A or SPRY2 155-315 mutants, together with mCherry-SPRY2 WT. In all cases, a fraction of SPRY2 proteins was consistently observed at the plasma membrane of cells (Fig. 4.11a). Furthermore, both EGFP-SPRY2 P154A and SPRY2 155-315 mutants co-localised with co-expressed mCherry-SPRY2 WT both visually and quantitatively, with Pearson's coefficient R_{tot} values close to +1 (i.e. positive linear correlation) (Fig. 4.11b). Thus,

the SPRY domain (plus a few extra amino acids) is *per se* sufficient for both S-acylation and plasma membrane localisation of SPRY2.

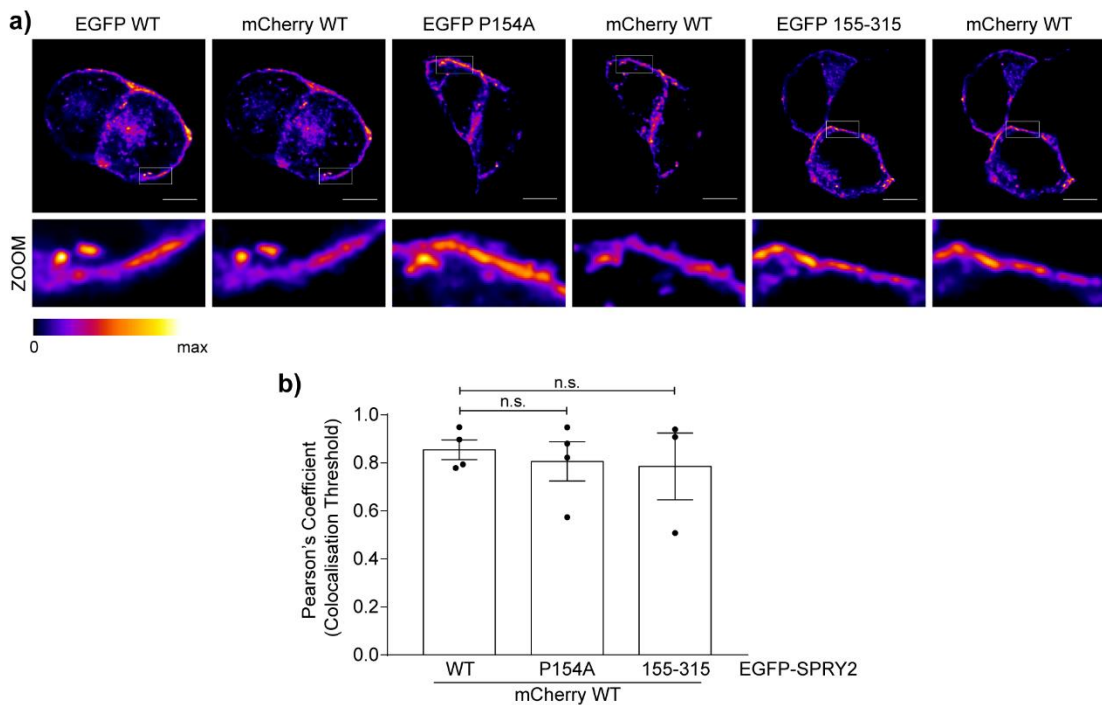


Figure 4.11 Intracellular localisation of SPRY2 P154 and 155-315 mutants in PC12 cells

a) Confocal imaging of PC12 cells co-transfected with plasmids encoding EGFP-SPRY2 WT, P154A, or 155-315 together with mCherry-SPRY2 WT. Representative images for mCherry and EGFP proteins are shown in the figure (*upper panels*) as well as magnified view of the indicated area for both channels (referred to as “ZOOM” in the *bottom panels*). Scale bars represent 5 μ m. **b)** Graph showing Pearson’s correlation coefficient (R_{tot}). Each bar shows mean values of R_{tot} \pm SEM; filled circles represent individual images. Results were analysed by Unpaired t-test (n.s. not significant denotes P > 0.05. SPRY2 WT and SPRY2 P154A, n=4; SPRY2 155-315, n=3).

4.3 Discussion

The importance of the ANK domain of zDHHC17 and zDHHC13 in substrate recognition and binding has been documented for several neuronal substrates, including SNAP25b, CSP α , and HTT (Greaves et al., 2010; Lemonidis et al., 2014; Singaraja et al., 2002). In these proteins, a highly conserved motif, in a cytosolic and unstructured protein region, known as the zDABM, is recognised and bound by the ANK domain of zDHHC17/13 (Lemonidis et al., 2015a). More than 200 proteins, including established substrates, as well as novel interactors, contain a validated zDABM and many more contain potential zDABM sequences (Lemonidis et al., 2017a). Those proteins with validated zDABMs include SPRY2, a tumour suppressor protein and a key regulator of the RTKs involved in cell differentiation, proliferation, and survival (Kim and Bar-Sagi, 2004). The aim of this chapter was to characterise the interaction of SPRY2 with the ANK domain of zDHHC17 and investigate the importance of zDABM sequences for SPRY2 S-acylation.

Based on the data presented in this chapter, there appears to be a second (low affinity) ANK17 binding site in SPRY2 that is linked to S-acylation. In contrast, the zDABM of SPRY2 and the corresponding binding pocket in ANK17 (N100, W130) are dispensable for S-acylation despite the finding that they constitute a major interaction site for these proteins. Where is this second site positioned? The results presented in this chapter do not provide a conclusive answer to this question, although peptide array experiments clearly highlighted the presence of a potential binding site at amino acids 106-120 in SPRY2. However, this observation appears contradictory to the results of truncation analyses of SPRY2, which suggested that residues 155-290 are sufficient for S-acylation by co-expressed zDHHC17 and indeed, a SPRY2 155-315 mutant is efficiently S-acylated by endogenous zDHC enzymes and also trafficked to the plasma membrane in PC12 cells. These data suggest that there may be an additional zDHHC17 binding site within the region 155-290 of SPRY2. In support of this idea, recent work performed by Liam Butler has found that the SPRY2 155-315 mutant co-immunoprecipitates with zDHHC17, albeit at a reduced level compared with wild-type SPRY2 (data not shown). However, peptide array

experiments did not identify an ANK17 binding site within this region of SPRY2. To explain these results we suggest the following possibilities that can be examined further in future work: (i) ANK17 displays a relatively high affinity for the zDABM in SPRY2 and a lower affinity for a site in amino acids 106-120 but neither of these interactions is required for S-acylation; (ii) there is an additional ANK17 binding site in the region 155-290 that is required for S-acylation but this site is either non-linear, and requires amino acids that are brought together within the 3-dimensional structure of SPRY2, or alternatively requires some form of post-translational modification to be recognised by ANK17 (which is missing in peptide array experiments); and (iii) the binding site in the region 155-290 interacts with a region of zDHHC17 outside the ANK domain (although this is inconsistent with the finding that the ANK domain is important for SPRY2 S-acylation). Although the exact modes of binding of SPRY2 to zDHHC17 have not yet been firmly established, the work presented in this chapter clearly suggests that S-acylation of SPRY2 by zDHHC17 involves a different binding mechanism from that previously reported for other zDHHC17 substrates, such as SNAP25b and HTT.

Previous studies on the zDHHC17-SNAP25b complex showed that this interaction specifically occurs between the amino acids 111-120 of SNAP25b and the ankyrin repeats 2 and 3 of zDHHC17. Within these ankyrin repeats, the most critical amino acids were shown to be Asn-100 (N100) and Trp-130 (W130), which contact specific residues in the zDABM of SNAP25b (Verardi et al., 2017). Hydrogen bonds are formed between N100 of the ANK domain of zDHHC17 and the valine at position 113 (V113) of SNAP25b. W130 contacts several residues in SNAP25b *via* favourable Van der Waals forces, and interaction with proline at position 117 (P117) (Verardi et al., 2017). The importance of these residues is highlighted by the fact that alanine-substitution at positions N100 and W130 of the ANK17 impairs SNAP25b and HTT binding and S-acylation (Verardi et al., 2017). Notably, the reported impairment of SNAP25b S-acylation by W130A and N100A mutants was primarily correlated with reduced substrate binding (Verardi et al., 2017). Pull-down assay experiments, in which we employed histidine-tagged versions of the ANK17 WT and ANK17 W130A

mutant, further support the importance of W130 for interaction not only with SNAP25b, but also with SPRY2 and a considerable number of other zDHHC17 interactors. These include the Sprouty-related proteins and key regulators of the RTK signalling SPRED1 and SPRED2; the vesicle trafficking protein CSP α ; HTT which in addition to being the causative of HD, is also a well-established zDHHC17 interacting protein; the cytoskeleton-associated proteins SLAIN1 and EVL-1; the MAPKs JNK1 α 2 and JNK3 α 2, fundamental in many cellular pathways; and the RNA-binding protein PAI-RBP1, which interacts with zDHHC17 through an RP instead of a canonical QP motif. For all of these substrates, the single point mutation W130A in the ANK domain greatly reduced the binding to zDHHC17. Interestingly, the non-S-acylated CSP α (i.e. fast migrating/bottom band) is the only form of the protein that was pulled down by the ANK17 WT, whereas the fully S-acylated form (i.e. slow migrating/upper band) could not be bound at all, this in agreement with a previous observation made by (Lemonidis et al., 2014). Thus, it is possible that substrates that are already S-acylated cannot be recruited or recognised by their specific zDHHC enzymes, perhaps due to conformational changes. On the other hand, strong binding of substrates does not always correlate with high S-acylation efficiency by zDHHC enzymes. For instance, zDHHC13, can strongly bind SNAP25b and CSP α but it is completely inactive towards both proteins (Lemonidis et al., 2014).

While it is clear that specific residues within the ANK domain of zDHHC17 are important for substrate recognition, integrity of zDABM sequences in substrate proteins is likewise a key requirement. Indeed, proline to alanine substitution at position 117 of SNAP25b abolished its binding to and S-acylation by zDHHC17 (Lemonidis et al., 2015a). Similarly, mutation of Val-113 (V113A), or Gln-116 (Q116A) at positions 2 and 5 of the zDABM, respectively, also reduced binding to ANK17 (Verardi et al., 2017). Like SNAP25b, SPRY2 contains a recognised zDABM motif, sufficient for the binding to the ANK domain of zDHHC17 with the key proline residue located at position 154 of the sequence (Lemonidis et al., 2017a). In addition, another three QP dipeptides (none of them recognised as zDABMs) exist at Pro-13, Pro-91, and Pro-96 of SPRY2 sequence. Based on this, we investigated whether the ANK17

binding pocket N100/W130 and the zDABM sequence of SPRY2 were required for efficient S-acylation of SPRY2 protein. To do so, we employed the two zDHHC17 mutants W130A and N100A in which either tryptophan at position 130 or asparagine at position 100 was mutated to alanine. Counterintuitively, both zDHHC17 W130A and zDHHC17 N100A mutants efficiently enhanced SPRY2 S-acylation, suggesting that integrity of the N100/W130 binding pocket in ANK17 is not necessary for S-acylation of this substrate. In agreement with this observation, mutation of either proline at position 154 of the recognised zDABM, or any of the other QP dipeptides, did not perturb SPRY2 S-acylation. Taken together, these data suggest that the interaction between the residues W130 and N100 of the ANK domain of zDHHC17, and the zDABM sequence is not a prerequisite for SPRY2 S-acylation. In contrast, the same zDHHC17 mutants (i.e. W130A and N100A) were found to be inactive towards SNAP25b, in agreement with previously published data (Verardi et al., 2017). Therefore, it is possible that S-acylation of SPRY2 occurs *via* a different mechanism from that previously described for SNAP25b.

Although the N100/W130 binding pocket appears to be dispensable for SPRY2 S-acylation, our initial pulldown experiments suggested that the SPRY2-ANK17 interaction was greatly reduced when Trp-130 is mutated. To confirm that this was the case and that our observation did not arise from the ANK17 W130A behaving anomalously in this set of experiments, we assessed the ability of ANK17 WT to bind SPRY2 QP mutant proteins (i.e. SPRY2 P154A and SPRY2 P13/91/96/154A). While SPRY2 wild-type was efficiently pulled down by ANK17, both SPRY2 mutants in which Pro-154 was mutated displayed reduced interactions. Nonetheless, some residual binding was observed with both SPRY2 QP mutants. Hence, we employed SPRY2 WT and the P154A mutant in immunoprecipitation (IP) experiments to co-immunoprecipitate a full-length catalytically inactive version of zDHHC17 (zDHHA17). Consistent with pull-down assays, mutation of Pro-154 correlated with reduced (but not abolished) binding to zDHHC17. These findings suggest that (i) the characterised zDABM sequence (including Pro-154) represents the major binding site to ANK17, and (ii) an additional, low affinity second binding site(s) might also exist, possibly linked

to S-acylation. In the same set of experiments, it was also evaluated whether the region of SPRY2 encompassing Asn-211 (N211), Asp-214 (D214) and Lys-223 (K223), was involved in binding of zDHHC17. These residues were identified as critical for correct SPRY2 S-acylation and plasma membrane localisation (Chapter 3). As the SPRY2 NDK mutant efficiently bound zDHHC17 in immunoprecipitation experiments, we suggest that this helical region does not participate in SPRY2-zDHHC17 interaction.

Based on the hypothesis that the additional ANK17 binding site in SPRY2 may be linked to S-acylation, we assessed the requirements of the N-terminal domain of the protein as the C-terminal SPRY region (amino acids 177-291) contains features indispensable for zDHHC17-mediated S-acylation, i.e. key cysteines and the NDK motif (Chapter 3). Removal of 100, 120, 140, or 155 amino terminal residues (i.e. SPRY2 100, 120, 140, 155-315 mutants) did not affect the ability of zDHHC17 to modify SPRY2. Likewise, removal of the C-terminal tail of SPRY2 (amino acids 291-315), previously implicated in the binding of proteins such as Grb2 and CIN85 (Haglund et al., 2005; Lao et al., 2006) did not disrupt S-acylation. Therefore, neither the N-terminal domain (i.e. amino acids 1-155) nor region 291-315 at the C-terminus of SPRY2 is required for its S-acylation by zDHHC17. Conversely, residues 155-290 of SPRY2, i.e. the SPRY domain plus a few upstream amino acids, are sufficient for zDHHC17-mediated S-acylation. It is possible that the hydrophobic character of this region (which partly overlaps with the CRD, corresponding to residues 178-301) mediates the association of SPRY2 with the membranes where zDHHC17 normally resides (i.e. *cis*-Golgi compartment), thus contributing to S-acylation. Indeed, the CRD of soluble proteins such as SNAP25b and CSP α has been previously found to be an important requirement for both membrane association and S-acylation of these substrates (Greaves et al., 2009a, 2008; Greaves and Chamberlain, 2006). While region 155-290 is sufficient for zDHHC17-mediated S-acylation of SPRY2, this also required an intact ANK domain in zDHHC17. Indeed, expression of a zDHHC17- Δ NANK17 mutant (i.e. lacking both the N-terminus domain and the seven ankyrin repeat domains) resulted in a loss of SPRY2 S-acylation. Although this suggests that

S-acylation of SPRY2 by zDHHC17 requires recognition by the ANK domain, it is important to note that the introduced deletion could possibly result in severe conformational changes, perturbing not only the overall structure of the enzyme but also its catalytic activity. Likewise, a zDHHC17- Δ C mutant (i.e. lacking the C-terminal domain (zDHHC17- Δ C) was unable to modify SPRY2. This latter observation is in line with another study reporting inactivity of the same mutant against both SNAP25b and CSP α (Lemonidis et al., 2014). More recently, the crystal structure of human zDHHC20 and zebrafish zDHHC15 was solved, revealing that the C-terminal domain is a key supporting structure for both the transmembrane helices and the DHHC catalytic domain of zDHHC enzymes (Rana et al., 2018a). Therefore, it is likely that removal of this domain in the zDHHC17- Δ C mutant leads to a catalytically dead enzyme. In contrast, the N-terminal domain of zDHHC17 is not required for SPRY2 S-acylation as its removal (i.e. zDHHC17- Δ N mutant) does not perturb SPRY2 S-acylation.

Although these observations suggest that the additional ANK17 binding site in SPRY2 may lay within residues 155-290, this was not consistent with the results of peptide binding experiments. Specifically, we adopted a peptide-based approach and screened the entire sequence of human SPRY2 for regions that bound to ANK17. In agreement with our previous observations and those of (Lemonidis et al., 2017a), the characterised zDABM of SPRY2 (corresponding to sequence 149-IIRVQP-154), was found to be the main SPRY2-ANK17 binding site. Also, SPRY2 peptides lacking Ile-149 and Ile-150 (at positions 1 and 2 of the zDBM, respectively) could not be bound by His₆-ANK17, highlighting the importance of these hydrophobic residues. Indeed, hydrophobic residues (particularly valine and isoleucine) are highly conserved within zDABM sequences and crucial for substrates recruitment by the ANK17 (Lemonidis et al., 2017a, 2015a). For instance, in SNAP25b, Val-113 (V113) at position 2 of the zDABM largely interacts with Asn-100 (N100) of the ANK17, and its mutation correlates with reduced binding (Verardi et al., 2017). In addition to the zDABM sequence, we also detected a second potential binding site, spanning from residue 106 to 120 of SPRY2, and corresponding to the sequence 106-PLSRISITVSSGSR-120.

Compared to the zDABM sequence, this second site was recognised more weakly, suggesting a lower affinity of binding, which was consistent with all other binding assays performed in this chapter. Surprisingly, this additional ANK17 binding site is found within the N-terminal domain of the protein and upstream of the zDABM. If this represents a *bona fide* ANK17 binding site in full-length SPRY2, then this second site might also not be required for S-acylation and rather serve other regulatory functions. Nonetheless, we must also consider the possibility that truncation mutants of SPRY2 do not accurately reflect properties of the full-length protein (e.g. they might alter the overall structure of the protein).

Intriguingly, amino acids 106-120, encompass the serine-rich motif (SRM) of SPRY2. Within the SRM, several serine residues, including Ser-112, Ser-115, and Ser-121 have been reported to undergo dynamic phosphorylation and have been linked to SPRY2 stability and activity (DaSilva et al., 2006; Lao et al., 2007). It will be interesting in future work to investigate if the phosphorylation status of some of these residues modulates interaction with ANK17. As a first step, this could be examined by performing additional peptide binding experiments using phospho-mimetic peptides. Indeed, Ser-112/121 have been previously reported to regulate the binding of SPRY2 with other proteins. For example, phosphorylation of both serines prevents SPRY2-B-Raf interaction (Brady et al., 2009). Conversely, binding of SPRY2 to the E3 ubiquitin ligase Nedd4 is promoted by phosphorylation at the very same serine residues, resulting in SPRY2 ubiquitination and subsequent degradation by the proteasome (Edwin et al., 2010). Thus, it was proposed that phosphorylation at Ser-112/121 determines binding to either B-Raf or Nedd4, thereby modulating duration and intensity of MAPK signalling (Edwin et al., 2010). The binding site of B-Raf to SPRY2 was mapped at region 87-139 of SPRY2 (also known as RBD2, Ras binding domain), thus overlapping with the novel ANK17 binding site (amino acids 106-120). However, the different subcellular localisation reported for zDHC17 and B-Raf makes it difficult to imagine that these proteins can compete for binding at this site. The exact binding region of Nedd4 on SPRY2 has not been defined. Also, as S-acylation promotes SPRY2 stability (Chapter 3), it will be interesting to investigate whether S-

acylation interferes with Nedd4-SPRY2 binding, whether phosphorylation at specific amino acids plays a role, and whether an interplay between phosphorylation at the SRM and S-acylation exists.

To examine the S-acylation of SPRY2 mutants without co-expression of zDHHC17, the P154A and 155-315 mutants were transfected into PC12 cells. When the S-acylation levels of SPRY2 were investigated using a “click-on-beads” approach, both SPRY2 P154A and 155-315 mutants were shown to be S-acylated endogenously as efficiently as SPRY2 WT. In line with this, in confocal microscopy the same mutants (i.e. SPRY2 P154A and 155-315) localised at the plasma membrane and within uncharacterised intracellular puncta, similarly to SPRY2 WT and as previously reported by others (Hausott et al., 2019; Impagnatiello et al., 2001; Lim et al., 2000). Also, in Pearson’s correlation analysis EGFP-SPRY2 P154A and 155-315 co-localised with co-expressed mCherry-SPRY2 WT. Thus, despite both SPRY2 P154A and 155-315 are characterised by defects in ANK17 binding (through the zDABM centred at Pro-154), their S-acylation and/or subcellular distribution is not affected. This is in clear contrast to SNAP25, which switches from a plasma membrane to a cytosolic localisation when the zDABM is mutated (Greaves et al., 2010).

In conclusion, the high affinity (zDABM) ANK17 binding site in SPRY2 is dispensable for S-acylation of SPRY2. Importantly, since the SPRY domain (plus a few amino acids) was found to be *per se* sufficient for S-acylation, it will be important in the future to investigate whether additional binding region(s) exist within this domain. On the other hand, it is possible that (i) the hydrophobicity of the SPRY domain, (ii) the presence of favourable cysteine residues, and (iii) an intact NDK motif are the “only” requisites for zDHHC17-mediated S-acylation of SPRY2.

Chapter 5 Homo- and hetero- multimerisation of zDHHC17, the enzyme that modifies SPRY2

5.1 Introduction

Despite recent advances on the structure and function of zDHHC enzymes, there is still little information available on how the activity of these enzymes is regulated (Chamberlain and Shipston, 2015). There is evidence that some zDHHC enzymes can be constitutively regulated by cofactors or other proteins. This is for example the case of zDHHC9 and its yeast homologue Erf2, which require an obligatory cofactor, GCP16 and Erf4, respectively (Swarthout et al., 2005). Erf4 appears to exert two regulatory effects on Erf2: stabilisation of the autoacylated enzyme intermediate and stabilisation of Erf2 protein by preventing its ubiquitination and degradation (Mitchell et al., 2012). GCP16 was also shown to enhance zDHHC9 expression levels (Swarthout et al., 2005) and affect the stability of the autoacylated zDHHC9 intermediate (Mitchell et al., 2014). In addition, the activity of zDHHC6 was suggested to require the cofactor protein Selenoprotein K (Fredericks and Hoffmann, 2015), whereas huntingtin (HTT) was suggested to act as a positive modulator of the zDHHC17 enzyme by affecting its autoacylation status (Huang et al., 2011). It is likely that many other members of the zDHHC family are regulated by co-factor proteins.

In addition to regulatory co-factors, there is also evidence that zDHHC enzymes can be regulated by dynamic changes in their intracellular localisation. For instance, sorting signals in the C-terminus of zDHHC2 dictate its cycling between endosomes and the plasma membrane (Greaves et al., 2011; Salaun et al., 2017). This cycling controls access to the substrate protein post-synaptic density protein 95 (PSD95) which is an important scaffolding protein for AMPA and NMDA receptors at the postsynaptic membranes (Noritake et al., 2009). The plasma membrane localisation of zDHHC5 is controlled by its phosphorylation state, which similarly affects accessibility to substrate proteins including δ -catenin (Brigidi et al., 2015). In this case, dephosphorylation of the tyrosine residue of a tyrosine-based sorting signal

facilitates clathrin-dependent endocytosis, allowing access to endosomally-localised δ -catenin (Brigidi et al., 2015). zDHHC5 has also been shown to undergo degradation following growth factor withdrawal as an additional mean of regulation (Li et al., 2012). Furthermore, the activity, localisation, and stability of zDHHC6 are regulated by dynamic S-acylation of its C-terminal tail by the opposing action of the S-acyltransferase zDHHC16 and the acyl protein thioesterase APT2 (Abrami et al., 2017).

Another suggested regulatory mechanism is *via* changes in the oligomeric state of zDHHC enzymes. Co-immunoprecipitation and cross-linking experiments suggested that the Golgi-localised enzymes zDHHC3 and zDHHC7 form homo- and hetero-multimers in HEK293T cells (Fang et al., 2006). Indeed, bioluminescence resonance energy transfer (BRET) and native gel electrophoresis experiments reported homo-multimer formation not only for zDHHC3 but also for zDHHC2 (Lai and Linder, 2013). For both of these enzymes, monomers and dimers were the major protein species detected rather than larger oligomeric complexes. Furthermore, the active state of these enzymes was suggested to correspond with the monomeric form and the inactive state with the oligomeric form. Thus, a potential monomer-dimer equilibrium was suggested to regulate zDHHC activity (Lai and Linder, 2013). However, the mechanisms controlling zDHHC enzyme multimerisation are not clear.

In this chapter, we investigated if the enzyme that regulates SPRY2 S-acylation, zDHHC17 also undergoes multimerisation. In particular, we investigated the role of the ANK domain, which is critical for substrate recognition and recruitment, in homo- and/or hetero- oligomerisation of zDHHC17 using a combination of pull-down experiments with purified proteins and cell-based co-immunoprecipitation assays.

5.2 Results

5.2.1 The ANK domain of zDHHC17 interacts with zDHHC17 and zDHHC13

As a first step in investigating potential oligomerisation of zDHHC17, we sought to determine if the ANK domain of zDHHC17 (ANK17) could mediate interactions with full-length zDHHC17 and with other Golgi-localised enzymes, including zDHHC13, zDHHC7, and zDHHC3. Both zDHHC7 and zDHHC3, localise at the *cis*-Golgi compartment with zDHHC17 and zDHHC13 (Ernst et al., 2018) and lack an ANK domain.

HA-tagged versions of zDHHC17, zDHHC13, zDHHC7, and zDHHC3 were expressed in HEK293T cells. The corresponding lysates were then incubated with His₆-ANK17 or PBS (negative control) to investigate whether they were able to interact with this region of zDHHC17. As shown in Figure 5.1, the ANK domain of zDHHC17 efficiently pulled down both HA-tagged zDHHC17 and zDHHC13. In contrast, binding to zDHHC7 and zDHHC3 was minimal, suggesting that the observed interaction of zDHHC17/zDHHC13 with ANK17 is specific.

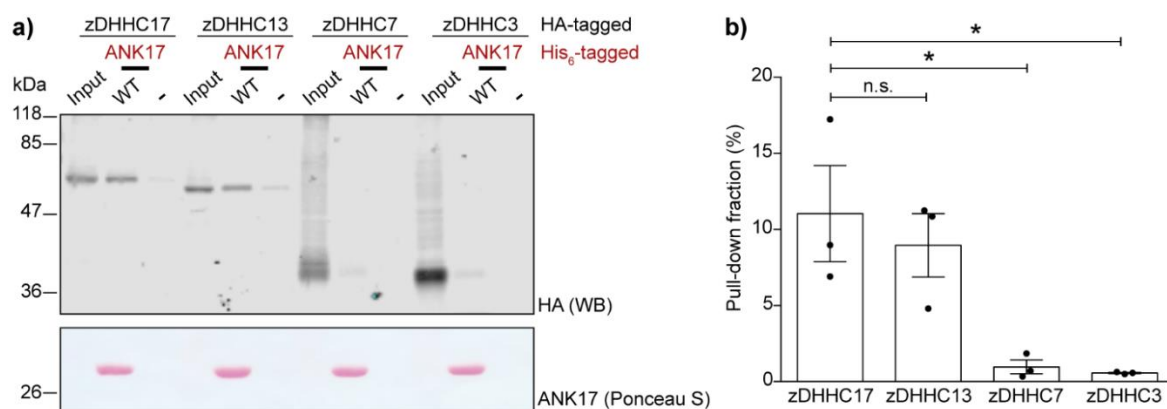


Figure 5.1 zDHC17 and zDHC13 bind to the ANK domain of zDHC17

a) Representative image of pull-down experiments. HA-tagged zDHC17, zDHC13, zDHC7, and zDHC3 were expressed in HEK293T cells, and the corresponding lysates were incubated with His₆-ANK17 (the ANK domain encompassed amino acid 54-288 of zDHC17) and captured on Ni²⁺-NTA agarose beads. The negative control samples (referred to as “-” in the figure) indicate where substrate proteins were incubated with Ni²⁺-NTA agarose beads in the absence of His₆-ANK17. 7.5% of the total input and 30% of the total bound fraction were run on 12% polyacrylamide gels and resolved by SDS-PAGE. After transfer to nitrocellulose, the membranes were stained by Ponceau S solution and probed with a HA antibody. The positions of molecular weight markers are shown on the left side of all immunoblots. **b)** Graph showing mean values of fractions pulled down by His₆-ANK17. Immunoblotting signals for bound proteins were normalised against the corresponding input signals. Error bars represent ± SEM; each replicate is shown with filled circles. Differences were analysed by one-way ANOVA (* denotes P < 0.05, n.s. not significant, n=3).

5.2.2 zDHHC17 interaction with the ANK domain reflects ANK-ANK interaction

As zDHHC17 and zDHHC13 both contain an ANK domain, the observed selective interactions of these enzymes with His₆-ANK17 (Fig. 5.1) highlight potential ANK domain homo- and hetero-dimerisation. To test this hypothesis, we investigated the interaction of a series of zDHHC17 truncation mutants with His₆-ANK17. A schematic representation of these constructs is provided in Figure 5.2a.

HA-tagged zDHHC17-ΔN, which lacks the N-terminus upstream of the ANK domain (construct encodes amino acids 54-632), zDHHC17-ΔNANK17, which lacks the N-terminus and ANK domain (construct encodes amino acids 287-632), and zDHHC17-ΔC, which lacks the cytosolic C-terminal region downstream of the sixth transmembrane domain (construct encodes amino acids 11-569) were used to transfect HEK293T cells. The corresponding lysates were incubated with His₆-ANK17 or PBS (negative control) and their capture on Ni²⁺-NTA resin was examined. Figure 5.2b and 5.2c show that both the N-terminal and C-terminal truncated versions of zDHHC17 (i.e. zDHHC17-ΔN and zDHHC17-ΔC) were pulled down by His₆-ANK17 as efficiently as the full-length zDHHC17. However, interaction with His₆-ANK17 was substantially reduced when the ankyrin repeat domain was removed (i.e. for zDHHC17-ΔNANK17), suggesting that the ANK domain undergoes self-association.

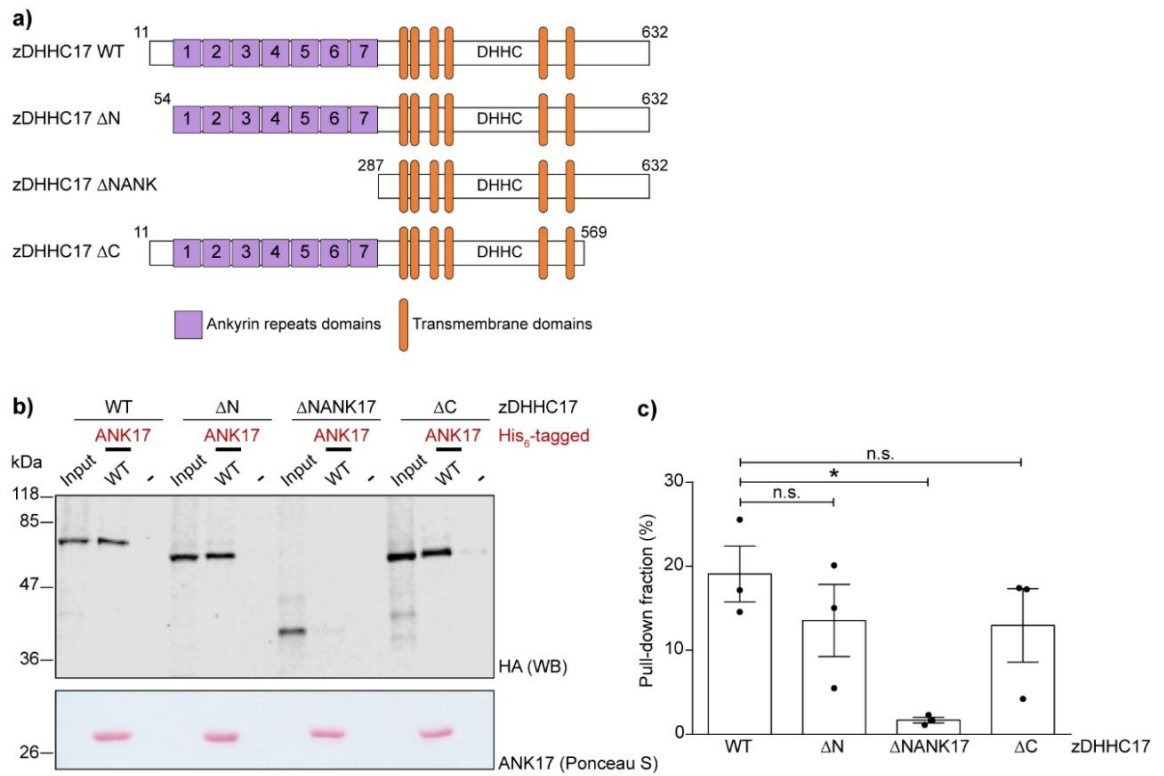


Figure 5.2 ANK17 displays a loss of interaction with a zDHHC17 mutant lacking the ANK domain

a) Schematic representation of the zDHHC17 mutants used in the experiments. **b)** Representative image of pull-down experiments. HA-tagged zDHHC17 full-length, zDHHC17-ΔN, zDHHC17-ΔNANK17, and zDHHC17-ΔC constructs were expressed in HEK293T cells. The corresponding lysates were incubated with His₆-ANK17 (the ANK domain encompassed amino acid 54-288 of zDHHC17) and captured on Ni²⁺-NTA agarose beads. The negative control samples (referred to as “-” in the figure) indicate where substrate proteins were incubated with Ni²⁺-NTA agarose beads in the absence of His₆-ANK17. 7.5% of the total input and 30% of the total bound fraction were run on 12% polyacrylamide gels and resolved by SDS-PAGE. After transfer to nitrocellulose, the membranes were stained by Ponceau S solution and probed with a HA antibody. The positions of molecular weight markers are shown on the left side of all immunoblots. **c)** Graph showing mean values of fractions pulled down by His₆-ANK17. Immunoblotting signals for bound protein were normalised against the corresponding Input signals. Error bars represent ± SEM; each replicate is shown with filled circles. Differences were analysed by one-way ANOVA (* denotes P < 0.05, n.s. not significant, n=3).

5.2.3 Self-association of the ANK domain of zDHHC17 requires the substrate binding pocket (Asn-100 and Trp-130)

The findings above highlight the importance of the ANK domain in dimerisation of zDHHC17. Previous work has shown the importance of this domain in mediating substrate recruitment to zDHHC17 (Lemonidis et al., 2017a; Verardi et al., 2017). In particular, Asn-100 (N100) and Trp-130 (W130) in the second and third ankyrin repeats were reported as being crucial for binding and S-acylation of SNAP25b and HTT (Verardi et al., 2017). In Chapter 4, we further showed that Trp-130 (W130) is also essential for efficient recruitment of many other substrates and interactors of zDHHC17, including SPRY2, SPRED and JNK3 proteins. As N100 and W130 form key interactions with multiple substrates of zDHHC17, we investigated if this binding pocket was also involved in the observed ANK-ANK interaction (Fig. 5.2). To do so, zDHHC17 W130A and zDHHC17 N100A mutants were employed in pull-down experiments and their ability to bind the purified ANK17 domain was compared with wild-type zDHHC17.

HEK293T cells were transfected with zDHHC17 WT, zDHHC17 W130A, or zDHHC17 N100A, and the corresponding lysates were incubated with His₆-ANK17 or PBS (negative control) and their capture on Ni²⁺-NTA resin examined. As shown in Figure 5.3, zDHHC17 W130A and zDHHC17 N100A mutants bound substantially less His₆-ANK17 than wild-type zDHHC17 did. However, residual binding could still be observed for both of these mutants suggesting either that other residues contribute to ANK dimerisation or that an intact N100/W130 binding pocket on one ANK domain (i.e. the purified ANK17) is sufficient to mediate a low level of dimerisation. This result is particularly interesting as if the same binding pocket is used for substrate binding and self-association, it is plausible that homo- or hetero- multimeric forms of the enzyme correspond to an inactive state, as previously suggested by others (Lai and Linder, 2013).

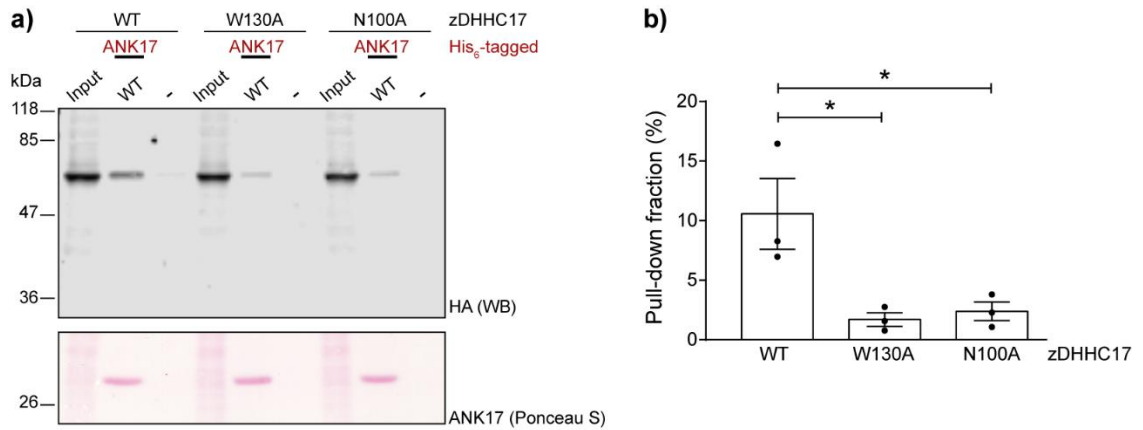


Figure 5.3 The N100/W130 binding pocket in the ANK domain is important for zDHHC17 homo-dimerisation

a) Representative image of pull-down experiments. HA-tagged zDHHC17 WT, zDHHC17 W130A, and zDHHC17 N100A were expressed in HEK293T cells. The corresponding lysates were incubated with His₆-ANK17 (the ANK domain encompassed amino acid 51-288 of zDHHC17) and captured on Ni²⁺-NTA agarose beads. The negative control samples (referred to as “-” in the figure) indicate where substrate proteins were incubated with Ni²⁺-NTA agarose beads in the absence of His₆-ANK17. 7.5% of the total input and 30% of the total bound fraction were run on 12% polyacrylamide gels and resolved by SDS-PAGE. After transfer to nitrocellulose, the membranes were stained by Ponceau S solution and probed with a HA antibody. The positions of molecular weight markers are shown on the left side of all immunoblots. **b)** Graph showing mean values of fractions pulled down by His₆-ANK17. Immunoblotting signals for bound protein were normalised against the corresponding Input signals. Error bars represent ± SEM; each replicate is shown with filled circles. Differences were analysed by one-way ANOVA (* denotes P < 0.05, n=3).

5.2.4 Co-immunoprecipitation experiments suggest a second mode of zDHHC17 self-association

zDHHC17 is a polytopic membrane protein and it was important to also study possible multimerisation of the full-length enzyme in cells. Therefore, to determine the importance of the ANK domain for homo- dimerisation of zDHHC17 in a cellular environment, we employed immunoprecipitation experiments (IP) in HEK293T cells. The ability of zDHHC17- Δ NANK17 and zDHHC17 W130A to bind full-length zDHHC17 was assessed using this approach. As shown above, zDHHC17- Δ NANK17 and zDHHC17 W130A both displayed reduced ANK17 binding in pull-down assays (Fig. 5.2 and 5.3).

Therefore, cells were transfected with either these plasmids or wild-type HA-zDHHC17, together with plasmids encoding either EGFP or EGFP-zDHHC17 wild-type. The corresponding lysates were incubated with beads conjugated to a GFP antibody and the amount of co-immunoprecipitated HA-zDHHC17 proteins was revealed by immunoblotting. Immunoprecipitation of EGFP-zDHHC17 WT (but not EGFP) resulted in efficient co-immunoprecipitation not only of HA-tagged zDHHC17 WT but also of zDHHC17- Δ NANK17 and zDHHC17 W130A mutants (Fig. 5.4). Furthermore, the level of co-IP was the same for all proteins, suggesting that besides ANK domains interaction, other domains/regions can mediate zDHHC17 self-association in cells.

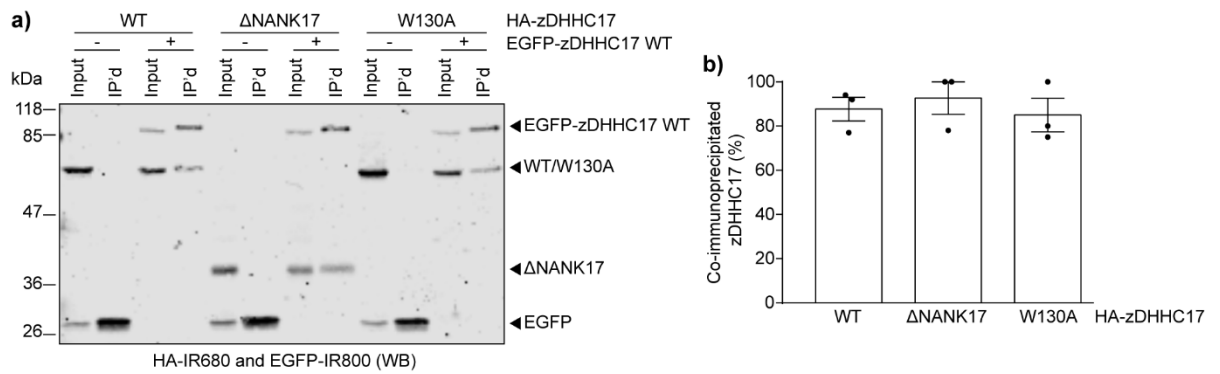


Figure 5.4 zDHHc17 self-association in cells does not require ANK domain dimerisation

a) HEK293T cells were transfected with plasmids encoding EGFP (control, referred to as “-” in the figure) or EGFP-tagged zDHHc17 WT (referred to as “+” in the figure) together with HA-tagged zDHHc17 WT, zDHHc17 ΔNANK17, or zDHHc17 W130A. Cell lysates were incubated with agarose beads conjugated to a GFP antibody. Bound proteins were collected, run on 10% polyacrylamide gels and resolved by SDS-PAGE. After transfer to nitrocellulose, membranes were probed with a GFP antibody to reveal EGFP and zDHHc17 WT (IR800) and with a HA antibody to reveal zDHHc17 (IR680). Protein levels of expression in each sample before immunoprecipitation experiments are shown (lane referred to as “Input” in the figure). Immunoprecipitated EGFP or EGFP-zDHHc17 proteins (IP’d) and co-immunoprecipitated zDHHc17 WT and mutants (Co-IP’d) (lane referred to as “IP’d” in the figure). The positions of molecular weight markers are shown on the left side of all immunoblots. **b)** Graph showing mean HA-zDHHc17 co-immunoprecipitated by EGFP-zDHHc17 WT, calculated as the ratio between HA and GFP signals (IR680/IR800) in the immunoprecipitated (IP’d) samples (IP’d lanes). Error bars represent ± SEM; each replicate is shown with filled circles. Differences were analysed by one-way ANOVA and found not different ($P > 0.05$, $n=3$).

5.3 Discussion

Multiple and different mechanisms have been reported and proposed to modulate zDHHC enzyme activity, including changes in their oligomeric state (Lai and Linder, 2013). Homo-multimerisation and hetero-multimerisation phenomena have been described for the Golgi-localised zDHHC7 and zDHHC3 (Fang et al., 2006) and for zDHHC2, which is found in recycling endosomes and at the plasma membrane of cells (Lai and Linder, 2013). In the study of Lai and Linder (2013), bioluminescence energy transfer (BRET), co-immunoprecipitation and blue native gel experiments were used to show that catalytic inactive versions of zDHHC2 (i.e. zDHHS2) and zDHHC3 (i.e. zDHHS3) self-associated more than the corresponding wild-type pairs suggesting that oligomers correspond to inactive enzymatic forms. In the same study, synthetic zDHHC2 and zDHHC3 dimers (that could be reversed into monomers) were found less active than the corresponding monomers, further supporting that the activity of these S-acyltransferases is regulated by their oligomeric status (Lai and Linder, 2013). These experiments used reversible cross-linking of recombinant purified zDHHC2 and zDHHC3 tandem dimers (separated by a thrombin cleavage site) in *in vitro* S-acylation assays to study dimers *versus* monomers relative activity. Understanding whether oligomerisation of zDHHC enzymes is a common feature, whether this mechanism could represent an extra level of regulation of their catalytic activity, and whether monomeric and di- or multimeric forms can bind different pools of substrates is a fundamental question in the S-acylation field. Based on this, in the present chapter, we interrogated whether the ankyrin repeat (ANK) domain of zDHHC17, crucial for substrate recognition and binding, can mediate oligomerisation of zDHHC17 with other Golgi-localised zDHHC enzymes.

The majority of S-acyltransferases are found at the Golgi apparatus and the endoplasmic reticulum (ER) (Ohno et al., 2006). zDHHC17 principally resides at the *cis*-Golgi membranes with other zDHHC family members including zDHHC13, zDHHC7, and zDHHC3 (Ernst et al., 2018). Based on this, we tested the ability of the ANK domain of zDHHC17 to bind these other zDHHC isoforms, as well as zDHHC17 itself. Lysates from HEK293T cells, transfected with plasmids encoding for zDHHC17,

zDHHC13, zDHHC7, and zDHHC3 were used in pull-down assays using a purified His₆-ANK17 protein. While the ANK domain of zDHHC17 could efficiently recognise and bind zDHHC17 itself and zDHHC13, only a minor amount of both zDHHC7 and zDHHC3 was pulled down. Together with zDHHC17, zDHHC13 is the only other S-acyltransferase characterised by an N-terminal ANK domain, suggesting that the observed homo- and hetero- dimerisation could be mediated by the ankyrin repeat domains of these isoforms.

To give body to this hypothesis, we further mapped the zDHHC17 region involved in its self-interaction employing a series of mutated versions of the enzyme. These included: (i) zDHHC17-ΔN, lacking the N-terminus, and encoding residues 54-632 (ii) zDHHC17-ΔNANK17, lacking the N-terminus and the ANK domain, and encoding residues 287-632 (iii) zDHHC17-ΔC, lacking the cytosolic C-terminal region downstream of the sixth transmembrane domain and encoding residues 11-569. In pull-down experiments using purified ANK17 as bait, the obtained evidence strongly suggested that interaction with zDHHC17 in cell lysates was mediated by ANK domain dimerisation. In fact, deletions of the -NH₂ or -COOH terminus did not affect the amount of zDHHC17 pulled down by His₆-ANK17 underlining that these domains are not interacting with the ANK domain. In contrast, when the construct lacking the ANK domain was expressed, the amount of captured zDHHC17 dropped drastically to levels next to the zero. Taken together, these results support that the observed self-association of zDHHC17 reflects the interaction between ANK domains rather than the interaction of this domain with other protein regions.

The importance of the ANK domain of zDHHC17/zDHHC13 as a recruitment module for substrate proteins was highlighted for the first time by studies conducted on Huntingtin protein (HTT) and its interaction with zDHHC17 (Huang et al., 2011). Subsequent research has shown that zDHHC17 and zDHHC13 recognise, *via* their ANK domain, specific zDHHC-ANK domain-binding motif (i.e. zDABM) sequences in several protein substrates (Lemonidis et al., 2017a). These motifs need to be present in unstructured regions of a protein (Lemonidis et al., 2015a). Recently, Verardi and colleagues solved a high-resolution crystal structure of zDHHC17 ankyrin repeat

domain in complex with a fragment peptide of SNAP25b (residues 111-120) containing the zDABM. Following this, the amino acids Trp-130 (W130) and Asn-100 (N100) within the ANK domain were established as critically important for SNAP25b recruitment and binding. The tryptophan at position 130 was pointed out as critical in establishing favourable interactions with the Pro-117 of SNAP25b (belonging to the dipeptide QP of the zDABM motif), whereas the asparagine at position 100 establishes hydrogen-bond (H-bond) with Val-113 (V113, also belonging to the zDABM sequence). Amino acid substitutions of either W130 or N100 to alanine completely abolished the ability of zDHHC17 to bind not only SNAP25b but also HTT, highlighting the importance of these residues and the binding pocket N100/W130 in substrate recruitment (Verardi et al., 2017). In addition, in Chapter 4, we showed that Trp-130 (W130) is important not only for binding of SNAP25b and HTT, but also of several other zDHHC17 interactors including vesicle trafficking and cytoskeleton-associated proteins, RTKs regulators, Ser/Thr protein kinases, and RNA-binding proteins.

Based on this, the importance of the binding pocket N100/W130 was investigated in the context of oligomerisation. zDHHC17 mutants, in which either tryptophan at position 130 or asparagine at position 100 were alanine-substituted (i.e. zDHHC17 W130A and N100A, respectively) were tested for binding to His₆-ANK17 in pull-down experiments. Interestingly, the amount of both zDHHC17 W130A and zDHHC17 N100A mutants captured by ANK17 was found to be significantly reduced compared to that of wild-type zDHHC17. This implies that the binding pocket N100/W130, important for substrate recognition and binding, is also important for zDHHC17 oligomerisation. Thus, a mechanism of mutual exclusion might exist between molecules of substrate and molecules of enzyme that tend to “occupy” the same binding site. Homo- and hetero- oligomerisation of zDHHC17 might then reflect inactive states of the enzyme in which the ANK domain, engaged in ANK-ANK interactions, is not accessible to substrate proteins. On the other hand, monomeric zDHHC17 would be free to engage in substrate interaction and S-acylation. In this regard, it is interesting to note that the study of Lai and Linder (2013) on zDHHC2 and

zDHHC3 suggested that a monomer-dimer equilibrium for zDHHC enzymes might exist in cells with monomers being the active forms of the enzymes and di-/oligomers the inactive. Although dimerisation might be mutually exclusive with substrate binding, it is also important to note that substrate binding could still occur for dimers if the N100/W130 pocket on one of the monomers is free for substrate engagement.

If the N100/W130 pocket does mediate ANK-ANK domain interaction, then it will be challenging to dissect the importance of dimerisation for enzyme activity using a mutational strategy (as mutations will block both substrate interaction and dimerisation). Nevertheless, it is interesting to speculate on the findings presented in Chapter 4. Here, we showed for SPRY2, which does not require the N100/W130 pocket for S-acylation by zDHHC17, that W130A and N100A mutants were fully active in co-expression S-acylation assays. Interestingly, there was a slight increase in SPRY2 S-acylation with these mutants, perhaps hinting that interfering with dimerisation can enhance enzyme activity. However, the evidence at this stage is weak and will require more rigorous assessments.

To further analyse the importance of ANK-ANK interaction and the binding pocket N100/W130 in mediating zDHHC17 self-association in a cellular context, immunoprecipitation (IP) experiments were carried out. A full-length and EGFP-tagged version of zDHHC17 was used to Co-IP HA-tagged zDHHC17 wild-type, zDHHC17- Δ NANK17, or zDHHC17 W130A mutant. Surprisingly, neither removal of the ANK domain (i.e. zDHHC17- Δ NANK17) nor mutation of Trp-130 (i.e. zDHHC17 W130A) impaired or reduced binding to full-length zDHHC17, compared to WT-WT interaction. Therefore, while ANK-ANK interaction can mediate zDHHC17 self-association, there may be additional modes of multimerisation in cells. It is interesting to speculate that zDHHC17 might exist primarily in a stable dimeric/oligomeric state and that fluctuations in ANK domain interactions could represent a mechanism to regulate substrate recruitment. For other proteins, such as SPRY2 for which integrity of the same binding pocket (i.e. N100/W130) is not required for S-acylation, dimerisation might have a different outcome (Chapter 4). Nonetheless, further analysis will be required to shed light on both the molecular

mechanisms and physiological consequences of zDHHC17 dimerisation. Furthermore, the combination of zDHHC17 interactions mediated by different regions of the enzyme could contribute to the formation of larger oligomeric complexes.

ANK domain dimerisation was recently reported by Kozlov and colleagues (2018) for the *Legionella pneumophila* protein AnkC (LegA12). The crystal structure of this protein reveals that two AnkC molecules, each characterised by seven ankyrin repeats, form symmetric and continuous dimers using their ankyrin repeats 2-6 as well as multiple surface contacts mediated by the outer hairpin loops of the ankyrin repeats. Importantly, such dimerisation interface runs along the back of the ankyrin grooves (i.e. binding pockets) and it does not interfere with the binding of target proteins (Kozlov et al., 2018). The dependence observed on W130 and N100 for ANK17 dimerisation implies that the mechanism of self-association of the ANK domain of zDHHC17 is distinct from that seen with AnkC.

What regions of zDHHC17 might mediate self-association in the absence of the ANK domain (as seen in co-immunoprecipitation experiments in Fig. 5.4)? Transmembrane domains (TMDs) have been reported to mediate homo-dimerisation of the *E. Coli* proton symporter UraA (corresponding to the SLC23 family in human) (Yu et al., 2017) and of the solute carrier family 26 in *Deinococcus geothermalis* (SLC26Dg, corresponding to the SLC26 family in human) (Chang et al., 2019). Crystal structures of these polytopic proteins (14 TMDs) have been solved and their dimerisation interfaces finely described. In UraA, on each monomer hydrophobic residues in several TMDs (i.e. TMD 5, 12, and 13) contribute to dimerisation (Yu et al., 2017). In contrast, the dimer interface in SLC26Dg is centred around a single TMD (TMD14) (Chang et al., 2019). Interestingly, UraA and SLC26Dg dimers were described as the catalytically active forms of the protein (Chang et al., 2019; Yu et al., 2017).

Analysis of transmembrane domains (TMDs) association in multipass proteins is still challenging, albeit several studies have highlighted general features important for helix-helix self-assembly (Cymer et al., 2012; Sal-Man et al., 2014; Sparr et al., 2005).

Studies on model membranes found that within the phospholipid bilayer TMDs associate preferentially using antiparallel α -helices (Sparr et al., 2005). The interactions with surrounding lipids are also important: hydrophobic mismatch has been suggested to promote helix-helix dimerisation (e.g. increase/decrease of membrane thickness or increase in cholesterol content) (Cymer et al., 2012; Sparr et al., 2005). The surface complementarity of the interacting helices and the presence of specific patterns, including the GxxxG motif and variations of it (Cymer et al., 2012) also play a role. Moreover, the presence of proline at the dimerisation interface has been suggested to stabilise TMD-TMD self-assembly despite proline being a helix breaker in solution (Sal-Man et al., 2014). It will be interesting to explore the possible role of each TMD of zDHHC17 in regulating self-association, and an initial step to examine this could be to perform TMD swapping experiments with other Golgi-localised zDHHC enzymes.

In the context of zDHHC enzymes, oligomerisation through transmembrane domains (TMDs) would allow a great degree of freedom in terms of possible combinations. zDHHC enzymes with little sequence similarity would be able to dimerise as it has been for instance previously reported for zDHHC3 and zDHHC7 hetero- dimerisation (Fang et al., 2006). Thus, it will be interesting to test this hypothesis perhaps using zDHHC versions in which the only means for dimerisation is represented by the transmembrane domains (e.g. zDHHC enzymes lacking both the N- and C-terminus ends). The ability to homo- or hetero- dimerise could then be tested for different zDHHC pairs using co-immunoprecipitation assays as well as techniques suitable for live-cell analysis such as bioluminescence resonance energy transfer (BRET) or fluorescence resonance energy transfer (FRET). It will also be important to analyse the amino acid sequence of zDHHC enzymes with particular regard to sequence similarities, or motifs reported as important for TMD self-association (e.g. proline at the membrane interface and GxxxG motifs) and whether they are found at the membrane-cytosol interface where they could favour such interactions.

Chapter 6 Final Discussion

Although S-acylation of SPRY1 and SPRY2 was first reported twenty years ago (Impagnatiello et al., 2001), to-date there has not been any comprehensive study investigating the cellular and/or physiological consequences of this post-translational modification (PTM) in this family of proteins. Likewise, the specific zDHHC enzymes involved in this process and how S-acylation is determined is not clear. This study represents the first in depth analysis of the mechanisms and outcomes of SPRY2 S-acylation and also identifies candidate zDHHC enzymes involved in this process. SPRY2 deregulation has been linked to a number of malignancies, developmental disorders as well as neurological diseases (Hausott and Klimaschewski, 2019; Kawazoe and Taniguchi, 2019; Masoumi-Moghaddam et al., 2014), and therefore generating a more comprehensive understanding of the molecular mechanisms regulating the cellular functions of this protein is important to develop new therapies and to improve the efficacy of already existing treatments. Collectively, the data presented in this thesis suggest that S-acylation may be a key requirement for SPRY2 function and therefore provides an important basis for future work.

The results presented in this thesis are schematically summarised in Figure 6.1.

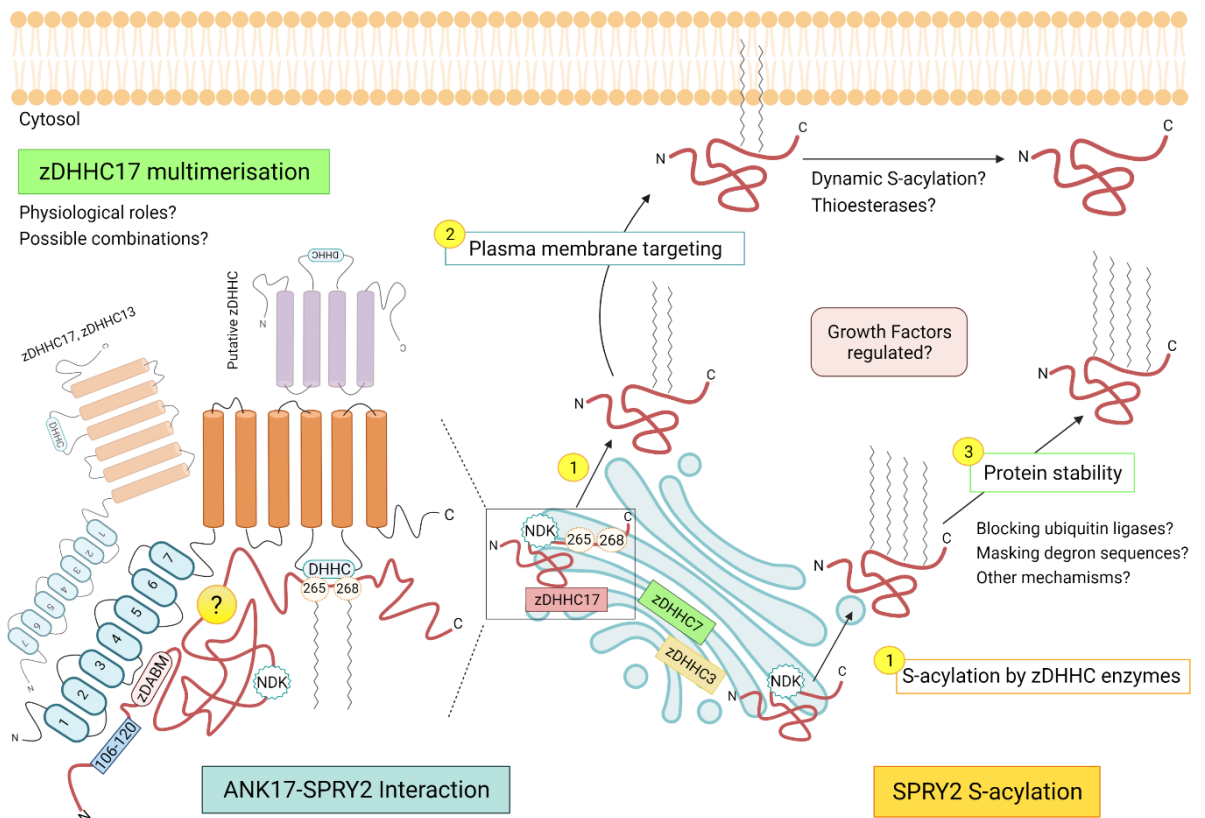


Figure 6.1 Main findings of this study and key outstanding questions

SPRY2 S-acylation: SPRY2 is the substrate of different S-acyltransferases, including zDHC17, zDHC7 and zDHC3 (*step 1*). Key features required for S-acylation are also depicted (i.e. C265/268 and NDK). Following S-acylation, SPRY2 can associate with the plasma membrane (*step 2*). S-acylation also increases SPRY2 stability (*step 3*) via unknown pathways. *Schematic of ANK17-SPRY2 interaction:* SPRY2 interacts with ANK17 primarily via the zDABM centred at P154 (*pink oval*). Also, there may be further binding sites at region 106-120 (*blue rectangle*) and within amino acids 155-290 (*yellow question mark*). The region of ANK17 that interacts with these additional binding sites is not known. *zDHC17 multimerisation:* interacting zDHC enzymes are depicted in light colours. zDHC17 homo- or hetero- dimerisation via ANK-ANK interaction is represented on the left (*both have orange TMDs and blue ANK domains*). On the top, a putative TMD-TMD interaction with another zDHC enzyme is also shown (*purple*). Some of the key outstanding questions that arose from this study are also included in the figure. Created with BioRender.com.

Click chemistry experiments revealed that SPRY2 is differentially S-acylated by zDHHC17, zDHHC7 and zDHHC3. Specifically, zDHHC17 targeted Cys-265/268, whereas zDHHC7 and zDHHC3 mediated more extensive S-acylation of the cysteine-rich domain (CRD). While this finding is in line with the previously reported low activity of zDHHC17, compared to the more promiscuous zDHHC7 and zDHHC3 (Lemonidis et al., 2014) in future studies it will be important to investigate the dynamics of S-acylation for both exogenous and endogenous SPRY2. This could use pulse-chase analyses in which cells are initially pulsed with palmitic acid analogues (e.g. palmitic acid azide/alkyne) and subsequently incubated (“chased”) with an excess of unlabelled palmitic acid for a range of different times. Beside this, the effect of several growth factors (e.g. FGF2, NGF, EGF) on S-acylation turnover should also be studied. If SPRY2 S-acylation is shown to be dynamically regulated, it will be of interest to determine whether turnover occurs on all cysteines or only on a defined subset. Acyl-PEG switch analyses, in which S-acylation of single cysteines can be measured as a mobility shift on SDS-PAGE could be used in combination with pulse-chase experiments to generate information on the number of cysteines undergoing dynamic S-acylation.

S-acylation of SPRY2 (by both zDHHC17 and zDHHC7) required the presence of non-cysteine residues, such as Asp-214 (N214), Lys-223 (K223), and to a lesser extent Asn-211 (N211), referred to as the “NDK motif”. This motif was found to be conserved across a number of species and to lay within a region predicted to fold into an α -helix where the negatively charged D214 orientated opposite to the positively charged K223. However, it is not clear how the NDK motif participates in the S-acylation process. Although the charged Asp-214 and Lys-223 may play a role in ensuring efficient membrane association of SPRY2 prior to S-acylation, in PC12 cells a SPRY2 NDK mutant was still tightly membrane-associated. Nevertheless, it could be valuable to explore whether the NDK motif mediates interaction of SPRY2 with specific intracellular membrane compartments and/or known S-acylation hot-spots (e.g. *cis*/*trans*-Golgi, ER membranes). Overall, the identification of SPRY2 S-acylation-deficient mutants (i.e. C265/268A and NDK) could help the identification of proteins

that interact with only the S-acylated form of SPRY2 as we currently lack any insight into how protein-protein interactions are affected by this modification. Perhaps S-acylation-dependent protein interactions are linked to the effects of S-acylation on plasma membrane targeting of SPRY2. One approach could employ immunoprecipitation experiments with mass-spectrometry analysis to identify proteins that differentially bind SPRY2 WT *versus* C265/268A and/or NDK mutants.

S-acylation also promoted SPRY2 stability and indeed, reduced protein levels were observed when S-acylation was blocked, for example, by mutating zDHHC17 (i.e. zDHHA17 mutant) or SPRY2 (i.e. C265/268A and NDK mutants). Also, stabilisation occurred independently of Tyr-55 phosphorylation, and thus the E3 ubiquitin ligase c-Cbl, which interacts with phospho-Tyr-55 (Fong et al., 2003). Further analyses are required to pinpoint the exact pathways by which S-acylation affects SPRY2 stability/degradation. This could be initially done by mutating sites linked to SPRY2 ubiquitination (e.g. Lys-313) and analysing how this affects expression levels of the resulting mutants. Apart from this, it could be examined whether S-acylation interferes with the action of other ubiquitin ligases that act *via* pathways independent of phospho-Y55 (e.g. Nedd4 and Siah2). It could be evaluated whether the binding of SPRY2 WT or S-acylation-deficient mutants (i.e. C265/268A and NDK) with Nedd4/Siah2 is enhanced and also whether these SPRY2 mutants show enhanced ubiquitination compared to wild-type protein. It would also be important to analyse the N- and the C-terminus of SPRY2 for the presence of degron sequences which may be masked following S-acylation, thus preventing SPRY2 degradation. Furthermore, since SPRY2 is functionally down-regulated in several tumours (Kawazoe and Taniguchi, 2019; Masoumi-Moghaddam et al., 2014), it will be of interest to investigate the S-acylation levels associated with SPRY2 in specific cancer cell lines. This could include prostate cancer cells (e.g. LNCaP, PC-3M, PC-3MLN4 and PC-3MPRO4) and glioblastoma cells (U251, U118MG, and U87MG) in which SPRY2 expression has been previously reported to be decreased (McKie et al., 2005) and increased (Walsh et al., 2015), respectively. If a correlation is found, targeting S-

acylation could provide the basis for the development of new treatments that aim to restore normal SPRY2 levels in these types of cancer.

As briefly mentioned above, fractionation experiments revealed that SPRY2 is tightly associated with cellular membranes regardless of S-acylation. Intriguingly, both C265/268A and NDK mutants displayed a different electrophoretic mobility compared to wild-type SPRY2. The electrophoretic mobility of SPRY2 is influenced by the phosphorylation status of specific serine and threonine residues (Brady et al., 2009; Impagnatiello et al., 2001). While this observation may suggest an interplay between S-acylation and phosphorylation, further evidence is required to support this hypothesis, and indeed to rule out that the change in mobility is more directly linked to S-acylation of the proteins. It could be useful to initially evaluate the S-acylation levels of specific phospho-null as well as phospho-mimetic versions of SPRY2 (e.g. S111A/D, S120A/D) in click chemistry assays.

Confocal analysis in PC12 cells revealed that S-acylation regulated plasma membrane targeting of SPRY2. A fraction of the wild-type protein was consistently observed at the plasma membrane, whereas both S-acylation deficient mutants (i.e. C265/268A and NDK) almost exclusively distributed in intracellular punctate structures. Comparison of the sub-cellular distribution from SPRY2 WT and S-acylation deficient mutants could provide an important tool to study the intracellular trafficking of SPRY2 (e.g. shuttling, recycling). Also, the observation that the SPRY2 C265/268A mutant failed to localise to the plasma membrane suggests that in PC12 cells SPRY2 S-acylation is mediated by zDHHC17. However, knock-down/-out strategies (e.g. siRNA, shRNA or CRISPR-Cas9) will be required to further support this hypothesis. Nonetheless, this approach should take into account the possibility of other zDHHC enzymes compensating for the loss of zDHHC17. Apart from this, it would be valuable to explore the interplay between dynamic S-acylation and dynamic trafficking/localisation of SPRY2 in response to a range of different growth factors. This could perhaps make use of live-imaging techniques in which changes in the sub-cellular localisation of fluorescently-tagged SPRY2 following GF treatments (at different time points) can be analysed.

This thesis also included the first thorough analysis of the interaction between SPRY2 and the ankyrin repeat (ANK) domain of zDHHC17 and its requirements for S-acylation. Previous studies identified residues important for S-acylation in both ANK17 and substrate proteins (Lemonidis et al., 2015a; Verardi et al., 2017). Specifically, in ANK17, the N100/W130 binding pocket was shown to be critical for recognition of zDABM sequences (i.e. QP motifs) in substrate proteins such as SNAP25b and HTT prior to S-acylation (Verardi et al., 2017). Binding assays, including pull-down, immunoprecipitation and peptide-array, confirmed that the association of SPRY2 with the ANK domain of zDHHC17 primarily involves the N100/W130 binding pocket in ANK17 and the zDABM sequence of SPRY2 centred around P154 (i.e. 149-IIRVQP-154). Interestingly however, S-acylation of SPRY2 occurred *via* a different mechanism (i.e. “non-canonical”) from that previously identified for SNAP25b. In fact, the N100/W130 binding pocket in ANK17 and the zDABM in SPRY2 were not required for S-acylation of SPRY2, which is in marked contrast to SNAP25b. Accordingly, in PC12 cells SPRY2 P154A and 155-315 mutants (both characterised by loss of the zDABM and defects in zDHHC17 binding) were endogenously S-acylated (presumably by zDHHC17) and correctly targeted to the plasma membrane. At present, it is unknown whether other zDHHC17 substrates are S-acylated *via* a similar non-canonical mechanism. To this end, it will of interest to assess the activity of zDHHC17 W130A and N100A mutants towards other zDHHC17 substrates (e.g. SPRED1 and SPRED2, JNK1 α 2 and JNK3 α 2, PAI-RBP1, SLAIN1 and EVL-I).

The data presented in the thesis is consistent with the idea that SPRY2 contains a second (low affinity) ANK17 binding site outside of the zDABM, that is linked to SPRY2 S-acylation. However, the results of different experimental approaches were somewhat conflicting regarding the position of this additional site. Click chemistry experiments suggested that this may lay within region 155-290 of SPRY2, which was *per se* sufficient for zDHHC17-mediated S-acylation. In contrast, peptide array screening revealed the presence of a second (low affinity) ANK17 binding site at position 106-120 of SPRY2. In support of our click chemistry data, recent work performed by Liam Butler found that the SPRY2 155-315 mutant co-

immunoprecipitated with zDHHC17, albeit at a reduced level compared with wild-type SPRY2 (data not shown). In future work, it will be important to narrow down the exact location of this site and evaluate its implications in SPRY2 S-acylation. This could be done by mutagenesis analysis (e.g. insertions of premature stop codons in SPRY2 155-315 mutant and analysis of the corresponding S-acylation levels), or by employing peptide arrays (e.g. ANK17 peptides could be screened for binding to SPRY2). However, this approach should take into consideration the possibility that the additional binding site may be a non-linear motif, undetectable in peptide-array experiments. If this binding site is identified, further analysis could reveal the presence of post-translational modifications which might account for the fact that we were not able to detect binding of this region with the ANK17 in peptide arrays. Besides this, if region 106-120 of SPRY2 is confirmed to be a *bona fide* ANK17 binding site, it will be interesting to investigate whether dynamic phosphorylation at specific residues modulates the binding with zDHHC17. This could be initially done in peptide binding experiments using phospho-mimetic peptides. If these modulate zDHHC17 binding, it could be relevant to also consider the binding of other proteins which recognise residues 106-120 (e.g. Nedd4). Overall, it is possible that SPRY2 binds ANK17 *via* three different sites (i) the zDABM, (ii) residues 106-120, and (iii) an unidentified site within region 155-290. While the zDABM and residues 106-120 are dispensable for S-acylation, they may mediate functions of SPRY2 that are yet to be uncovered. On the other hand, a novel binding site within region 155-290 may be indispensable for S-acylation.

This study also included the first evidence that zDHHC17, the enzyme that modifies SPRY2, undergoes multimerisation. In pull-down experiments (which employed a purified His-tagged version of ANK17) zDHHC17 formed both homodimers and heterodimers with zDHHC13, whereas it did not interact with zDHHC7 or zDHHC3. Pull-down assays also revealed that zDHHC17 self-association may occur *via* multiple means. First, the ANK domain of zDHHC17 can directly mediate homo-dimerisation with the N100/W130 binding pocket contributing to ANK-ANK interactions. These observations raise questions about whether dimers could correspond to inactive

forms of the enzyme, e.g. by precluding substrate recognition and binding. Nevertheless, in the context of SPRY2, which does not require binding to the N100/W130 binding pocket, dimerisation may have different outcomes. Indeed, it is feasible that dimerisation *via* the N100/W130 pocket underlies selective interactions of zDHHC17 with specific substrate proteins (e.g. dimers might selectively interact with SPRY2 and monomers with other substrates such as SNAP25). It will be important to explore these hypotheses in cross-linking experiments and fluorescence resonance energy transfer (FRET) experiments. For example, these could evaluate the rate of association of zDHHC17 WT-WT *versus* W130A-W130A *versus* DHHA-DHHA in the presence of substrates such as SNAP25b and SPRY2. Second, immunoprecipitation experiments (in which full-length proteins were employed) highlighted that other regions/sites outside of the ANK domain can mediate zDHHC17 self-association. Although the nature of these sites was not characterised their identification will be valuable. As a starting point, the implications of the transmembrane domains (TMDs) could be explored, as oligomerisation through these domains would allow a great degree of freedom in terms of possible zDHHC combinations. This approach could initially use zDHHC enzymes in which both the N- and C-termini have been truncated, and the ability of these mutants to undergo oligomerisation could be examined in immunoprecipitation experiments. If these are found to associate, it could also be relevant to analyse the protein sequence for features previously reported to facilitate TMD-TMD interactions, including proline residues at the membrane interface or GxxxG motifs (Cymer et al., 2012; Sal-Man et al., 2014).

Overall, this study has provided new insight into the mechanisms and outcomes of SPRY2 S-acylation and highlighted novel pathways for S-acylation by zDHHC17 that might be relevant to other substrates of this enzyme. As S-acylation appears to regulate both the stability and localisation of SPRY2, further characterisation of this process might uncover novel therapeutic pathways to treat conditions linked to changes in SPRY2 expression.

Chapter 7 Bibliography

- Abrami, L., Audagnotto, M., Ho, S., Marcaida, M.J., Mesquita, F., Anwar, M., Sandoz, P., Fonti, G., Pojer, F., Peraro, M.D., van der Goot, F.G., 2020. Molecular mode of action of an Acyl Protein thioesterase. <https://doi.org/10.1101/2020.06.18.157545>
- Abrami, L., Dallavilla, T., Sandoz, P.A., Demir, M., Kunz, B., Savoglidis, G., Hatzimanikatis, V., van Der Goot, F.G., 2017. Identification and dynamics of the human ZDHHC16-ZDHHC6 palmitoylation cascade. *Elife* 6. <https://doi.org/10.7554/eLife.27826>
- Abrami, L., Kunz, B., Iacovache, I., Van Der Goot, F.G., 2008. Palmitoylation and ubiquitination regulate exit of the Wnt signaling protein LRP6 from the endoplasmic reticulum. *Proc. Natl. Acad. Sci. U. S. A.* 105, 5384–5389. <https://doi.org/10.1073/pnas.0710389105>
- Abrami, L., Leppla, S.H., Gisou Van Der Goot, F., 2006. Receptor palmitoylation and ubiquitination regulate anthrax toxin endocytosis. *J. Cell Biol.* 172, 309–320. <https://doi.org/10.1083/jcb.200507067>
- Aicart-Ramos, C., Valero, R.A., Rodriguez-Crespo, I., 2011. Protein palmitoylation and subcellular trafficking. *Biochim. Biophys. Acta - Biomembr.* 1808, 2981–2994. <https://doi.org/10.1016/j.bbamem.2011.07.009>
- Aikawa, Y., Xia, X., Martin, T.F.J., 2006. SNAP25, but not syntaxin 1A, recycles via an ARF6-regulated pathway in neuroendocrine cells. *Mol. Biol. Cell* 17, 711–722. <https://doi.org/10.1091/mbc.E05-05-0382>
- Akbulut, S., Reddi, A.L., Aggarwal, P., Ambardekar, C., Canciani, B., Kim, M.K.H., Hix, L., Vilimas, T., Mason, J., Basson, M.A., Lovatt, M., Powell, J., Collins, S., Quatela, S., Phillips, M., Licht, J.D., 2010. Sprouty proteins inhibit receptor-mediated activation of phosphatidylinositol-specific phospholipase C. *Mol. Biol. Cell* 21, 3487–3496. <https://doi.org/10.1091/mbc.E10-02-0123>

- Akimzhanov, A.M., Boehning, D., Snyder, S.H., 2015. Rapid and transient palmitoylation of the tyrosine kinase Lck mediates Fas signaling. *Proc. Natl. Acad. Sci. U. S. A.* 112, 11876–11880. <https://doi.org/10.1073/pnas.1509929112>
- Alland, L., Peseckis, S.M., Atherton, R.E., Berthiaume, L., Resh, M.D., 1994. Dual myristylation and palmitoylation of Src family member p59(fyn) affects subcellular localization. *J. Biol. Chem.* 269, 16701–16705.
- Apolloni, A., Prior, I.A., Lindsay, M., Parton, R.G., Hancock, J.F., 2000. H-ras but Not K-ras Traffics to the Plasma Membrane through the Exocytic Pathway. *Mol. Cell. Biol.* 20, 2475–2487. <https://doi.org/10.1128/mcb.20.7.2475-2487.2000>
- Aranda, S., Alvarez, M., Turró, S., Laguna, A., de la Luna, S., 2008. Sprouty2-Mediated Inhibition of Fibroblast Growth Factor Signaling Is Modulated by the Protein Kinase DYRK1A. *Mol. Cell. Biol.* 28, 5899–5911. <https://doi.org/10.1128/mcb.00394-08>
- Arrasate, M., Mitra, S., Schweitzer, E.S., Segal, M.R., Finkbeiner, S., 2004. Inclusion body formation reduces levels of mutant huntingtin and the risk of neuronal death. *Nature.* <https://doi.org/10.1038/nature02998>
- Asmat, U., Abad, K., Ismail, K., 2016. Diabetes mellitus and oxidative stress—A concise review. *Saudi Pharm. J.* 24, 547–553. <https://doi.org/10.1016/j.jsps.2015.03.013>
- Baird, K., Davis, S., Antonescu, C.R., Harper, U.L., Walker, R.L., Chen, Y., Glatfelter, A.A., Duray, P.H., Meltzer, P.S., 2005. Gene expression profiling of human sarcomas: Insights into sarcoma biology. *Cancer Res.* 65, 9226–9235. <https://doi.org/10.1158/0008-5472.CAN-05-1699>
- Bartels, D.J., Mitchell, D.A., Dong, X., Deschenes, R.J., 1999. Erf2, a Novel Gene Product That Affects the Localization and Palmitoylation of Ras2 in *Saccharomyces cerevisiae*. *Mol. Cell. Biol.* 19, 6775–6787. <https://doi.org/10.1128/mcb.19.10.6775>
- Basson, M.A., Akbulut, S., Watson-Johnson, J., Simon, R., Carroll, T.J., Shakya, R.,

- Gross, I., Martin, G.R., Lufkin, T., McMahon, A.P., Wilson, P.D., Costantini, F.D., Mason, I.J., Licht, J.D., 2005. Sprouty1 is a critical regulator of GDNF/RET-mediated kidney induction. *Dev. Cell* 8, 229–239. <https://doi.org/10.1016/j.devcel.2004.12.004>
- Basson, M.A., Watson-Johnson, J., Shakya, R., Akbulut, S., Hyink, D., Costantini, F.D., Wilson, P.D., Mason, I.J., Licht, J.D., 2006. Branching morphogenesis of the ureteric epithelium during kidney development is coordinated by the opposing functions of GDNF and Sprouty1. *Dev. Biol.* 299, 466–477. <https://doi.org/10.1016/j.ydbio.2006.08.051>
- Bates, G.P., Dorsey, R., Gusella, J.F., Hayden, M.R., Kay, C., Leavitt, B.R., Nance, M., Ross, C.A., Scahill, R.I., Wetzel, R., Wild, E.J., Tabrizi, S.J., 2015. Huntington disease. *Nat. Rev. Dis. Prim.* 1, 1–21. <https://doi.org/10.1038/nrdp.2015.5>
- Beck, M., Schmidt, A., Malmstroem, J., Claassen, M., Ori, A., Szymborska, A., Herzog, F., Rinner, O., Ellenberg, J., Aebersold, R., 2011. The quantitative proteome of a human cell line. *Mol. Syst. Biol.* 7. <https://doi.org/10.1038/msb.2011.82>
- Berchtold, L.A., Størling, Z.M., Ortis, F., Lage, K., Bang-Berthelsen, C., Bergholdt, R., Hald, J., Brorsson, C.A., Eizirik, D.L., Pociot, F., Brunak, S., Størling, J., 2011. Huntingtin-interacting protein 14 is a type 1 diabetes candidate protein regulating insulin secretion and beta-cell apoptosis. *Proc. Natl. Acad. Sci. U. S. A.* 108, E681-8. <https://doi.org/10.1073/pnas.1104384108>
- Bijlmakers, M.-J.J.J.E., Marsh, M., 1999. Trafficking of an acylated cytosolic protein: Newly synthesized p56(lck) travels to the plasma membrane via the exocytic pathway. *J. Cell Biol.* 145, 457–468. <https://doi.org/10.1083/jcb.145.3.457>
- Biosciences, L., 2015. Western Blot Normalization: Challenges and Considerations for Quantitative Analysis. LI-COR Biosci. <https://doi.org/10.1103/PhysRevC.78.054322>
- Blanc, M., David, F., Abrami, L., Migliozi, D., Armand, F., Bürgi, J., van der Goot, F.G., 2015. SwissPalm: Protein Palmitoylation database. *F1000Research* 4.

<https://doi.org/10.12688/f1000research.6464.1>

Blanc, M., David, F., van der Goot, F.G., 2019. SwissPalm 2: Protein S-Palmitoylation Database, in: Protein Lipidation. New York, NY: Springer New York, New York, pp. 203–214. <https://doi.org/10.4324/9781351218986-16>

Blanpain, C., Wittamer, V., Vanderwinden, J.M., Boom, A., Renneboog, B., Lee, B., Le Poul, E., El Asmar, L., Govaerts, C., Vassart, G., Doms, R.W., Parmentier, M., 2001. Palmitoylation of CCR5 Is Critical for Receptor Trafficking and Efficient Activation of Intracellular Signaling Pathways. *J. Biol. Chem.* 276, 23795–23804. <https://doi.org/10.1074/jbc.M100583200>

Blaskovic, S., Blanc, M., Van Der Goot, F.G., 2013. What does S-palmitoylation do to membrane proteins? *FEBS J.* 280, 2766–2774. <https://doi.org/10.1111/febs.12263>

Bloethner, S., Chen, B., Hemminki, K., Müller-Berghaus, J., Ugurel, S., Schadendorf, D., Kumar, R., 2005. Effect of common B-RAF and N-RAS mutations on global gene expression in melanoma cell lines. *Carcinogenesis* 26, 1224–1232. <https://doi.org/10.1093/carcin/bgi066>

Brady, S.C., Coleman, M.L., Munro, J., Feller, S.M., Morrice, N.A., Olson, M.F., 2009. Sprouty2 association with B-Raf is regulated by phosphorylation and kinase conformation. *Cancer Res.* 69, 6773–6781. <https://doi.org/10.1158/0008-5472.CAN-08-4447>

Brigidi, G.S., Santyr, B., Shimell, J., Jovellar, B., Bamji, S.X., 2015. Activity-regulated trafficking of the palmitoyl-acyl transferase DHHC5. *Nat. Commun.* 6. <https://doi.org/10.1038/ncomms9200>

Buchan, D.W.A., Jones, D.T., 2019. The PSIPRED Protein Analysis Workbench: 20 years on. *Nucleic Acids Res.* 47, W402–W407. <https://doi.org/10.1093/nar/gkz297>

Buchanan, B.W., Lloyd, M.E., Engle, S.M., Rubenstein, E.M., 2016. Cycloheximide chase analysis of protein degradation in *Saccharomyces cerevisiae*. *J. Vis. Exp.*

2016, 53975. <https://doi.org/10.3791/53975>

Butland, S.L., Sanders, S.S., Schmidt, M.E., Riechers, S.P., Lin, D.T.S., Martin, D.D.O., Vaid, K., Graham, R.K., Singaraja, R.R., Wanker, E.E., Conibear, E., Hayden, M.R., 2014. The palmitoyl acyltransferase HIP14 shares a high proportion of interactors with huntingtin: Implications for a role in the pathogenesis of Huntington's disease. *Hum. Mol. Genet.* 23, 4142–4160. <https://doi.org/10.1093/hmg/ddu137>

Cabrita, M.A., Christofori, G., 2008. Sprouty proteins, masterminds of receptor tyrosine kinase signaling. *Angiogenesis.* <https://doi.org/10.1007/s10456-008-9089-1>

Cabrita, M.A., Christofori, G., 2003. Sprouty proteins: Antagonists of endothelial cell signaling and more. *Thromb. Haemost.* 90, 586–590. <https://doi.org/10.1160/th03-04-0217>

Cabrita, M.A., Jäggi, F., Widjaja, S.P., Christofori, G., 2006. A functional interaction between sprouty proteins and Caveolin-1. *J. Biol. Chem.* 281, 29201–29212. <https://doi.org/10.1074/jbc.M603921200>

Camp, L.A., Hofmann, S.L., 1993. Purification and properties of a palmitoyl-protein thioesterase that cleaves palmitate from H-Ras. *J. Biol. Chem.* 268, 22566–22574. [https://doi.org/10.1016/S0021-9258\(18\)41567-0](https://doi.org/10.1016/S0021-9258(18)41567-0)

Carreno, S., Gouze, M.E., Schaak, S., Emorine, L.J., Maridonneau-Parini, I., 2000. Lack of palmitoylation redirects p59(Hck) from the plasma membrane to p61(Hck)-positive lysosomes. *J. Biol. Chem.* 275, 36223–36229. <https://doi.org/10.1074/jbc.M003901200>

Casci, T., Vinós, J., Freeman, M., 1999. Sprouty, an intracellular inhibitor of Ras signaling. *Cell* 96, 655–665. [https://doi.org/10.1016/S0092-8674\(00\)80576-0](https://doi.org/10.1016/S0092-8674(00)80576-0)

Casey, P.J., Solski, P.A., Der, C.J., Buss, J.E., 1989. P21Ras Is Modified By a Farnesyl Isoprenoid. *Proc. Natl. Acad. Sci. U. S. A.* 86, 8323–8327.

<https://doi.org/10.1073/pnas.86.21.8323>

- Chamberlain, L.H., Lemonidis, K., Sanchez-Perez, M., Werno, M.W., Gorleku, O.A., Greaves, J., 2013. Palmitoylation and the trafficking of peripheral membrane proteins, in: *Biochemical Society Transactions*. pp. 62–66. <https://doi.org/10.1042/BST20120243>
- Chamberlain, L.H., Shipston, M.J., 2015. The Physiology of Protein S-acylation. *Physiol. Rev.* 95, 341–376. <https://doi.org/10.1152/physrev.00032.2014>
- Chambers, D., Medhurst, A.D., Walsh, F.S., Price, J., Mason, I., 2000. Differential display of genes expressed at the midbrain - hindbrain junction identifies sprouty2: An FGF8-inducible member of a family of intracellular FGF antagonists. *Mol. Cell. Neurosci.* 15, 22–35. <https://doi.org/10.1006/mcne.1999.0801>
- Chandramouli, S., Chye, Y.Y., Yusoff, P., Lao, D.H., Hwei, F.L., Mizuno, K., Guy, G.R., 2008. *Tesk1* interacts with *Spry2* to abrogate its inhibition of ERK phosphorylation downstream of receptor tyrosine kinase signaling. *J. Biol. Chem.* 283, 1679–1691. <https://doi.org/10.1074/jbc.M705457200>
- Chang, Y.N., Jaumann, E.A., Reichel, K., Hartmann, J., Oliver, D., Hummer, G., Joseph, B., Geertsma, E.R., 2019. Structural basis for functional interactions in dimers of SLC26 transporters. *Nat. Commun.* 10. <https://doi.org/10.1038/s41467-019-10001-w>
- Chen, F.J., Lee, K.W., Lai, C.C., Lee, S.P., Shen, H.H., Tsai, S.P., Liu, B.H., Wang, L.M., Liou, G.G., 2013. Structure of native oligomeric Sprouty2 by electron microscopy and its property of electroconductivity. *Biochem. Biophys. Res. Commun.* 439, 351–356. <https://doi.org/10.1016/j.bbrc.2013.08.083>
- Chen, S., Han, C., Miao, X., Li, X., Yin, C., Zou, J., Liu, M., Li, S., Stawski, L., Zhu, B., Shi, Q., Xu, Z.X., Li, C., Goding, C.R., Zhou, J., Cui, R., 2019. Targeting MC1R depalmitoylation to prevent melanomagenesis in redheads. *Nat. Commun.* 10. <https://doi.org/10.1038/s41467-019-08691-3>

- Chen, X., Hao, A., Li, X., Ye, K., Zhao, C., Yang, H., Ma, H., Hu, Lei, Zhao, Z., Hu, Lizhu, Ye, F., Sun, Q., Zhang, H., Wang, H., Yao, X., Fang, Z., 2020. Activation of JNK and p38 MAPK mediated by ZDHHC17 drives glioblastoma multiforme development and malignant progression. *Theranostics* 10, 998–1015. <https://doi.org/10.7150/thno.40076>
- Ching, S.T., Cunha, G.R., Baskin, L.S., Basson, M.A., Klein, O.D., 2014. Coordinated activity of *spry1* and *spry2* is required for normal development of the external genitalia. *Dev. Biol.* 386, 1–11. <https://doi.org/10.1016/j.ydbio.2013.12.014>
- Chisari, M., Saini, D.K., Kalyanaraman, V., Gautam, N., 2007. Shuttling of G protein subunits between the plasma membrane and intracellular membranes. *J. Biol. Chem.* 282, 24092–24098. <https://doi.org/10.1074/jbc.M704246200>
- Chow, S.Y., Yu, C.Y., Guy, G.R., 2009. Sprouty2 interacts with protein Kinase C δ and disrupts phosphorylation of protein kinase D1. *J. Biol. Chem.* 284, 19623–19636. <https://doi.org/10.1074/jbc.M109.021600>
- Choy, E., Chiu, V.K., Silletti, J., Feoktistov, M., Morimoto, T., Michaelson, D., Ivanov, I.E., Philips, M.R., 1999. Endomembrane trafficking of ras: The CAAX motif targets proteins to the ER and Golgi. *Cell* 98, 69–80. [https://doi.org/10.1016/S0092-8674\(00\)80607-8](https://doi.org/10.1016/S0092-8674(00)80607-8)
- Clevers, H., 2006. Wnt/ β -Catenin Signaling in Development and Disease. *Cell*. <https://doi.org/10.1016/j.cell.2006.10.018>
- Collins, M.O., Woodley, K.T., Choudhary, J.S., 2017. Global, site-specific analysis of neuronal protein S-acylation. *Sci. Rep.* 7, 1–14. <https://doi.org/10.1038/s41598-017-04580-1>
- Craven, S.E., El-Husseini, A.E., Bredt, D.S., 1999. Synaptic targeting of the postsynaptic density protein PSD-95 mediated by lipid and protein motifs. *Neuron* 22, 497–509. [https://doi.org/10.1016/S0896-6273\(00\)80705-9](https://doi.org/10.1016/S0896-6273(00)80705-9)
- Cymer, F., Veerappan, A., Schneider, D., 2012. Transmembrane helix-helix

interactions are modulated by the sequence context and by lipid bilayer properties. *Biochim. Biophys. Acta - Biomembr.* 1818, 963–973. <https://doi.org/10.1016/j.bbamem.2011.07.035>

Dallavilla, T., Abrami, L., Sandoz, P.A., Savoglidis, G., Hatzimanikatis, V., van der Goot, F.G., 2016. Model-Driven Understanding of Palmitoylation Dynamics: Regulated Acylation of the Endoplasmic Reticulum Chaperone Calnexin. *PLoS Comput. Biol.* 12. <https://doi.org/10.1371/journal.pcbi.1004774>

DaSilva, J., Xu, L., Kim, H.J., Miller, W.T., Bar-Sagi, D., 2006. Regulation of Sprouty Stability by Mnk1-Dependent Phosphorylation. *Mol. Cell. Biol.* 26, 1898–1907. <https://doi.org/10.1128/mcb.26.5.1898-1907.2006>

Davies, S.W., Turmaine, M., Cozens, B.A., DiFiglia, M., Sharp, A.H., Ross, C.A., Scherzinger, E., Wanker, E.E., Mangiarini, L., Bates, G.P., 1997. Formation of neuronal intranuclear inclusions underlies the neurological dysfunction in mice transgenic for the HD mutation. *Cell* 90, 537–548. [https://doi.org/10.1016/S0092-8674\(00\)80513-9](https://doi.org/10.1016/S0092-8674(00)80513-9)

De Maximy, A.A., Nakatake, Y., Moncada, S., Itoh, N., Thiery, J.P., Bellusci, S., 1999. Cloning and expression pattern of a mouse homologue of *Drosophila* sprouty in the mouse embryo. *Mech. Dev.* 81, 213–216. [https://doi.org/10.1016/S0925-4773\(98\)00241-X](https://doi.org/10.1016/S0925-4773(98)00241-X)

Diez-Ardanuy, C., Greaves, J., Munro, K.R., Tomkinson, N.C.O., Chamberlain, L.H., 2017. A cluster of palmitoylated cysteines are essential for aggregation of cysteine-string protein mutants that cause neuronal ceroid lipofuscinosis. *Sci. Rep.* 7, 10. <https://doi.org/10.1038/s41598-017-00036-8>

Ding, W., Bellusci, S., Shi, W., Warburton, D., 2003. Functional analysis of the human *Sprouty2* gene promoter. *Gene* 322, 175–185. <https://doi.org/10.1016/j.gene.2003.09.004>

Du, K., Murakami, S., Sun, Y., Kilpatrick, C.L., Luscher, B., 2017. DHHC7 palmitoylates glucose transporter 4 (Glut4) and regulates Glut4 membrane translocation. *J.*

Biol. Chem. 292, 2979–2991. <https://doi.org/10.1074/jbc.M116.747139>

Ducker, C.E., Griffel, L.K., Smith, R.A., Keller, S.N., Zhuang, Y., Xia, Z., Diller, J.D., Smith, C.D., 2006. Discovery and characterization of inhibitors of human palmitoyl acyltransferases. *Mol. Cancer Ther.* 5, 1647–1659. <https://doi.org/10.1158/1535-7163.MCT-06-0114>

Ducker, C.E., Stettler, E.M., French, K.J., Upson, J.J., Smith, C.D., 2004. Huntingtin interacting protein 14 is an oncogenic human protein: Palmitoyl acyltransferase. *Oncogene* 23, 9230–9237. <https://doi.org/10.1038/sj.onc.1208171>

Duncan, J.A., Gilman, A.G., 2002. Characterization of *Saccharomyces cerevisiae* acyl-protein thioesterase 1, the enzyme responsible for G protein α subunit deacylation in vivo. *J. Biol. Chem.* 277, 31740–31752. <https://doi.org/10.1074/jbc.M202505200>

Duncan, J.A., Gilman, A.G., 1998. A cytoplasmic acyl-protein thioesterase that removes palmitate from G protein α subunits and p21(RAS). *J. Biol. Chem.* 273, 15830–15837. <https://doi.org/10.1074/jbc.273.25.15830>

Edwin, F., Anderson, K., Patel, T.B., 2010. HECT domain-containing E3 ubiquitin ligase Nedd4 interacts with and ubiquitinates sprouty2. *J. Biol. Chem.* 285, 255–264. <https://doi.org/10.1074/jbc.M109.030882>

Edwin, F., Anderson, K., Ying, C., Patel, T.B., 2009. Intermolecular Interactions of Sprouty Proteins and Their Implications in Development and Disease. *Mol. Pharmacol.* 76, 679–691. <https://doi.org/10.1124/mol.109.055848>

Edwin, F., Singh, R., Endersby, R., Baker, S.J., Patel, T.B., 2006. The tumor suppressor PTEN is necessary for human sprouty 2-mediated inhibition of cell proliferation. *J. Biol. Chem.* 281, 4816–4822. <https://doi.org/10.1074/jbc.M508300200>

Egan, J.E., Hall, A.B., Yatsula, B.A., Bar-Sagi, D., 2002. The bimodal regulation of epidermal growth factor signaling by human Sprouty proteins. *Proc. Natl. Acad. Sci.* 99, 6041–6046. <https://doi.org/10.1073/pnas.052090899>

- El-Husseini, A.E., Craven, S.E., Chetkovich, D.M., Firestein, B.L., Schnell, E., Aoki, C., Brecht, D.S., 2000. Dual palmitoylation of PSD-95 mediates its vesiculotubular sorting, postsynaptic targeting, and ion channel clustering. *J. Cell Biol.* 148, 159–171. <https://doi.org/10.1083/jcb.148.1.159>
- El-Husseini, A.E.D., Brecht, D.S., 2002. Protein palmitoylation: A regulator of neuronal development and function. *Nat. Rev. Neurosci.* 3, 791–802. <https://doi.org/10.1038/nrn940>
- El-Husseini, A.E.D., Schnell, E., Dakoji, S., Sweeney, N., Zhou, Q., Prange, O., Gauthier-Campbell, C., Aguilera-Moreno, A., Nicoll, R.A., Brecht, D.S., 2002. Synaptic strength regulated by palmitate cycling on PSD-95. *Cell* 108, 849–863. [https://doi.org/10.1016/S0092-8674\(02\)00683-9](https://doi.org/10.1016/S0092-8674(02)00683-9)
- Erales, J., Coffino, P., 2014. Ubiquitin-independent proteasomal degradation. *Biochim. Biophys. Acta - Mol. Cell Res.* 1843, 216–221. <https://doi.org/10.1016/j.bbamcr.2013.05.008>
- Ernst, A.M., Syed, S.A., Zaki, O., Bottanelli, F., Zheng, H., Hacke, M., Xi, Z., Rivera-Molina, F., Graham, M., Rebane, A.A., Björkholm, P., Baddeley, D., Toomre, D., Pincet, F., Rothman, J.E., 2018. S-Palmitoylation Sorts Membrane Cargo for Anterograde Transport in the Golgi. *Dev. Cell* 47, 479-493.e7. <https://doi.org/10.1016/j.devcel.2018.10.024>
- Ernst, A.M., Toomre, D., Bogan, J.S., 2019. Acylation - A new means to control traffic through the Golgi. *Front. Cell Dev. Biol.* 7. <https://doi.org/10.3389/fcell.2019.00109>
- Fang, C., Deng, L., Keller, C.A., Fukata, M., Fukata, Y., Chen, G., Luscher, B., 2006. GODZ-Mediated Palmitoylation of GABAA Receptors Is Required for Normal Assembly and Function of GABAergic Inhibitory Synapses. *J. Neurosci.* 26, 12758–12768. <https://doi.org/10.1523/JNEUROSCI.4214-06.2006>
- Feng, Y., Davis, N.G., 2000. Akr1p and the Type I Casein Kinases Act prior to the Ubiquitination Step of Yeast Endocytosis: Akr1p Is Required for Kinase

Localization to the Plasma Membrane. *Mol. Cell. Biol.* 20, 5350–5359.
<https://doi.org/10.1128/mcb.20.14.5350-5359.2000>

Feng, Y.H., Wu, C.L., Tsao, C.J., Chang, J.G., Lu, P.J., Yeh, K.T., Uen, Y.H., Lee, J.C., Shiau, A.L., 2011. Deregulated expression of sprouty2 and microRNA-21 in human colon cancer: Correlation with the clinical stage of the disease. *Cancer Biol. Ther.* 11, 111–121. <https://doi.org/10.4161/cbt.11.1.13965>

Fong, C.W., Chua, M.S., McKie, A.B., Ling, S.H.M., Mason, V., Li, R., Yusoff, P., Lo, T.L., Leung, H.Y., So, S.K.S., Guy, G.R., 2006. Sprouty 2, an inhibitor of mitogen-activated protein kinase signaling, is down-regulated in hepatocellular carcinoma. *Cancer Res.* 66, 2048–2058. <https://doi.org/10.1158/0008-5472.CAN-05-1072>

Fong, C.W., Leong, H.F., Wong, E.S.M., Lim, J., Yusoff, P., Guy, G.R., 2003. Tyrosine phosphorylation of Sprouty2 enhances its interaction with c-Cbl and is crucial for its function. *J. Biol. Chem.* 278, 33456–33464. <https://doi.org/10.1074/jbc.M301317200>

Frank, M.J., Dawson, D.W., Bensinger, S.J., Hong, J.S., Knosp, W.M., Xu, L., Balatoni, C.E., Allen, E.L., Shen, R.R., Bar-Sagi, D., Martin, G.R., Teitell, M.A., 2009. Expression of sprouty2 inhibits B-cell proliferation and is epigenetically silenced in mouse and human B-cell lymphomas. *Blood* 113, 2478–2487. <https://doi.org/10.1182/blood-2008-05-156943>

Fredericks, G.J., Hoffmann, F.W., Hondal, R.J., Rozovsky, S., Urschitz, J., Hoffmann, P.R., 2018. Selenoprotein K increases efficiency of DHH6 catalyzed protein palmitoylation by stabilizing the acyl-DHH6 intermediate. *Antioxidants* 7. <https://doi.org/10.3390/antiox7010004>

Fredericks, G.J., Hoffmann, P.R., 2015. Selenoprotein K and protein palmitoylation. *Antioxidants Redox Signal.* <https://doi.org/10.1089/ars.2015.6375>

Fritzsche, S., Kenzelmann, M., Hoffmann, M.J., Müller, M., Engers, R., Gröne, H.J., Schulz, W.A., 2006. Concomitant down-regulation of SPRY1 and SPRY2 in

- prostate carcinoma. *Endocr. Relat. Cancer* 13, 839–849.
<https://doi.org/10.1677/erc.1.01190>
- Fukata, M., Fukata, Y., Adesnik, H., Nicoll, R.A., Brecht, D.S., 2004. Identification of PSD-95 Palmitoylating Enzymes. *Neuron* 44, 987–996.
<https://doi.org/10.1016/J.NEURON.2004.12.005>
- Fukata, Y., Dimitrov, A., Boncompain, G., Vielemeyer, O., Perez, F., Fukata, M., 2013. Local palmitoylation cycles define activity-regulated postsynaptic subdomains. *J. Cell Biol.* 202, 145–161. <https://doi.org/10.1083/jcb.201302071>
- Fukata, Y., Fukata, M., 2010. Protein palmitoylation in neuronal development and synaptic plasticity. *Nat. Rev. Neurosci.* 11, 161–175.
<https://doi.org/10.1038/nrn2788>
- Fukata, Y., Murakami, T., Yokoi, N., Fukata, M., 2016. Local Palmitoylation Cycles and Specialized Membrane Domain Organization, *Current Topics in Membranes*. Elsevier Ltd. <https://doi.org/10.1016/bs.ctm.2015.10.003>
- Gao, M., Patel, R., Ahmad, I., Fleming, J., Edwards, J., Mccracken, S., Sahadevan, K., Seywright, M., Norman, J., Sansom, O., Leung, H.Y., 2012. SPRY2 loss enhances ErbB trafficking and PI3K/AKT signalling to drive human and mouse prostate carcinogenesis. *EMBO Mol. Med.* 4, 776–790.
<https://doi.org/10.1002/emmm.201100944>
- Gao, X., Hannoush, R.N., 2018. A Decade of Click Chemistry in Protein Palmitoylation: Impact on Discovery and New Biology. *Cell Chem. Biol.*
<https://doi.org/10.1016/j.chembiol.2017.12.002>
- Gök, C., Fuller, W., 2020. Topical review: Shedding light on molecular and cellular consequences of NCX1 palmitoylation. *Cell. Signal.*
<https://doi.org/10.1016/j.cellsig.2020.109791>
- Gök, C., Plain, F., Robertson, A.D., Howie, J., Baillie, G.S., Fraser, N.J., Fuller, W., 2020. Dynamic Palmitoylation of the Sodium-Calcium Exchanger Modulates Its

- Structure, Affinity for Lipid-Ordered Domains, and Inhibition by XIP. *Cell Rep.* 31. <https://doi.org/10.1016/j.celrep.2020.107697>
- González Montoro, A., Quiroga, R., Maccioni, H.J.F., Valdèz Taubas, J., 2009. A novel motif at the C-terminus of palmitoyltransferases is essential for Swf1 and Pfa3 function in vivo. *Biochem. J.* 419, 301–308. <https://doi.org/10.1042/BJ20080921>
- González Montoro, A., Quiroga, R., Valdez Taubas, J., 2013. Zinc co-ordination by the DHHC cysteine-rich domain of the palmitoyltransferase Swf1. *Biochem. J.* 454, 427–435. <https://doi.org/10.1042/BJ20121693>
- Gonzalo, S., Greentree, W.K., Linder, M.E., 1999. SNAP-25 is targeted to the plasma membrane through a novel membrane-binding domain. *J. Biol. Chem.* 274, 21313–21318. <https://doi.org/10.1074/jbc.274.30.21313>
- Gonzalo, S., Linder, M.E., 1998. SNAP-25 palmitoylation and plasma membrane targeting require a functional secretory pathway. *Mol. Biol. Cell* 9, 585–597. <https://doi.org/10.1091/mbc.9.3.585>
- Goodnough, L.H., Brugmann, S.A., Hu, D., Helms, J.A., 2007. Stage-dependent craniofacial defects resulting from sprouty2 overexpression. *Dev. Dyn.* 236, 1918–1928. <https://doi.org/10.1002/dvdy.21195>
- Goodwin, J.S., Drake, K.R., Rogers, C., Wright, L., Lippincott-Schwartz, J., Philips, M.R., Kenworthy, A.K., 2005. Depalmitoylated Ras traffics to and from the Golgi complex via a nonvesicular pathway. *J. Cell Biol.* 170, 261–272. <https://doi.org/10.1083/jcb.200502063>
- Gorenberg, E., Zhao, H., Bishai, J., Chou, V., Wirak, G., Lam, T., Chandra, S., 2020. Identification of palmitoyl protein thioesterase 1 substrates defines roles for synaptic depalmitoylation. <https://doi.org/10.1101/2020.05.02.074302>
- Gorleku, O.A., Barns, A.M., Prescott, G.R., Greaves, J., Chamberlain, L.H., 2011. Endoplasmic reticulum localization of DHHC palmitoyltransferases mediated by lysine-based sorting signals. *J. Biol. Chem.* 286, 39573–39584.

<https://doi.org/10.1074/jbc.M111.272369>

Gottlieb, C.D., Linder, M.E., 2017. Structure and function of DHHC protein S-acyltransferases. *Biochem. Soc. Trans.* <https://doi.org/10.1042/BST20160304>

Gottlieb, C.D., Zhang, S., Linder, M.E., 2015. The cysteine-rich domain of the DHHC3 palmitoyltransferase is palmitoylated and contains tightly bound zinc. *J. Biol. Chem.* 290, 29259–29269. <https://doi.org/10.1074/jbc.M115.691147>

Goytain, A., Hines, R.M., Quamme, G.A., 2008. Huntingtin-interacting proteins, HIP14 and HIP14L, mediate dual functions, palmitoyl acyltransferase and Mg²⁺ transport. *J. Biol. Chem.* 283, 33365–33374. <https://doi.org/10.1074/jbc.M801469200>

Greaves, J., Carmichael, J. a, Chamberlain, L.H., 2011. The palmitoyl transferase DHHC2 targets a dynamic membrane cycling pathway: regulation by a C-terminal domain. *Mol. Biol. Cell* 22, 1887–1895. <https://doi.org/10.1091/mbc.E10-11-0924>

Greaves, J., Chamberlain, L.H., 2011a. Differential palmitoylation regulates intracellular patterning of SNAP25. *J. Cell Sci.* 124, 1351–1360. <https://doi.org/10.1242/jcs.079095>

Greaves, J., Chamberlain, L.H., 2011b. DHHC palmitoyl transferases: Substrate interactions and (patho)physiology. *Trends Biochem. Sci.* 36, 245–253. <https://doi.org/10.1016/j.tibs.2011.01.003>

Greaves, J., Chamberlain, L.H., 2010. S-acylation by the DHHC protein family. *Biochem. Soc. Trans.* 38, 522–524. <https://doi.org/10.1042/BST0380522>

Greaves, J., Chamberlain, L.H., 2007. Palmitoylation-dependent protein sorting. *J. Cell Biol.* 176, 249–254. <https://doi.org/10.1083/jcb.200610151>

Greaves, J., Chamberlain, L.H., 2006. Dual role of the cysteine-string domain in membrane binding and palmitoylation-dependent sorting of the molecular chaperone cysteine-string protein. *Mol.Biol.Cell* 17, 4748–4759.

<https://doi.org/10.1091/mbc.E06>

Greaves, J., Gorleku, O.A., Salaun, C., Chamberlain, L.H., 2010. Palmitoylation of the SNAP25 protein family: Specificity and regulation by DHHC palmitoyl transferases. *J. Biol. Chem.* 285, 24629–24638. <https://doi.org/10.1074/jbc.M110.119289>

Greaves, J., Munro, K.R., Davidson, S.C., Riviere, M., Wojno, J., Smith, T.K., Tomkinson, N.C.O., Chamberlain, L.H., 2017. Molecular basis of fatty acid selectivity in the zDHHC family of S-acyltransferases revealed by click chemistry. *Proc. Natl. Acad. Sci.* 114, E1365–E1374. <https://doi.org/10.1073/pnas.1612254114>

Greaves, J., Prescott, G.R., Fukata, Y., Fukata, M., Salaun, C., Chamberlain, L.H., 2009a. The Hydrophobic Cysteine-rich Domain of SNAP25 Couples with Downstream Residues to Mediate Membrane Interactions and Recognition by DHHC Palmitoyl Transferases. *Mol. Biol. Cell* 20, 1845–1854. <https://doi.org/10.1091/mbc.E08-09-0944>

Greaves, J., Prescott, G.R., Gorleku, O.A., Chamberlain, L.H., 2009b. The fat controller: Roles of palmitoylation in intracellular protein trafficking and targeting to membrane microdomains (Review). *Mol. Membr. Biol.* 26, 67–79. <https://doi.org/10.1080/09687680802620351>

Greaves, J., Salaun, C., Fukata, Y., Fukata, M., Chamberlain, L.H., 2008. Palmitoylation and membrane interactions of the neuroprotective chaperone cysteine-string protein. *J. Biol. Chem.* 283, 25014–25026. <https://doi.org/10.1074/jbc.M802140200>

Gross, I., Armant, O., Benosman, S., de Aguilar, J.L.G., Freund, J.N., Kedinger, M., Licht, J.D., Gaiddon, C., Loeffler, J.P., 2007. Sprouty2 inhibits BDNF-induced signaling and modulates neuronal differentiation and survival. *Cell Death Differ.* 14, 1802–1812. <https://doi.org/10.1038/sj.cdd.4402188>

Gross, I., Bassit, B., Benezra, M., Licht, J.D., 2001. Mammalian Sprouty Proteins Inhibit Cell Growth and Differentiation by Preventing Ras Activation. *J. Biol. Chem.* 276,

46460–46468. <https://doi.org/10.1074/jbc.M108234200>

- Gschwind, A., Fischer, O.M., Ullrich, A., 2004. The discovery of receptor tyrosine kinases: Targets for cancer therapy. *Nat. Rev. Cancer* 4, 361–370. <https://doi.org/10.1038/nrc1360>
- Gundersen, C.B., Mastrogiacomot, A., Faull, K., Umbach, J.A., 1994. Extensive lipidation of a Torpedo cysteine string protein. *J. Biol. Chem.* 269, 19197–19199.
- Gutierrez, L., Magee, A.I., Marshall, C.J., Hancock, J.F., 1989. Post-translational processing of p21(ras) is two-step and involve carboxyl-methylation and carboxy-terminal proteolysis. *EMBO J.* 8, 1093–1098. <https://doi.org/10.1002/j.1460-2075.1989.tb03478.x>
- Guy, G.R., Jackson, R.A., Yusoff, P., Chow, S.Y., 2009. Sprouty proteins: Modified modulators, matchmakers or missing links? *J. Endocrinol.* 203, 191–202. <https://doi.org/10.1677/JOE-09-0110>
- Guy, G.R., Wong, E.S.M., Yusoff, P., Chandramouli, S., Lo, T.L., Lim, J., Fong, C.W., 2003. Sprouty: How does the branch manager work? *J. Cell Sci.* 116, 3061–3068. <https://doi.org/10.1242/jcs.00652>
- Hacohen, N., Kramer, S., Sutherland, D., Hiromi, Y., Krasnow, M.A., 1998. sprouty encodes a novel antagonist of FGF signaling that patterns apical branching of the *Drosophila* airways. *Cell* 92, 253–263. [https://doi.org/10.1016/S0092-8674\(00\)80919-8](https://doi.org/10.1016/S0092-8674(00)80919-8)
- Haglund, K., Schmidt, M.H.H., Wong, E.S.M., Guy, G.R., Dikic, I., 2005. Sprouty2 acts at the Cbl/CIN85 interface to inhibit epidermal growth factor receptor downregulation. *EMBO Rep.* 6, 635–641. <https://doi.org/10.1038/sj.embor.7400453>
- Hall, A.B., Jura, N., Dasilva, J., Jang, Y.J., Gong, D., Bar-sagi, D., 2003. hSpry2 Is Targeted to the Ubiquitin-Dependent Proteasome Pathway by c-Cbl. *Curr. Biol.* 13, 308–314.

- Hall, R.A., 2004. Studying Protein-Protein Interactions via Blot Overlay or Far Western Blot, in: Fu, H. (Ed.), *Protein-Protein Interactions: Methods and Applications*. Humana Press, Totowa, NJ, pp. 167–174. <https://doi.org/10.1385/1-59259-762-9:167>
- Hallak, H., Muszbek, L., Laposata, M., Belmonte, E., Brass, L.F., Manning, D.R., 1994. Covalent binding of arachidonate to G protein α subunits of human platelets. *J. Biol. Chem.* 269, 4713–4716.
- Hanafusa, H., Torii, S., Yasunaga, T., Matsumoto, K., Nishida, E., 2004. Shp2, an SH2-containing protein-tyrosine phosphatase, positively regulates receptor tyrosine kinase signaling by dephosphorylating and inactivating the inhibitor sprouty. *J. Biol. Chem.* 279, 22992–22995. <https://doi.org/10.1074/jbc.M312498200>
- Hanafusa, H., Torii, S., Yasunaga, T., Nishida, E., 2002. Sprouty1 and Sprouty2 provide a control mechanism for the Ras/MAPK signalling pathway. *Nat. Cell Biol.* 4, 850–858. <https://doi.org/10.1038/ncb867>
- Hancock, J.F., Magee, A.I., Childs, J.E., Marshall, C.J., 1989. All ras proteins are polyisoprenylated but only some are palmitoylated. *Cell* 57, 1167–1177. [https://doi.org/10.1016/0092-8674\(89\)90054-8](https://doi.org/10.1016/0092-8674(89)90054-8)
- Hausott, B., Klimaschewski, L., 2019. Sprouty2—a Novel Therapeutic Target in the Nervous System? *Mol. Neurobiol.* <https://doi.org/10.1007/s12035-018-1338-8>
- Hausott, B., Park, J.-W., Valovka, T., Offterdinger, M., Hess, M.W., Geley, S., Klimaschewski, L., 2019. Subcellular Localization of Sprouty2 in Human Glioma Cells. *Front. Mol. Neurosci.* 12. <https://doi.org/10.3389/fnmol.2019.00073>
- Hayashi, T., Rumbaugh, G., Huganir, R.L., 2005. Differential regulation of AMPA receptor subunit trafficking by palmitoylation of two distinct sites. *Neuron* 47, 709–723. <https://doi.org/10.1016/j.neuron.2005.06.035>
- Hayashi, T., Thomas, G.M., Huganir, R.L., 2009. Dual Palmitoylation of NR2 Subunits Regulates NMDA Receptor Trafficking. *Neuron* 64, 213–226.

<https://doi.org/10.1016/j.neuron.2009.08.017>

- Heindel, U., Schmidt, M.F., Veit, M., 2003. Palmitoylation sites and processing of synaptotagmin I, the putative calcium sensor for neurosecretion. *FEBS Lett.* 544, 57–62. [https://doi.org/10.1016/S0014-5793\(03\)00449-6](https://doi.org/10.1016/S0014-5793(03)00449-6)
- Hellsten, E., Vesa, J., Olkkonen, V.M., Jalanko, A., Peltonen, L., 1996. Human palmitoyl protein thioesterase: Evidence for lysosomal targeting of the enzyme and disturbed cellular routing in infantile neuronal ceroid lipofuscinosis. *EMBO J.* 15, 5240–5245. <https://doi.org/10.1002/j.1460-2075.1996.tb00909.x>
- Hemmings, B.A., Restuccia, D.F., 2012. PI3K-PKB/Akt pathway. *Cold Spring Harb. Perspect. Biol.* 4. <https://doi.org/10.1101/cshperspect.a011189>
- Hernandez, J.L., Davda, D., Cheung See Kit, M., Majmudar, J.D., Won, S.J., Gang, M., Pasupuleti, S.C., Choi, A.I., Bartkowiak, C.M., Martin, B.R., 2017. APT2 Inhibition Restores Scribble Localization and S-Palmitoylation in Snail-Transformed Cells. *Cell Chem. Biol.* 24, 87–97. <https://doi.org/10.1016/j.chembiol.2016.12.007>
- Hess, D.T., Slater, T.M., Wilson, M.C., Skene, J.H.P., 1992. The 25 kDa synaptosomal-associated protein SNAP-25 is the major methionine-rich polypeptide in rapid axonal transport and a major substrate for palmitoylation in adult CNS. *J. Neurosci.* 12, 4634–4641. <https://doi.org/10.1523/jneurosci.12-12-04634.1992>
- Hirano, T., Kishi, M., Sugimoto, H., Taguchi, R., Obinata, H., Ohshima, N., Tatei, K., Izumi, T., 2009. Thioesterase activity and subcellular localization of acylprotein thioesterase 1/lysophospholipase 1. *Biochim. Biophys. Acta - Mol. Cell Biol. Lipids* 1791, 797–805. <https://doi.org/10.1016/j.bbalip.2009.05.001>
- Holgren, C., Dougherty, U., Edwin, F., Cerasi, D., Taylor, I., Fichera, A., Joseph, L., Bissonnette, M., Khare, S., 2010. Sprouty-2 controls c-Met expression and metastatic potential of colon cancer cells: Sprouty/c-Met upregulation in human colonic adenocarcinomas. *Oncogene* 29, 5241–5253. <https://doi.org/10.1038/onc.2010.264>

- Huang, K., Sanders, S., Singaraja, R., Orban, P., Cijssouw, T., Arstikaitis, P., Yanai, A., Hayden, M.R., El-Husseini, A., 2009. Neuronal palmitoyl acyl transferases exhibit distinct substrate specificity. *FASEB J.* 23, 2605–2615. <https://doi.org/10.1096/fj.08-127399>
- Huang, K., Sanders, S.S., Kang, R., Carroll, J.B., Sutton, L., Wan, J., Singaraja, R., Young, F.B., Liu, L., El-Husseini, A., Davis, N.G., Hayden, M.R., 2011. Wild-type HTT modulates the enzymatic activity of the neuronal palmitoyl transferase HIP14. *Hum. Mol. Genet.* 20, 3356–3365. <https://doi.org/10.1093/hmg/ddr242>
- Huang, K., Yanai, A., Kang, R., Arstikaitis, P., Singaraja, R.R., Metzler, M., Mullard, A., Haigh, B., Gauthier-Campbell, C., Gutekunst, C.-A., Hayden, M.R., El-Husseini, A., 2004. Huntingtin-Interacting Protein HIP14 Is a Palmitoyl Transferase Involved in Palmitoylation and Trafficking of Multiple Neuronal Proteins polarized protein targeting, and clustering of scaffolding and signaling proteins (El-Husseini and Bredt, 2002; Gauthi, *Neuron*. <https://doi.org/10.1016/j.neuron.2004.11.027>
- Huttlin, E.L., Bruckner, R.J., Paulo, J.A., Cannon, J.R., Ting, L., Baltier, K., Colby, G., Gebreab, F., Gygi, M.P., Parzen, H., Szpyt, J., Tam, S., Zarraga, G., Pontano-Vaites, L., Swarup, S., White, A.E., Schweppe, D.K., Rad, R., Erickson, B.K., Obar, R.A., Guruharsha, K.G., Li, K., Artavanis-Tsakonas, S., Gygi, S.P., Wade Harper, J., 2017. Architecture of the human interactome defines protein communities and disease networks. *Nature* 545, 505–509. <https://doi.org/10.1038/nature22366>
- Iiri, T., Backlund, P.S., Jones, T.L.Z., Wedegaertner, P.B., Bourne, H.R., 1996. Reciprocal regulation of G α , by palmitate and the $\beta\gamma$ subunit. *Proc. Natl. Acad. Sci. U. S. A.* 93, 14592–14597. <https://doi.org/10.1073/pnas.93.25.14592>
- Impagnatiello, M.A., Weitzer, S., Gannon, G., Compagni, A., Cotten, M., Christofori, G., 2001. Mammalian sprouty-1 and -2 are membrane-anchored phosphoprotein inhibitors of growth factor signaling in endothelial cells. *J. Cell Biol.* 152, 1087–1098. <https://doi.org/10.1083/jcb.152.5.1087>
- Jahn, R., Scheller, R.H., 2006. SNAREs - Engines for membrane fusion. *Nat. Rev. Mol.*

Cell Biol. 7, 631–643. <https://doi.org/10.1038/nrm2002>

- Janosi, L., Li, Z., Hancock, J.F., Gorfe, A.A., 2012. Organization, dynamics, and segregation of Ras nanoclusters in membrane domains. *Proc. Natl. Acad. Sci. U. S. A.* 109, 8097–8102. <https://doi.org/10.1073/pnas.1200773109>
- Jarvis, L.A., Toering, S.J., Simon, M.A., Krasnow, M.A., Smith-Bolton, R.K., 2006. Sprouty proteins are in vivo targets of Corkscrews/SHP-2 tyrosine phosphatases. *Development* 133, 1133–1142. <https://doi.org/10.1242/dev.02255>
- Jennings, B.C., Linder, M.E., 2012. DHHC protein S-acyltransferases use similar ping-pong kinetic mechanisms but display different Acyl-CoA specificities. *J. Biol. Chem.* 287, 7236–7245. <https://doi.org/10.1074/jbc.M111.337246>
- Jennings, B.C., Linder, M.E., 2010. Regulation of G proteins by covalent modification, Second Edition, *Handbook of Cell Signaling*, 2/e. Elsevier Inc. <https://doi.org/10.1016/B978-0-12-374145-5.00200-X>
- Jones, D.T., 1999. Protein secondary structure prediction based on position-specific scoring matrices. *J. Mol. Biol.* 292, 195–202. <https://doi.org/10.1006/jmbi.1999.3091>
- Joseph, M., Nagaraj, R., 1995. Conformations of peptides corresponding to fatty acylation sites in proteins. A circular dichroism study. *J. Biol. Chem.* <https://doi.org/10.1074/jbc.270.33.19439>
- Kádková, A., Radecke, J., Sørensen, J.B., 2019. The SNAP-25 Protein Family. *Neuroscience* 420, 50–71. <https://doi.org/10.1016/j.neuroscience.2018.09.020>
- Kang, R., Swayze, R., Lise, M.F., Gerrow, K., Mullard, A., Honer, W.G., El-Husseini, A., 2004. Presynaptic trafficking of synaptotagmin I is regulated by protein palmitoylation. *J. Biol. Chem.* 279, 50524–50536. <https://doi.org/10.1074/jbc.M404981200>
- Kang, R., Wan, J., Arstikaitis, P., Takahashi, H., Huang, K., Bailey, A.O., Thompson, J.X., Roth, A.F., Drisdell, R.C., Mastro, R., Green, W.N., Yates, J.R., Davis, N.G., El-

- Husseini, A., 2008. Neural palmitoyl-proteomics reveals dynamic synaptic palmitoylation. *Nature*. <https://doi.org/10.1038/nature07605>
- Kang, R., Wang, L., Sanders, S.S., Zuo, K., Hayden, M.R., Raymond, L.A., 2019. Altered regulation of striatal neuronal N-methyl-D-aspartate receptor trafficking by palmitoylation in Huntington disease mouse model. *Front. Synaptic Neurosci.* 11. <https://doi.org/10.3389/fnsyn.2019.00003>
- Kasahara, K., Nakayama, Y., Kihara, A., Matsuda, D., Ikeda, K., Kuga, T., Fukumoto, Y., Igarashi, Y., Yamaguchi, N., 2007. Rapid trafficking of c-Src, a non-palmitoylated Src-family kinase, between the plasma membrane and late endosomes/lysosomes. *Exp. Cell Res.* 313, 2651–2666. <https://doi.org/10.1016/j.yexcr.2007.05.001>
- Kathayat, R.S., Cao, Y., Elvira, P.D., Sandoz, P.A., Zaballa, M.E., Springer, M.Z., Drake, L.E., Macleod, K.F., Van Der Goot, F.G., Dickinson, B.C., 2018. Active and dynamic mitochondrial S-depalmitoylation revealed by targeted fluorescent probes. *Nat. Commun.* 9. <https://doi.org/10.1038/s41467-017-02655-1>
- Kawazoe, T., Taniguchi, K., 2019. The Sprouty/Spred family as tumor suppressors: Coming of age. *Cancer Sci.* <https://doi.org/10.1111/cas.13999>
- Kim, H.J., Bar-Sagi, D., 2004. Modulation of signalling by sprouty: A developing story. *Nat. Rev. Mol. Cell Biol.* 5, 441–450. <https://doi.org/10.1038/nrm1400>
- Kim, H.J., Taylor, L.J., Bar-Sagi, D., 2007. Spatial Regulation of EGFR Signaling by Sprouty2. *Curr. Biol.* 17, 455–461. <https://doi.org/10.1016/j.cub.2007.01.059>
- Kim, S.J., Zhang, Z., Sarkar, C., Tsai, P.C., Lee, Y.C., Dye, L., Mukherjee, A.B., 2008. Palmitoyl protein thioesterase-1 deficiency impairs synaptic vesicle recycling at nerve terminals, contributing to neuropathology in humans and mice. *J. Clin. Invest.* 118, 3075–3086. <https://doi.org/10.1172/JCI33482>
- Klein, O.D., Minowada, G., Peterkova, R., Kangas, A., Yu, B.D., Lesot, H., Peterka, M., Jernvall, J., Martin, G.R., 2006. Sprouty Genes Control Diastema Tooth

- Development via Bidirectional Antagonism of Epithelial-Mesenchymal FGF Signaling. *Dev. Cell* 11, 181–190. <https://doi.org/10.1016/j.devcel.2006.05.014>
- Ko, P.J., Woodrow, C., Dubreuil, M.M., Martin, B.R., Skouta, R., Bassik, M.C., Dixon, S.J., 2019. A ZDHHC5-GOLGA7 Protein Acyltransferase Complex Promotes Nonapoptotic Cell Death. *Cell Chem. Biol.* 26, 1716-1724.e9. <https://doi.org/10.1016/j.chembiol.2019.09.014>
- Koegl, M., Zlatkine, P., Ley, S.C., Courtneidge, S.A., Magee, A.I., 1994. Palmitoylation of multiple Src-family kinases at a homologous N-terminal motif. *Biochem. J.* 303, 749–753. <https://doi.org/10.1042/bj3030749>
- Kong, E., Peng, S., Chandra, G., Sarkar, C., Zhang, Z., Bagh, M.B., Mukherjee, A.B., 2013. Dynamic palmitoylation links cytosol-membrane shuttling of acyl-protein thioesterase-1 and acyl-protein thioesterase-2 with that of proto-oncogene H-Ras product and growth-associated protein-43. *J. Biol. Chem.* 288, 9112–9125. <https://doi.org/10.1074/jbc.M112.421073>
- Kosloff, M., Elia, N., Selinger, Z., 2002. Structural homology discloses a bifunctional structural motif at the N-termini of G α proteins. *Biochemistry* 41, 14518–14523. <https://doi.org/10.1021/bi026729x>
- Kozlov, G., Wong, K., Wang, W., Skubák, P., Muñoz-Escobar, J., Liu, Y., Siddiqui, N., Pannu, N.S., Gehring, K., 2018. Ankyrin repeats as a dimerization module. *Biochem. Biophys. Res. Commun.* 495, 1002–1007. <https://doi.org/10.1016/j.bbrc.2017.11.135>
- Kramer, S., Okabe, M., Hacohen, N., Krasnow, M.A., Hiromi, Y., 1999. Sprouty: A common antagonist of FGF and EGF signaling pathways in *Drosophila*. *Development* 126, 2515–2525.
- Kwak, H.J., Kim, Y.J., Chun, K.R., Woo, Y.M., Park, S.J., Jeong, J.A., Jo, S.H., Kim, T.H., Min, H.S., Chae, J.S., Choi, E.J., Kim, G., Shin, S.H., Gwak, H.S., Kim, S.K., Hong, E.K., Lee, G.K., Choi, K.H., Kim, J.H., Yoo, H., Park, J.B., Lee, S.H., 2011. Downregulation of Spry2 by miR-21 triggers malignancy in human gliomas.

- Oncogene 30, 2433–2442. <https://doi.org/10.1038/onc.2010.620>
- Lai, J., Linder, M.E., 2013. Oligomerization of DHHC protein S-acyltransferases. *J. Biol. Chem.* 288, 22862–22870. <https://doi.org/10.1074/jbc.M113.458794>
- Lakkaraju, A.K.K., Abrami, L., Lemmin, T., Blaskovic, S., Kunz, B., Kihara, A., Dal Peraro, M., Van Der Goot, F.G., 2012. Palmitoylated calnexin is a key component of the ribosome-translocon complex. *EMBO J.* 31, 1823–1835. <https://doi.org/10.1038/emboj.2012.15>
- Lane, S.R., Liu, Y., 1997. Characterization of the palmitoylation domain of SNAP-25. *J. Neurochem.* 69, 1864–1869. <https://doi.org/10.1046/j.1471-4159.1997.69051864.x>
- Lao, D.H., Chandramouli, S., Yusoff, P., Chee, W.F., Tzuen, Y.S., Lai, P.T., Chye, Y.Y., Hwei, F.L., Guy, G.R., 2006. A Src homology 3-binding sequence on the C terminus of sprouty2 is necessary for inhibition of the Ras/ERK pathway downstream of fibroblast growth factor receptor stimulation. *J. Biol. Chem.* 281, 29993–30000. <https://doi.org/10.1074/jbc.M604044200>
- Lao, D.H., Yusoff, P., Chandramouli, S., Philp, R.J., Chee, W.F., Jackson, R.A., Tzuen, Y.S., Chye, Y.Y., Guy, G.R., 2007. Direct binding of PP2A to Sprouty2 and phosphorylation changes are a prerequisite for ERK inhibition downstream of fibroblast growth factor receptor stimulation. *J. Biol. Chem.* 282, 9117–9126. <https://doi.org/10.1074/jbc.M607563200>
- Lehtovirta, M., Kyttälä, A., Eskelinen, E.L., Hess, M., Heinonen, O., Jalanko, A., 2001. Palmitoyl protein thioesterase (PPT) localizes into synaptosomes and synaptic vesicles in neurons: Implications for infantile neuronal ceroid lipofuscionosis (INCL). *Hum. Mol. Genet.* 10, 69–75. <https://doi.org/10.1093/hmg/10.1.69>
- Lemmon, M.A., Schlessinger, J., 2010. Cell signaling by receptor tyrosine kinases. *Cell.* <https://doi.org/10.1016/j.cell.2010.06.011>
- Lemonidis, K., Gorleku, O.A., Sanchez-Perez, M.C., Grefen, C., Chamberlain, L.H.,

2014. The Golgi S-acylation machinery comprises zDHHC enzymes with major differences in substrate affinity and S-acylation activity. *Mol. Biol. Cell* 25, 3870–83. <https://doi.org/10.1091/mbc.E14-06-1169>
- Lemonidis, K., MacLeod, R., Baillie, G.S., Chamberlain, L.H., 2017a. Peptide array-based screening reveals a large number of proteins interacting with the ankyrin-repeat domain of the zDHHC17 S-acyltransferase. *J. Biol. Chem.* 292, 17190–17202. <https://doi.org/10.1074/jbc.M117.799650>
- Lemonidis, K., Salaun, C., Kouskou, M., Diez-Ardanuy, C., Chamberlain, L.H., Greaves, J., 2017b. Substrate selectivity in the zDHHC family of S-acyltransferases. *Biochem. Soc. Trans.* 45, 751–758. <https://doi.org/10.1042/BST20160309>
- Lemonidis, K., Sanchez-Perez, M.C., Chamberlain, L.H., 2015a. Identification of a novel sequence motif recognized by the ankyrin repeat domain of zDHHC17/13 S-acyltransferases. *J. Biol. Chem.* 290, 21939–21950. <https://doi.org/10.1074/jbc.M115.657668>
- Lemonidis, K., Werno, M.W., Greaves, J., Diez-Ardanuy, C., Sanchez-Perez, M.C., Salaun, C., Thomson, D.M., Chamberlain, L.H., 2015b. The zDHHC family of S-acyltransferases. *Biochem. Soc. Trans.* 43, 217–221. <https://doi.org/10.1042/BST20140270>
- Levental, I., Lingwood, D., Grzybek, M., Coskun, Ü., Simons, K., 2010. Palmitoylation regulates raft affinity for the majority of integral raft proteins. *Proc. Natl. Acad. Sci. U. S. A.* 107, 22050–22054. <https://doi.org/10.1073/pnas.1016184107>
- Li, X., Brunton, V.G., Burgar, H.R., Wheldon, L.M., Heath, J.K., 2004. FRS2-dependent SRC activation is required for fibroblast growth factor receptor-induced phosphorylation of Sprouty and suppression of ERK activity. *J. Cell Sci.* 117, 6007–6017. <https://doi.org/10.1242/jcs.01519>
- Li, Y., Martin, B.R., Cravatt, B.F., Hofmann, S.L., 2012. DHHC5 protein palmitoylates flotillin-2 and is rapidly degraded on induction of neuronal differentiation in cultured cells. *J. Biol. Chem.* 287, 523–530.

<https://doi.org/10.1074/jbc.M111.306183>

- Liang, X., Nazarian, A., Erdjument-Bromage, H., Bornmann, W., Tempst, P., Resh, M.D., 2001. Heterogeneous Fatty Acylation of Src Family Kinases with Polyunsaturated Fatty Acids Regulates Raft Localization and Signal Transduction. *J. Biol. Chem.* 276, 30987–30994. <https://doi.org/10.1074/jbc.M104018200>
- Lievens, P.M.-J., Kuznetsova, T., Kochlamazashvili, G., Cesca, F., Gorinski, N., Galil, D.A., Cherkas, V., Ronkina, N., Lafera, J., Gaestel, M., Ponimaskin, E., Dityatev, A., 2016. ZDHHC3 Tyrosine Phosphorylation Regulates Neural Cell Adhesion Molecule Palmitoylation. *Mol. Cell. Biol.* 36, 2208–2225. <https://doi.org/10.1128/mcb.00144-16>
- Lim, J., Wong, E.S.M., Siew Hwa Ong, Yusoff, P., Boon Chuan Low, Guy, G.R., 2000. Sprouty proteins are targeted to membrane ruffles upon growth factor receptor tyrosine kinase activation: Identification of a novel translocation domain. *J. Biol. Chem.* 275, 32837–32845. <https://doi.org/10.1074/jbc.M002156200>
- Lim, J., Yusoff, P., Sook, E., Wong, M., Chandramouli, S., Lao, D.-H., Fong, C.W., Guy, G.R., 2002. The Cysteine-Rich Sprouty Translocation Domain Targets Mitogen-Activated Protein Kinase Inhibitory Proteins to Plasma Membranes The Cysteine-Rich Sprouty Translocation Domain Targets Mitogen-Activated Protein Kinase Inhibitory Proteins to Phosphatidylinos. *Mol. Cell. Biol.* 22, 7953–7966. <https://doi.org/10.1128/MCB.22.22.7953>
- Lin, D.T.S., Conibear, E., 2015. ABHD17 proteins are novel protein depalmitoylases that regulate N-Ras palmitate turnover and subcellular localization. *Elife* 4, 1–14. <https://doi.org/10.7554/eLife.11306>
- Linder, M.E., Deschenes, R.J., 2007. Palmitoylation: Policing protein stability and traffic. *Nat. Rev. Mol. Cell Biol.* 8, 74–84. <https://doi.org/10.1038/nrm2084>
- Linder, M.E., Middleton, P., Hepler, J.R., Taussig, R., Gilman, A.G., Mumby, S.M., 1993. Lipid modifications of G proteins: α Subunits are palmitoylated. *Proc. Natl. Acad. Sci. U. S. A.* 90, 3675–3679. <https://doi.org/10.1073/pnas.90.8.3675>

- Lito, P., Mets, B.D., Kleff, S., O'Reilly, S., Maher, V.M., McCormick, J.J., 2008. Evidence that sprouty 2 is necessary for sarcoma formation by H-Ras oncogene-transformed human fibroblasts. *J. Biol. Chem.* 283, 2002–2009. <https://doi.org/10.1074/jbc.M709046200>
- Lo, T.L., Yusoff, P., Fong, C.W., Guo, K., McCaw, B.J., Phillips, W.A., Yang, H., Wong, E.S.M., Leong, H.F., Zeng, Q., Putti, T.C., Guy, G.R., 2004. The Ras/mitogen-activated protein kinase pathway inhibitor and likely tumor suppressor proteins, sprouty 1 and sprouty 2 are deregulated in breast cancer. *Cancer Res.* 64, 6127–6136. <https://doi.org/10.1158/0008-5472.CAN-04-1207>
- Lobo, S., Greentree, W.K., Linder, M.E., Deschenes, R.J., 2002. Identification of a Ras palmitoyltransferase in *Saccharomyces cerevisiae*. *J. Biol. Chem.* 277, 41268–41273. <https://doi.org/10.1074/jbc.M206573200>
- Long, J.Z., Cravatt, B.F., 2011. The metabolic serine hydrolases and their functions in mammalian physiology and disease. *Chem. Rev.* 111, 6022–6063. <https://doi.org/10.1021/cr200075y>
- Lynch, S.J., Snitkin, H., Gumper, I., Philips, M.R., Sabatini, D., Pellicer, A., 2015. The Differential palmitoylation states of N-Ras and H-Ras determine their distinct golgi subcompartment localizations. *J. Cell. Physiol.* 230, 610–619. <https://doi.org/10.1002/jcp.24779>
- Lynes, E.M., Raturi, A., Shenkman, M., Sandoval, C.O., Yap, M.C., Wu, J., Janowicz, A., Myhill, N., Benson, M.D., Campbell, R.E., Berthiaume, L.G., Lederkremer, G.Z., Simmen, T., 2013. Palmitoylation is the switch that assigns calnexin to quality control or ER Ca²⁺ signaling. *J. Cell Sci.* 126, 3893–3903. <https://doi.org/10.1242/jcs.125856>
- Magee, A.I., Gutierrez, L., McKay, I.A., Marshall, C.J., Hall, A., 1987. Dynamic fatty acylation of p21N-ras. *EMBO J.* 6, 3353–3357. <https://doi.org/10.1002/j.1460-2075.1987.tb02656.x>
- Mailleux, A.A., Tefft, D., Ndiaye, D., Itoh, N., Thiery, J.P., Warburton, D., Bellusci, S.,

2001. Evidence that SPROUTY2 functions as an inhibitor of mouse embryonic lung growth and morphogenesis. *Mech. Dev.* 102, 81–94. [https://doi.org/10.1016/S0925-4773\(01\)00286-6](https://doi.org/10.1016/S0925-4773(01)00286-6)
- Marrari, Y., Crouthamel, M., Irannejad, R., Wedegaertner, P.B., 2007. Assembly and trafficking of heterotrimeric G proteins. *Biochemistry.* <https://doi.org/10.1021/bi700338m>
- Martin, B.R., Wang, C., Adibekian, A., Tully, S.E., Cravatt, B.F., 2012. Global profiling of dynamic protein palmitoylation. *Nat. Methods* 9, 84–89. <https://doi.org/10.1038/nmeth.1769>
- Martínez, N., García-Domínguez, C.A., Domingo, B., Oliva, J.L., Zarich, N., Sánchez, A., Gutiérrez-Eisman, S., Llopis, J., Rojas, J.M., 2007. Sprouty2 binds Grb2 at two different proline-rich regions, and the mechanism of ERK inhibition is independent of this interaction. *Cell. Signal.* 19, 2277–2285. <https://doi.org/10.1016/j.cellsig.2007.07.008>
- Mason, J.M., Morrison, D.J., Bassit, B., Dimri, M., Band, H., Licht, J.D., Gross, I., 2004. Tyrosine Phosphorylation of Sprouty Proteins Regulates Their Ability to Inhibit Growth Factor Signaling: A Dual Feedback Loop. *Mol. Biol. Cell* 15, 2176–2188. <https://doi.org/10.1091/mbc.E03-07-0503>
- Mason, J.M., Morrison, D.J., Basson, M.A., Licht, J.D., 2006. Sprouty proteins: Multifaceted negative-feedback regulators of receptor tyrosine kinase signaling. *Trends Cell Biol.* <https://doi.org/10.1016/j.tcb.2005.11.004>
- Masoumi-Moghaddam, S., Amini, A., Morris, D.L., 2014. The developing story of Sprouty and cancer. *Cancer Metastasis Rev.* <https://doi.org/10.1007/s10555-014-9497-1>
- Masoumi-Moghaddam, S., Amini, A., Wei, A.Q., Robertson, G., Morris, D.L., 2015. Sprouty 2 protein, but not Sprouty 4, is an independent prognostic biomarker for human epithelial ovarian cancer. *Int. J. Cancer* 137, 560–570. <https://doi.org/10.1002/ijc.29425>

- Matsumura, K., Taketomi, T., Yoshizaki, K., Arai, S., Sanui, T., Yoshiga, D., Yoshimura, A., Nakamura, S., 2011. Sprouty2 controls proliferation of palate mesenchymal cells via fibroblast growth factor signaling. *Biochem. Biophys. Res. Commun.* 404, 1076–1082. <https://doi.org/10.1016/j.bbrc.2010.12.116>
- McKie, A.B., Douglas, D.A., Olijslagers, S., Graham, J., Omar, M.M., Heer, R., Gnanapragasam, V.J., Robson, C.N., Leung, H.Y., 2005. Epigenetic inactivation of the human sprouty (hSPRY2) homologue in prostate cancer. *Oncogene* 24, 2166–2174. <https://doi.org/10.1038/sj.onc.1208371>
- Microsystems Leica, 2018. LIGHTNING. Image information extraction by adaptive deconvolution.
- Milligan, G., Kostenis, E., 2006. Heterotrimeric G-proteins: A short history. *Br. J. Pharmacol.* <https://doi.org/10.1038/sj.bjp.0706405>
- Minowada, G., Jarvis, L.A., Chi, C.L., Neubüser, A., Sun, X., Hacohen, N., Krasnow, M.A., Martin, G.R., 1999. Vertebrate Sprouty genes are induced by FGF signaling and can cause chondrodysplasia when overexpressed. *Development* 126, 4465–4475.
- Mitchell, D.A., Hamel, L.D., Ishizuka, K., Mitchell, G., Schaefer, L.M., Deschenes, R.J., 2012. The Erf4 subunit of the yeast Ras palmitoyl acyltransferase is required for stability of the Acyl-Erf2 intermediate and palmitoyl transfer to a Ras2 substrate. *J. Biol. Chem.* 287, 34337–34348. <https://doi.org/10.1074/jbc.M112.379297>
- Mitchell, D.A., Hamel, L.D., Reddy, K.D., Farh, L., Rettew, L.M., Sanchez, P.R., Deschenes, R.J., 2014. Mutations in the X-linked intellectual disability gene, zDHHC9, alter autopalmitoylation activity by distinct mechanisms. *J. Biol. Chem.* 289, 18582–18592. <https://doi.org/10.1074/jbc.M114.567420>
- Mitchell, D.A., Mitchell, G., Ling, Y., Budde, C., Deschenes, R.J., 2010. Mutational analysis of *Saccharomyces cerevisiae* Erf2 reveals a two-step reaction mechanism for protein palmitoylation by DHHC enzymes. *J. Biol. Chem.* 285, 38104–38114. <https://doi.org/10.1074/jbc.M110.169102>

- Mitchell, D.A., Vasudevan, A., Linder, M.E., Deschenes, R.J., 2006. Protein palmitoylation by a family of DHHC protein S-acyltransferases. *J. Lipid Res.* <https://doi.org/10.1194/jlr.R600007-JLR200>
- Mól, A.R., Castro, M.S., Fontes, W., 2018. NetWheels: A web application to create high quality peptide helical wheel and net projections. <https://doi.org/10.1101/416347>
- Montojo, M.T., Aganzo, M., González, N., 2017. Huntington's Disease and Diabetes: Chronological Sequence of its Association. *J. Huntingtons. Dis.* <https://doi.org/10.3233/JHD-170253>
- Mumby, S.M., Kleuss, C., Gilman, A.G., 1994. Receptor regulation of G-protein palmitoylation. *Proc. Natl. Acad. Sci. U. S. A.* 91, 2800–2804. <https://doi.org/10.1073/pnas.91.7.2800>
- Muszbek, L., Haramura, G., Cluette-Brown, J.E., Van Cott, E.M., Laposata, M., 1999. The pool of fatty acids covalently bound to platelet proteins by thioester linkages can be altered by exogenously supplied fatty acids, in: *Lipids*. American Oil Chemists Society. <https://doi.org/10.1007/bf02562334>
- Nadeau, R.J., Toher, J.L., Yang, X., Kovalenko, D., Friesel, R., 2007. Regulation of Sprouty2 stability by mammalian seven-in-absentia homolog 2. *J. Cell. Biochem.* 100, 151–160. <https://doi.org/10.1002/jcb.21040>
- Nadolski, M.J., Linder, M.E., 2007. Protein lipidation. *FEBS J.* 274, 5202–5210. <https://doi.org/10.1111/j.1742-4658.2007.06056.x>
- Neve, K.A., Qanbar, R., Bouvier, M., 2003. Role of palmitoylation/depalmitoylation reactions in G-protein-coupled receptor function. *Pharmacol. Ther.* [https://doi.org/10.1016/S0163-7258\(02\)00300-5](https://doi.org/10.1016/S0163-7258(02)00300-5)
- Ng, C., Jackson, R.A., Buschdorf, J.P., Sun, Q., Guy, G.R., Sivaraman, J., 2008. Structural basis for a novel intrapeptidyl H-bond and reverse binding of c-Cbl-TKB domain substrates. *EMBO J.* 27, 804–816. <https://doi.org/10.1038/emboj.2008.18>

- Noritake, J., Fukata, Y., Iwanaga, T., Hosomi, N., Tsutsumi, R., Matsuda, N., Tani, H., Iwanari, H., Mochizuki, Y., Kodama, T., Matsuura, Y., Bredt, D.S., Hamakubo, T., Fukata, M., 2009. Mobile DHHC palmitoylating enzyme mediates activity-sensitive synaptic targeting of PSD-95. *J. Cell Biol.* 186, 147–160. <https://doi.org/10.1083/jcb.200903101>
- Ohlendieck, K., Harding, S.E., 2017. Centrifugation and Ultracentrifugation.
- Ohno, Y., Kihara, A., Sano, T., Igarashi, Y., 2006. Intracellular localization and tissue-specific distribution of human and yeast DHHC cysteine-rich domain-containing proteins. *Biochim. Biophys. Acta - Mol. Cell Biol. Lipids* 1761, 474–483. <https://doi.org/10.1016/j.bbalip.2006.03.010>
- Ohyama, T., Verstreken, P., Ly, C. V., Rosenmund, T., Rajan, A., Tien, A.C., Haueter, C., Schulze, K.L., Bellen, H.J., 2007. Huntingtin-interacting protein 14, a palmitoyl transferase required for exocytosis and targeting of CSP to synaptic vesicles. *J. Cell Biol.* 179, 1481–1496. <https://doi.org/10.1083/jcb.200710061>
- Ozaki, K.I., Miyazaki, S., Tanimura, S., Kohno, M., 2005. Efficient suppression of FGF-2-induced ERK activation by the cooperative interaction among mammalian Sprouty isoforms. *J. Cell Sci.* 118, 5861–5871. <https://doi.org/10.1242/jcs.02711>
- Paik, J.H., Kollipara, R., Chu, G., Ji, H., Xiao, Y., Ding, Z., Miao, L., Tothova, Z., Horner, J.W., Carrasco, D.R., Jiang, S., Gilliland, D.G., Chin, L., Wong, W.H., Castrillon, D.H., DePinho, R.A., 2007. FoxOs Are Lineage-Restricted Redundant Tumor Suppressors and Regulate Endothelial Cell Homeostasis. *Cell* 128, 309–323. <https://doi.org/10.1016/j.cell.2006.12.029>
- Park, J.W., Wollmann, G., Urbiola, C., Fogli, B., Florio, T., Geley, S., Klimaschewski, L., 2018. Sprouty2 enhances the tumorigenic potential of glioblastoma cells. *Neuro. Oncol.* 20, 1044–1054. <https://doi.org/10.1093/neuonc/noy028>
- Parsons, S.J., Parsons, J.T., 2004. Src family kinases, key regulators of signal transduction. *Oncogene* 23, 7906–7909. <https://doi.org/10.1038/sj.onc.1208160>

- Patel, R., Fleming, J., Mui, E., Loveridge, C., Repiscak, P., Blomme, A., Harle, V., Salji, M., Ahmad, I., Teo, K., Hamdy, F.C., Hedley, A., van den Broek, N., Mackay, G., Edwards, J., Sansom, O.J., Leung, H.Y., 2018. Sprouty2 loss-induced IL 6 drives castration-resistant prostate cancer through scavenger receptor B1. *EMBO Mol. Med.* 10, 1–19. <https://doi.org/10.15252/emmm.201708347>
- Patel, R., Gao, M., Ahmad, I., Fleming, J., Singh, L.B., Rai, T.S., McKie, A.B., Seywright, M., Barnetson, R.J., Edwards, J., Sansom, O.J., Leung, H.Y., 2013. Sprouty2, PTEN, and PP2A interact to regulate prostate cancer progression. *J. Clin. Invest.* 123, 1157–1175. <https://doi.org/10.1172/JCI63672>
- Percherancier, Y., Planchenault, T., Valenzuela-Fernandez, A., Virelizier, J.L., Arenzana-Seisdedos, F., Bachelier, F., 2001. Palmitoylation-dependent Control of Degradation, Life Span, and Membrane Expression of the CCR5 Receptor. *J. Biol. Chem.* 276, 31936–31944. <https://doi.org/10.1074/jbc.M104013200>
- Philippe, J.M., Jenkins, P.M., 2019. Spatial organization of palmitoyl acyl transferases governs substrate localization and function. *Mol. Membr. Biol.* 35, 60–75. <https://doi.org/10.1080/09687688.2019.1710274>
- Phizicki, E.M., Fields, S., 1995. Protein-protein interactions (PPIs): Types, methods for detection and analysis, in: *Protein-Protein Interactions: Methods for Detection and Analysis*. pp. 1–165.
- Plowman, S.J., Muncke, C., Parton, R.G., Hancock, J.F., 2005. H-ras, K-ras, and inner plasma membrane raft proteins operate in nanoclusters with differential dependence on the actin cytoskeleton. *Proc. Natl. Acad. Sci.* 102, 15500–15505. <https://doi.org/10.1073/PNAS.0504114102>
- Prior, I.A., Muncke, C., Parton, R.G., Hancock, J.F., 2003. Direct visualization of ras proteins in spatially distinct cell surface microdomains. *J. Cell Biol.* 160, 165–170. <https://doi.org/10.1083/jcb.200209091>
- Purcell, P., Jheon, A., Vivero, M.P., Rahimi, H., Joo, A., Klein, O.D., 2012. Spry1 and Spry2 are essential for development of the temporomandibular joint. *J. Dent.*

Res. 91, 387–393. <https://doi.org/10.1177/0022034512438401>

Putilina, T., Wong, P., Gentleman, S., 1999. The DHHC domain: A new highly conserved cysteine-rich motif. *Mol. Cell. Biochem.* 195, 219–226. <https://doi.org/10.1023/A:1006932522197>

Rana, M.S., Kumar, P., Lee, C.J., Verardi, R., Rajashankar, K.R., Banerjee, A., 2018a. Fatty acyl recognition and transfer by an integral membrane S-acyltransferase. *Science (80-.)*. 359, eaao6326. <https://doi.org/10.1126/science.aao6326>

Rana, M.S., Lee, C.-J., Banerjee, A., 2018b. The molecular mechanism of DHHC protein acyltransferases. *Biochem. Soc. Trans.* BST20180429. <https://doi.org/10.1042/BST20180429>

Rathmanner, N., Haigl, B., Vanas, V., Doriguzzi, A., Gsur, A., Sutterlüty-Fall, H., 2013. Sprouty2 but not Sprouty4 is a potent inhibitor of cell proliferation and migration of osteosarcoma cells. *FEBS Lett.* 587, 2597–2605. <https://doi.org/10.1016/j.febslet.2013.06.040>

Reich, A., Sapir, A., Shilo, B., 1999. Sprouty inhibits RTK signaling. *Development* 126, 4139–4147.

Reilly, L., Howie, J., Wypijewski, K., Ashford, M.L.J., Hilgemann, D.W., Fuller, W., 2015. Palmitoylation of the Na/Ca exchanger cytoplasmic loop controls its inactivation and internalization during stress signaling. *FASEB J.* 29, 4532–4543. <https://doi.org/10.1096/fj.15-276493>

Ren, W., Sun, Y., Du, K., 2013. DHHC17 Palmitoylates ClipR-59 and Modulates ClipR-59 Association with the Plasma Membrane. *Mol. Cell. Biol.* 33, 4255–4265. <https://doi.org/10.1128/mcb.00527-13>

Ren, X., Nicoll, D.A., Galang, G., Philipson, K.D., 2008. Intermolecular cross-linking of Na⁺-Ca²⁺ exchanger proteins: Evidence for dimer formation. *Biochemistry* 47, 6081–6087. <https://doi.org/10.1021/bi800177t>

Resh, M.D., 1999. Fatty acylation of proteins: New insights into membrane targeting

of myristoylated and palmitoylated proteins. *Biochim. Biophys. Acta - Mol. Cell Res.* 1451, 1–16. [https://doi.org/10.1016/S0167-4889\(99\)00075-0](https://doi.org/10.1016/S0167-4889(99)00075-0)

Rikani, A.A., Choudhry, Z., Choudhry, A.M., Rizvi, N., Ikram, H., Mobassarrah, N.J., Tulli, S., 2014. The mechanism of degeeration of striatal neuronal subtypes in Huntington disease. *Ann. Neurosci.* <https://doi.org/10.5214/ans.0972.7531.210308>

Rocks, O., Peyker, A., Kahms, M., Verveer, P.J., Koerner, C., Lumbierres, M., Kuhlmann, J., Waldmann, H., Wittinghofer, A., Bastiaens, P.I.H., 2005. An acylation cycle regulates localization and activity of palmitoylated ras isoforms. *Science (80-.)*. 307, 1746–1752. <https://doi.org/10.1126/science.1105654>

Rodenburg, R.N.P., Snijder, J., Van De Waterbeemd, M., Schouten, A., Granneman, J., Heck, A.J.R., Gros, P., 2017. Stochastic palmitoylation of accessible cysteines in membrane proteins revealed by native mass spectrometry. *Nat. Commun.* 8. <https://doi.org/10.1038/s41467-017-01461-z>

Roth, A.F., Feng, Y., Chen, L., Davis, N.G., 2002. The yeast DHHC cysteine-rich domain protein Akr1p is a palmitoyl transferase. *J. Cell Biol.* 159, 23–28. <https://doi.org/10.1083/jcb.200206120>

Roth, A.F., Wan, J., Bailey, A.O., Sun, B., Kuchar, J.A., Green, W.N., Phinney, B.S., Yates, J.R., Davis, N.G., 2006. Global Analysis of Protein Palmitoylation in Yeast. *Cell* 125, 1003–1013. <https://doi.org/10.1016/j.cell.2006.03.042>

Roy, S., Plowman, S., Rotblat, B., Prior, I.A., Muncke, C., Grainger, S., Parton, R.G., Henis, Y.I., Kloog, Y., Hancock, J.F., 2005. Individual Palmitoyl Residues Serve Distinct Roles in H-Ras Trafficking, Microlocalization, and Signaling. *Mol. Cell Biol.* 25, 6722–6733. <https://doi.org/10.1128/mcb.25.15.6722-6733.2005>

Rubin, C., Litvak, V., Medvedovsky, H., Zwang, Y., Lev, S., Yarden, Y., 2003. Sprouty fine-tunes EGF signaling through interlinked positive and negative feedback loops. *Curr. Biol.* 13, 297–307. [https://doi.org/10.1016/S0960-9822\(03\)00053-8](https://doi.org/10.1016/S0960-9822(03)00053-8)

- Rubin, C., Zwang, Y., Vaisman, N., Ron, D., Yarden, Y., 2005. Phosphorylation of carboxyl-terminal tyrosines modulates the specificity of sprouty-2 inhibition of different signaling pathways. *J. Biol. Chem.* 280, 9735–9744. <https://doi.org/10.1074/jbc.M408308200>
- Saini, D.K., Chisari, M., Gautam, N., 2009. Shuttling and translocation of heterotrimeric G proteins and Ras. *Trends Pharmacol. Sci.* 30, 278–286. <https://doi.org/10.1016/j.tips.2009.04.001>
- Saini, M., Verma, A., Mathew, S.J., 2018. SPRY2 is a novel MET interactor that regulates metastatic potential and differentiation in rhabdomyosarcoma. *Cell Death Dis.* 9. <https://doi.org/10.1038/s41419-018-0261-2>
- Sal-Man, N., Gerber, D., Shai, Y., 2014. Proline localized to the interaction interface can mediate self-association of transmembrane domains. *Biochim. Biophys. Acta - Biomembr.* 1838, 2313–2318. <https://doi.org/10.1016/j.bbamem.2014.05.006>
- Salaün, C., Gould, G.W., Chamberlain, L.H., 2005a. The SNARE proteins SNAP-25 and SNAP-23 display different affinities for lipid rafts in PC12 cells: Regulation by distinct cysteine-rich domains. *J. Biol. Chem.* 280, 1236–1240. <https://doi.org/10.1074/jbc.M410674200>
- Salaün, C., Gould, G.W., Chamberlain, L.H., Salaun, C., Gould, G.W., Chamberlain, L.H., 2005b. Lipid raft association of SNARE proteins regulates exocytosis in PC12 cells. *J. Biol. Chem.* 280, 19449–19453. <https://doi.org/10.1074/jbc.M501923200>
- Salaun, C., Greaves, J., Chamberlain, L.H., 2010. The intracellular dynamic of protein palmitoylation. *J. Cell Biol.* 191, 1229–1238. <https://doi.org/10.1083/jcb.201008160>
- Salaun, C., Greaves, J., Tomkinson, N.C.O., Chamberlain, L.H., 2020a. The linker domain of the SNARE protein SNAP25 acts as a flexible molecular spacer that ensures efficient S-acylation. *J. Biol. Chem.*

<https://doi.org/10.1074/jbc.RA120.012726>

Salaün, C., James, D.J., Chamberlain, L.H., 2004. Lipid rafts and the regulation of exocytosis. *Traffic*. <https://doi.org/10.1111/j.1600-0854.2004.0162.x>

Salaun, C., Locatelli, C., Zmuda, F., Cabrera González, J., Chamberlain, L.H., 2020b. Accessory proteins of the zDHHC family of S-acylation enzymes. *J. Cell Sci.* <https://doi.org/10.1242/jcs.251819>

Salaun, C., Ritchie, L., Greaves, J., Bushell, T.J., Chamberlain, L.H., 2017. The C-terminal domain of zDHHC2 contains distinct sorting signals that regulate intracellular localisation in neurons and neuroendocrine cells. *Mol. Cell. Neurosci.* 85, 235–246. <https://doi.org/10.1016/j.mcn.2017.07.007>

Sanders, S.S., Parsons, M.P., Mui, K.K.N., Southwell, A.L., Franciosi, S., Cheung, D., Walzl, S., Raymond, L.A., Hayden, M.R., 2016. Sudden death due to paralysis and synaptic and behavioral deficits when *Hip14/Zdhhc17* is deleted in adult mice. *BMC Biol.* 14, 108. <https://doi.org/10.1186/s12915-016-0333-7>

Sasaki, A., Taketomi, T., Kato, R., Saeki, K., Nonami, A., Sasaki, M., Kuriyama, M., Saito, N., Shibuya, M., Yoshimura, A., 2003. Mammalian Sprouty4 suppresses Ras-independent ERK activation by binding to Raf1. *Nat. Cell Biol.* 5, 427–432. <https://doi.org/10.1038/ncb978>

Sasaki, A., Taketomi, T., Wakioka, T., Kato, R., Yoshimura, A., 2001. Identification of a Dominant Negative Mutant of Sprouty that Potentiates Fibroblast Growth Factor-but Not Epidermal Growth Factor-induced ERK Activation. *J. Biol. Chem.* 276, 36804–36808. <https://doi.org/10.1074/jbc.C100386200>

Sato, I., Obata, Y., Kasahara, K., Nakayama, Y., Fukumoto, Y., Yamasaki, T., Yokoyama, K.K., Saito, T., Yamaguchi, N., 2009. Differential trafficking of Src, Lyn, Yes and Fyn is specified by the state of palmitoylation in the SH4 domain. *J. Cell Sci.* 122, 965–975. <https://doi.org/10.1242/jcs.034843>

Schaaf, G., Hamdi, M., Zwijnenburg, D., Lakeman, A., Geerts, D., Versteeg, R., Kool,

- M., 2010. Silencing of SPRY1 triggers complete regression of rhabdomyosarcoma tumors carrying a mutated RAS gene. *Cancer Res.* 70, 762–771. <https://doi.org/10.1158/0008-5472.CAN-09-2532>
- Schmidt, M.F.G., Bracha, M., Schlesinger, M.J., 1979. Evidence for covalent attachment of fatty acids to Sindbis virus glycoproteins (membranes/sodium dodecyl sulfate/polyacrylamide gel/palmitate), *Biochemistry*.
- Schutzman, J.L., Martin, G.R., 2012. Sprouty genes function in suppression of prostate tumorigenesis. *Proc. Natl. Acad. Sci. U. S. A.* 109, 20023–20028. <https://doi.org/10.1073/pnas.1217204109>
- Segal-Salto, M., Sapir, T., Reiner, O., 2016. Reversible cysteine acylation regulates the activity of human palmitoyl-protein thioesterase 1 (PPT1). *PLoS One* 11. <https://doi.org/10.1371/journal.pone.0146466>
- Sezgin, E., Levental, I., Mayor, S., Eggeling, C., 2017. The mystery of membrane organization: Composition, regulation and roles of lipid rafts. *Nat. Rev. Mol. Cell Biol.* <https://doi.org/10.1038/nrm.2017.16>
- Shahinian, S., Silvius, J.R., 1995. Doubly-Lipid-Modified Protein Sequence Motifs Exhibit Long-Lived Anchorage to Lipid Bilayer Membranes. *Biochemistry* 34, 3813–3822. <https://doi.org/10.1021/bi00011a039>
- Shenoy-Scaria, A.M., Dietzen, D.J., Kwong, J., Link, D.C., Lublin, D.M., 1994. Cysteine3 of Src family protein tyrosine kinases determines palmitoylation and localization in caveolae. *J. Cell Biol.* 126, 353–363. <https://doi.org/10.1083/jcb.126.2.353>
- Shim, K., Minowada, G., Coling, D.E., Martin, G.R., 2005. Sprouty2, a mouse deafness gene, regulates cell fate decisions in the auditory sensory epithelium by antagonizing FGF signaling. *Dev. Cell* 8, 553–564. <https://doi.org/10.1016/j.devcel.2005.02.009>
- Shipston, M.J., 2014a. S-acylation dependent post-translational cross-talk regulates large conductance calcium- and voltage- activated potassium (BK) channels.

Front. Physiol. 5 JUL, 1–9. <https://doi.org/10.3389/fphys.2014.00281>

Shipston, M.J., 2014b. Ion channel regulation by protein S-acylation. *J. Gen. Physiol.* <https://doi.org/10.1085/jgp.201411176>

Shukla, A., Rai, K., Shukla, V., Chaturvedi, N.K., Bociek, R.G., Pirruccello, S.J., Band, H., Lu, R., Joshi, S.S., 2016. Sprouty 2: A novel attenuator of B-cell receptor and MAPK-Erk signaling in CLL. *Blood* 127, 2310–2321. <https://doi.org/10.1182/blood-2015-09-669317>

Sievers, F., Wilm, A., Dineen, D., Gibson, T.J., Karplus, K., Li, W., Lopez, R., McWilliam, H., Remmert, M., Söding, J., Thompson, J.D., Higgins, D.G., 2011. Fast, scalable generation of high-quality protein multiple sequence alignments using Clustal Omega. *Mol. Syst. Biol.* 7. <https://doi.org/10.1038/msb.2011.75>

Singaraja, R.R., Hadano, S., Metzler, M., Givan, S., Wellington, C.L., Warby, S., Yanai, A., Gutekunst, C.-A., Leavitt, B.R., Yi, H., Fichter, K., Gan, L., McCutcheon, K., Chopra, V., Michel, J., Hersch, S.M., Ikeda, J.-E., Hayden, M.R., 2002. HIP14, a novel ankyrin domain-containing protein, links huntingtin to intracellular trafficking and endocytosis. *Hum. Mol. Genet.* 11, 2815–28. <https://doi.org/10.1093/hmg/11.23.2815>

Singaraja, R.R., Huang, K., Sanders, S.S., Milnerwood, A.J., Hines, R., Lerch, J.P., Franciosi, S., Drisdell, R.C., Vaid, K., Young, F.B., Doty, C., Wan, J., Bissada, N., Henkelman, R.M., Green, W.N., Davis, N.G., Raymond, L.A., Hayden, M.R., 2011. Altered palmitoylation and neuropathological deficits in mice lacking HIP14. *Hum. Mol. Genet.* 20, 3899–3909. <https://doi.org/10.1093/hmg/ddr308>

Sirivatanauskorn, Y., Sirivatanauskorn, V., Srisawat, C., Khongmanee, A., Tongkham, C., 2012. Differential expression of sprouty genes in hepatocellular carcinoma. *J. Surg. Oncol.* 105, 273–276. <https://doi.org/10.1002/jso.22095>

Skotte, N.H., Sanders, S.S., Singaraja, R.R., Ehrnhoefer, D.E., Vaid, K., Qiu, X., Kannan, S., Verma, C., Hayden, M.R., 2017. Palmitoylation of caspase-6 by HIP14 regulates its activation. *Cell Death Differ.* 24, 433–444.

<https://doi.org/10.1038/cdd.2016.139>

Slow, E.J., van Raamsdonk, J., Rogers, D., Coleman, S.H., Graham, R.K., Deng, Y., Oh, R., Bissada, N., Hossain, S.M., Yang, Y.Z., Li, X.J., Simpson, E.M., Gutekunst, C.A., Leavitt, B.R., Hayden, M.R., 2003. Selective striatal neuronal loss in a YAC128 mouse model of Huntington disease. *Hum. Mol. Genet.* <https://doi.org/10.1093/hmg/ddg169>

Smotrys, J.E., Linder, M.E., 2004. Palmitoylation of Intracellular Signaling Proteins: Regulation and Function. *Annu. Rev. Biochem.* 73, 559–587. <https://doi.org/10.1146/annurev.biochem.73.011303.073954>

Solis, G.P., Valnohova, J., Alvarez, C., Katanaev, V.L., 2020. Local and substrate-specific S-palmitoylation determines subcellular localization of Gαo. *bioRxiv* 2020.08.25.266692.

Sparr, E., Ash, W.L., Nazarov, P. V., Rijkers, D.T.S., Hemminga, M.A., Tieleman, D.P., Killian, J.A., 2005. Self-association of transmembrane α -helices in model membranes: Importance of helix orientation and role of hydrophobic mismatch. *J. Biol. Chem.* 280, 39324–39331. <https://doi.org/10.1074/jbc.M502810200>

Strathmann, M.P., Simon, M.I., 1991. G α 12 and G α 13 subunits define a fourth class of G protein α subunits. *Proc. Natl. Acad. Sci. U. S. A.* 88, 5582–5586. <https://doi.org/10.1073/pnas.88.13.5582>

Sugimoto, H., Hayashi, H., Yamashita, S., 1996. Purification, cDNA cloning, and regulation of lysophospholipase from rat liver. *J. Biol. Chem.* 271, 7705–7711. <https://doi.org/10.1074/jbc.271.13.7705>

Sutterlüty, H., Mayer, C.E., Setinek, U., Attems, J., Ovtcharov, S., Mikula, M., Mikulits, W., Micksche, M., Berger, W., 2007. Down-regulation of Sprouty2 in non-small cell lung cancer contributes to tumor malignancy via extracellular signal-regulated kinase pathway-dependent and -independent mechanisms. *Mol. Cancer Res.* 5, 509–520. <https://doi.org/10.1158/1541-7786.MCR-06-0273>

- Swarthout, J.T., Lobo, S., Farh, L., Croke, M.R., Greentree, W.K., Deschenes, R.J., Linder, M.E., 2005. DHHC9 and GCP16 constitute a human protein fatty acyltransferase with specificity for H- and N-Ras. *J. Biol. Chem.* 280, 31141–31148. <https://doi.org/10.1074/jbc.M504113200>
- Sweet, S.M.M., Mardakheh, F.K., Ryan, K.J.P., Langton, A.J., Heath, J.K., Cooper, H.J., 2008. Targeted online liquid chromatography electron capture dissociation mass spectrometry for the localization of sites of in vivo phosphorylation in human Sprouty2. *Anal. Chem.* 80, 6650–6657. <https://doi.org/10.1021/ac800963a>
- Taketomi, T., Yoshiga, D., Taniguchi, K., Kobayashi, T., Nonami, A., Kato, R., Sasaki, M., Sasaki, A., Ishibashi, H., Moriyama, M., Nakamura, K.I., Nishimura, J., Yoshimura, A., 2005. Loss of mammalian Sprouty2 leads to enteric neuronal hyperplasia and esophageal achalasia. *Nat. Neurosci.* 8, 855–857. <https://doi.org/10.1038/nn1485>
- Taniguchi, K., Ayada, T., Ichiyama, K., Kohno, R. ichiro, Yonemitsu, Y., Minami, Y., Kikuchi, A., Maehara, Y., Yoshimura, A., 2007. Sprouty2 and Sprouty4 are essential for embryonic morphogenesis and regulation of FGF signaling. *Biochem. Biophys. Res. Commun.* 352, 896–902. <https://doi.org/10.1016/j.bbrc.2006.11.107>
- Taylor, B.S., Schultz, N., Hieronymus, H., Gopalan, A., Xiao, Y., Carver, B.S., Arora, V.K., Kaushik, P., Cerami, E., Reva, B., Antipin, Y., Mitsiades, N., Landers, T., Dolgalev, I., Major, J.E., Wilson, M., Socci, N.D., Lash, A.E., Heguy, A., Eastham, J.A., Scher, H.I., Reuter, V.E., Scardino, P.T., Sander, C., Sawyers, C.L., Gerald, W.L., 2010. Integrative Genomic Profiling of Human Prostate Cancer. *Cancer Cell* 18, 11–22. <https://doi.org/10.1016/j.ccr.2010.05.026>
- Tefft, D., Lee, M., Smith, S., Crowe, D.L., Bellusci, S., Warburton, D., 2002. mSprouty2 inhibits FGF10-activated MAP kinase by differentially binding to upstream target proteins. *Am. J. Physiol. - Lung Cell. Mol. Physiol.* 283, 700–706. <https://doi.org/10.1152/ajplung.00372.2001>

- Tian, L., McClafferty, H., Knaus, H.G., Ruth, P., Shipston, M.J., 2012. Distinct acyl protein transferases and thioesterases control surface expression of calcium-activated potassium channels. *J. Biol. Chem.* 287, 14718–14725. <https://doi.org/10.1074/jbc.M111.335547>
- Tomatis, V.M., Trenchi, A., Gomez, G.A., Daniotti, J.L., 2010. Acyl-protein thioesterase 2 catalyzes the deacylation of peripheral membrane-associated GAP-43. *PLoS One* 5, 15045. <https://doi.org/10.1371/journal.pone.0015045>
- Topinka, J.R., Brecht, D.S., 1998. N-terminal palmitoylation of PSD-95 regulates association with cell membranes and interaction with K⁺ channel K(v)1.4. *Neuron* 20, 125–134. [https://doi.org/10.1016/S0896-6273\(00\)80440-7](https://doi.org/10.1016/S0896-6273(00)80440-7)
- Tortosa, E., Adolfs, Y., Fukata, M., Pasterkamp, R.J., Kapitein, L.C., Hoogenraad, C.C., 2017. Dynamic Palmitoylation Targets MAP6 to the Axon to Promote Microtubule Stabilization during Neuronal Polarization. *Neuron* 94, 809-825.e7. <https://doi.org/10.1016/j.neuron.2017.04.042>
- Toyoda, T., Sugimoto, H., Yamashita, S., 1999. Sequence, expression in *Escherichia coli*, and characterization of lysophospholipase II. *Biochim. Biophys. Acta - Mol. Cell Biol. Lipids* 1437, 182–193. [https://doi.org/10.1016/S1388-1981\(99\)00007-4](https://doi.org/10.1016/S1388-1981(99)00007-4)
- Tsavachidou, D., Coleman, M.L., Athanasiadis, G., Li, S., Licht, J.D., Olson, M.F., Weber, B.L., 2004. SPRY2 is an inhibitor of the Ras/extracellular signal-regulated kinase pathway in melanocytes and melanoma cells with wild-type BRAF but not with the V599E mutant. *Cancer Res.* 64, 5556–5559. <https://doi.org/10.1158/0008-5472.CAN-04-1669>
- Tsutsumi, R., Fukata, Y., Noritake, J., Iwanaga, T., Perez, F., Fukata, M., 2009. Identification of G Protein α Subunit-Palmitoylating Enzyme. *Mol. Cell. Biol.* 29, 435–447. <https://doi.org/10.1128/mcb.01144-08>
- Udeshi, N.D., Svinkina, T., Mertins, P., Kuhn, E., Mani, D.R., Qiao, J.W., Carr, S.A., 2013. Refined preparation and use of anti-diglycine remnant (k- ϵ -gg) antibody enables

routine quantification of 10,000s of ubiquitination sites in single proteomics experiments. *Mol. Cell. Proteomics* 12, 825–831. <https://doi.org/10.1074/mcp.O112.027094>

Valdez-Taubas, J., Pelham, H., 2005. Swf1-dependent palmitoylation of the SNARE Tlg1 prevents its ubiquitination and degradation. *EMBO J.* 24, 2524–2532. <https://doi.org/10.1038/sj.emboj.7600724>

Van 't Hof, W., Resh, M.D., 1997. Rapid plasma membrane anchoring of newly synthesized p59(fyn): Selective requirement for NH₂-terminal myristoylation and palmitoylation at cysteine-3. *J. Cell Biol.* 136, 1023–1035. <https://doi.org/10.1083/jcb.136.5.1023>

Vaquero, M., Cuesta, S., Anerillas, C., Altés, G., Ribera, J., Basson, M.A., Licht, J.D., Egea, J., Encinas, M., 2019. Sprouty1 controls genitourinary development via its N-terminal tyrosine. *J. Am. Soc. Nephrol.* 30, 1398–1411. <https://doi.org/10.1681/ASN.2018111085>

Vartak, N., Papke, B., Grecco, H.E., Rossmannek, L., Waldmann, H., Hedberg, C., Bastiaens, P.I.H., 2014. The autodepalmitoylating activity of APT maintains the spatial organization of palmitoylated membrane proteins. *Biophys. J.* 106, 93–105. <https://doi.org/10.1016/j.bpj.2013.11.024>

Veit, M., Reverey, H., Schmidt, M.F.G., 1996a. Cytoplasmic tail length influences fatty acid selection for acylation of viral glycoproteins. *Biochem. J.* 318, 163–172. <https://doi.org/10.1042/bj3180163>

Veit, M., Söllner, T.H., Rothman, J.E., 1996b. Multiple palmitoylation of synaptotagmin and the t-SNARE SNAP-25. *FEBS Lett.* 385, 119–123. [https://doi.org/10.1016/0014-5793\(96\)00362-6](https://doi.org/10.1016/0014-5793(96)00362-6)

Velasco, A., Pallares, J., Santacana, M., Gatus, S., Fernandez, M., Domingo, M., Valls, J., Yeramian, A., Encinas, M., Dolcet, X., Matias-Guiu, X., 2011. Promoter hypermethylation and expression of sprouty 2 in endometrial carcinoma. *Hum. Pathol.* 42, 185–193. <https://doi.org/10.1016/j.humpath.2010.08.001>

- Verardi, R., Kim, J.S., Ghirlando, R., Banerjee, A., 2017. Structural Basis for Substrate Recognition by the Ankyrin Repeat Domain of Human DHHC17 Palmitoyltransferase. *Structure* 25, 1337-1347.e6. <https://doi.org/10.1016/j.str.2017.06.018>
- Verkruyse, L.A., Hofmann, S.L., 1996. Lysosomal targeting of palmitoyl-protein thioesterase. *J. Biol. Chem.* 271, 15831–15836. <https://doi.org/10.1074/jbc.271.26.15831>
- Vogel, K., Roche, P.A., 1999. SNAP-23 and SNAP-25 are palmitoylated in vivo. *Biochem. Biophys. Res. Commun.* 258, 407–410. <https://doi.org/10.1006/bbrc.1999.0652>
- Walsh, A.M., Kapoor, G.S., Buonato, J.M., Mathew, L.K., Bi, Y., Davuluri, R. V, Martinez-Lage, M., Simon, M.C., O'Rourke, D.M., Lazzara, M.J., 2015. Sprouty2 drives drug resistance and proliferation in Glioblastoma. *Mol. Cancer Res.* 13, 1227–1237. <https://doi.org/10.1158/1541-7786.MCR-14-0183-T>
- Wang, J.H., Zhou, W.W., Cheng, S.T., Liu, B.X., Liu, F.R., Song, J.Q., 2015. Downregulation of Sprouty homolog 2 by microRNA-21 inhibits proliferation, metastasis and invasion, however promotes the apoptosis of multiple myeloma cells. *Mol. Med. Rep.* 12, 1810–1816. <https://doi.org/10.3892/mmr.2015.3567>
- Wang, Z., Qin, C., Zhang, J., Han, Z., Tao, J., Cao, Q., Zhou, W., Xu, Z., Zhao, C., Tan, R., Gu, M., 2017. MiR-122 promotes renal cancer cell proliferation by targeting Sprouty2. *Tumor Biol.* 39. <https://doi.org/10.1177/1010428317691184>
- Wedegaertner, P.B., 2012. G Protein Trafficking. *Subcell. Biochem.* 63, 193–223. https://doi.org/10.1007/978-94-007-4765-4_11
- Wedegaertner, P.B., Bourne, H.R., 1994. Activation and depalmitoylation of G α . *Cell* 77, 1063–1070. [https://doi.org/10.1016/0092-8674\(94\)90445-6](https://doi.org/10.1016/0092-8674(94)90445-6)
- Wepy, J.A., Galligan, J.J., Kingsley, P.J., Xu, S., Goodman, M.C., Tallman, K.A., Rouzer, C.A., Marnett, L.J., 2019. Lysophospholipases cooperate to mediate lipid

- homeostasis and lysophospholipid signaling. *J. Lipid Res.* 60, 360–374.
<https://doi.org/10.1194/jlr.M087890>
- Wimley, W.C., White, S.H., 1996. Experimentally determined hydrophobicity scale for proteins at membrane interfaces. *Nat. Struct. Biol.* 3, 842–848.
<https://doi.org/10.1038/nsb1096-842>
- Won, S.J., Cheung See Kit, M., Martin, B.R., 2018. Protein depalmitoylases. *Crit. Rev. Biochem. Mol. Biol.* 53, 83–98.
<https://doi.org/10.1080/10409238.2017.1409191>
- Won, S.J., Davda, D., Labby, K.J., Hwang, S.Y., Pricer, R., Majmudar, J.D., Armacost, K.A., Rodriguez, L.A., Rodriguez, C.L., Chong, F.S., Torossian, K.A., Palakurthi, J., Hur, E.S., Meagher, J.L., Brooks, C.L., Stuckey, J.A., Martin, B.R., 2016. Molecular Mechanism for Isoform-Selective Inhibition of Acyl Protein Thioesterases 1 and 2 (APT1 and APT2). *ACS Chem. Biol.* 11, 3374–3382.
<https://doi.org/10.1021/acscchembio.6b00720>
- Wong, E.S.M., Fong, C.W., Lim, J., Yusoff, P., Low, B.C., Langdon, W.Y., Guy, G.R., 2002. Sprouty2 attenuates epidermal growth factor receptor ubiquitylation and endocytosis, and consequently enhances Ras/ERK signalling. *EMBO J.* 21, 4796–4808. <https://doi.org/10.1093/emboj/cdf493>
- Wong, E.S.M., Lim, J., Low, B.C., Chen, Q., Guy, G.R., 2001. Evidence for Direct Interaction between Sprouty and Cbl. *J. Biol. Chem.* 276, 5866–5875.
<https://doi.org/10.1074/jbc.M006945200>
- Woodley, K.T., Collins, M.O., 2019. S-acylated Golga7b stabilises DHHC 5 at the plasma membrane to regulate cell adhesion. *EMBO Rep.* 20, 1–19.
<https://doi.org/10.15252/embr.201847472>
- Xu, Y.-F., Liu, H.-D., Liu, Z.-L., Pan, C., Yang, X.-Q., Ning, S.-L., Zhang, Z.-L., Guo, S., Yu, J.-M., 2018. Sprouty2 suppresses progression and correlates to favourable prognosis of intrahepatic cholangiocarcinoma via antagonizing FGFR2 signalling. *J. Cell. Mol. Med.* 1–11. <https://doi.org/10.1111/jcmm.13833>

- Yanai, A., Huang, K., Kang, R., Singaraja, R.R., Arstikaitis, P., Gan, L., Orban, P.C., Mullard, A., Cowan, C.M., Raymond, L.A., Drisdell, R.C., Green, W.N., Ravikumar, B., Rubinsztein, D.C., El-Husseini, A., Hayden, M.R., 2006. Palmitoylation of huntingtin by HIP14 is essential for its trafficking and function. *Nat. Neurosci.* 9, 824–831. <https://doi.org/10.1038/nn1702>
- Yang, G., Cynader, M.S., 2011. Palmitoyl acyltransferase zD17 mediates neuronal responses in acute ischemic brain injury by regulating JNK activation in a signaling module. *J. Neurosci.* 31, 11980–11991. <https://doi.org/10.1523/jneurosci.2510-11.2011>
- Yang, W., Di Vizio, D., Kirchner, M., Steen, H., Freeman, M.R., 2010. Proteome scale characterization of human S-acylated proteins in lipid raft-enriched and non-raft membranes. *Mol. Cell. Proteomics* 9, 54–70. <https://doi.org/10.1074/mcp.M800448-MCP200>
- Yang, X., Kilgallen, S., Andreeva, V., Spicer, D.B., Pinz, I., Friesel, R., 2010. Conditional expression of Spry1 in neural crest causes craniofacial and cardiac defects. *BMC Dev. Biol.* 10, 1–12. <https://doi.org/10.1186/1471-213X-10-48>
- Yigzaw, Y., Poppleton, H.M., Sreejayan, N., Hassid, A., Patel, T.B., 2003. Protein-tyrosine phosphatase-1B (PTP1B) mediates the anti-migratory actions of sprouty. *J. Biol. Chem.* 278, 284–288. <https://doi.org/10.1074/jbc.M210359200>
- Yim, D.G.R., Ghosh, S., Guy, G.R., Virshup, D.M., 2015. Casein kinase 1 regulates Sprouty2 in FGF-ERK signaling. *Oncogene* 34, 474–484. <https://doi.org/10.1038/onc.2013.564>
- Yokoi, N., Fukata, Y., Sekiya, A., Murakami, T., Kobayashi, K., Fukata, M., 2016. Identification of PSD-95 depalmitoylating enzymes. *J. Neurosci.* 36, 6431–6444. <https://doi.org/10.1523/JNEUROSCI.0419-16.2016>
- Yu, X., Yang, G., Yan, C., Baylon, J.L., Jiang, J., Fan, H., Lu, G., Hasegawa, K., Okumura, H., Wang, T., Tajkhorshid, E., Li, S., Yan, N., 2017. Dimeric structure of the uracil:proton symporter UraA provides mechanistic insights into the SLC4/23/26

- transporters. *Cell Res.* 27, 1020–1033. <https://doi.org/10.1038/cr.2017.83>
- Yurchak, L.K., Sefton, B.M., 1995. Palmitoylation of either Cys-3 or Cys-5 is required for the biological activity of the Lck tyrosine protein kinase. *Mol. Cell. Biol.* 15, 6914–6922. <https://doi.org/10.1128/mcb.15.12.6914>
- Yusoff, P., Lao, D.H., Ong, S.H., Miin Wong, E.S., Lim, J., Lo, T.L., Leong, H.F., Fong, C.W., Guy, G.R., 2002. Sprouty2 inhibits the Ras/MAP kinase pathway by inhibiting the activation of Raf. *J. Biol. Chem.* 277, 3195–3201. <https://doi.org/10.1074/jbc.M108368200>
- Zaballa, M.E., van der Goot, F.G., 2018. The molecular era of protein S-acylation: spotlight on structure, mechanisms, and dynamics. *Crit. Rev. Biochem. Mol. Biol.* <https://doi.org/10.1080/10409238.2018.1488804>
- Zeidman, R., Buckland, G., Cebecauer, M., Eissmann, P., Davis, D.M., Magee, A.I., 2011. DHHC2 is a protein S-acyltransferase for Lck. *Mol. Membr. Biol.* 28, 473–486. <https://doi.org/10.3109/09687688.2011.630682>
- Zhang, F., Di, Y., Li, J., Shi, Y., Zhang, L., Wang, C., He, X., Liu, Y., Wan, D., Huo, K., Gu, J., 2006. Molecular cloning and characterization of human Aph2 gene, involved in AP-1 regulation by interaction with JAB1. *Biochim. Biophys. Acta - Gene Struct. Expr.* 1759, 514–525. <https://doi.org/10.1016/j.bbaexp.2006.10.002>
- Zhang, W., Lv, Y., Xue, Y., Wu, C., Yao, K., Zhang, C., Jin, Q., Huang, R., Li, J., Sun, Y., Su, X., Jiang, T., Fan, X., 2016. Co-expression modules of NF1, PTEN and sprouty enable distinction of adult diffuse gliomas according to pathway activities of receptor tyrosine kinases. *Oncotarget* 7, 59098–59114. <https://doi.org/10.18632/oncotarget.10359>
- Zhao, L., Lobo, S., Dong, X., Ault, A.D., Deschenes, R.J., 2002. Erf4p and Erf2p form an endoplasmic reticulum-associated complex involved in the plasma membrane localization of yeast Ras proteins. *J. Biol. Chem.* 277, 49352–49359. <https://doi.org/10.1074/jbc.M209760200>

Zhao, Q., Chen, S., Zhu, Z., Yu, L., Ren, Y., Jiang, M., Weng, J., Li, B., 2018. miR-21 promotes EGF-induced pancreatic cancer cell proliferation by targeting Spry2. *Cell Death Dis.* 9. <https://doi.org/10.1038/s41419-018-1182-9>

Zingler, P., Särchen, V., Glatter, T., Caning, L., Saggau, C., Kathayat, R.S., Dickinson, B.C., Adam, D., Schneider-Brachert, W., Schütze, S., Fritsch, J., 2019. Palmitoylation is required for TNF-R1 signaling. *Cell Commun. Signal.* 17, 1–16. <https://doi.org/10.1186/s12964-019-0405-8>

Books

Alberts, B., Johnson, A., Lewis, J. Raff, M., Roberts, K., & Walter, P. (2015). 6th edition. *Molecular biology of the cell*. New York, Garland Science.

Deschenes, Rj. (2013). 2nd edition. *Encyclopaedia of Biological Chemistry*. Academic Press

Linder, M. E. (2019). *Protein Lipidation: Methods and Protocols*. New York, Humana Press [_https://www.springer.com/gp/book/9781493995318](https://www.springer.com/gp/book/9781493995318)

Web Links

<https://www.uniprot.org/uniprot/O43609> (hSPRY1 - UniProtKB)

<https://www.uniprot.org/uniprot/O43597> (hSPRY2 - UniProtKB)

<https://www.uniprot.org/uniprot/Q9QXV8> (mSPRY2 - UniProtKB)

<https://www.uniprot.org/uniprot/O43610> (hSPRY3 - UniProtKB)

<https://www.uniprot.org/uniprot/Q9C004> (hSPRY4 - UniProtKB)

<https://www.ncbi.nlm.nih.gov/gene/10252> (SPRY1 - GeneBank)

<https://www.ncbi.nlm.nih.gov/gene/10253> (SPRY2 - GeneBank)

<https://www.ncbi.nlm.nih.gov/gene/10251> (SPRY3 - GeneBank)

<https://www.ncbi.nlm.nih.gov/gene/81848> (SPRY4 - GeneBank)



University of Strathclyde

Protein interactions mediated by the Ankyrin - Repeat Domain of the S-acyltransferase zDHHC17

Carolina Locatelli¹, Kimon Lemonidis², Christine Salami¹ and Luke Chamberlain¹

¹ Strathclyde Institute of Pharmacy and Biomedical Sciences, University of Strathclyde, Glasgow, UK.
² Institute of Molecular, Cell and Systemic Biology, University of Glasgow, Glasgow, UK.
 carolina.locatelli@strath.ac.uk



Chamberlain Lab
UNIVERSITY OF STRATHCLYDE

Introduction

zDHC enzymes mediate protein S-acylation: a post-translational modification in which a long fatty acid chain is reversibly attached onto free cysteines. S-acylation affects protein trafficking and membrane binding [1].

There are 23 highly conserved zDHC enzyme isoforms all defined by a 'DHC' motif with the two Cys/CoI localized zDHHC13 and zDHHC17 characterized by an additional *N-terminal ankyrin-repeat domain* (AR domain, Fig. 1).

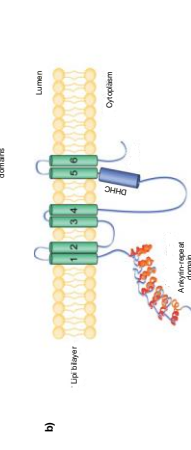


Fig. 1. zDHHC17 schematic structure and functional domains

a) and b) zDHHC17 protein consists of an NH₂-terminal seven ankyrin-repeat domain (in orange, zD structure are in six transmembrane domains (in green, numbered 1-6) and a zDHC-CR catalytic domain (in blue, numbered 1-4) and a DHC-CR catalytic domain (in blue, numbered 1-4). Both catalytic domain and AR domain lay in the cytoplasm where substrates are recognised (based on [2]).

→ The AR domain of zDHHC17 actively recognizes and binds a consensus sequence [VAP]VTXXQP in the substrates (zDAMB in Fig. 2 [3-4]).

→ Specific amino acids in zDHHC17 within residues 100-130 of the AR domain are involved in recognition and binding of partner proteins [5].

Here, we report that while specific amino acid mutations, within the above mentioned residues 100-130 of the AR domain of zDHHC17 completely impair S-acylation of SNAP25b they appear to be not that crucial for SPRY2 S-acylation.

In addition to that, we found that SPRY2 expression levels are influenced by zDHHC17-mediated S-acylation.

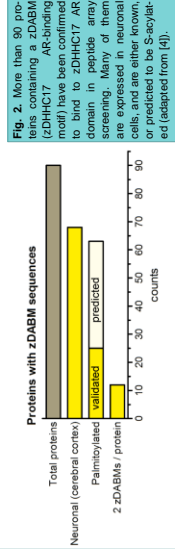


Fig. 2. More than 90 proteins containing a zDABM (zDHHC17 AR-binding motif) have been confirmed to bind to zDHHC17 AR domain in peptide array screening. Many of them are not in our cell lines, and are either known or predicted to be S-acylated (adapted from [4]).

Data Analysis

→ Quantification of protein bands was by densitometry, using Image Studio software.

→ Statistical analysis was conducted using Prism Software (GraphPad 5.0).

→ One way ANOVA with Dunnett's multiple comparison was used for comparison of the means between each condition and the control (corresponding to pEF-BOS HA).

→ All error bars represent standard error of the mean (SEM).

Results

zDHHC17 W130A and N100A mutants are inactive towards SNAP25b

Fig. 3. Western blot of SNAP25b in which S-acylation is revealed by click-chemistry (left) and relative quantification (right). Overexpression of zDHHC17 WT significantly increases S-acylation of SNAP25b, while both W130A and N100A mutants are completely inactive (***) denotes P < 0.001, (n=3).

zDHHC17 W130A and N100A mutants are active towards SPRY2

Fig. 4. Western blot of SPRY2 in which S-acylation is revealed by click-chemistry (left) and relative quantification (right). Overexpression of zDHHC17 WT, as well as both W130A and N100A mutants significantly increases S-acylation of SPRY2 (** denotes P < 0.01, *** denotes P < 0.001, n=3).

The AR domain of zDHHC17 binds to multiple regions on SPRY2

Fig. 5. Western blot of SPRY2 in which S-acylation is revealed by click-chemistry (left) and relative quantification (right). Proline to Alanine substitution at position 154, as well as R177A mutations at any of the other SPRY2 Cys' does not abolish S-acylation by zDHHC17 (***) denotes P < 0.001, (n=3).

zDHHC17 AR domain binds to SPRY2 wild-type and mutants to a different extent. His₁₅₄AR₁₅₄ efficiently binds SPRY2 wild-type and to a lesser extent SPRY2 Cys mutants. His₁₅₄AR₁₅₄ is able to pull-down SPRY2 truncated at Arg-177 but not SPRY2 truncated at Cys-146. Mutation of His₁₅₄ to Proline at position 154 of SPRY2 (R177A mutant) completely impairs interaction with zDHHC17.

Fig. 6. zDHHC17 AR domain binds to SPRY2 wild-type and mutants to a different extent. His₁₅₄AR₁₅₄ efficiently binds SPRY2 wild-type and to a lesser extent SPRY2 Cys mutants. His₁₅₄AR₁₅₄ is able to pull-down SPRY2 truncated at Arg-177 but not SPRY2 truncated at Cys-146. Mutation of His₁₅₄ to Proline at position 154 of SPRY2 (R177A mutant) completely impairs interaction with zDHHC17.

Overexpression of HA-tagged zDHHC17 significantly increases EGFP-tagged SPRY2 S-acylation and expression levels. (***) denotes P < 0.001, (n=3). SPRY2 S-acylation is revealed by click chemistry, relative expression levels are quantified using total protein stain.

Fig. 7. Overexpression of HA-tagged zDHHC17 significantly increases EGFP-tagged SPRY2 S-acylation and expression levels. (***) denotes P < 0.001, (n=3). SPRY2 S-acylation is revealed by click chemistry, relative expression levels are quantified using total protein stain.

zDHHC17 W130A and N100A substitutions impair S-acylation of SNAP25b but not S-acylation of SPRY2 protein.

→ None of the Proline to Alanine substitutions at the Cys prevent zDHHC17-mediated S-acylation of SPRY2.

→ zDHHC17 AR domain mainly binds to the consensus sequence [VAP]VTXXQP at position 154 of SPRY2. Furthermore, an additional AR domain binding site might exist downstream Arginine 177 of SPRY2.

→ zDHHC17 S-acylation stabilizes SPRY2 level of expression.

Discussion

→ zDHHC17 W130A and N100A substitutions impair S-acylation of SNAP25b but not S-acylation of SPRY2 protein.

→ None of the Proline to Alanine substitutions at the Cys prevent zDHHC17-mediated S-acylation of SPRY2.

→ zDHHC17 AR domain mainly binds to the consensus sequence [VAP]VTXXQP at position 154 of SPRY2. Furthermore, an additional AR domain binding site might exist downstream Arginine 177 of SPRY2.

→ zDHHC17 S-acylation stabilizes SPRY2 level of expression.

References

[1] Chamberlain and Shipston, 2015


[2] Butland et al., 2014

[3] Lemonidis, Sanchez-Perez and Chamberlain, 2015

[4] Lemonidis et al., 2017

[5] Verardi et al., 2017

Appendix II




University of Strathclyde

zDHHC17 protein-protein interactions mediated by the Ankyrin-Repeat Domain

Carolina Locatelli¹, Kimon Lemonidis² and Luke H. Chamberlain¹

¹ Strathclyde Institute of Pharmacy and Biomedical Sciences, University of Strathclyde, Glasgow, UK.
² Institute of Molecular, Cell and Systems Biology, University of Glasgow, Glasgow, UK.



BIOCHEMICAL SOCIETY

Introduction

zDHHC enzymes mediate protein S-acylation, a major post-translational modification that regulates many cellular processes (Verardi et al. 2017). There are 23 different zDHHC enzyme isoforms, all defined by the presence of a "DHHC" motif (Chamberlain and Shipston, 2015) with the two Golgi localized *zDHHC13* and *zDHHC17* characterized by an additional N-terminal *ankyrin-repeat domain* (AR domain) (Fig.1). This domain is actively involved in substrate binding and recognizes a consensus sequence [VIAP][VT]XXQP in them (Lemonidis et al. 2015, 2017). Here, we report that specific amino acid mutations, within residues 100-130 of the AR domain of zDHHC17 (reported by Verardi et al. 2017), completely impair the binding of a number of proteins. Additionally, we observed the ability for the AR domain of zDHHC17 to dimerise.

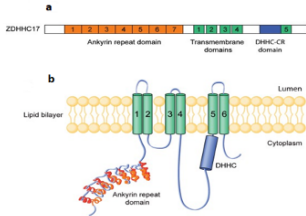


Fig. 1. zDHHC17 schematic structure and functional domains. a) and b) zDHHC17 protein consists of an NH2 terminal seven ankyrin-repeat domain (orange, 3D structure in b); six transmembrane domains, (TMDs, in green) and a 51 amino acid DHHC-CR catalytic domain, located between the TMD 4 and 5. Both catalytic domain and AR domain lay in the cytoplasm (based on fig from Butland et al. 2014).

Results

- ❖ Quantification of protein bands was by densitometry, using Image Studio software.
- ❖ Statistical analysis was conducted using Prism Software (GraphPad 5.0).
- ❖ One way ANOVA with Dunnett's multiple comparison was used for comparisons of the means either between wild-type and mutant zDHHC17 or between zDHHC17 and the other zDHHCs.
- ❖ All error bars represent standard error of the mean.

zDHHC17 undergoes homo and hetero-dimerization mediated by its ankyrin-repeat domain

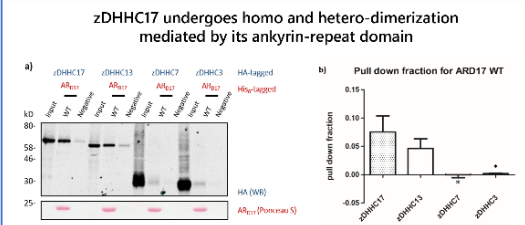
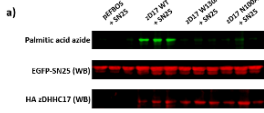


Fig. 4. zDHHC17 and zDHHC13 but not zDHHC7 and zDHHC3 are able to form homo and hetero-dimers interacting with the AR domain of zDHHC17. a) Western blot of a representative experiment b) relative quantification (n=4, * denotes p<0.05).

zDHHC17 W130A and N100A mutants are inactive towards SNAP25b

a)



b) Effect of zDHHC17 mutants on SNAP25b palmitoylation

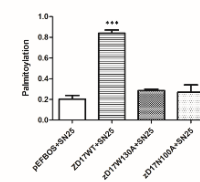
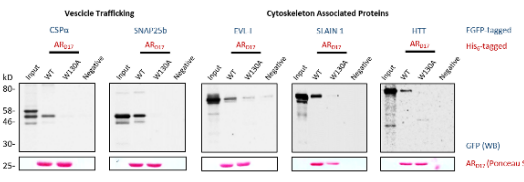


Fig. 2. Western blot of SNAP25b in which palmitoylation is revealed by click-chemistry (top) and relative quantification (bottom). Overexpression of zDHHC17 WT significantly (***) denotes p<0.0001, n=3) increases palmitoylation of SNAP25b while both W130A and N100A mutants are completely inactive.

The W130A substitution in the ankyrin-repeat domain severely impairs the ability of zDHHC17 to bind several partners

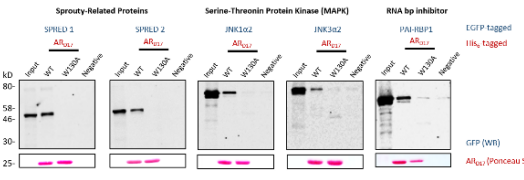
Vesicle Trafficking

CSF1R, SNAP25b, EVI1, STAIN 1, NIT1, FGFP-tagged



Cytoskeleton Associated Proteins

AR, AR, AR, AR, AR, AR



Sprouty-Related Proteins

SPR1D1, SPR1D2, JNK3G2, JNK3G2, PAK-HSP1, RNA bp inhibitor

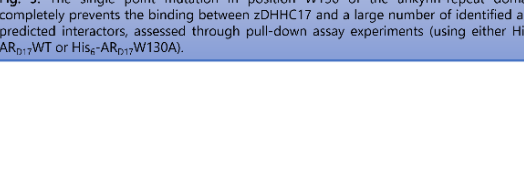
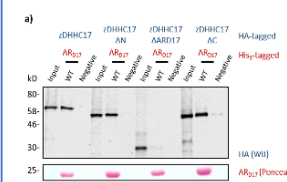


Fig. 3. The single point mutation in position W130 of the ankyrin-repeat domain completely prevents the binding between zDHHC17 and a large number of identified and predicted interactors, assessed through pull-down assay experiments (using either His₆-ARD17-WT or His₆-ARD17-W130A).

The self-association observed for zDHHC17 is mediated by its ankyrin-repeat domain

a)



b) Pull down fraction for ARD17 WT

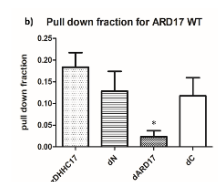
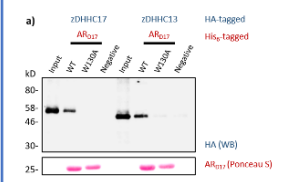


Fig. 5. zDHHC17 self-associates through its ankyrin-repeat domain. a) Western blot of a representative experiment b) relative quantification (n=3, * denotes p<0.05). Truncation mutants: zDHHC17 ΔN (residues 54-632), zDHHC17 ΔARD17 (residues 267-632) and zDHHC17 ΔC (residues 11-569) (Lemonidis et al. 2014).

Both zDHHC17 and zDHHC13 lose the ability to form dimers in the presence of the W130A substitution

a)



b) Pull down fraction for ARD17 WT

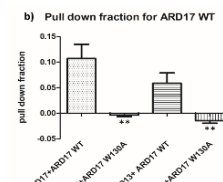


Fig. 6. The residue W130 is crucial in the observed dimerization. Both zDHHC17 and zDHHC13 can be pulled down by His₆-ARD17-WT but not by His₆-ARD17-W130A. a) Western blot of a representative experiment b) relative quantification (n=3, ** denotes p<0.001).

Discussion

- ❖ zDHHC17 W130A and N100A substitutions impair the palmitoylation of SNAP25b by zDHHC17.
- ❖ The W130A substitution in zDHHC17 ankyrin-repeat domain impairs the binding to a large number of zDHHC17 substrates.
- ❖ The AR domain of zDHHC17 is able to bind zDHHC17 itself and zDHHC13 but not zDHHC7 or zDHHC3 underlying oligomerization mechanisms.
- ❖ zDHHC17 W130A substitution impairs the binding of both zDHHC17 and zDHHC13.

Acknowledgments - This work is funded by the University of Strathclyde.